UNIVERSIDAD COMPLUTENSE DE MADRID
FACULTAD DE MEDICINA

TESIS DOCTORAL

Experimental treatments for retinitis pigmentosa in animal models: targeting insulin receptor, GSK-3 and Toll-like receptors

Tratamientos experimentales para la retinosis pigmentaria en modelos animales: el receptor de insulina, GSK-3 y los receptores tipo Toll como dianas terapéuticas

MEMORIA PARA OPTAR AL GRADO DE DOCTOR

PRESENTADA POR

Alonso Sánchez Cruz

DIRECTORES

Ignacio Lizasoain Hernández
Catalina Hernández Sánchez

Madrid

UNIVERSIDAD COMPLUTENSE DE MADRID

FACULTAD DE MEDICINA

TESIS DOCTORAL

Experimental treatments for retinitis pigmentosa in animal models: Targeting insulin receptor, GSK-3 and Toll-like receptors

Tratamientos experimentales para la retinosis pigmentaria en modelos animales: El receptor de insulina, GSK-3 y los receptores tipo Toll como dianas terapéuticas

MEMORIA PARA OPTAR AL GRADO DE DOCTOR

PRESENTADA POR

Alonso Sánchez Cruz

DIRECTOR

Ignacio Lizasoain Hernández
Catalina Hernández Sánchez

UNIVERSIDAD COMPLUTENSE MADRID

FACULTAD DE MEDICINA

Experimental treatments for retinitis pigmentosa in animal models: targeting insulin receptor, GSK-3, and Toll-like receptors

Tratamientos experimentales para la retinosis pigmentaria en modelos animales: receptor de insulina, GSK-3 y receptores tipo Toll como dianas terapéuticas

Alonso Sánchez Cruz

Directores: Ignacio Lizasoain Hernández
Catalina Hernández Sánchez

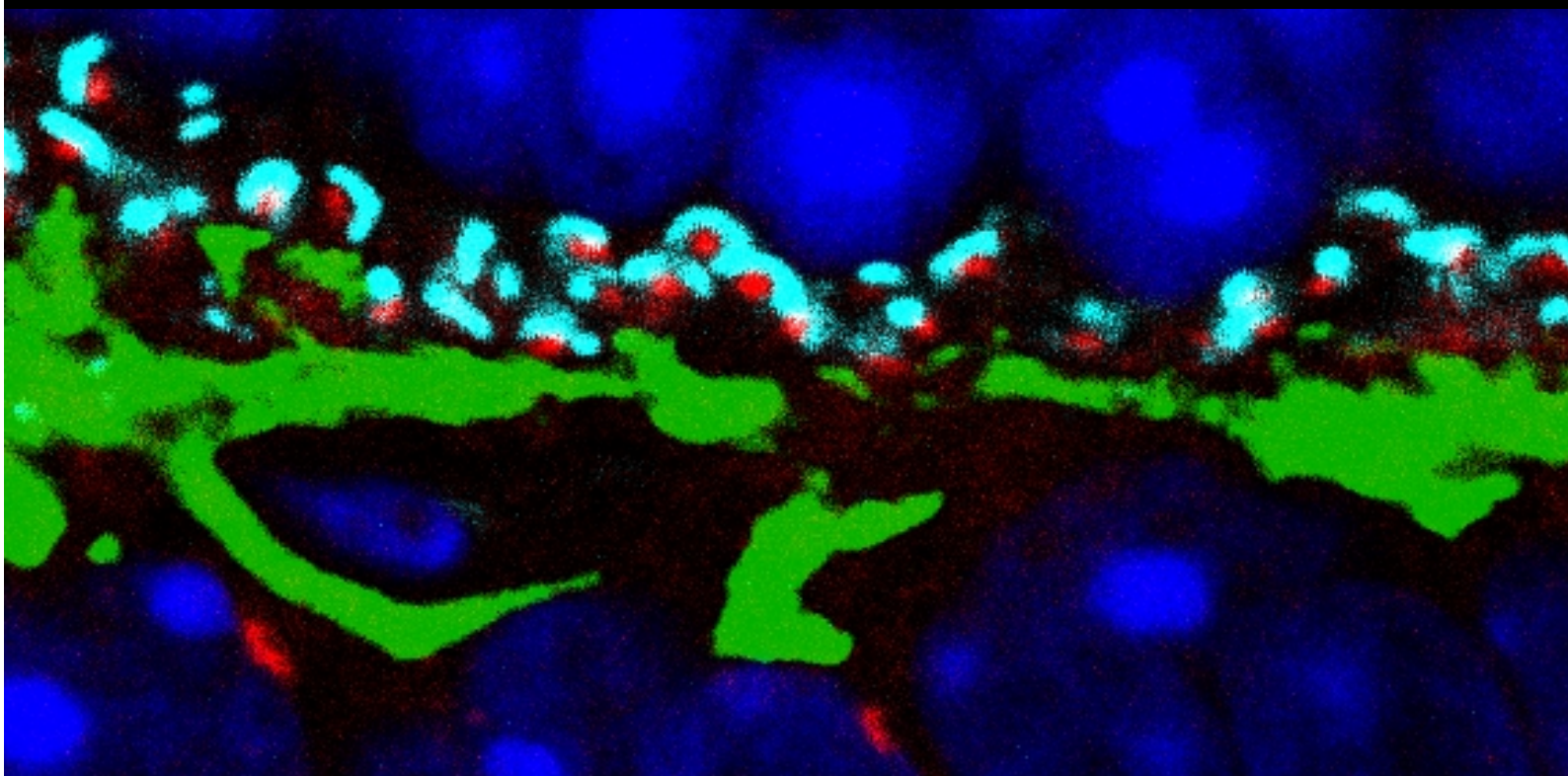

Esta memoria ha sido presentada para optar al grado de Doctor en Investigación Biomédica en la Universidad Complutense de Madrid por el Graduado en Biotecnología Alonso Sánchez Cruz.

Para su realización se ha contado con un contrato UCM perteneciente a la convocatoria CT45/15-CT46/15

Agradecimientos

En primer lugar, querría agradecer todo el apoyo a mi director de tesis el Dr. Ignacio Lizasoain. Muchas gracias por darme la oportunidad de realizar una tesis bajo tu dirección. Sin tu ayuda no hubiera podido presentar esta tesis doctoral.

También desearía agradecer a mi codirectora de tesis la Dra. Catalina Hernández por toda su dedicación a lo largo de estos años. Gracias por tener la puerta de tu despacho siempre abierta, proponer continuamente nuevos experimentos y por seguir de forma permanente el trabajo experimental.

Agradezco también las continuas sugerencias y consejos de todos los miembros de los laboratorios de la UCM y del CIB. Gracias a los Dres. Enrique de la Rosa, Teresa Suárez, Flora de Pablo, María Ángeles Moro, Patricia Boya y Consuelo González. En especial agradezco al Dr. Enrique de la Rosa sus útiles discusiones y consejos científicos y a la Dra. Teresa Suarez el acogerme en el 105.

Querría reconocer muy especialmente el trabajo de Tany y Maria D. Hernández. Sin vuestro trabajo y ayuda (genotipajes, inmunos, criostato, cuantitativas y un largo etc) esta tesis hubiera sido mucho peor. También quiero agradecer la labor formativa de Jose, Tany, Alberto, y Miguel Marchena, que me ayudaron en mucho en mis primeros pasos en el laboratorio. En este sentido, agradezco también la actitud de Noemí, siempre dispuesta a echar una mano. Gracias también a toda la gente con la que he compartido laboratorio durante las diferentes etapas: María P, Marisa, Patricia L., María A, Aina, Cristina, Marta, Pilar y Mateo. Muchas gracias también a Mariano por estar dispuesto siempre a echar un cable. Agradezco también la ayuda de Violeta Medina que respondió a todas mis dudas y me ayudó a encontrar siempre los ratones que necesitaba. Extiendo estos agradecimientos al conjunto del grupo de la UCM por todas su ayuda y sugerencias en los seminarios.

Además, querría reconocer todo el trabajo que han hecho todos nuestros colaboradores para que esta tesis fuera mejor. En primer lugar, querría agradecer al Dr. Pedro de la Villa todo su trabajo ayudándonos con la electrofisiología. En particular, ha sido fundamental para esta tesis la instalación de un equipamiento de ERG portátil en nuestro laboratorio. También quiero agradecer a Laura que me enseñara a hacer ERG y a Mateo y a Santi por toda su ayuda con la electrofisiología. Además, es necesario agradecer a las Dras. Ana Martínez y a Valle Palomo por sintetizar y cedernos el VP3.15 para los experimentos. También es necesario agradecer a la Dra. Fátima Bosch por la generación de los vectores adenoasociados con el gen de la proinsulina. Además, la ayuda de la Dra. Concepción Lillo, realizando los estudios de microscopía electrónica,

ha sido fundamental para estudiar las sinapsis del ratón *rd10*. Querría agradecer también al grupo de la Dra. Patricia Boya sus consejos, colaboración y cesión de reactivos siempre que fue necesario. Gracias Raquel, Bea, Nacho, Elena, Petra, Lorena, Iñaqui, Sergio, Patricia, Katherina y Ana.

Además, me gustaría agradecer al Dr. Uri Saragovi y a todo su grupo que me acogiera en su laboratorio de Montreal y me diera la oportunidad de aprender nuevas técnicas y formas de trabajar. Me gustaría agradecer especialmente toda la ayuda a Alba Galán y a Sean Jmaeff. A ellos dos y a Arturo Papaluca quiero agradecer también los buenos ratos que pasé en la estancia.

También es necesario agradecer el trabajo previo del grupo en los estudios de proinsulina y GSK-3. En particular me gustaría reconocer el trabajo de Alberto Hernández, Carolina Isiegas, Silvia Corrochano y Ryan Steel con la proinsulina y el trabajo de Miguel Marchena y Beatriz Villarejo con el VP3.15.

Gracias también a todo el personal del animalario que siempre han ayudado en todo los posible. En especial querría agradecer el trabajo de Carlos, Meri y Melanie manteniendo y cuidando nuestras colonias de ratones. Querría reconocer nuevamente el trabajo de Carlos que me enseñó muchas técnicas de manejo de los animales y valorar el trabajo de Angélica que ha puesto a punto el anestesiado de los animales. También quería agradecer al personal de los servicios de confocal tanto del CIB como de la UCM que nos han ayudado en todo lo posible y han aumentado mucho la calidad de nuestras imágenes. Gracias Maite, Gema, Juanjo y Alfonso. También me gustaría agradecer a todo el personal del servicio de proteómica por toda su ayuda durante mi breve estancia allí, gracias Tamar, Vivi y Paco. Además, querría reconocer también a todos los diferentes investigadores que nos han dejado reactivos a lo largo de esta tesis. Agradezco especialmente al laboratorio del Dr. Manuel Fresno que nos permitiera utilizar los animales deficientes para *Tlr2*.

Querría acabar agradeciendo a todos los miembros de los miembros presentes y pasados del laboratorio (por orden alfabético): Aina, Alberto, Ana R., Andrés, Bea, Cati, Consuelo, Cristina, Diana, Enrique, Flora, Gerardo, Isa, Jose, Maria A, Maria D, Marco, Mariano, Maria P, Marina, Marisa, Marta, Mateo, Miguel Marchena, Pablo, Patri L, Patri V, Pilar, Raquel, Tany y Tere. Muchas gracias por todos los buenos ratos dentro del laboratorio y también fuera de él.

Agradezco también a mi familia y a Andréa, esta tesis es también gracias a vosotros.

Contenido

RESUMEN

La retinosis pigmentaria (RP) es una enfermedad rara causante de la mayoría de los casos de ceguera hereditaria. La RP es una enfermedad genéticamente heterogénea causada por más de 3000 mutaciones en más de 60 genes, para la cual no existe actualmente ningún tratamiento. Independientemente de la mutación subyacente, todos los casos de RP presentan muerte de los fotorreceptores e inflamación de la retina. En esta tesis hemos estudiado tres posibles estrategias terapéuticas, independientes del tipo de mutación, para el tratamiento de la RP.

El receptor de insulina (IR) es un importante controlador metabólico, pero también regula la supervivencia neuronal y la actividad sináptica. En esta tesis relacionamos también la disminución de la señalización del IR con la RP. En condiciones fisiológicas, el IR se expresa en todas las capas de las retinas, pero su expresión está enriquecida en las fibras de las células horizontales y ganglionares. En el modelo murino de RP *rd10*, el receptor de insulina y su efector fosfo-S6 estaban selectivamente disminuidos en las células horizontales. En paralelo, observamos sinapsis aberrantes entre los bastones y las células horizontales y bipolares. Sin embargo, mediante una terapia génica que inducía una producción continua de proinsulina restauramos la señalización del receptor de insulina en las células horizontales del *rd10*, aumentando la fosforilación de la proteína S6. Además, la proinsulina preservaba el número de fotorreceptores y sus conexiones sinápticas. Estos resultados abren una nueva línea de investigación dirigida a preservar la sinapsis de los bastones y apoyan el uso de la proinsulina como potencial terapia en la RP.

GSK-3 es una enzima multifuncional siendo uno de sus funciones regular el balance inflamatorio, por lo que tiene potencial terapéutico en enfermedades con un componente inflamatorio. En esta tesis observamos que la expresión de GSK-3β (ARNm y proteína) no cambiaba durante la degeneración del *rd10*. Sin embargo, los niveles de pGSK-3β^{Ser9} y de su regulador pAKT^{Ser473} aumentaban en las retinas *rd10* en comparación con las silvestres. La administración *in vivo* del inhibidor de GSK-3 VP3.15, permitió retrasar la perdida de los fotorreceptores y de los segmentos externos de conos y bastones. Además, VP3.15 disminuyó la activación del regulador inflamatorio NF-κB en explantes de retina *rd10*. Estos resultados son una prueba de concepto del potencial terapéutico de VP3.15 en la RP.

Los receptores tipo *Toll* (TLRs), además de participar en la defensa contra patógenos, responden al daño celular y tisular. Su activación ha sido asociada a los procesos inflamatorios involucrados en la neurodegeneración. Aquí mostramos que la expresión de los *Tlr1-9* y sus

adaptadores estaba aumentada en los ratones *rd10* y por lo menos *Tlr2* y *Tlr4* en el modelo de RP P23H. La haploinsuficiencia para *Tlr4* aceleraba la pérdida de función visual en *rd10*, correlacionándose con una peor preservación de la integridad de los fotorreceptores. Este fenotipo se agravaba por la total deleción de *Tlr4*, en los ratones *rd10* y P23H. El análisis de la microglia en el ratón *rd10*, mostró un aumento de la microglia fagocítica y una disminución de la homeostática, en las capas de los fotorreceptores después de la total deleción de *Tlr4*. Por el contrario, la deleción de un solo alelo de *Tlr2* no alteraba el curso de la RP en el ratón *rd10*. Sin embargo, su completa deleción extendía la función visual en *rd10* y P23H. Estos resultados sugieren que TLR4 tiene un papel protector en la RP, y que la inhibición farmacológica de TLR2 podría ser una potencial diana terapéutica en la enfermedad.

En resumen, en esta tesis concluimos que la administración de proinsulina o del inhibidor de GSK-3 VP3.15 pueden ser potenciales abordajes terapéuticos para el tratamiento de la RP. Adicionalmente, hemos observado que la expresión local del IR y su señalización están alterados en la RP, pudiendo participar en la pérdida de la función y la estructura de la retina propias de la enfermedad. Además, mostramos que los TLRs tienen un papel dual en la progresión de la RP: TLR4 tiene un papel protector, mientras que TLR2 resulta perjudicial. Los resultados de esta tesis indican que TLR2 podría ser una diana terapéutica para el tratamiento de RP, mientras que sugieren que presencia de TLR4 resulta beneficiosa para la progresión de la RP.

ABSTRACT

Retinitis pigmentosa (RP) is a rare disease responsible for the majority of the cases of hereditary blindness. RP is a genetically heterogeneous disease caused by more than 3000 mutations in over 60 genes without an effective treatment. Irrespectively of the causative mutation, there are common traits to RP: photoreceptor cell death and retinal inflammation. In this thesis we have studied three potential mutation-independent therapeutic strategies for RP treatment.

The insulin receptor, a key controller of metabolism, also regulates neuronal survival and synaptic formation, maintenance, and activity. Here we present evidence linking impaired insulin receptor signaling with RP. In physiological conditions, insulin receptor is expressed in all the retinal layers depicting prominent levels in horizontal and ganglion cells fibers. In the *rd10* retinas, a mouse model of RP, the insulin receptor and its downstream effector phospho-S6 were selectively decreased in the horizontal cells. In parallel, we observed aberrant synapses between rod photoreceptors and the post-synaptic terminals of horizontal and bipolar cells. A gene therapy strategy to induce sustained proinsulin production restored retinal insulin receptor signaling, increasing S6 phosphorylation. Moreover, proinsulin preserved photoreceptor cells and synaptic connectivity. These results open a new line of research into interventions aimed at preserving rod connectivity and support the therapeutic potential of proinsulin in RP.

GSK-3 is a multitask enzyme involved in the regulation of the pro-inflammatory and anti-inflammatory balance among other multiple cellular functions. Consequently, it is considered a potential therapeutic target for diseases with an inflammatory component. In this thesis we show that GSK-3β expression (mRNA and protein) remained unchanged during the retinal degeneration period in the *rd10* model. However, levels of pGSK-3β^{Ser9} and its regulator pAKT^{Ser473} were increased in *rd10* versus wild-type retinas. *In vivo* administration of VP3.15, a small-molecule GSK-3 inhibitor, delayed the loss of photoreceptors and preserved the outer segments of cones and rods without interfering with other retinal populations. Moreover, VP3.15 attenuated the activation of NF-κB, a key regulator of the inflammatory response, in *rd10* retinal explants. These results provide proof of concept of the therapeutic potential of VP3.15 for the treatment of RP.

Toll-like receptors (TLRs), besides being key players in the defense against pathogens, are responders to cellular and tissue damage. TLR activation has been associated to inflammatory processes involved in neurodegenerative conditions. Here we show that the expression of TLR1-

9 and of TLR-adaptor proteins are increased in the retinas of two RP models, *rd10* and at least *Tlr2* and *Tlr4* in P23H mice. Haploinsufficiency of *Tlr4* accelerates visual function loss in both RP models, correlating with a worse preservation of photoreceptor integrity. This phenotype was aggravated by the total deletion of *Tlr4*. Microglia analysis in the *rd10* retina showed increased phagocytic and decreased homeostatic microglia in the photoreceptor layers upon *Tlr4* total deletion. On the contrary, single *Tlr2* allele deletion did not affect RP progression in the *rd10* mouse, but complete elimination of *Tlr2* extended the visual function in the *rd10* and P23H mice. These results suggest that TLR4 plays a protective role during RP and that pharmacological inhibition of TLR2 is a potential therapeutic target for RP.

Overall, in this thesis we have concluded that proinsulin or the GSK-3 inhibitor VP3.15 could be potential therapies for RP. Moreover, we have shown that local IR expression and signaling are altered in the RP context and could participate in the retinal structural and functional decline of the disease. In addition, we showed that TLRs have a dual role on RP progression: TLR4 is protective, while TLR2 is detrimental. The results of this thesis indicate that TLR2 could be a potential therapeutic target for RP treatment, but suggest that TLR4 has a beneficial role in RP progression.

ABBREVIATIONS

***A2m*:** alpha-2-macroglobulin gene

AAV: Adeno-associated viral vector

AD: Alzheimer's disease

AKT/PKB: protein kinase B

AMD: Age-related macular degeneration

AP1: Activator protein 1

APP: amyloid precursor protein

ARVO: Association for Research in Vision and Ophthalmology

Aβ: Amiloid β

bFGF: basic fibroblast growth factor

CCL: Chemokine (C-C motif) ligand 2

***Cd68*/CD68:** cluster of differentiation 68

cDNA: complementary desoxyribonucleic acid

cGMP: cyclic guanosine monophosphate

ChR: Channel rhodopsin

CNS: Central nervous system

CNTF: Ciliary neurotrophic factor

CREB: cyclic AMP-response element-binding protein

CRISPR/Cas9: Clustered regularly interspaced short palindromic repeats/CRISPR associated protein 9

CSIC: Consejo Superior de Investigaciones Científicas

CtBP2: c-terminal binding protein 2

DAMPs: Damage associated molecular patterns

DAPI: 4´,6-diamidino-2-phenylindole

EC_{50}: Half maximal effective concentration

EDTA: Ethylenediaminetetraacetic acid

EGTA: Egtazic acid

ELISA: Enzyme-Linked ImmunoSorbent Assay

EMA: European Medicines Agency

ERG: Electroretinography

ERK: Extracellular signal regulated kinases

ESCs: Embryonic stem cells

FDA: Food and Drug Administration

GABA: *gamma*-aminobutyric acid

GAPDH: glyceraldehyde 3-phosphate dehydrogenase

GCL: Ganglion cell layer

GDNF: Glial-cell derived neurotrophic factor

GluA2: ionotropic glutamate receptor A2

GSK-3: glycogen synthase kinase-3

HMGB1: High mobility group box 1 protein

hPi: human proinsulin

HSP: Heat-shock proteins

Iba1*/Iba1*: Ionized calcium-binding adapter molecule 1

IC_{50}: Half maximal inhibitory concentration

IFN: Interferon

IGF-1: insulin-like growth factor 1

IGF1R: insulin-like growth factor 1 receptor

IGF-2: insulin-like growth factor 2

IKK: Inhibitor of kappa B kinase

IL: Interleukin

ILM: Inner limiting membrane

INL: Inner nuclear layer

***Ins2*:** insulin 2 gene

***Insr*:** Insulin receptor gene

IPL: Inner plexiform layer

iPSCs: Induced pluripotent stem cells

IR: Insulin receptor protein

IRAK: IL-1R-associated kinase

IRF: Interferon regulatory factor

IRS: insulin receptor substrate

IS: Inner segment

JNK: JUN N-terminal kinase

L/M-opsin: Long/medium wavelength opsin

LPS: Lipopolysaccharides

LRR: Leucine-rich repeat

MAPK: mitogen activated protein kinase

***Mertk*:** MER receptor tyrosine kinase gene

MG: Müller glia

mGluR6: metabotropic glutamate receptor 6

MKK: MAP kinase kinase

MnTBAP: Mn (III) tetrakis (4-benzoic acid) porphyrin chloride

MNU: methylnitrosourea

MPTP: 1-methyl-4-phenyl-1,2,3,6-tetrahydropyridine

mRNA: messenger RNA

mTOR: mammalian target of rapamycin

MYD88/*MyD88*: Myeloid differentiation primary response 88

NFL: Nerve fiber layer

NF-M: Neurofilament medium

NF-κB: nuclear factor kappa light-chain enhancer of activated B-cells

NGF: nerve growth factor

NMDA: N-methyl-D-aspartate

OLM: Outer limiting membrane

ON: Optic nerve

ONL: Outer nuclear layer

OP: Oscillatory potential

OPL: Outer plexiform layer

OS: Outer segment

p: p-value

PAMPs: Pathogen associated molecular patterns

PBS: Phosphate buffer saline

PD: Parkinson's disease

***Pde6*/PDE6:** phosphodiesterase 6

***Pde7*/PDE7:** phosphodiesterase 7

PEDF: Pigment epithelium-derived factor

PI3K: phosphoinositide 3-kinase

PKA: protein kinase A

PKC-α: protein kinase C alpha

PLGA: poly lactic-*co*-glycolic acid

***Prph2*:** Peripherin gene

PRR: Pattern recognition receptors

qPCR: quantitative polymerase chain reaction

RBPMS: RNA-binding protein with multiple splicing

RdCVF: Rod-derived cone viability factor

***RLBP1*:** Retinal aldehyde binding protein 1 gene

RNA: Ribonucleic acid

RNAi: RNA interference

RP: Retinitis pigmentosa

RPE: Retinal pigment epithelium

***Rpe65*/RPE65:** retinoid isomerohydrolase RPE65

***RPGR*:** Retinitis pigmentosa GTPase regulator gene

RT: reverse transcription

S6: ribosomal S6 protein

S6K: ribosomal protein S6 kinase

SD-OCT: Spectral domain optical coherence tomography

SEM: Standard error of the mean

Shc: Src homologous and collagen protein

S-opsin: Short wavelength opsin

SPB: Sörensen's phosphate buffer

STR: Scotopic threshold response

SUnSET: surface sensing of translation

***Tbp*:** TATA binding protein gene

TGF-β: Transforming growth factor β

***Ticam*/TICAM**: TIR domain-containing adapter molecule

TIR: Toll/interleukin-1 receptor/resistance protein domain

TIRAP/*Tirap*: TIR domain containing adaptor protein

TLR/*Tlr*: Toll like receptor

***Tnf*/TNF-α:** Tumor necrosis factor α

TNF-R1: tumor necrosis factor receptor 1

TRAF: TNF receptor-associated factors

TRAM: TRIF-related adaptor molecule

TRIF: TIR-domain-containing adapter-inducing interferon-β

TUDCA: Tauroursodeoxycholic acid

VPA: Valproic acid

WT: Wild-type

SECTION 1
INTRODUCTION

1. INTRODUCTION

1.1. Retina

The retina is the part of the central nervous system (CNS) that is localized in the back of the eye. It is responsible for converting light into electrochemical signals and is thus indispensable for vision. This conversion is called phototransduction. Retina is divided in two parts: the retinal pigment epithelium (RPE) and the neural part, the neuroretina. The RPE is formed by a monolayer of hexagonal epithelial cells that contain melanosomes, responsible for its pigmented color. The RPE is located in the back of the eye and is in close contact with the neuroretina, the translucent neural component of the retina with photosensitive properties. The cytoarchitecture of the neuroretina was initially described by Cajal (1892). It is formed by 6 neuronal types and 3 glial cell types distributed in three nuclear layers (Figure 1.1). The outer nuclear layer (ONL) is the closest to the RPE and contains the nuclei of the photoreceptors. The second nuclear layer is the inner nuclear layer (INL) that contains the nuclei of the interneurons: bipolar, horizontal and amacrine cells. The most internal nuclear layer is called the ganglion cell layer (GCL) and is formed by the nuclei of the ganglion cells and of the displaced amacrine cells. The axons of the ganglion cells form the nerve fiber layer (NFL) and give rise to the optic nerve, which projects to the brain. Between the nuclear layer there are two fiber layers: the outer plexiform layer (OPL) and the inner plexiform layer (IPL) formed by synaptic contacts of the retinal neurons (Figure 1.1).

Photoreceptors are specialized neurons that are in charge of phototransduction. There are two types of photoreceptors: rods and cones. Rods response in low light conditions (scotopic conditions) and allow for night vision, while cones are responsible for color vision in daylight conditions (photopic vision). The number of rods in the retina is much higher than the number of cones, for instance in human retinas rods outnumber the cones in a 20:1 ratio (Mustafi et al., 2009). The differential light response of both cell types is conferred by the particular opsin expressed by each photoreceptor cell type. Rods express rhodopsin that is able to be stimulated even with just a single photon. Cones express different types of opsins, each one specific for a different part of the visual spectrum. For example, cones in humans have three types of opsins red-sensitive (long wavelength), green-sensitive (middle wavelength) and blue-sensitive (short wavelength). Rhodopsin and cone opsins are located in membranous discs of the outer segment (OS) of photoreceptors. The inner segment (IS) of photoreceptors contains organelles and a great quantity of mitochondria mainly devoted to the energy-consuming phototransduction process. In fact, it has been reported that the retina consumes more oxygen per gram than the

brain, becoming one of highest oxygen consuming tissues in the body (Anderson, 1968; Yu and Cringle, 2001).

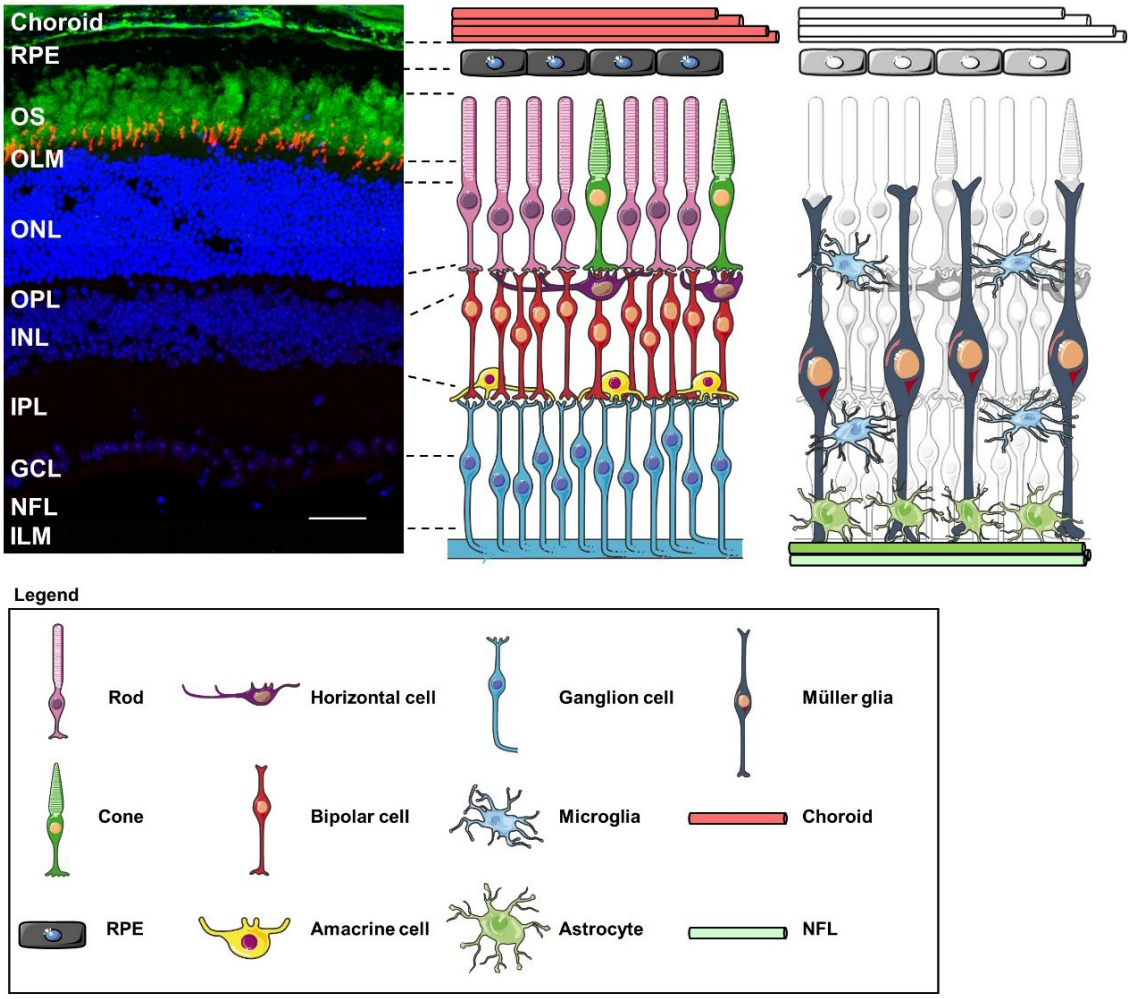

Figure 1.1. Retinal structure. The neuroretina is comprised of three nuclear layers. The first nuclear layer that is contact with the retinal pigment epithelium (RPE) is the outer nuclear layer (ONL) that has the nuclei of rods and cones. These cells have a specialized structure called the outer segment (OS), where the photopigment is located. The nuclei of the interneurons horizontal, bipolar and amacrine cells are located in the inner nuclear layer (INL). The ganglion cells are located in the ganglion cell layer (GCL) and their axons form the nerve fiber layer (NFL). Between the nuclear layers there are two fiber layers: the outer plexiform layer (OPL) and the inner plexiform layer IPL (IPL). The choroid is the vascular layer of the eye. The retina has two limiting membranes: the outer limiting membrane (OLM) and the inner limiting membrane (ILM). The glial cells present in the retina are the Müller glia (with nuclei in the INL and projections from the OLM to the ILM), the microglia (present in the OPL and IPL) and astrocytes (located in GCL and NFL). Nuclei are stained with DAPI and the OS of rods and cones are immunostained with anti-rhodopsin and anti-L/M-opsin antibodies respectively. Scale bar: 35µm.

Photoreceptor synaptic terminals are called spherules in the case of rods and pedicles in the case of cones. Both contain electro-dense structures of 200-1000 nm of length called ribbons, where the synaptic vesicles are tethered by fine filaments (Figure 1.2). The ribbon is a common structure in sensory neurons and allows for acute and sustained release of neurotransmitters (glutamate in the case of photoreceptors). Photoreceptors synapse in the OPL with bipolar and horizontal terminals in a structure named triad because it is formed by three neuronal cell types.

Each rod spherule has a single ribbon, forming a ribbon synapse with horizontal and bipolar cell processes; while each cone pedicle has 20-50 ribbons depending on the species, each one forming a triad synapse (see Figure 1.2). The postsynaptic side of the triad has as central element one bipolar cell dendritic terminal (in cones) or two bipolar cell dendritic terminals (in rods). As lateral elements rod and cone synapses have two horizontal cell processes. Photoreceptors form a direct synapse with bipolar cells, that relies on the neurotransmitter glutamate; however, the synapse with horizontal cells is more complex. In this case, horizontal cells receive glutamatergic input from photoreceptors but they provide feedback and feedforward signals to photoreceptors and bipolar cells respectively. The feedback signaling modulates the glutamate release by the photoreceptor and may employ three different mechanisms: ephaptic, proton-mediated or *gamma*-aminobutyric acid (GABA-mediated), as reviewed in (Chapot et al., 2017). The feedforward signaling from horizontal cells to bipolar cells is less studied and may rely on the neurotransmitter GABA.

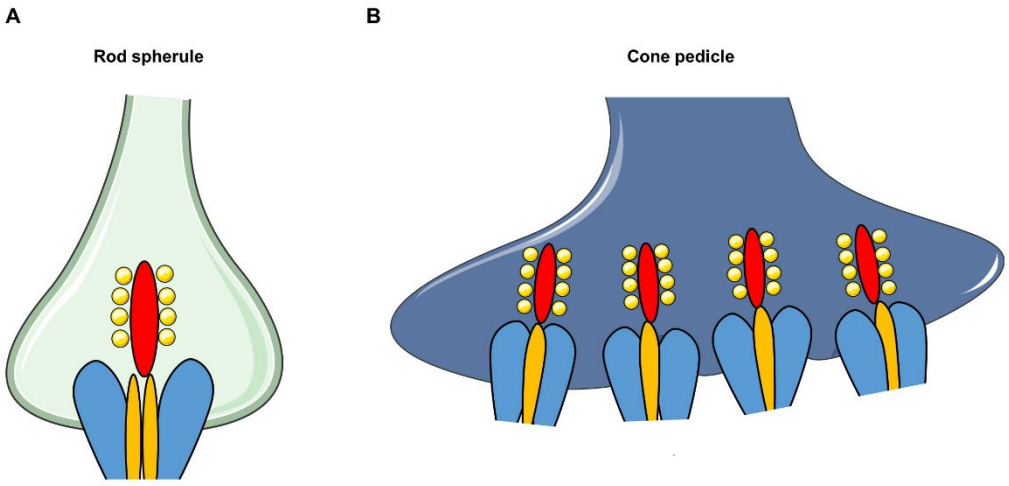

Figure 1.2. Rod and cone synapses. A. Rod spherule. Each rod spherule has a single ribbon (red). Glutamate synaptic vessels (yellow) are tethered to the ribbon. The postsynaptic elements are two horizontal cell processes (blue) and two bipolar cell dendritic terminals (orange). **B.** Cone pedicle. Each cone pedicle has between 20 and 50 ribbons depending on the species. The postsynaptic elements for each ribbon are two horizontal cell processes and one bipolar cell dendritic terminal.

Bipolar cells allow the direct communication of photoreceptors with ganglion cells. For this purpose, they have a dendritic arbor that, as previously mentioned, synapse onto photoreceptors and a large axon that synapses onto ganglion cells. This second synapse also relies on the presence of ribbons, in this case in the IPL. On the contrary, horizontal cells are responsible for the modulation of photoreceptor output and key players in the early processing of the visual information, contributing to contrast enhancement and color opponency. In the INL there are also nuclei of the interneurons called amacrine cells (Figure 1.1). These cells are synaptically active in the IPL, where they make inhibitory synapses onto bipolar and ganglion

cells, modulating the visual information transmitted from bipolar cells to ganglion cells. In addition, there is also a population of amacrine cells with nuclei in the GCL, called displaced amacrine cells.

Ganglion cells are the projection neurons of the retina, they convey the visual information of the rest of the retinal neurons, and their axons (nerve fiber layer, NFL, Figure 1.1) form the optic nerve that projects to the brain.

In addition to neurons, in the neuroretina there are glia cells, the macroglia (Müller glia and astrocytes) and the microglia. The Müller glia (MG) are the endogenous retinal glia and represent about 90% of the total glia population (Vecino et al., 2016). MG have their nuclei in the INL and extend radial projections through-out the retina, from the outer limiting membrane (OLM) to the inner limiting membrane (ILM) as depicted in Figure 1.1. MG are important for retinal structure and essential for maintaining retinal homeostasis. They have trophic functions, supplying the end-products of anaerobic metabolism (lactate/pyruvate) to neurons and are key cells in the reuptake of glutamate, protecting neurons from excessive amount of this neurotransmitter. MG regulate water, bicarbonate and ion transport, and the blood-retinal barrier permeability. MG are also capable of acting as fibers, guiding the light throughout the retina to the photoreceptors. Besides the homeostatic functions, MG is an important player in the retinal response to injury. MG undergo a process of reactive gliosis, that involves structural, physiological and biochemical alterations, and in some cases proliferation. All these changes aim to restore homeostasis, however prolonged reactive gliosis can exacerbate retinal damage (Goldman, 2014; de Hoz et al., 2016).

Astrocytes, the other macroglial cells, enter the retina through the optic nerve during development. Astrocytes are located exclusively in the GCL and NFL. As in the brain, they insulate and protect neurons. They also have trophic functions, regulate the metabolism of neurotransmitters (such as glutamate and GABA), protect neurons from oxidative stress and regulate blood-retinal barrier. Upon injury, astrocytes can also proliferate and undergo a process of reactive gliosis.

Microglia are the tissue resident mononuclear phagocytes of the retina. They derive from myeloid progenitors that arise early in development (Ginhoux et al., 2010). Retinal microglia population is maintained, in steady-state conditions, by self-renewal (Ajami et al., 2007). In physiological conditions, microglia are located in the plexiform layers where they display a ramified morphology and are in charge of immunosurveillance. In addition, microglia participate in the developmental synaptic pruning (Li et al., 2019) and in the maintenance of the retinal

synapses of the adult animal (Wang et al., 2016). In the case of trauma or disease, microglia acquire a reactive state and undergo dramatic physiological and morphological changes. Microglia migrate to the affected area in order to restore homeostasis, but as in the case of the macroglia, the persistence of this reactive state may aggravate the disease progression (Rashid et al., 2019).

RPE is in close contact with the photoreceptor OS (Figure 1.1). RPE cells extend microvilli from the apical membrane to surround rod and cone OS and participate in OS daily renewal. RPE is crucial in the phosphotransduction process since it participates in the recycling and in the reisomerization of the retinal (see below). In addition, the melanin of the melanosomes quenches the excess of light, impeding an abnormal reflex of light in the sclera that would alter vision. RPE also participates in the transport of glucose, retinol or fatty acids from the choroid blood vessels. It is important to highlight that RPE is indispensable for vision and that due to its tight interaction with photoreceptors, degeneration of the RPE causes degeneration of photoreceptors and vice-versa as reviewed in Strauss (2005).

Although the RPE is part of the retina, the term retina is commonly applied exclusively to the neuroretina. Therefore, to be consistent with the literature, for the rest of the thesis we will refer to the neuroretina as retina.

1.2. Phototransduction

The light enters the eye through the cornea and the lens and is projected onto the retina where it travels through-out all the retinal layers until it reaches the photoreceptors, where the phototransduction cascade takes place (Figure 1.3).

In the dark, the OS of the photoreceptors have high levels of cyclic GMP (cGMP) that keep the cGMP cathionic channels open. This allows the entrance of Na^+ and Ca^{2+}, resulting in membrane depolarization. In the IS there are outward non-gated K^+ channels, which are compensated with active transport Na^+/K^+ pumps. These pumps allow the entrance of K^+ and the outward movement of Na^+, maintaining photoreceptors in a partially depolarized state. This depolarization causes that, in the dark, the voltage-gated Ca^{2+} channels of the synapses are open. This allows the entrance of Ca^{2+} and a continuous glutamate release in dark conditions.

In the presence of light, rhodopsin is stimulated in the rod OS. Rhodopsin consists on a protein part, the opsin, that belongs to the G-protein-coupled receptor family; and the retinal, the light-absorbing part of the molecule. When stimulated by light photons, the retinal undergoes an isomerization from 11 –*cis* retinal to all-*trans* retinal, forming *meta*-rhodopsin II, that catalyzes

the GDP to GTP exchange in the G- protein transducin. The *meta*-rhodopsin II is unstable and within several minutes it splits into the protein component and all-*trans* retinal. The all-*trans* retinal is reisomerized in the RPE, where it is reduced to all-trans retinol (vitamin A), the precursor in the synthesis of 11-*cis* retinal, which is transported back to the OS of rods.

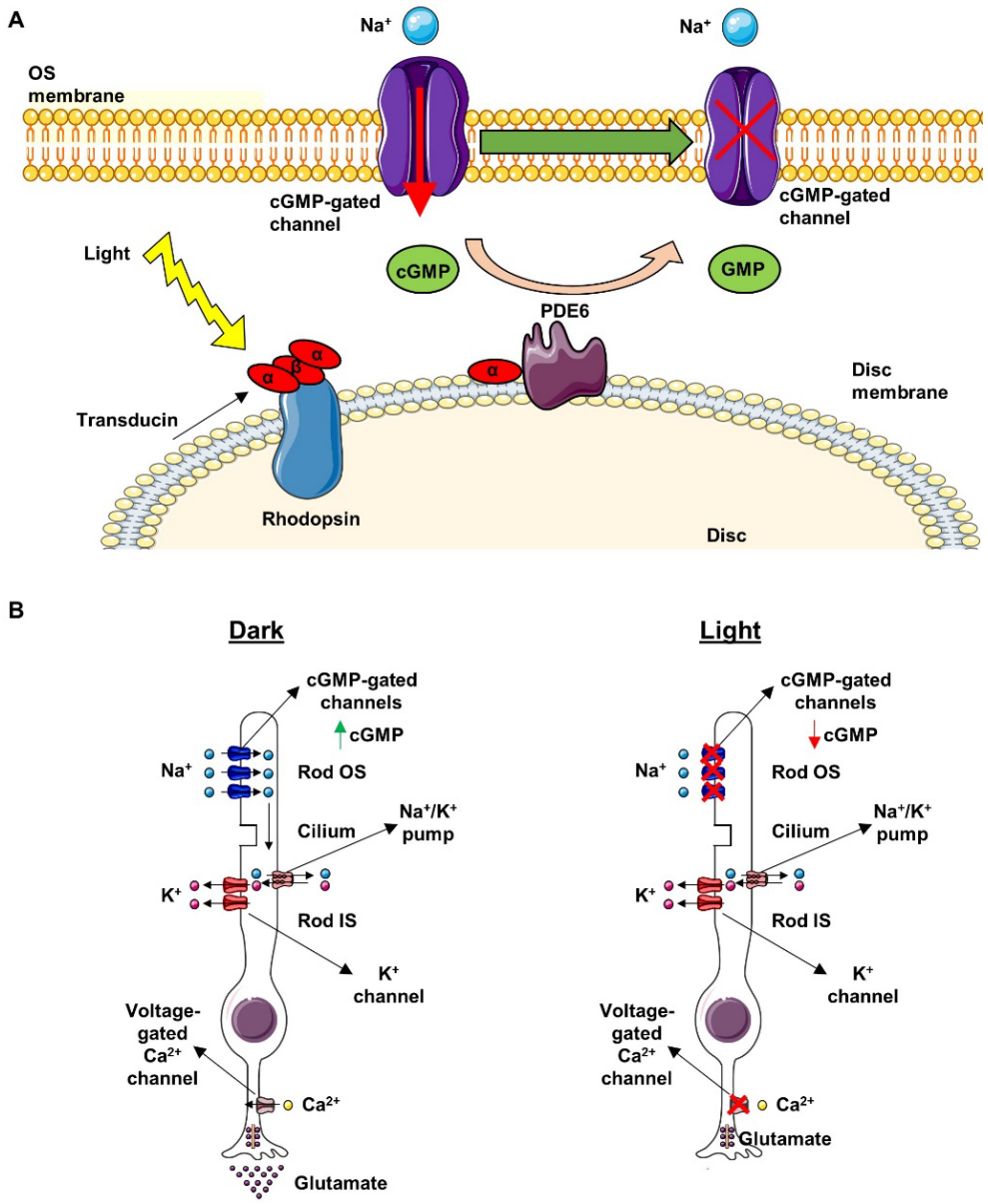

Figure 1.3. Phototransduction cascade. A. The light activation of rhodopsin results in the cleavage of the α subunit of the transducin. This activated transducin prompts phosphodiesterase 6 (PDE6), which catalyzes the hydrolysis of cGMP. The decrease of the cGMP leads to the closure of the cGMP-gated cannels of the outer segment (OS) of the photoreceptor and consequently to a decreased Na^+ entrance. **B.** In scotopic conditions, cGMP levels are increased leading to the entrance of Na^+ through cGMP-channels in the OS of photoreceptors. In the inner segment (IS) there are outward K^+ channels that are compensated with Na^+/K^+ pumps, resulting in a partial depolarization of the photoreceptor. This, in turn leads to the opening of the voltage-gated Ca^{2+} channels of the synaptic terminal, promoting the entrance of Ca^{2+} and triggering the release of glutamate to the synaptic cleft. The stimulation of the photoreceptor with light, leads to the decreased cGMP levels and therefore to the closure of the cGMP-gated channels, resulting in a hyperpolarization of the photoreceptor. This hyperpolarization leads to the closure of the Ca^{2+}-channels and to a decreased release of glutamate.

The phototransduction cascade continues as follows, in the activated transducin the catalytic subunit α is released from the β and γ subunits and, in turn, it activates phosphodiesterase 6 (PDE6). The activation of PDE6 consists on the release of the catalytic subunits α and β from the inhibitory subunit γ. Activation of PDE6 produces the breakdown of cGMP and as a consequence of the decreased cGMP levels, cGMP channels close, leading to a hyperpolarization of the membrane of the photoreceptors. This leads to the closure of the voltage-gated Ca^{2+} channels and to a decrease in the glutamate released by the photoreceptor. The degree of photoreceptor hyperpolarization can be measured in electroretinographic recordings (the amplitude of the a-wave, see section 3.10).

1.3. Retinitis pigmentosa

Retinitis pigmentosa (RP) is a group of retinal hereditary dystrophies responsible for most of the cases of hereditary blindness, affecting more than 1.5 million patients in the world (Verbakel et al., 2018). The global prevalence is considered to be 1:4000 (Pagon, 1988), however it is highly dependent on the cohort of studied patients. In Spain there are about 15,000 RP patients and 1 out of every 80 people is a carrier of a RP gene (Flores-Rodríguez, 2013).

RP is a heterogeneous genetic disease with more than 3000 mutations identified in over 60 genes (https://sph.uth.edu/retnet/sum-dis.htm). These genes have functions in different retinal processes, including phototransduction, retinal metabolism, RNA splicing, cellular structure (in particular photoreceptor structure) and retinal development (Nash, 2015). The first RP causative mutation was identified 30 years ago in the rhodopsin gene (Dryja et al., 1990). Since then, the number of genes associated with the disease has increased dramatically, however the causative mutation is still unknown in around 30% of the patients (Verbakel et al., 2018). The RP inheritance pattern is also diverse. RP can be autosomical dominant (30-40% of the cases), autosomical recessive (50-60%) or X-linked (5-15%) (Hartong et al., 2006). In a small percentage of patients, the inheritance is non-mendelian (digenic or mitochondrial). Despite this heterogeneous genetic origin, there are common traits to the different RP forms. The disease courses with dysfunction and death of rods followed by cone loss, resulting in blindness. This process takes place in both eyes (bilateral disease). The clinical manifestations start with loss of night vision (nyctalopia) due to the death of rods, followed by the loss of peripheral daylight vision, due to the death of cones resulting in tunnel vision that progressively ends in legal blindness (Figure 1.4).

Although the age of onset and severity of the disease progression are highly dependent on the causative mutation, RP patients typically start losing night vision at adolescence and mid-peripheral vision field is evident at young adulthood (Verbakel et al., 2018).

Figure 1.4. Loss of vision of retinitis pigmentosa (RP) patients. In early stages of the disease, rod cell death causes RP patients to lose night vision. In later stages, the disease evolves to produce cone cell death, leading to daylight vision loss. This vision loss starts in the peripheral area of the vision field, producing tunnel vision and evolves towards the central area of the vision field, ending up in legal blindness.

Since RP is a genetic disease, family history is critical in the diagnosis of RP. However, around 40% of the patients of RP are isolated (or simplex) cases (Hayakawa et al., 1997; Neveling et al., 2012; Bravo-Gil et al., 2016). This means that they do not have a first-degree relative affected and no reported cases in other family members.

In the clinical practice, RP diagnosis relies on noninvasive procedures as electroretinography (ERG). Alterations in ERG recordings are observed even before the first night blindness symptoms are detected. Also, at early stages the shortening of the photoreceptor outer segments can be observed by spectral-domain optical coherence tomography (SD-OCT). At more advanced stages, RP patients display abnormal eye fundi. Intraretinal pigmentation (also known as bone-spicule deposits) due to RPE cell migration into the neuroretina is a hallmark of RP, and gives name to the disease. Other alterations of RP eye fundi are attenuated retinal vessels and optic-disc pallor. Furthermore, RP patients suffer from other ocular complications as a consequence of the disease such as nystalgmus, macular complications or posterior subcapsular cataracts, reviewed in Verbakel et al. (2018). The progression of the disease can be monitored

measuring the vision field by perimetry, observing the retinal structure by SD-OCT and assessing the retinal function by ERG.

The heterogeneous genetic etiology of the disease is a challenge, not only for the characterization and molecular diagnosis of RP but also for the disease treatment. Nowadays for most of the types of RP there is not available treatment to cure or prevent the disease. Neverthless, recently a gene therapy strategy has been approved by the FDA for a subtype of RP, caused by mutations in the RPE gene, retinoid isomerohydrolase RPE65, *RPE65* (as explained in 1.5.1). The complexity and diversity of mutations causing RP will require a lot of time and investment to develop gene-specific therapies as a general treatment. Consequently, there is an urgent demand for novel therapies, independent of the causative gene mutation, that could ameliorate the course of the disease.

1.4. State of the art of therapies for retinitis pigmentosa

As previously mentioned, nowadays RP patients do not have any treatment available that can cure or prevent the disease besides the gene therapy for a particular gene aforementioned. However, there are several options available to improve their quality of life and to allow them to adapt better to disease progression.

When there is a RP diagnosis, the patient experiences a process of acceptance of the disease, which sometimes needs psychological help. From early stages the majority of RP patients have difficulties with light adaptation and night vision. These difficulties can be partially overcome with the help of different types of torches, flashlights or night googles. RP patients can also benefit from orientation and mobility training, to allow them to perform better activities of daily living. Actions like reading can be better perform with the use of different types of magnifiers or using text-to-speech software. Also, their mobility can be improved with electronic travel aids and some patients can benefit from the help of a guide dog.

As already stated, RP patients have associated other ocular conditions that can be treated accordingly. The cataract associated to RP can be surgically removed, resulting in an improvement of visual acuity (Yoshida et al., 2015). Regarding to the development of cystoid macular edema, the classic treatment is the administration of carbonic anhydrase inhibitors dorzolamide or acetazolamide, although it is unclear to what extend this results in a preservation of visual acuity (Huang et al., 2017).

The treatment with several vitamins and dietary supplements is available, however their effects at best are marginal (Rayapudi et al., 2013; Brito-Garcia et al., 2017). As described above,

vitamin A is an indispensable element of the visual cycle. Therefore, vitamin A supplements have been used to treat RP patients since the 1960s. Conversely, their real efficacy is still under debate. The clinical trial of Berson and colleagues showed a mild preservation of retinal function in RP patients treated with vitamin A (Berson et al., 1993), although in a meta-analysis a clear effect was not observed (Rayapudi et al., 2013). Similarly, the effects of retinal precursor β-carotene have been studied in RP patients in clinical trials. The study in a small number of patients of Dr. Harats group observed a mild preservation of visual function in treated patients, but failed to find differences between both groups in visual acuity (Rotenstreich et al., 2013). Also, the efficacy of carotenoid lutein was assessed finding a small delay of disease progression in treated patients (Bahrami et al., 2006; Berson et al., 2010).

Another option available for RP patients in an end-stage of the disease is the implantation of electronic devices. These devices are light sensitive and capable of stimulating inner retinal layers, thus allowing visual information to be transferred to the brain in the absence of photoreceptors. Nowadays two devices have received European approval: The Argus II epiretinal implant (Second Sight Medical Products, USA) and the Alpha AMS subretinal implant (Retinal Implant AG, Germany). Development of novel implants capable of restoring vision is a very attractive solution. However, the equipment that is available right now provides only basic black and white vision. Although this weak vision can help the patient in daily activities, it is not comparable to vision of a healthy eye. Moreover, these devices require to be surgically implanted, can have important side effects, need visual adaptation and their long-term safety is not well studied.

1.5. Novel therapies for retinitis pigmentosa

The lack of therapies for RP has prompted researchers world-wide to investigate novel therapies to treat the disease. The therapeutic strategies can be divided in two groups i) therapies that are dependent on the causative mutation and ii) therapies that are independent of the mutation (Figure 1.5).

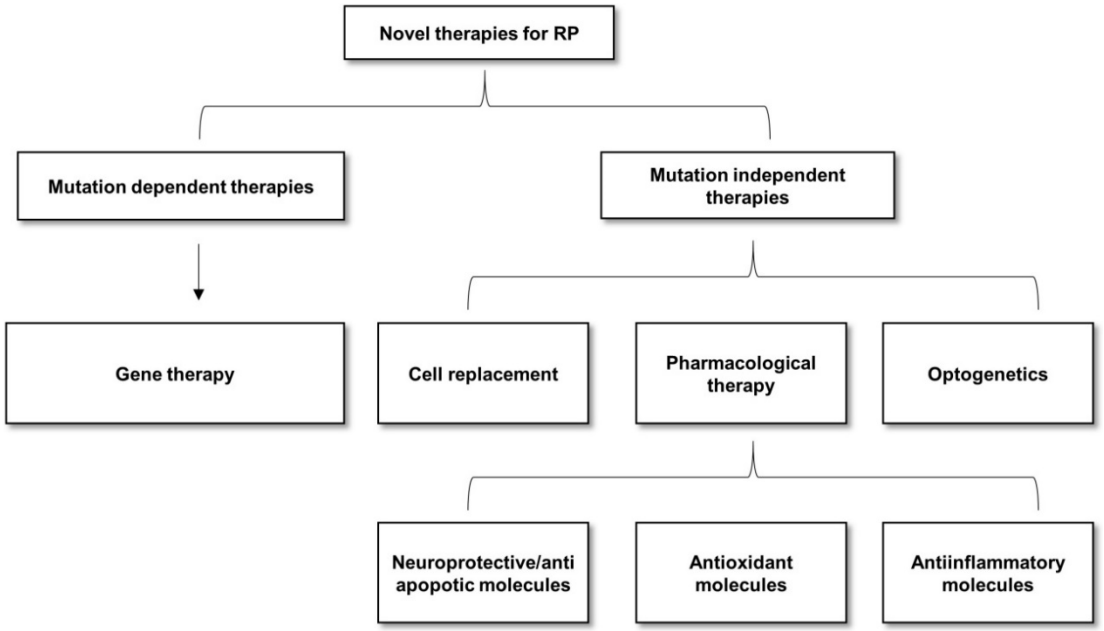

Figure 1.5. Classification of novel therapies for retinitis pigmentosa (RP).

1.5.1. Gene therapy

Due to the genetic origin of RP, gene therapy directed to edit the mutation or supply with the wild-type (WT) copy of the gene could be a definitive curative strategy. Gene therapy in the eye and in the retina has several advantages in comparison with other organs (Trapani and Auricchio, 2019). The eye is easily accessible, allowing the supplementation of the vectors near to the affected tissues. Also, as the eye is a compartmentalized structure, the probability of vector diffusion is low, increasing the safety of the procedure. Moreover, the eye has special immune properties, decreasing the risk of undesirable immune reactions.

In fact, as previously mentioned the most successful gene therapy strategy has been the administration of voretigene neparvovec (Luxturna) to treat retinal dystrophies (RP and Leber congenital amaurosis) produced by mutations in the RPE gene *RP65*. In this case, AAV carrying *RP65* cDNA are injected subretinally in patients. This drug was administered to 40 patients and resulted in an improvement in vision function over 4 years after the administration and was considered safe (Maguire et al., 2019). Those results led to United States Food and Drug Administration (FDA) and European Medicine Agency (EMA) approval as a novel drug, becoming the first approved gene therapy drug. Luxturna is based on gene augmentation, the most assayed gene therapy strategy until the development of CRISPR/Cas9 technology (see below) as reviewed in Diakatou et al. (2019). In this case, the correct version of the mutated cDNA is administered via a specific viral vector. The most commonly employed vectors are adeno-associated viral vectors, AVV. Importantly, an increasing number of clinical trials are ongoing

employing this strategy to treat different retinal dystrophies with mutations in: Mer proto-oncogene tyrosine kinase, *MERTK* (Ghazi et al., 2016), *PDE6A* (NCT02759952), *PDE6B* (NCT03328130), retinitis pigmentosa GTPase regulator, *RPGR* (NCT03316560 and NCT03252847) and retinaldehyde binding protein 1, *RLBP1* (NCT03374657). Given that mutations within the rhodopsin gene are the most frequent cause of RP in patients, gene augmentation has been studied predominantly for this gene in animal models. Increasing the wild-type copies of rhodopsin has been proven effective at delaying disease progression in a dominant mouse model of RP with a mutation within the rhodopsin gene (Mao et al., 2011). Also, gene augmentation approaches have been carried out for mutations in the RP gene peripherin (*Prph2*). In these cases, the administration wild-type cDNA in the form of nanoparticles or alternatively of AAV vectors encoding a functional *Prph2* copy, has been successful at delaying RP progression in mouse models with mutations within *Phrp2* (Cai et al., 2010)(Ali et al., 2000). The administration of wild-type *Mertk* using viral vectors has been also studied with positive results in a rat model with mutations in this gene (Vollrath et al., 2001). Another gene that was studied in animal models of RP is PDE6A. In this regard, AAV carrying canine *Pde6a* were administered to dog model of RP with a naturally-occurring mutation in the gene. Treated animals showed slight improvements in dim light vision (Mowat et al., 2017).

However, in the case of dominant negative mutation or gain-of-function mutations, it is not sufficient to increase the amount of wild-type protein by gene augmentation. In order to obtain better results, the wrong version of the gene should be silenced before gene augmentation or the mutant copy directly replaced by a correct version of the gene. Importantly, this is the case of mutations within the rhodopsin gene, that cause protein misfolding and aberrant glycosylation that lead to protein aggregation and result in cell toxicity (Ferrari et al., 2011). There are several examples of successful gene silencing in animal models of RP. The administration with AAV of Zinc-finger proteins design to silence rhodopsin expression has ameliorated disease progression in a mouse model of dominant RP (Mussolino et al., 2011; Botta et al., 2016). There have been strategies also to knockdown rhodopsin RNA using ribozymes in wild-type mice (Gorbatyuk et al., 2005) or specifically design to target mutated copies that have been assessed *in vitro* (Drenser et al., 1998). Also, RNA interference strategies have been used to this purpose, using short hairpin RNA to target rhodopsin in a dog model of dominant RP (Cideciyan et al., 2018) or anti-sense oligo nucleotides to specifically target the mutated version of rhodopsin in a dominant RP rat model (Murray et al., 2015).

However, the most promising tool in gene therapy strategies is CRISPR/Cas technology. This technology can be used to silence the mutated genes or to directly substitute the mutated gene

for a corrected copy. An example of the former is the approach that Bakondi and colleagues use to treat a dominant rat model of RP. In this case they were able to selectively disrupt the mutated allele of the heterozygous model, without affecting the wild-type copy and resulting in an improvement of retinal function (Bakondi et al., 2016). Also, the gene silencing approach can be combined with gene supplementation. This was done by Tsai and colleagues in different types of rhodopsin-mutant mice. They used two AAV: one with modified CRISPR/Cas to silence the rhodopsin gene and the other to supplement with a wild-type rhodopsin copy. This strategy resulted in a significant preservation of retinal function in treated animals (Tsai et al., 2018).

Although significant advances have been made in gene therapy for retinal diseases, there are still many drawbacks. First, gene therapy is only applicable at very early stages of the disease when preservation of photoreceptors is still high. This makes gene therapy not suitable for patients that have a late diagnosis of the disease or for dystrophies with very fast progression. Second, it is still not clear how long the gene therapy effect will last. Recent studies suggest that gene therapy does not "last forever" (Aguirre, 2017). Third, gene therapy strategies are mutation or gene specific what hinders its general applicability and increases dramatically the cost of the treatment. The cost of Luxturna is about $425,000 per eye. As mentioned above, another limitation for gene therapy is the treatment of dominant mutations. In addition there are technical aspects that need to be considered: i) the expression of the transgene should be finely tuned to achieve sufficient levels of the wild-type protein but avoiding toxic effects of excessive expression (Price et al., 2012); ii) the limited cargo capacity of the AAV that hinders the delivery of transgenes larger than 4.7 kb (Schon et al., 2015); iii) the immunogenicity of the viral vectors and of the administered proteins of bacterial origin like Cas (Trapani and Auricchio, 2019).

1.5.2. Cell replacement therapy

This approach is based on the functional substitution of dead photoreceptors by healthy exogenous ones. Although this technique is very attractive, the origin of the incorporated cells is still not solved. In the first clinical trials, retinal sheets were obtained from post-mortem adult human eyes (Kaplan et al., 1997) or from human fetuses (Radtke et al., 1999; Radtke et al., 2008) and transplanted to patients of various retinal diseases, including advanced RP. In those clinical trials, the number of transplant rejections was very low and in some case retinal sheets of fetal origin resulted in some extend of vision improvement (Radtke et al., 1999; Radtke et al., 2004; Radtke et al., 2008). Although, retinal sheet transplant has produced some benefits in patients with RP. Those studies revealed that the morphology and orientation of the graft is critical for success. Moreover, in some cases, the retinal graft leaded to a formation of a double retina and

consequently to synaptic defects. Other source of exogenous photoreceptors is retinal progenitor cells. Clinical trials injecting retinal progenitor cells obtained from human fetuses in the vitreous of RP patients have shown safety in phase I (jCell, NCT02320812). The efficacy of the procedure is currently being assessed in a phase II study (NCT03073733). Even in the case that these clinical trials show promising results, the scarcity of material to be transplanted limits the number of patients that could benefit from these techniques.

Good results have been obtained in preclinical studies with young post-mitotic photoreceptors directly obtained from early-postnatal retinas and transplanted as cell suspensions in retinas of different RP mouse models (MacLaren et al., 2006). This approach led to an increase of visual function. However, in humans, post-mitotic photoreceptors are formed during the second trimester of pregnancy, what raises ethical and legal concerns.

Therefore, a translational option would be the administration of photoreceptors derived from embryonic stem cells (ESCs) or ideally from induced pluripotent stem cells (iPSCs) that do not raise ethical concerns, however iPSCs generated from patients carrying a mutation would need gene therapy to supply the wild type copy or to correct the mutation by gene editing techniques. ESCs and iPSCs have been successfully differentiated to photoreceptors, although with very low efficiency, less than 20% of the cells end up differentiating into photoreceptors (Osakada et al., 2008; Hirami et al., 2009). Another subject of broad interest is the developing of retinal organoids from both ESCs and iPSCs in order to obtain higher numbers of photoreceptors. The research team of Sasai and colleagues reported for the first time, the formation of an 3D organoid retina from human ESCs (Nakano et al., 2012).

Even though these approaches are very attractive, there are several concerns to be solved before a genuine applicability. First, the incorporation of novel photoreceptors to the retinal neuronal circuits has been questioned since it has been shown that many of the transplanted photoreceptors fuse their cytoplasm with photoreceptors of the recipient retina (Singh et al., 2014; Ortin-Martinez et al., 2017). Also, immunological safety of the exogenous cell transplant is still being studied (Gasparini et al., 2019). Other roadblocks that should be overcome are the low efficiency of the cell transplant and the high cost of these therapies.

1.5.3. Optogenetics

Optogenetics is the genetic photosensitization of neuronal tissues. To this purpose, neurons are transduced by a viral vector that expresses a light sensitive protein, commonly a light-sensitive ion channel (Sahel and Roska, 2013). Currently there are several investigations to

generate novel photosensitive cells in the RP retinas to overcome the lack of photoreceptors. In this context, the most studied molecules are channelrhodopsins (ChRs), a family of algal opsins that have rhodopsin-like functions. *ChR2* has been administer using AVV technology to retinal cells in different RP mouse models, resulting in an increase of retinal function (Lagali et al., 2008; Doroudchi et al., 2011). Different strategies have been assayed to transduce retinal cells (from viral vectors to electroporation) as well as different target cells, including bipolar, ganglion or all retinal cells as reviewed in Simunovic et al. (2019). Interestingly, clinical trials are being carried out administering channelrhodopsin genes to RP patients (RST-001, NCT02556736; GS030, NCT03326336).

Another protein employed to photosensitize retinal neurons in preclinical models is melanopsin. This light sensitive protein, physiologically present in a subtype of retinal ganglion cells, has been transduced in all ganglion cells, resulting in a partial restoration of vision in a *Pde6b* mutant mouse model (Lin et al., 2008).

Optogenetics is a relatively novel technique that provides hope for patients with advanced RP, in which gene therapy or neuroprotective therapies are not feasible. However, some factors such as the type of vectors and promoters used, the target cell type for transduction or the photosensitive molecule to be expressed are still under debate. Therefore, optogenetics will not provide at least in the short-term the adaptive vision that photoreceptors offer.

1.5.4. Pharmacological therapy of RP

Another area of broad investigation interest is the pharmacological treatment of RP. In this approach, the objective is to delay the progression of the disease rather than providing a definitive cure, increasing the time of functional vision of the patient. It is important to take into account that a small preservation of rod cell number can result in a much greater preservation of cones, resulting in a significant delay of vision loss (Guadagni et al., 2015). Also, considering that RP is a genetically heterogeneous disease, drugs that target common RP processes are desirable. Most of the drugs that are being currently studied for RP treatment are neuroprotective, antiapoptotic, antioxidative or antiinflamatory molecules. An important factor to take into account to treat RP is the presence of the blood-retinal barrier that acts as a filter and may difficult the penetrance of our drug of interest to the retina.

1.5.4.1. Neuroprotective and antiapoptotic drugs

Neurotrophic factors are released in the retina mainly by RPE and Müller glia cells. Exogenous supply of neurotrophic factors is one of the most studied approaches to promote photoreceptor

survival. Some of these neurotrophic factors have been demonstrated to delay retinal degeneration in RP animal models, however their performance in RP patients is still under study.

The pioneer study by LaVail and colleagues first described that intravitreal administration of basic fibroblast growth factor (bFGF) resulted in a delayed retinal degeneration in a rat animal model with a mutation within a RPE-specific gene (Faktorovich et al., 1990). Likewise, the treatment of a rat model of RP with AAV carrying the bFGF gene resulted in a decrease of photoreceptor cell death and in a preservation of retinal function (Lau et al., 2000).

Similarly, the intravitreal administration of nerve growth factor (NGF) resulted in photoreceptor preservation in a RP mouse model (Lambiase and Aloe, 1996). Moreover, NGF has been assayed in clinical trials in RP patients. In a pilot study, the administration of eye-drops with NGF was demonstrated to be safe and resulted in a mild subjective vision improvement in a subset of patients (Falsini et al., 2016), however there is not yet available complete information about its efficacy in the ongoing clinical trials (NCT02110225).

Ciliary neurotrophic factor (CNTF) has been shown to be protective in different animal models of RP (Cayouette and Gravel, 1997; Cayouette et al., 1998; LaVail et al., 1998). In clinical trials to allow stable release of the molecule, CNTF has been administrated in the form of cell implants (trade name NT-501) that were surgically placed in vitreous to allow for continuous release of the molecule. Although this approach showed safety (Sieving et al., 2006), it failed to produce significant therapeutic benefit even though, in some cases, it resulted in a delay of photoreceptor cell loss (Birch et al., 2013; Zein et al., 2014).

Also, glial-cell derived neurotrophic factor (GDNF) has received considerable attention in RP preclinical studies. Subretinal administration of GDNF delayed the electroretinographic response loss in a RP animal model (Frasson et al., 1999). To provide a continuous administration of GDNF, different approaches have been employed in posterior studies with RP animal models. Both, the administration of the GDNF by gene therapy with AAV (McGee Sanftner et al., 2001) or by poly lactic-*co*-glycolic acid (PLGA) microspheres carrying encapsulated GDNF (Andrieu-Soler et al., 2005) resulted in a delay of vision loss. Protective results were also obtained when RP animal models were treated with GDNF-mimetic small molecules (Saragovi et al., 2014).

Another molecule that has received considerable attention is rod-derived cone viability factor (RdCVF). This molecule is secreted by rods to promote cone survival under physiological conditions. Primary loss of rods in RP and the consequent decrease of RdCVF availability have been postulated as, at least one of the reasons for the death of cones. Therefore, it has been

proposed that the exogenous administration of RdCVF to RP retinas would decrease cone cell death (Leveillard et al., 2004). Indeed, the same group demonstrated that subretinal administration of RdCVF resulted in a preservation of retinal function in a rat model of RP (Yang et al., 2009).

Pigment epithelium-derived factor (PEDF) is a neurotrophic factor produced by the cells of the RPE in physiological condition and has also provided benefit in animal models of RP (Cayouette et al., 1999; Hernandez-Pinto et al., 2019). However, clinical trials with PEDF in RP patients have not been initiated yet.

Besides neurotrophic factors, other molecules have been demonstrated to confer neuroprotection in the retina. Valproic acid (VPA) is a histone deacetylase inhibitor approved for the treatment of epilepsy, bipolar disorder and migraine that has also intensively studied for the treatment of RP with controversial outcomes (Guadagni et al., 2015). In a first report, considerable clinical benefit was obtained in patients treated with VPA (Clemson et al., 2011). However, later studies failed to reproduce this positive effect, and even a negative effect for some patients was reported (Sisk, 2012; Bhalla et al., 2013). Differences in the underlying mutations may account for paradoxical effects of VPA in patients as it has been shown in animal models (Vent-Schmidt et al., 2017).

Another promising molecule is the synthetic progesterone analogue, Norgestrel. This molecule is FDA-approved for its use in oral contraceptives and has shown to reduce photoreceptor cell death in animal models of RP (Doonan et al., 2011; Roche et al., 2019). However, no clinical trials in RP patients have been started yet.

As a common mechanism of all RP types is photoreceptor cell death, considerable effort has been made to develop drugs that target the death pathways. Nevertheless, this is hindered by the fragmentary picture that we have of the different executive pathways underlying RP (Doonan et al., 2005; Sahni et al., 2011). Nevertheless, several molecules have been shown to interfere with photoreceptor death. Tauroursodeoxycholic acid (TUDCA), a component of bear bile used in traditional Chinese medicine to treat blindness, decreased photoreceptor death and improved retinal function in RP animal models (Boatright et al., 2006; Phillips et al., 2008; Drack et al., 2012). In addition, Rasagiline, an anti-Parkinsonian drug can preserve photoreceptor cells and retinal function in animal models (Eigeldinger-Berthou et al., 2012; Garcia-Delgado et al., 2018). Likewise, myriocin, a pharmacological inhibitor of the biosynthesis of the death effector ceramide, preserved retinal structure and function in animal RP model (Strettoi et al., 2010; Piano et al., 2013).

1.5.4.2. Antioxidant molecules

Oxidative stress has been postulated, together with the aforementioned decreased RdCVF levels, as one of the causes of cone death upon rod loss (Komeima et al., 2006). The absence of rods gives rise to a hyperoxic environment toxic for cones (Yu et al., 2004), therefore strategies to diminish the oxidative stress have been assayed. As a proof of principle, AAV carrying antioxidant genes, like catalase, superoxide dismutase (Usui et al., 2009) and glutathione peroxidase (Lu et al., 2009), have been administered to RP animal models, resulting in a reduction of cone cell death. Also, some anti-oxidant dietary supplements like curcumin, saffron, lutein or N-acetyl-cysteine have been reported to be protective in RP (Cuenca et al., 2014). However, both the presence of the blood-retinal barrier and the soluble nature of some of these molecules, limit their retinal accessibility and decrease their efficacy (Guadagni et al., 2015). One solution could be the administration of a cocktail of antioxidant molecules. In this direction, a cocktail containing α-tocopherol, ascorbic acid, α-lipoic acid and MnTBAP could slow photoreceptor death and improve retinal function in RP mouse models (Komeima et al., 2006; Komeima et al., 2007). In addition, the unoprostone, employed in the treatment of glaucoma to lower intraocular pressure, has antioxidant properties (Tsuruma et al., 2011), and RP clinical trials with unoprostone reported some positive effects in (Yamamoto et al., 2012; Akiyama et al., 2014), although they did not reach statistical significance in phase III clinical trial (NCT01786395).

1.5.4.3. Antiinflammatory molecules

In RP, photoreceptor cell death has been associated temporary and spatially to an inflammatory condition (Silverman and Wong, 2018). First, in homeostatic conditions, microglial cell bodies are located in the retinal plexiform layers and are in charge of immune surveillance. They display a ramified morphology and have low levels of phagocytic activity. In animal models of RP it is well-stablished that microglia migrate towards the ONL (Roque et al., 1996; Zeiss and Johnson, 2004; Karlstetter et al., 2015). There, microglia show an ameboid morphology and have cytoplasmic inclusions that contain rhodopsin (Zhao et al., 2015).

In patients, the first report that involved inflammation in photoreceptor cell death, was the discovery that microglia accumulate in the areas of the ONL with active rod cell death (Gupta et al., 2003). Now, it is well stablished that there is a chronic inflammatory process in RP patients, that courses with an increase of proinflammatory cytokines and chemokines (Yoshida et al., 2013a). The same study found out that increased number of inflammatory cells in the vitreous cavity correlated with lower visual function.

Studies in RP animal models showed that retinal degeneration courses with increased production of proinflammatory cytokines (TNF-α and IL-1β) (Yoshida et al., 2013b) and chemokines (CCL-2, CCL-3 or CCL-7) (Zeng et al., 2005) that are described to be produced by microglia, but also by Müller glia and astrocytes (Vecino et al., 2016; Galan et al., 2017). The general consensus is that the exacerbated inflammatory process aggravates photoreceptor cell death and therefore it accelerates disease progression (Silverman and Wong, 2018). Remarkably, it has been observed that microglia phagocyte living photoreceptors (Zhao et al., 2015). When RP animal models were treated with anti-inflammatory drugs dexamethasone or fluocinolone acetonide, photoreceptor survival was increased (Glybina et al., 2010; Peng et al., 2014; Guadagni et al., 2019). In the same direction, the administration of clodronate liposomes to RP mice to deplete microglia, results in a moderate reduction in photoreceptor cell death. However, microglia are necessary to mediate IGF-1 protective effects in those animals (Arroba et al., 2011). Also, it has been described that microglia migration to the subretinal space in RP mouse models confers RPE protection (O'Koren et al., 2019). Both factors suggest a dual role of microglia in retinal degeneration.

Interestingly, some of the compounds that were mentioned before as neuroprotective or anti-oxidative drugs, like rasagiline, norgestrel, curcumin or lutein, have also been reported to have an anti-inflammatory activity that could contribute to reduce photoreceptor cell death (Cuenca et al., 2014).

All these data, support the view that inflammation has an active role in the pathogenesis of RP and that the modulation of inflammation should be considered as a potential therapy for RP.

1.6. Insulin receptor as a neuroprotective pathway

The insulin receptor (IR) belongs to the tyrosine kinase receptor family. The functional IR is a homodimer, formed by two monomers bound by a disulfide bond. Each monomer is formed by an α subunit and a β subunit also bound by disulfide bonds (Figure 1.6). The α subunit is extracellular and has the ligand binding domain, while the β subunit has extracellular, transmembrane and intracellular domains. In this intracellular domain resides the kinase activity of the receptor. In addition, there are two IR isoforms that differ in the presence of the 12-residue product of the exon 11, IR-A excludes this exon while IR-B includes it in the α subunit of the molecule.

IR-A can bind insulin, proinsulin (the insulin precursor) and insulin-like growth factor 2 (IGF2), while IR-B only binds insulin (Malaguarnera et al., 2012; Belfiore et al., 2017). In addition, insulin

receptor can form heterodimers with the insulin-like growth factor 1 receptor (IGF1R), when both molecules are co-expressed. This heterodimer can bind with high affinity insulin-like growth factor 1 (IGF1) (Malaguarnera et al., 2012; Belfiore et al., 2017).

As represented in Figure 1.6, upon ligand binding there is a conformational change of the IR that induces its autophosphorylation in tyrosine residues of the cytoplasmic domain of the β subunit. This induces the IR to phosphorylate members of the insulin receptor substrate (IRS) family and of Src homologous and collagen protein (Shc), which lead to the subsequent activation of the mitogen activated protein kinase (MAPK) and phosphoinositide 3-kinase (PI3K) pathways. The activation of these pathways produces respectively increased levels of phosphorylated extracellular signal regulated kinases (ERK) and of phosphorylated protein kinase B (PKB or AKT). The stimulation of PI3K/AKT pathway results in the inhibition of glycogen synthase kinase 3 (GSK-3), which in turn, targets β-catenin to proteasomal degradation. The activation of AKT also leads to the activation of mammalian target of rapamycin (mTOR), that subsequently activates ribosomal protein S6 kinase (S6K). This activation leads to the phosphorylation of ribosomal protein S6 (S6). As shown in figure 1.6, IR activation results in multiple effects that vary depending on the cell type; these effects include increased cell survival, proliferation, augmented protein synthesis, increased energy storage and increased anabolism.

IR has been traditionally studied as a peripheral metabolic regulator, with clear roles in muscle, adipose tissue, pancreas and liver where it regulates glucose homeostasis and promotes anabolism. The brain has been classically studied as an “insulin-insensitive” organ because glucose transport to the brain is mainly insulin-independent (Blázquez et al., 2014). However, IR expression in the brain was reported decades ago (Havrankova et al., 1978; Marks et al., 1990), suggesting a specific role for IR in the nervous system. Since the description that IR is expressed in neurons, an increasing number of CNS non-metabolic functions have been assigned to IR signaling in neurons, including synaptic maintenance and activity (Chiu et al., 2008; Urwyler et al., 2019), stimulation of neurite growth (Recio-Pinto et al., 1984; Choi et al., 2005), modulation of long term potentiation and depression (van der Heide et al., 2005), release and reuptake of neurotransmitters (Sauter et al., 1983) and promotion of neuronal survival (Valenciano et al., 2006). In addition, IR has been proposed to participate in key brain functions such as learning and memory (Zhao et al., 1999; Dou et al., 2005). Therefore, the consideration of the brain as an “insulin-insensitive” organ is being called into question and it is now acknowledged that insulin receptor signaling is associated with neural function and survival (Hamer et al., 2019).

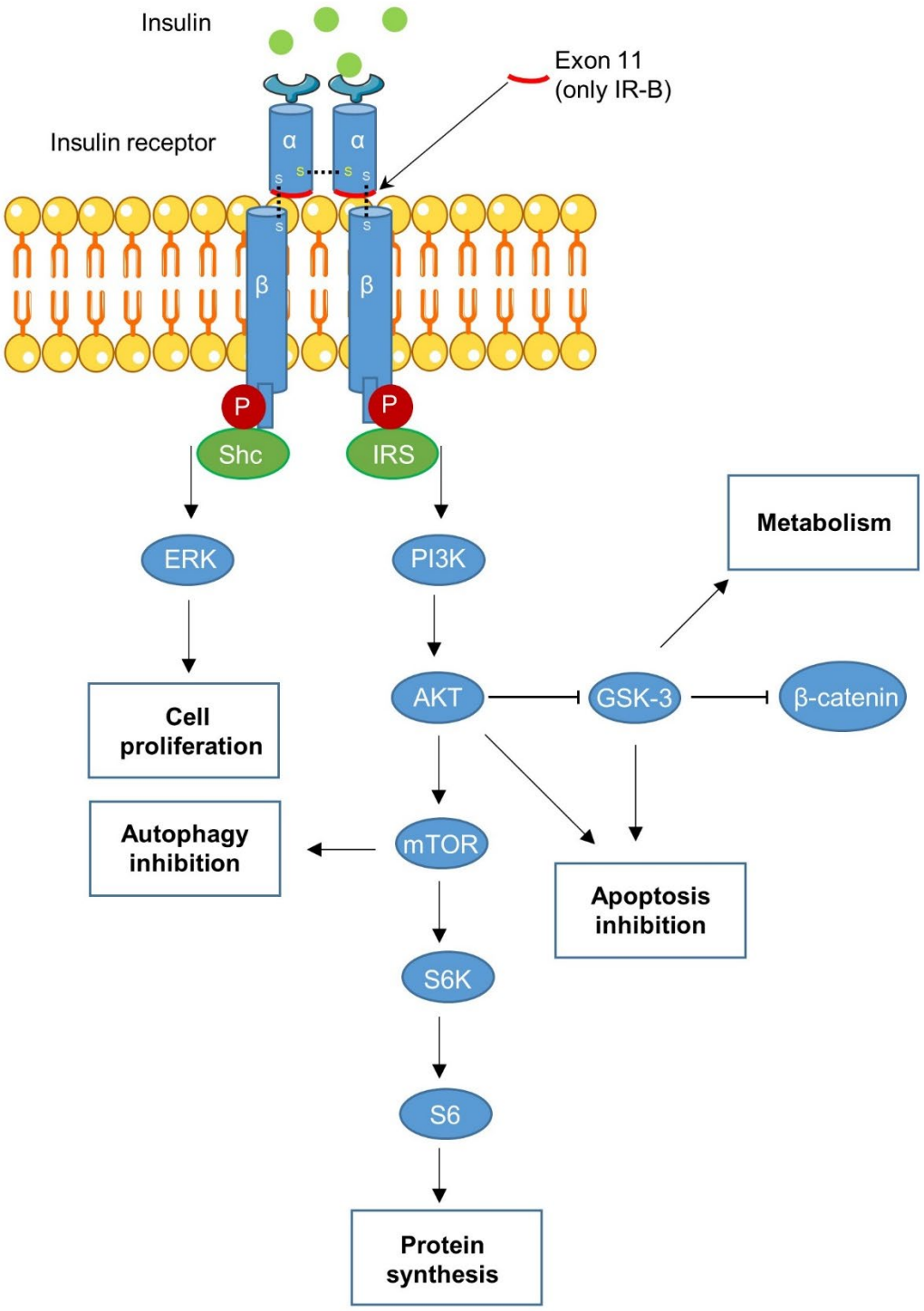

Figure 1.6. Insulin receptor (IR) signaling. IR is a homodimer, formed by two monomers bound by a disulfide bond (dashed lines). Each monomer is formed by an α and a β subunit bound by disulfide bonds. The α subunit has the insulin-binding domain of the receptor. In the isoform B of the receptor (IR-B) the product of the exon 11 is included, but not in the IR-A isoform. The binding of insulin to the α subunit causes the autophosphorylation of the β subunit and the phosphorylation of Src homologous and collagen protein (Shc) and of members of the IRS family. This leads to the activation of the mitogen activated protein kinase/extracellular signal-regulated kinases (MAPK/ERK) and phosphoinositide 3-kinase/protein kinase B (PI3K/AKT) pathways. This results in the activation of mammalian target of rapamycin (mTOR), which activates ribosomal protein S6 kinase (S6K), that phosphorylates the ribosomal protein S6 (S6). The activation of AKT results in the inhibition of glycogen synthase kinase 3 (GSK-3). GSK-3 activity results in the phosphorylation of β-catenin, targeting it to proteasomal degradation. The activation of IR leads to multiple effects that can include cell proliferation, promotion of anabolism, inhibition of apoptosis, increased protein synthesis and inhibition of autophagy.

Moreover, deregulation of IR signaling has been associated to neurodegenerative disorders, in particular to Alzheimer's disease (AD). The first reported links between insulin signaling and dementia came with the discovery that diabetes mellitus patients had memory and cognitive impairments (Perlmuter et al., 1984). In addition, animal models with altered glucose metabolism displayed memory deficits and synaptic abnormalities (Mayer et al., 1990; Ramos-Rodriguez et al., 2013). In addition, it was found that AD human brains showed decreased insulin receptor expression levels and insulin resistance (Steen et al., 2005; Talbot et al., 2012). Along the same lines, amyloid beta (Aβ) oligomers have been reported to directly decrease insulin receptor expression in dendrites in animal models (Zhao et al., 2008). All those data indicate that insulin could be of therapeutic use for AD patients. Indeed, several clinical trials have been carried out administrating intranasally insulin to AD patients, as reviewed in Chapman et al. (2018). Although additional research is needed, many of those studies (Reger et al., 2006; Craft et al., 2012; Craft et al., 2017), but not all (Rosenbloom et al., 2014) showed clinical benefits in insulin-treated patients. However, in patients carrying the ApoE4 allele the results are more controversial (Reger et al., 2008; Claxton et al., 2013).

The influence of IR signaling in neurodegeneration is not constrained to AD, in addition IR signaling deficiency has also been related to Parkinson's disease, PD (Moroo et al., 1994; Athauda and Foltynie, 2016). In a pilot study, intranasal administration of insulin resulted in an increased verbal fluency and motor capacities of the treated patients (Novak et al., 2019), however the study involved only a small number of patients and consequently more studies are necessary to provide consistent evidence of clinical benefits of insulin administration in PD.

The presence of insulin receptor expression in the retina was described decades ago (Rodrigues et al., 1988). IR signaling deficiency has mainly been studied in the context of diabetes. One of the most common complications of diabetes is the damage of the blood vessels that irrigate the retina, leading to development of diabetic retinopathy, a major cause of blindness. Diabetes is also considered a risk factor for the development of glaucoma (Song et al., 2016). Interestingly, exogenous insulin administration could delay cone cell death in a RP animal model and promote ganglion cell regeneration after axonal injury (Punzo et al., 2009; Agostinone et al., 2018). In addition, a few studies have shown local effects of insulin action in the developing retina promoting neuronal proliferation and decreasing cell death (Hernandez-Sanchez et al., 1995; Valenciano et al., 2006). Despite these insulin beneficial effects, systemic metabolic actions of insulin are a limitation to its therapeutic use. Studies of our group have shown that proinsulin, the insulin precursor, is similarly effective promoting neuronal differentiation and decreasing neuronal cell death during retinal development (Hernandez-

Sanchez et al., 1995; Valenciano et al., 2006). Moreover, systemic proinsulin treatment delayed photoreceptor cell death and visual function loss in RP mouse models without significant alteration of glucose homeostasis (Corrochano et al., 2008; Fernandez-Sanchez et al., 2012; Isiegas et al., 2016). The low metabolic profile of proinsulin (Lazarus et al., 1970; Galloway et al., 1992) could be related to its selective binding of IR-A isoform of the receptor, while insulin binds with high affinity both IR-A and IR-B (Malaguarnera et al., 2012). Nevertheless, the state of insulin receptor in the context of RP degeneration as well as the neuroprotective mechanism of action of proinsulin are barely known.

1.7. GSK-3 and neurodegeneration

The enzyme glycogen synthase kinase- 3 (GSK-3) was named for its role in glycogen synthesis, however now it is recognized as a protein with important functions in many cellular processes besides glucose metabolism, including cell growth, survival, differentiation, inflammation and apoptosis. The multifaceted activity of GSK-3 is due to the high number and variety of substrates that can be recognized and phosphorylated by this enzyme. There are more than 100 described and over 500 predicted substrates (Linding et al., 2007; Sutherland, 2011). In addition, GSK-3 has two isoforms: GSK-3α and GSK-3β. Although, GSK-3α and GSK-3β are commonly referred as isoforms, these molecules are not isoforms, but paralogs because they derive from different genes. However, their great sequence similarity has made difficult to design isoform-specific inhibitors, making difficult to unravel the different regulations and functions of both isoforms (Hoeflich et al., 2000). The plethora of GSK-3 actions imply that GSK-3 has to be finely regulated (Beurel et al., 2015). Unlike most kinases, GSK-3 is constitutively active and its regulator pathways –mainly insulin and Wnt signaling– regulate negatively its activity by phosphorylation (in Ser21 in the α isoform and Ser9 in the β). In addition, most GSK-3 substrates need to be previously-phosphorylated (primed) by another kinase, thus the availability of primed substrates is another mechanism to regulate GSK-3 activity.

Since GSK-3 participates in such many cellular processes and regulatory pathways, its deregulation is involved in a great variety of disorders. The potential therapeutic applications of GSK-3 modulators include cancer, cardiovascular diseases, diabetes and inflammatory conditions. However, the implication in GSK-3 in neurodegenerative and psychiatric diseases has attracted more attention.

The observation that GSK-3 could mediate hyper-phosphorylation of tau protein, a key process in the pathogenesis of AD, provided the first evidence implicating GSK-3 in neurodegenerative processes (Hanger et al., 1992). Subsequent studies confirmed that GSK-3

takes part in all the hallmarks of Alzheimer's disease: deposition of amyloid plaques by promoting the cleavage of amyloid precursor protein (APP) into amiloid β peptides, Aβ (Phiel et al., 2003), formation of neurofibrillary tangles by hyper-phosphorylation of Tau (Lovestone et al., 1999) and promotion of apoptosis (Mines et al., 2011).

Lithium has been the standard treatment for patients with bipolar disorder since the 1950s. Lithium inhibits GSK-3 by competing with the Mg^{2+} for its binding site (Klein and Melton, 1996) and this inhibition accounts, at least, for part of the clinical effect of lithium treatment (Freland and Beaulieu, 2012). These observations prompted many research groups to investigate the efficacy of lithium in AD preclinical studies and clinical trials (Eldar-Finkelman and Martinez, 2011). The treatment with lithium enhanced the performance in spatial memory tests of different AD animal models (Ghosal et al., 2009), but only when administered before the onset of the major pathological features of AD (Sudduth et al., 2012). Lithium is considered to have none or small effects on cognition in healthy individuals (Wingo et al., 2009). However, patients with bipolar disorders that are continuously treated with lithium have a decreased rate of dementia (Kessing et al., 2010). Clinical trials of lithium administration in AD patients produced mixed findings: some of them showed beneficial effects (Nunes et al., 2013), while others did not (Hampel et al., 2009). The promising, albeit limited, effects of lithium prompted the search for alternative and more selective GSK-3 inhibitors (Palomo and Martinez, 2017; Palomo et al., 2017). One such compound is tideglusib, which showed safety in clinical trials for AD (del Ser et al., 2013) but only some signs of efficacy in phase II clinical trial (Lovestone et al., 2015).

GSK-3 inhibitors have been assayed for other neurodegenerative diseases. Tideglusib was proven safe in clinical trials for progressive supranuclear palsy (Tolosa et al., 2014) and has shown to reduce the progression of brain atrophy (Hoglinger et al., 2014). Lithium could rescue short-memory deficits in MPTP-induced Parkinson's disease in rats (Castro et al., 2012). In addition, lithium could ameliorate the severity of autoimmune encephalomyelitis (model of multiple sclerosis in animals) (De Sarno et al., 2008), effect that was reproduced with other GSK-3 inhibitors (Beurel et al., 2013).

While many studies have investigated the therapeutic potential of GSK-3 inhibitors in neurodegenerative disorders of the brain, little attention has been paid to the role of GSK-3 in neurodegenerative disorders of another part of the CNS, the retina. However, GSK-3 inhibitors reduced hypoxia, promoting a correct neovascularization in a murine model of diabetic retinopathy (Hoang et al., 2010). Also, in an animal model of glaucoma, the systemic administration of lithium chloride reduced intraocular pressure, the main cause of glaucoma

progression (Sun et al., 2014). Moreover, drugs that showed beneficial effects in glaucoma animal models (forskolin, homotaurine and L-carnositine) were associated with GSK-3 inhibition (Russo et al., 2015). Our group showed that two different GSK-3 inhibitors reduced NMDA-induced ganglion cell death in an *ex vivo* glaucoma model (Marchena et al., 2017). In the context of RP, studies with VPA (described above) that also inhibits GSK-3 both directly and indirectly (Chen et al., 1999; De Sarno et al., 2002), yielded controversial results in clinical trials (Clemson et al., 2011; Iraha et al., 2016; Birch et al., 2018). Recently, our group showed that three different GSK-3 inhibitors (VP3.15, VP3.16 and Tideglusib) decreased *ex vivo* photoreceptor cell death in a mouse model of retinitis pigmentosa (Marchena et al., 2017).

A different aspect of GSK-3 that has aroused interest is its role in retinal regeneration. The WNT-GSK-3 axis participates in zebra fish retinal regeneration, and lithium administration was sufficient to induce that regeneration (Ramachandran et al., 2011). Similarly, downregulation of GSK-3 activity has been used a first step to exogenously induce retinal regeneration in mammals (Yao et al., 2016).

The broad spectrum of potential therapeutic applications of GSK-3 inhibitors is probably due to the intervention of GSK-3 intervention at various cellular levels. It has been reported that inhibition of GSK-3 reduced apoptosis (Beurel and Jope, 2006), decreased inflammation (Jope et al., 2017), modulated axon and dendrite growth and repair (Jiang et al., 2005; Rui et al., 2013) and regulated synaptic plasticity (Bradley et al., 2012). At the same time, the plethora of GSK-3 substrates has raised concerns as to possible undesirable effects caused by its total inhibition. Therefore, modulators of GSK-3 that achieved mild GSK-3 inhibition, but sufficient to recover cellular homeostasis rather than GSK-3 blockers are preferred (Martinez et al., 2013; Palomo et al., 2017).

1.8. Toll-like receptors in neurodegeneration

Toll-like receptors (TLRs) are pattern recognition receptors (PRR) that recognize pathogen associated molecular patterns (PAMPs) or damage associated molecular patterns (DAMPs), triggering the activation of innate immune response. Toll-like receptor family is comprised by 13 proteins in mammals (Kawai and Akira, 2009). TLR1 to TLR9 are conserved between humans and mice, but TLR10 is not functional in mice and TLR11, TLR12 and TLR13 are not present in humans. Consequently, the family of TLRs is comprised of 10 molecules in humans and 12 in mice.

TLRs are formed by a Leucine-rich repeat (LRR) motif that is responsible for the binding of the ligand and therefore is specific of each member of the TLR family, a transmembrane helix

domain and the intracellular Toll/interleukin-1 receptor/resistance protein domain (TIR), responsible for the downstream transduction of the signal (see below). In basal conditions, most of the TLRs are located in the plasma membrane, but TLR3, TLR7, TLR8 and TLR9 are located in intracellular compartments, including endosomes, lysosomes or the endoplasmic reticulum (Figure 1.7).

Each individual TLR-family member recognizes a subset of PAMPs and DAMPs (Table 1.1). PAMPs include bacterial and viral components like bacterial lipopolysaccharides (LPS), flagelin, defensin or viral nucleic acids. DAMPs are cellular molecules released after tissue damage such as heat-shock-proteins (HSPs), high mobility group box 1 protein (HMGB1) and endogenous DNA and RNA. Upon binding of the ligand, TLRs homo- or heterodimerize and trigger different pathways depending on the adaptor protein associated with the TIR domain. The functional significance of heterodimerization is not clear but it has been proposed that heterodimerization may potentiate (TLR1-TLR2) or inhibit signaling (TLR1-TLR4) (Ozinsky et al., 2000; Spitzer et al., 2002).

TLR signaling pathways, which are represented in Figure 1.7, are broadly classified into the MYD88-dependent pathway (myeloid differentiation primary response 88) and the MYD88-independent pathway. All TLRs except TLR3 signal through the MYD88-dependent pathway. In this pathway, the MYD88 adaptor protein in recruited directly or in collaboration with the adaptor protein TIR Domain Containing Adaptor Protein (TIRAP). The activation of this pathway then involves the activation of the IL-1R-associated kinases (IRAKs) and the adaptor molecules TNF receptor-associated factors (TRAFs), which in turn activate MAP kinase kinases (MKKs) and the inhibitor of kappa B kinase (IKK) complex. This result in the activation of the mitogen-activated protein kinases (MAPKs), JUN N-terminal kinase (JNK) and p38 and the nuclear factor kappa light-chain enhancer of activated B-cells (NF-κB) pathway. The activation of JNK and p38 results in the activation of cyclic AMP-response element-binding protein (CREB), activator protein 1 (AP1) pathways. The activation of those pathways results in the production of proinflammatory cytokines. Also in the case of TLRs 7, 8 and 9, the activation of TRAFs and IRAKs leads to the activation of interferon regulatory factors (IRF) and the production of type I interferons (IFN).

MYD88-independent pathway is employed for TLR3 and TLR4 signaling and requires the adaptor molecule TIR-domain-containing adapter-inducing interferon-β (TRIF). In addition to TRIF, TLR4 signaling through TRIF-dependent pathway requires the collaboration of the TRIF-related adaptor molecule (TRAM). The activation of the TRIF dependent pathways results in a

delayed activation of the NF-κB, CREB and AP-1 transcription factors and in the production of type I interferon cytokines. Interestingly, TLR4 is the only TLR that can signal employing all four adaptor molecules.

The binding of PAMPs to TLRs to activate innate immunity has prompted the research of TLR activators as adjuvants in the development of vaccines and has put the focus on TLRs to find novel treatments for sepsis. However, since DAMPs are also ligands of TLRs, targeting TLRs has attracted attention in the context of autoimmune diseases, cancer and inflammatory conditions. In particular, TLRs have been studied in the context of sterile inflammation. Sterile inflammation is defined to the inflammatory response that occurs in the absence of any microorganisms, typically as a result of trauma, ischemia-reperfusion injury or chemically induced injury (Chen and Nuñez, 2010) and it is gaining importance in the pathogenesis of neurodegenerative diseases.

	PAMPS	DAMPS
TLR1	Lipopeptides	
TLR2	Lipoproteins, lipopeptides, peptidoglycanx, zymosan, lipotheichoid acids (LTA)	Heat shock proteins (HSP60, HSP70, HSP Gp96), hyaluronic acid, HMGB1
TLR3	Double-stranded RNA	mRNA
TLR4	LPS	HSP60, HSP70, HSPGp96, hyaluronic acid, HMGB1, heparan sulfate, fibrinogen
TLR5	Flagellin	
TLR6	Diacyl lipopeptides, LTA	
TLR7	Single-stranded RNA	Endogenous RNA
TLR8	Single stranded RNA	Endogenous RNA
TLR9	Unmethylated CpG DNA	Endogenous DNA

Table 1.1. Toll-like receptor ligands. The principal ligands of each Toll-like receptor (TLR), both pathogen associated molecular patterns (PAMPs) and damage associated molecular patterns (DAMPs) are depicted in this table. Adapted from Fadakar et al. (2014).

TLR expression has been described in different cell types of the CNS. Microglia has been reported to express TLRs (Bsibsi et al., 2002; Olson and Miller, 2004). Also expression of TLRs has been observed in neurons (Chakravarty and Herkenham, 2005; Tang et al., 2007), astrocytes (Jou et al., 2006) and oligodendrocytes (Kigerl et al., 2007).

The influence of TLRs (especially TLR2 and TLR4) in the pathogenesis of brain neurodegenerative diseases has been thoroughly studied, although with controversial results in some cases. The presence of TLR4 has been associated with microglia-dependent neurotoxicity in neuronal cultures (Lehnardt et al., 2003). Moreover, it has been reported that *MyD88* deficient mice had decreased β-amyloidosis (Lim et al., 2011). Also, a TLR4 polymorphism that decreased its function was protective against AD (Minoretti et al., 2006). On the other hand, TLR4 has been reported to have a protective function in AD animal models promoting Aβ phagocytosis and clearance (Tahara et al., 2006). In addition, other authors have obtained different results for *MyD88* depletion in the context of AD: it has been reported that animals with decreased expression of *MyD88* have increased levels of soluble Aβ oligomers and accelerated memory deficits (Michaud et al., 2011) and other authors did not observe any difference in AD progression in *MyD88* deficient or heterozygous animals (Weitz et al., 2014). Along the same lines, the administration of the TLR4 agonist LPS decreased the levels of phosphorylated Tau and increased cognitive function in AD mouse models (Qin et al., 2016). These results suggest that the presence of TLR4 may be a double-edged sword owing to its interaction with several adaptor proteins (Leitner et al., 2019). The influence of TLR2 in AD progression has been less studied, but also controversial results have been reported. It has been described that TLR2 participates in Aβ clearance in AD mouse models and that its depletion resulted in an accelerated cognitive decline (Richard et al., 2008). However, other authors reported that the treatment with anti-TLR2 reduced Aβ plaques accumulation and improved spatial learning in AD mouse models (McDonald et al., 2016).

Regarding α-synucleinopathies, it has been reported that TLR4 promotes α-synuclein clearance in animal models and that animals with abnormal α-synuclein expression have increased motor disability if *Tlr4* is depleted (Stefanova et al., 2011). On the contrary it has been described that *Tlr4* depletion reduced α-synuclein accumulation in a PD mouse model (Campolo et al., 2019). The studies of the role of TLR2 in PD are less abundant. TLR2 has been described to be increased in the brains of PD patients (Dzamko et al., 2017). Also, its inhibition in PD animal models with anti-TLR2 antibodies resulted in decreased α-synuclein accumulation and neurodegeneration (Kim et al., 2018).

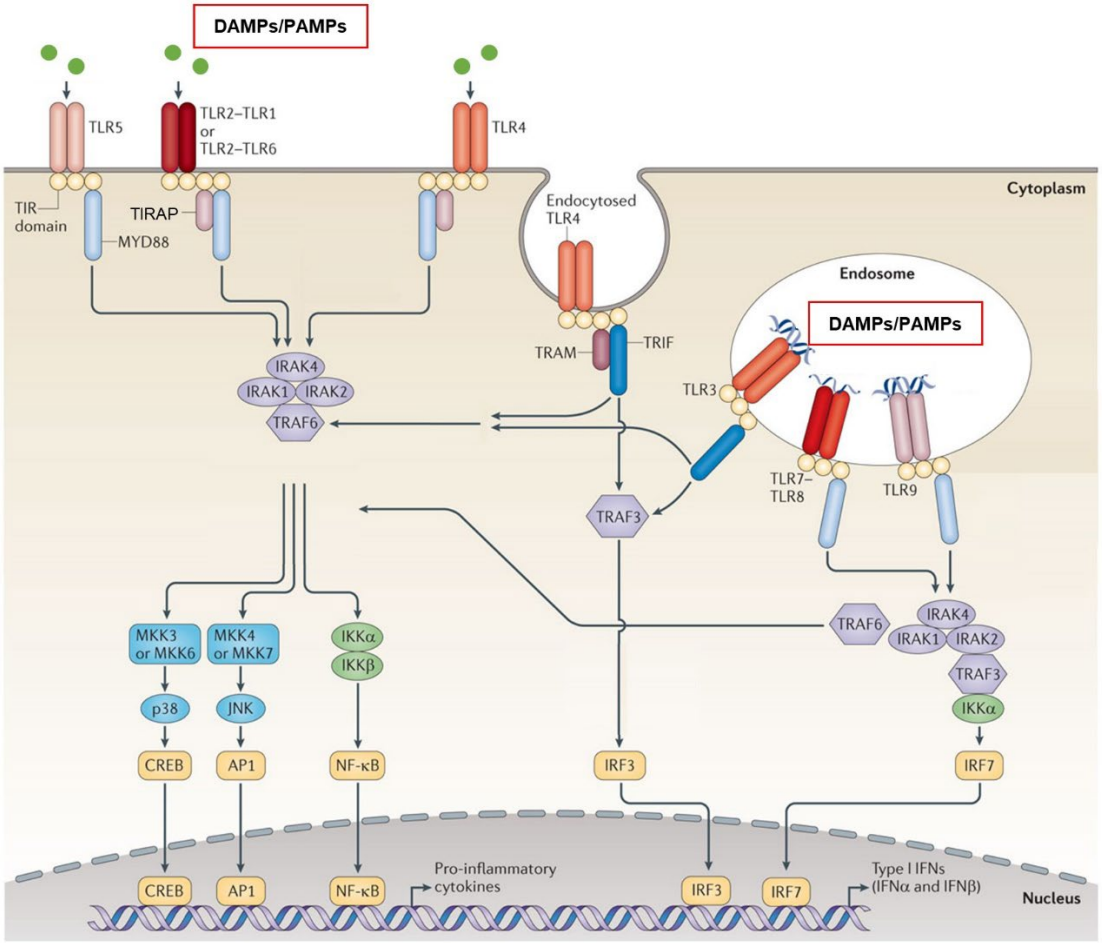

Figure 1.7. Toll-like receptor signaling. Toll like receptors (TLRs) 1, 2, 4, 5 and 6 reside in the plasmatic membrane, while TLRs 3, 7, 8 and 9 are in the endosomal membrane. TLRs can act as homodimers or heterodimers. Upon binding of Pathogen Associated Molecular Patters (PAMPs) or Damage Associated Molecular Patterns (DAMPs) to the different TLRs, the myeloid differentiation primary-response protein 88 (MYD88) (all TLRs but TLR3) or MYD88-indepent pathways (TLR3 and TLR4) are activated. MYD88-dependent pathway also employs the adaptor TIR Domain Containing Adaptor Protein (TIRAP) and TLR4 MYD88-independent signaling also employs the TRIF-related adaptor molecule (TRAM) adaptor. The activation of these pathways involves the activation of the IL-1R-associated kinases (IRAKs) and the adaptor molecules TNF receptor-associated factors (TRAFs) This leads to the subsequent activation of MAP kinase kinases (MKKs) and therefore the mitogen activated protein kinases (MAPKs) JUN N-terminal kinase (JNK) and p38. Also, it leads to the activation of the IκB kinase (IKK) protein complex. The activation of these pathways results in the activation of the transcription factors cyclic AMP-response element-binding protein (CREB), activator protein 1 (AP1), nuclear factor-κB (NF-κB) and the interferon regulatory factors (IRFs). The activation of TLR signaling results in the production of pro-inflammatory cytokines and in the production of type I interferons (IFNs). Adapted from O'Neill et al. (2013).

In experimental stroke, animals deficient for *Tlr4* have decreased infarct volumes and decreased brain inflammation (Cao et al., 2007; Caso et al., 2007). Along the same lines, aptamers that act as TLR4 antagonists reduced infarct volume (Fernández et al., 2018). On the contrary, TLR4 activity has been demonstrated to have a protective role participating in ischemic preconditioning (Tasaki et al., 1997; Rosenzweig et al., 2007; Pradillo et al., 2009). TLR2 deficient mice have also been reported to have decreased brain injury after ischemic stroke (Tang et al., 2007).

The physio-pathological role of TLRs in the retina has been less studied. TLR4 has been proposed to participate in the physiological photoreceptor outer segment phagocytosis by the RPE (Kindzelskii et al., 2004). In pathological conditions, the first report that linked TLRs with retinal neurodegeneration showed that a TLR4 variant was associated with increased susceptibility to age-related macular degeneration (AMD) (Zareparsi et al., 2005). Also, *Tlr4* deletion in an animal model of AMD decreased photoreceptor cell death upon light damage (Kohno et al., 2013). In a mouse model of glaucoma mouse, the absence of TLR4 decreased ganglion cell death (Kilic et al., 2008). In the context of RP, TLRs have not been intensively studied. It has been reported an increased expression of some TLRs in the retinas of canine models of RP (Sudharsan et al., 2017). Moreover, other authors reported that depletion or pharmacological inhibition of MyD88 resulted in decreased photoreceptor cell death and delayed in retinal function loss (Syeda et al., 2015; Garces et al., 2020). Due to the scarcity of studies of TLRs in a retinal context, further studies are necessary to gain more insight into the role of TLRs in retinal dystrophies.

SECTION 2

HYPOTHESES AND OBJECTIVES

2. HYPOTHESES AND OBJECTIVES

Loss of photoreceptor cells and visual functional decline leading to blindness are common signs of RP, a genetically heterogeneous group of inherited retinal dystrophies. This point of no return is preceded by other molecular and cellular alterations, particularly photoreceptor dysfunction and inflammatory response. Remarkably, in many cases, vision is maintained to a certain degree as far as surviving photoreceptor cells are present.

Our **general hypothesis** is that strategies directed to preserve photoreceptor integrity as well as those to interfere with relatively early, common processes that contribute to the retinal damage, could be potential treatments to extent time of visual function in RP patients independently of the causative mutations. Particularly, in this Thesis we hypothesized that potentiating insulin receptor signaling and GSK3 inhibition contribute to maintain photoreceptor integrity and visual function. In addition, we postulate that interference with the early retinal innate immune response has a beneficial effect on the disease progression.

The **global objective** of this Thesis is **to increase the knowledge** of the physiopathological basis of RP by characterizing the neuroprotective role of proinsulin and GSK3 inhibitors, and analyzing the involvement of the innate immune response in the course of the disease. The **specific objectives** of this Thesis are:

1.1 Characterization of the insulin receptor and insulin receptor signaling in the retinas of wild-type (WT) mice and in the model of retinitis pigmentosa *rd10.*

1.2 Assessment of photoreceptor connectivity in the *rd10* model of retinitis pigmentosa.

1.3 Characterization of the effects of human proinsulin administration in *rd10* mice focusing on insulin receptor signaling activation and photoreceptor connectivity.

2.1 Characterization of GSK-3 activity in retinas of WT and *rd10* mice.

2.2 Evaluation of the neuroprotective properties of the GSK-3 inhibitor VP3.15 in the *rd10* model.

3.1 Characterization of Toll-like receptor expression in wild-type and retinitis pigmentosa mouse retinas.

3.2 Evaluation of the deficiency of TLR4 in the course of retinitis pigmentosa degenerative process.

3.3 Evaluation of the deficiency of TLR2 in the course of retinitis pigmentosa degenerative process.

SECTION 3

MATERIALS AND METHODS

3. MATERIALS AND METHODS

3.1. Animals

All animals were in C57BL/6J background or backcrossed for 8-10 generations into C57BL/6J background before using them. The *rd10* (Pang et al., 2008), P23H (Sakami et al., 2011) and *Tlr4* null (Poltorak et al., 1998) mice were obtained from The Jackson Laboratory (Bar Harbor, ME, USA). The *Tlr2*$^{-/-}$ were kindly provided by Dr. M. Fresno (Centro de Biología Molecular Severo Ocho, Madrid, Spain) and were originally generated by Dr. Akira's group (Osaka University, Japan) as explained in Takeuchi et al. (1999).

The *rd10* and P23H RP mouse models carry different mutations and have different hereditary and temporal progression patterns. The *rd10* mice carry a recessive homozygous spontaneous point mutation (Arg 560 for Cys) in the rod-specific phosphodiesterase 6b gene (*Pde6b*$^{rd10/rd10}$). Mutations in *Pde6b* account for 3-4% of all the cases of autosomal recessive RP in humans (Ferrari et al., 2011). The *Pde6b*$^{rd10/rd10}$ mutation causes decreased PDE6 activity that leads to increased cGMP levels and elevated calcium influx to the rods, resulting in rod dysfunction and death (Wang et al., 2018). The loss of the majority of rods in *rd10* mice takes place from post-natal age (P) P18 to P35 (Pang et al., 2008), while cone defects start about P30 (Barhoum et al., 2008). Representative images of retinal sections of WT and *rd10* animals at different time points are shown in Figure 3.1A. Electroretinographic response of the *rd10* mice is null around P50. As explained in section 1.3, RP patients typically start losing night-vision and peripheral vision at adolescence and young adulthood, respectively, and become legally blind by middle-age (Verbakel et al., 2018). Vision loss in *rd10* at P50 would be equivalent to vision loss at puberty in humans (Dutta and Sengupta, 2016), therefore *rd10* is an aggressive model of RP.

The P23H mouse carries a dominant mutation in the rhodopsin gene (substitution of proline at position 23 by histidine) that was generated by a knock-in strategy (Sakami et al., 2011). The mutations in the rhodopsin gene account for 30-40% of all the cases of autosomal dominant RP in patients (Ferrari et al., 2011). The P23H replacement produces misfolding, deficient glycosylation and aggregation of the rhodopsin protein, leading to cell toxicity (Sakami et al., 2011). Rod degeneration takes place in the heterozygous P23H (*Rho*$^{P23H/+}$) from P60 to P270 (Sakami et al., 2011), a much slower pace than that of *rd10* mice and closer to that of RP patients. Representative images of retinal sections of WT and P23H mice at different time points are shown in Figure 3.1B.

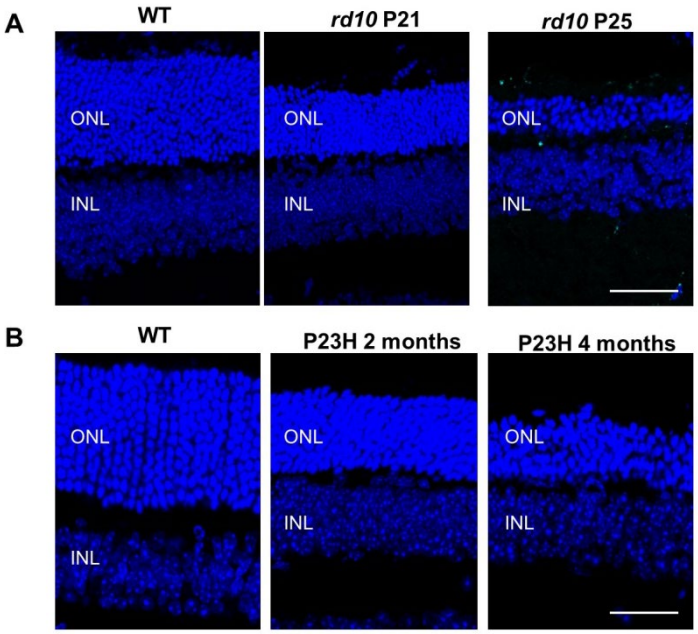

Figure 3.1. A. Representative images of retinal sections of WT (P23) and *rd10* at P21 and P25. **B.** Representative images of WT (2 months) and P23H of 2 and 4 months of age. Nuclei were stained with DAPI. ONL, outer nuclear layer; INL, inner nuclear layer. Scale bar: 90 µm in A and 60 µm in B.

All animals were housed and handled in accordance with the ARVO statement for the Use of Animals in Ophthalmic and Vision Research, European Union guidelines, and those of the local ethics committees of the CSIC and the Comunidad de Madrid. Mice were bred in the Centro de Investigaciones Biológicas Margarita Salas (Madrid, Spain) core facilities on a 12/12-h light/dark cycle. Light intensity was maintained at 3-5 lx.

3.2. N9 cell line

The murine N9 microglial cell line, originally provided by Dr. Paola Ricciardi-Castagnoli (Singapore Immunology Network, Agency for Science, Technology and Research, Singapore), was obtained from Dr. Labandeira-García (University of Santiago de Compostela, Santiago de Compostela, Spain). N9 microglial cells were cultured in DMEM supplemented with 5% (v/v) FBS, 2 mM L-Glutamine, 100 U/ml penicillin, and 100 mg/ml streptomycin, and maintained at 37ºC, 95% air, and 5% CO_2 in a humidified incubator.

3.3. Pharmacological compounds and drug delivery

3.3.1. Human proinsulin administration

For insulin receptor signaling studies, methyonilated human proinsulin (hPi, custom-synthesized by Biotecnol Limited, Batch F148510 2 1-1, Hertfordshire, UK) (Isiegas et al., 2016) was administered intraperitoneally at a dose of 1 µg/g of body weight in saline with 10 mM HCl.

For sustained hPi production a gene therapy strategy was employed. AAV serotype 1 viral vectors bearing the cDNA from the human proinsulin (hPi) gene under control of the

cytomegalovirus promoter (AAV-hPi) or without hPi cDNA (AAV-null) were generated in the Center of Animal Biotechnology and Gene Therapy at the Universitat Autònoma de Barcelona (Barcelona, Spain) as previously described Corpas et al. (2017). *rd10* mice received a single intramuscular injection at a dose of 0.72 x 10^9 vector genomes/g of body weight of AAV-hPi or control (AAV-null) at P10-12. The total dose of vectors was distributed equally between the gastrocnemius muscles of both hind limbs. AAV vectors were chosen because they are non-replicative, show a good safety profile and because after intramuscular injection most of the vector remains in the injected muscle (Callejas et al., 2013; Corpas et al., 2017).

3.3.2. VP3.15 administration

VP3.15 was synthesized in Dr. A. Martínez laboratory (Centro de Investigaciones Biológicas Margarita Salas, Madrid, Spain) as previously described (Palomo et al., 2012). This small molecule is a member of the iminothiadiazole family, the first group of substrate-competitive GSK-3 inhibitors described. The dose administrated had been previously selected based on pharmacokinetic and IC_{50} data (0.88 µM for GSK-3 recombinant protein as assessed by the kinase luminometric assay decribed in Baki et al.,) and on previous functional studies (Medina-Rodríguez et al., 2017). Mice received daily intraperitoneal injections (100 µL each day) of vehicle (10% DMSO, 0.9% NaCl) or VP3.15 dissolved in vehicle (10 mg/kg of body weight) for the indicated period of time. Intraperitoneal injection was selected based on the ability of VP3.15 to cross the brain blood barrier (Medina-Rodríguez et al., 2017) and the necessity of performing repetitive administration without damaging the eye. VP3.15 has a good safety profile in regard to genotoxicity or mutagenic potential (Ames test) (Redondo *et al*., 2012). Animals treated with VP3.15 did not show any sign of distress and their body weights were similar to those of the control mice along the treatment (up to 1 month). The chemical structure of the compound is shown in Figure 3.2.

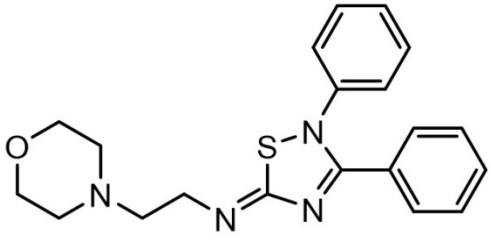

VP3.15

Figure 3.2. Chemical structure of VP3.15

3.4. Retinal organotypic cultures

Mice were euthanized, and their eyes were enucleated. Retinas were dissected and cultured free-floating in M24 multiwell plates for 16 h in 1 ml of the complex R16 medium (Marchena et al., 2017). Retinas were subsequently processed for immunoblots as described below.

3.5. Measurement of proinsulin levels

Human proinsulin levels were measured with the Proinsulin ELISA kit (EZHPI-15K, Millipore, Darmstadt, Germany) according to the manufacturer's instructions and as previously described (Isiegas et al., 2016). Briefly, mouse blood was obtained from the mouse submandibular vein and was left at room temperature for 30 minutes to let it clot. The clotted blood was centrifuged at 2,500 g at 4°C for 15 minutes. The supernatant was used for hPi ELISA determination. Samples with gross hemolysis were discarded.

3.6. RNA isolation and RT-PCR

Total RNA from tissues was isolated using Trizol reagent (Invitrogen,Waltham, MA, USA). Extracted RNA was quantified employing Nanodrop 1000 spectrophotomer (ThermoFischer Scientific) and its integrity was checked by electrophoresis (0.8% agarose in RNAse free water). Before reverse transcription (RT) possible contaminating DNA was eliminated with DNAse I (ThermoFischer Scientific). The RT was typically performed with 1 µg RNA and with the Superscript III Kit and random primers (all from ThermoFisher Scientific). Quantitative PCR (qPCR) was performed with the ABI Prism 7900HT Sequence Detection System using TaqMan Universal PCR Master Mix, no-AmpErase UNG, and Taqman assays (listed below) for detection (all from Thermo Fisher). The relative change in gene expression was calculated using the ΔCt method, normalizing to expression levels of the *Tbp* (TATA-binding protein) gene. The primer-probe sets used are listed in Table 3.1.

Gene	Taqman assay	Gene	Taqman assay	Gene	Taqman assay
A2m	Mm00558642_m1	*MyD88*	Mm00440338_m1	*Tlr4*	Mm00445273_m1
Ccl3	Mm00441259_g1	*Tbp*	Mm00446971_m1	*Tlr5*	Mm00546288_s1
Cd68	Mm03047343_m1	*Ticam1*	Mm00844508_s1	*Tlr6*	Mm02529782_s1
Gsk-3β	Mm00444911_m1	*Ticam2*	Mm01260003_m1	*Tlr7*	Mm00446590_m1
Iba1	Mm00479862_g1	*Tirap*	Mm00446502_m1	*Tlr8*	Mm04209873_m1
Il1b	Mm00434228_m1	*Tlr1*	Mm00446095_m1	*Tlr9*	Mm00446193_m1
Ins2	Mm00731595_gH	*Tlr2*	Mm00442346_m1	*Tnf*	Mm00443258_m1
Insr	Mm01211875_m1	*Tlr3*	Mm01207404_m1		

Table 3.1. TaqMan assays used in this thesis.

3.7. Western blot

Individual retinas were sonicated in RIPA lysis buffer pH 7.4 (containing 150 mM NaCl, 5 mM EDTA, 1mM EGTA, 0.25% sodium deoxycholate, 0.5% SDS, 1% NP40, 2 mM Na_3VO_4, 10 mM NaF, 4 mM $Na_4P_2O_7$, 10% glycerol, 2mM protease inhibitor Pefabloc (which was included for better sample preservation, catalog number 11429868001, Roche, Basel, Switzerland) and 1X protease inhibitor cocktail, catalog number 11836170001, Roche). After 30 min of incubation on ice, the lysates were centrifuged (12,000 x *g* 15 min) and the supernatant was collected. Protein concentration was quantified with Pierce BCA protein assay kit (23225, Thermo Scientific). Proteins (30 µg) from each sample were fractionated by electrophoresis on precast 10–12% (w/v) SDS-polyacrylamide gels (Criterion TGX, Bio-Rad, Munich, Germany), and then transferred to PVDF membranes using the Trans-Blot Turbo system (Bio-Rad). Blots were incubated overnight at 4 °C with primary antibodies (Table 3.2) diluted in TBS (Tris-buffered saline) containing 1% (w/v) Triton-X100, followed by incubation with the appropriate peroxidase-conjugated secondary antibody during 2 hours at room temperature (Table 3.2). To assess the levels of $pAKT^{Ser473}$, $pERK^{Thr202/Tyr204}$ or $pGSK\text{-}3\beta^{Ser9}$ blots were subjected to stripping followed by reprobing for total AKT, ERK and GSK-3β respectively. For IR, recoverin, GSK-3β, β-catenin and $pNF\text{-}\kappa B^{Ser536}$ the membranes were stripped and reblotted for GAPDH. Immunoreactive proteins were visualized using the Pierce® ECL Western Blotting Substrate (ThermoFisher Scientific), and quantified using ChemiDoc™ Touch Imaging System (Bio-Rad). Densitometric analysis was done with Fiji (ImageJ) software. The samples to compare were always immunoreacted in the same blot.

Specificity	Host species	Dilution	Manufacturer	Catalog number
AKT	Rabbit	1:1000	Cell Signaling Technology (Danvers, MA, USA)	9272
$pAKT^{Ser473}$	Rabbit	1:1000	Cell Signaling	9271L
β-catenin	Mouse	1:1000	BD Biosciences	610153
ERK	Rabbit	1:2000	Cell Signaling	9102
$pERK^{Thr202/Tyr204}$	Rabbit	1:1000	Cell Signaling	9101S
GAPDH	Mouse	1:5000	Abcam (Cambridge, UK)	AB8245
GSK-3β	Mouse	1:1000	Cell Signaling	9832S
$pGSK\text{-}3\beta^{Ser9}$	Rabbit	1:1000	Cell Signaling	9323S
Insulin receptor (IR)	Rabbit	1:1000	Santa Cruz (Santa Cruz, CA, USA)	C19; SC-711
Recoverin	Rabbit	1:5000	Millipore (Burlington, MA, USA)	AB5585
$pNF\text{-}\kappa B^{Ser536}$	Rabbit	1:500	Cell Signaling	3033

Table 3.2. Antibodies used for Western blot in this thesis.

3.8. Immunofluorescence and image capture

Animals were euthanized, their eyes were enucleated, fixated for 50 minutes in freshly prepared 4% paraformaldehyde (PFA) in Sörensen's phosphate buffer (SPB) (0.1M, pH 7.4) and then processed for either retinal sectioning or whole-mount immunostaining.

For the immunostaining of retinal sections, eyes were cryoprotected by incubation in increasing concentrations of sucrose (final concentration 50% in SPB) and stored at -80ºC until further use. Before sectioning, eyes were embedded in Tissue-Tek Optimal Cutting Temperature compound (Sakura Finetec, Torrance, CA, USA), and snap-frozen in dry-ice cold isopenthane. Cryostat (CM3050S, Leica Microsystems, Wetzlar, Germany) eye equatorial sections (12 µm) were obtained and mounted on Superfrost Plus slides (ThermoFisher Scientific). Sections were dried at room temperature and stored at -20ºC until the day of the assay. Then, retinal sections were rinsed with phosphate-buffered saline (PBS, pH 7.4) and permeated with 0.2% (w/v) Triton X-100 in PBS. Next, sections were incubated with blocking buffer (5% normal goat serum, 1% Tween-20, 1M glycine in PBS) for 1 h at room temperature, followed by incubation with primary antibodies (Table 3.3) diluted in the blocking buffer overnight at 4ºC. Then, sections were rinsed with PBS and incubated with DAPI (4´,6-diamidino-2-phenylindole; 1 µg/mL; Sigma-Aldrich Corp., St. Louis, MO, USA) and the appropriate secondary antibodies during 2 hours at room temperature: mouse-Igs and rabbit-Igs that were Alexa 488-568-647 labeled (A-11001, A-11004, A-11008, A-11011, A-21235, ThermoFisher Scientific), goat-Igs that were Alexa 568-labeled (A11057, Invitrogen) and rat-Igs that were Alexa 568-labeled (A11011, Invitrogen). Finally, sections were rinsed with PBS, mounted with Fluoromount-G (ThermoFisher Scientific) and coverslipped. For GluA2 and mGluR6 immunostaining, antigen retrieval step prior to incubation in blocking buffer was performed. Thus, sections were incubated in citrate buffer (10 mM sodium citrate, 0.05% Tween-20 pH 6.0) in boiling water for 10 minutes. After cooling to room temperature, sections were rinsed with PBS and then incubated in freshly prepared 0.2% sodium borohydride in PBS before continuing with the blocking reaction described above.

For the whole-mount immunostaining, retinas were carefully dissected after eye fixation and incubated with the primary antibody in PBS containing 1% Triton-X100 during three days at 4ºC, then rinsed with PBS containing 0.05% Tween-20 and incubated with the secondary antibody in PBS containing 1% Triton-X100 for three additional days at 4ºC. After that, the retinas were rinsed with PBS containing 0.05% Tween-20 and incubated with DAPI (1 µg/mL) at room temperature during 30 minutes. In order to flat-mount the retinas, four opposite cuts were

made in the retina as shown in Figure 3.3 and then mounted with Fluoromount-G between two coverslips.

Retinal sections or explants incubated in the absence of primary antibody were used as negative controls.

Specificity	Host species	Dilution	Manufacturer	Catalog number
pAKT^{Ser473}	Rabbit	1:100	Cell Signaling Technology	4060
Calbindin	Mouse	1:500	Sigma (St. Louis, MO, USA)	C9848
CD68	Rat	1:200	Biorad	MCA1957
CtBP2	Mouse	1:300	BD Biosciences (San Jose, CA, USA)	612044
GluA2	Mouse	1:300	Neuromab (Davis, CA, USA)	75-002
GSK-3β	Mouse	1:400	Cell Signaling	9832S
pGSK-3β^{Ser9}	Mouse	1:100	Cell Signaling	9323S
Iba1	Rabbit	1:200	Wako (Neuss, Germany)	019-19741
Insulin receptor (IR)	Rabbit	1:200	Santa Cruz	C19; SC-711
L/M-opsin	Rabbit	1:200	Abcam	AB5405
mGluR6	Rabbit	1:200	Alomone (Jerusalem, Israel)	AGC-026
Neurofilament Medium (NF-M)	Mouse	1:500	Developmental Studies Hybridoma Bank (Iowa City, IA, USA)	DH-3
P2Y12	Rabbit	1:300	AnaSpec (Fremont, CA, USA)	AS-55043A
PKC-α	Mouse	1:500	Abcam	AB11723
pS6$^{Ser240/Ser244}$	Rabbit	1:200	Cell Signaling	5364
RBPMS	Rabbit	1:500	Abcam	AB194213
Ribeye	Rabbit	1:400	Synaptic Systems (Goettingen, Germany)	192103
Rhodopsin	Mouse	1:500	Abcam	AB3267
S-opsin	Goat	1:100	Santa Cruz	SC-14363

Table 3.3. Antibodies used for immunofluorescence in this thesis.

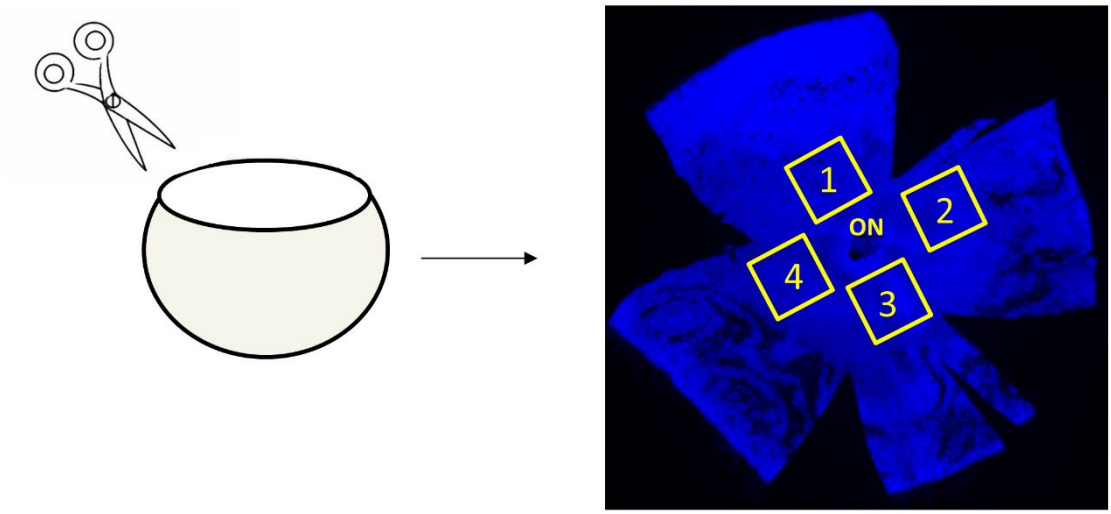

Figure 3.3. Retinal flat-mount. Four cuts were made in the mice retinas as shown in the figure. Image acquisition in flat-mounted retinas was done in four areas adjacent to the optic nerve (ON).

3.9. Image processing and analysis

Retinal sections and whole-mount retinas were analyzed in a laser confocal microscope (TCS SP5 and TCS SP8; Leica Microsystems). Samples to be compared were immunostained and imaged under identical conditions. For whole-mount retinas, four images near the optic nerve were acquired as represented in Figure 3.3. The area of each of the four images is 0.034 mm^2 and the outer segment and the ONL were imaged with a z-section of 1 µm. The number of infiltrating mononuclear monocytes was scored in those areas with the Cell counter plugin of the open source software Fiji (ImageJ).

For histological analysis of retinal sections, three sections per eye were analyzed: for each section, one image was captured for each of the 6 retinal zones (T1, T2, T3, T4, T5, and T6; Figure 3.4). To assess preservation of the photoreceptor layer, we compared the thickness of the ONL (which primarily contains photoreceptors) with that of the corresponding INL (which contains bipolar, horizontal, and amacrine neurons and Müller glial cell bodies). The ONL thickness was normalized to that of the INL, not affected by the degeneration at the analyzed ages (Barhoum et al., 2008; Sakami et al., 2011), to correct for possible inclinations of the sectioning plane. The length of rod and cone outer segments (OS) was evaluated by measuring the length of rhodopsin, L/M cone and S-cone staining. In each image, 3 measurements were recorded at random positions to obtain an average value per retinal zone per section. Measurements were performed using the “freehand line” and “measure” tools in Fiji software.

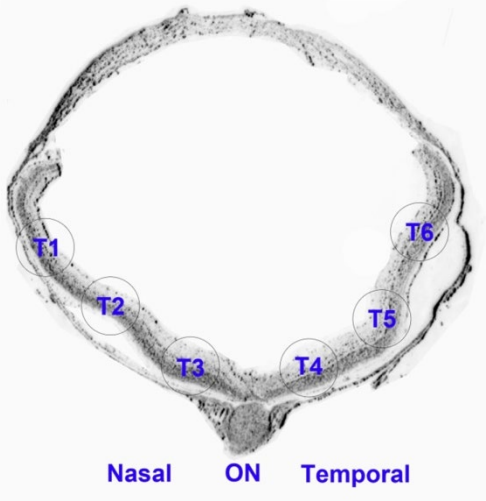

Figure 3.4. Selection of retinal areas for retinal section histology. The 6 retinal zones defined for quantification as T1, T2, T3, T4, T5 and T6 are indicated. ON, optic nerve.

To measure the area occupied by IR and NF-M staining the Fiji software was used. First, images were converted into black and white, then a threshold intensity to separate background from specific signal was selected for all the images and finally the area covered by the signal over that threshold was measured. To quantify the number of horizontal cell tips with associated $pS6^{Ser240/244}$ puncta staining, over 200 horizontal cell tips per animal in 4 areas of the retina were analyzed. Similarly, for synapse quantification, over 200 rod ribbons per animal in 4 areas of the retina were assessed for associated GluA2 (horizontal cell postsynaptic terminal) or mGluR6 (bipolar cell postsynaptic terminal) puncta staining. 3D reconstructions were done with LAS X Life Software (Leica Microsystems).

3.10. Electroretinographic (ERG) recordings

Mice were maintained overnight in dark conditions for dark-adaptation. The next day, electroretinographic responses were recorded employing home-made devices designed by Dr. P. de la Villa (Universidad de Alcala, Madrid, Spain). This device was designed using the amplifier CP511 (Grass Instruments, Quincy, MA, USA). Animals were anesthetized in scotopic conditions with ketamine (Ketolar, Pfizer, New York, NY, 50 mg/kg of body weight) and medetomidine (Domtor, Orion Corporation, Espoo, Finland, 0.3mg/kg of body weight). Their pupils were dilated with a drop of tropicamide (Alcon, Fort Worth, TX, USA). Then, as shown in Figure 3.5, the ground electrode was located parallel to the tail of the animals and the reference electrode was placed in the mouth of the mice. Methocel (Colorcon, Harleysville, PA, USA) was applied to their corneas to avoid eye drying and corneal electrodes were placed in contact with the Methocel. Animals were subjected to increasing light stimuli. For photopic conditions, mice were light-

adapted with an intensity of light of 30-50 cd/m^2 and ERG response to increasing light stimuli was measured.

For WT and *Tlr4*$^{-/-}$ mice the stimuli that were applied in dark-reared mice were: 0.0001, 0.0126, and 8 cd·s/m^2, while in light-adapted mice the applied stimulus was 8 cd·s/m^2. The scotopic threshold response (STR) was evaluated for the lowest stimulus (0.0001 cd·s/m^2). STR measures the response to light stimuli near the minimum rod threshold, it shows the activity of the ganglion cells, reflecting thus the prior response of rods. Then, the a- and b-waves were recorded. These waves are a measurement of the hyperpolarization of the photoreceptors and of the depolarization of the bipolar cells, respectively. When dark-reared mice are stimulated with dim stimuli only rods respond (scotopic waves, 0.0126 cd·s/m^2). However, when the intensity of the stimulus is increased, the response corresponds to both rods and cones (mixed waves, 8 cd·s/m^2). In light-adapted animals, the rod response is bleached and the response is exclusively of cones (photopic waves). In dark-reared mice the oscillatory potential (OP) was measured for a stimulus of 8 cd·s/m^2. The OP is a measurement of the synaptic interactions of bipolar, amacrine and ganglion cells.

For *rd10* mice the light stimuli in dark-adapted animals were: 0.1, 1, 10 and 50 cd·s/m^2, and in light-adapted animals were 1, 10 and 50 cd·s/m^2. P23H mice were subjected to stimuli of 0.001, 0.01, 0.1, 1, 10 and 50 cd·s/m^2 in dark-adapted animals and 0.1, 1 and 10 cd·s/m^2 in light-adapted animals. In *rd10* animals, the applied stimuli are high enough to stimulate rods and cones, therefore the a- and b-was are considered mixed responses. The cone response in light-adapted animals was recorded for the three previously-mentioned stimuli for each model.

For light-adapted animals from all strains the flicker response was measured. The flicker is the cone response to a flickering (20 Hz) stimulus of 8 cd·s/m^2 (WT and *Tlr4*$^{-/-}$), 50 cd·s/m^2 (*rd10*) and 10 cd·s/m^2 (P23H).

After ERG recording, animal sedation was interrupted with atipamezol (Antisedan, Orion Corporation, Espoo, Finland, 1mg/kg of body weight).

All measurements were performed by an observer blind to the experimental condition of the animal. The amplitude of the waves was analyzed with Labchart 7.0 software (AD Instruments, Oxford, UK)

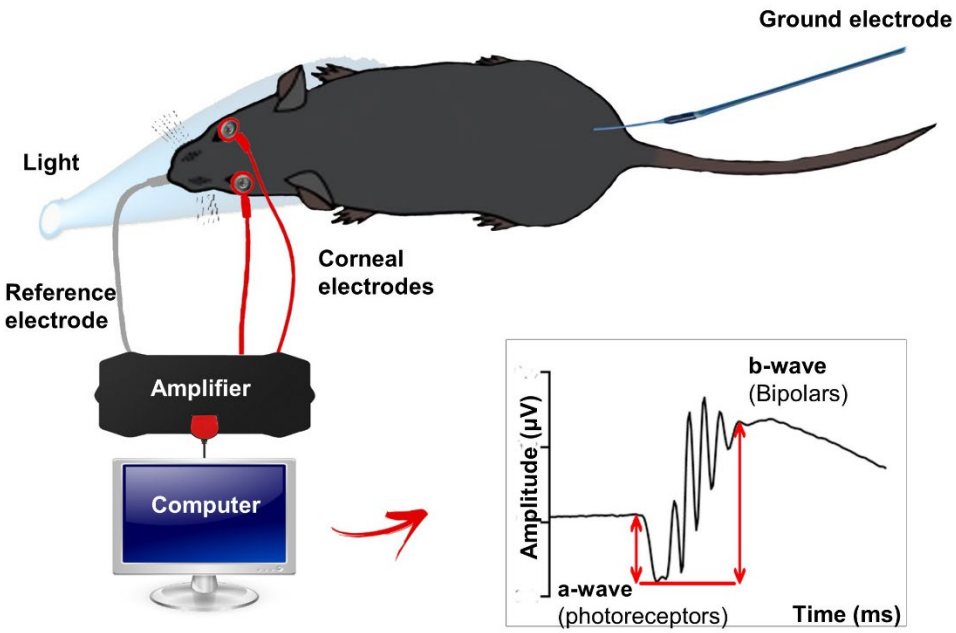

Figure 3.5. Diagram of the recording of the electroretinographic response. Mice were maintained in scotopic conditions 14-16 hours. Then, they were anaesthetized and electrodes were placed near in the mouth (reference electrode), near the corneas (corneal electrodes) and in parallel to the tail of the animal (ground electrode). The electroretinographic response to defined flashes of light was recorded. The amplitude of the a-wave and the b-wave were measured. Scheme kindly provided by Dr. N. Álvarez-Lindo (Centro de Investigaciones Biológicas Margarita Salas, Madrid, Spain)

3.11. Statistical analysis

Statistical analysis was performed with GraphPad Prism software 8.0 (GraphPad Software Inc., La Jolla, CA, USA).

In order to compare two groups, first normality was assessed for each group using Shapiro-Wilk normality test. If normality was confirmed, two-tailed unpaired t-test was employed in the case of unpaired data, while paired t-test was applied in the case of paired data sets. When normality was not confirmed, Mann Whitney test was used. The analysis of more than two data sets was done using one-way ANOVA and to compare values at the different time points with those of a specific time point, Dunnett's multiple comparison test was used. Tukeys's post-test was used for the comparisons between all the different time points. Comparisons of two variables were done using 2-way ANOVA and the Sidak's multiple comparison post-test was performed only when a significant interaction between both variables was found. In all the cases, statistical significance was established at p-value (p) <0.05. The different obtained p-values were indicated in the figures with star (or dollar/ampersand) symbols. **** p<0.0001; *** p<0.001; ** p<0.01; * p<0.05.

SECTION 4
RESULTS

4. RESULTS

4.1. Insulin receptor signaling potentiation in retinitis pigmentosa

IR signaling has been reported to be a key player in neurodegenerative diseases of brain and retina (Song et al., 2016; Bloom et al., 2018). This section is focused on the characterization of insulin receptor expression and signaling in the retina during course of RP, and on the analysis of the consequences of the potentiation of IR signaling in the disease progression.

4.1.1. Insulin receptor expression in WT and RP retinas

In mice, there are two insulin genes, *Ins1* and *Ins2*. *Ins2* is the most ancestral one and the one expressed predominantly in the brain and retina (Mehran et al., 2012; Hernández-Sánchez personal communication). Therefore, the expression of *Ins2* was analyzed by qPCR in WT and *rd10* retinas from the onset of retinal degeneration (P19) until the degeneration is well established (P25) (Barhoum et al., 2008). No differences were observed between the two genotypes along the analyzed time period (Figure 4.1A). However, when the insulin receptor gene (*Insr)* was analyzed at the same ages, a small but statistically significant increase of *Insr* expression in the *rd10* retinas was observed compared to WT (Figure 4.1B). We next analyzed IR protein levels by Western blot employing the C19 antibody directed against the IR-β subunit and previously tested in the CNS (Bruning et al., 2000; Dixon-Salazar et al., 2014). As shown in Figure 4.1C and D, we observed higher IR levels in *rd10* in comparison with WT retinas. To get more insight into IR retinal distribution, we first examined IR expression pattern by immunohistochemistry in the WT retinas. IR staining was observed in all retinal layers, according to its versatile nature. However, prominent immunostaining was visualized in the OPL and in the NFL (Figure 4.1E).

The OPL is the synaptic layer where the photoreceptors synapse with bipolar and horizontal cell terminals (section 1.1). Co-immunostaining for IR and the horizontal cell marker calbindin showed that IR labeling in the OPL was restricted to a subset of calbindin positive fibers (Figure 4.2A). On the contrary, no colocalization was found with the ON-bipolar cell dendrites that were immunostained with PKC-α (Figure 4.2D). To determine the type (axon or dendrite) of the horizontal cell IR-positive processes, we performed immunostaining for Neurofilament Medium (NF-M), which is selectively expressed in axons (Peichl and Gonzalez-Soriano, 1993) (Figure 4.2C). Co-immunostaining for IR and NF-M, showed that IR expression in the OPL was restricted to the NF-M-positive horizontal cell axons (Figure 4.2B). In addition, the NF-M-positive ganglion

cell axons showed also robust IR expression (Figure 4.2E). Horizontal cells collect the rod and cone pathways separately, while horizontal cell axons terminals receive inputs from rods, dendrites collect contacts from cone pedicles (Kolb, 1970; Kolb, 1974; Peichl and Gonzalez-Soriano, 1994; Feigenspan and Babai, 2015). Therefore, our immunostaining results show preferential IR location in the horizontal cell axons that synapse with rod spherules.

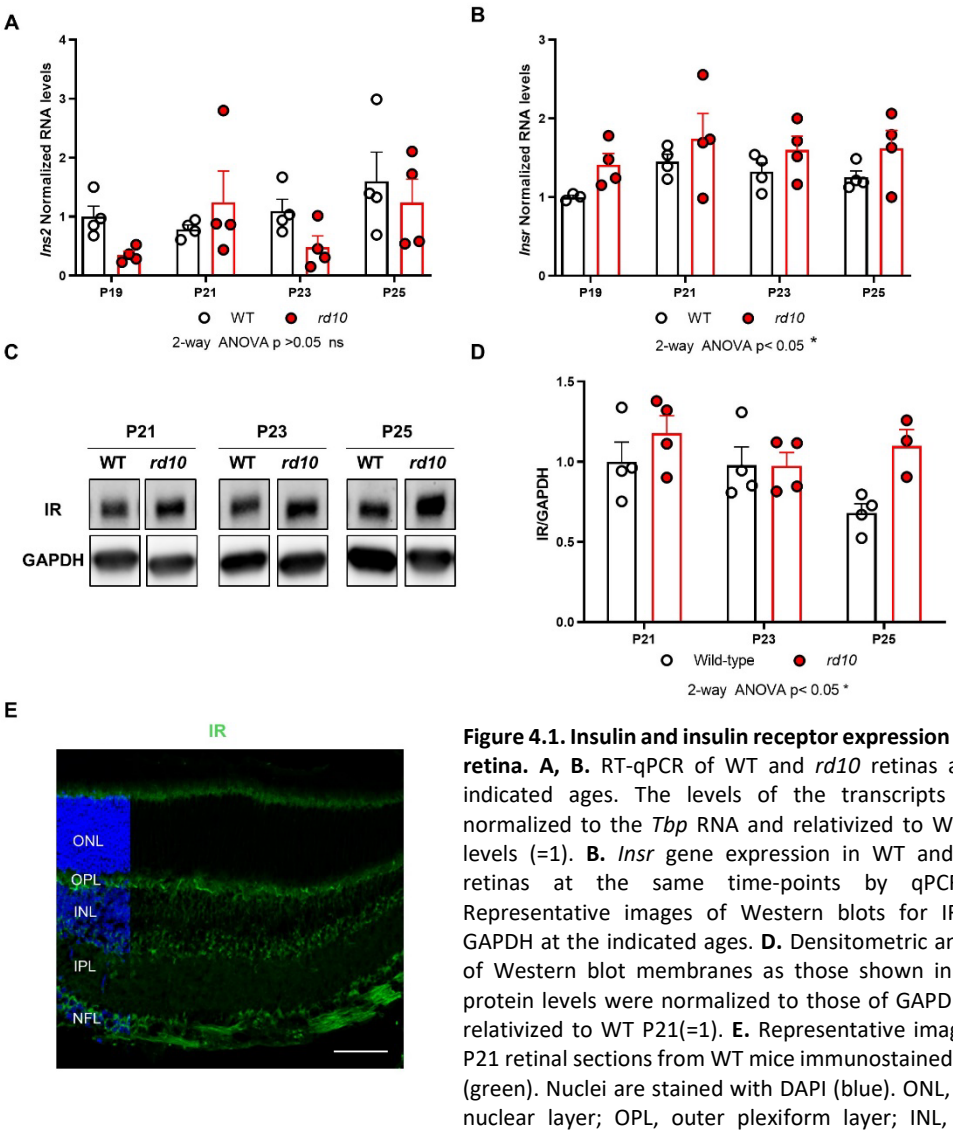

Figure 4.1. Insulin and insulin receptor expression in the retina. A, B. RT-qPCR of WT and *rd10* retinas at the indicated ages. The levels of the transcripts were normalized to the *Tbp* RNA and relativized to WT P19 levels (=1). **B.** *Insr* gene expression in WT and *rd10* retinas at the same time-points by qPCR. **C.** Representative images of Western blots for IR and GAPDH at the indicated ages. **D.** Densitometric analysis of Western blot membranes as those shown in C. IR protein levels were normalized to those of GAPDH and relativized to WT P21(=1). **E.** Representative images of P21 retinal sections from WT mice immunostained for IR (green). Nuclei are stained with DAPI (blue). ONL, outer nuclear layer; OPL, outer plexiform layer; INL, inner nuclear layer; IPL, inner plexiform layer. Scale bar: 60 µm. For A, B and D, dots represent individual mice and bars represent the mean value for each group +SEM. n=3-4 mice per group. 2-way ANOVA was used for statistical analysis *p < 0.05.

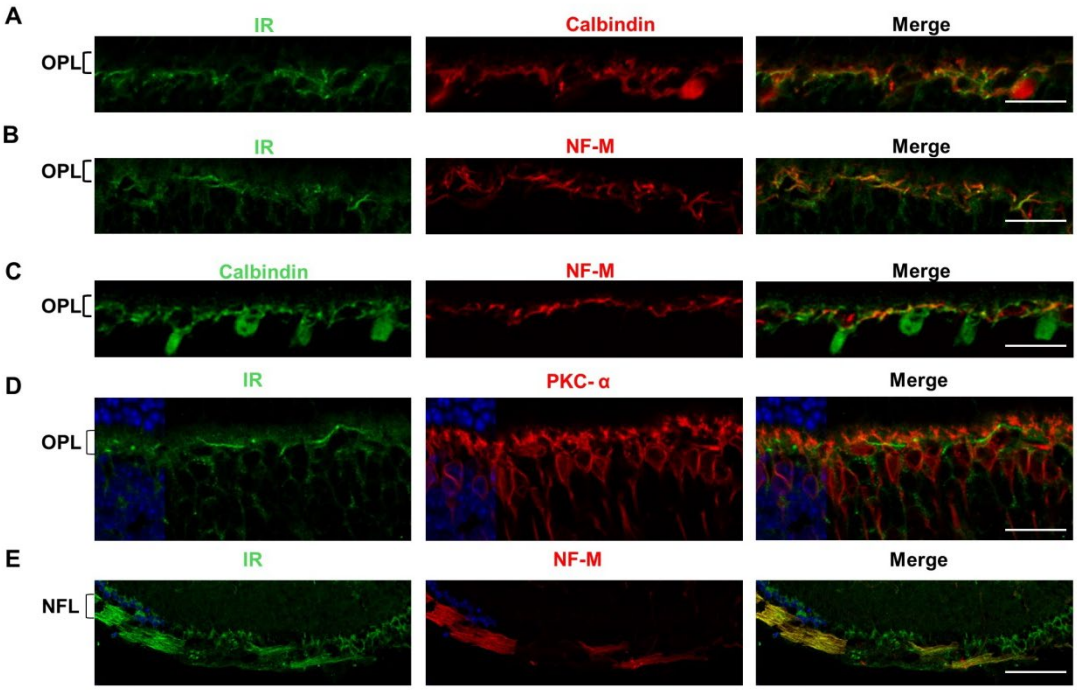

Figure 4.2. Characterization of IR expression in the OPL and NFL of P21 WT retinas. A-D. Magnified images of the OPL showing double immunostaining for IR (green) and calbindin (red) (A), IR (green) and NF-M (red) (B), calbindin (green) and NF-M (red) (C) and IR (green) and PKC-α (red) (D). **E.** Magnified images of the NFL showing double immunostaining for IR (green) and NF-M (red). Nuclei are stained with DAPI (blue). OPL, outer plexiform layer; NFL, nerve fiber layer. Scale bars: A, B and C 25 µm; D 20 µm and E 75 µm.

Next, we checked for a differential IR expression pattern associated to retinal dystrophy. At stages previous to any significant rod cell disturbance (P16), the relative IR/NF immunostaining of the OPL and NFL was globally similar in the WT and *rd10* retinas (Figure 4.3A and B). Conversely, during the course of rod degeneration (P21-P23) the IR immunostaining found in horizontal cell axons was selectively decreased in the *rd10* retina as depicted in Figure 4.3C-F. This decrease was not due to the loss of horizontal cells since similar number of calbindin^{+} cells was found in WT and *rd10* animals at P23 (Figure 4.4) nor horizontal cell axon degeneration as derived from the preserved NF-M staining. Moreover, the down-regulation of IR levels was specific for horizontal cell axons since no significant changes were observed in the IR immunostaining in the ganglion cell axons at any of the analyzed ages (Figure 4.3).

The IR downregulation on horizontal axons was not observed when analyzing whole retina extracts by qPCR or Western blot (Figure 4.1) most likely because this local decrease gets diluted by the IR expression in the rest of the tissue. Alternatively, changes in the retinal cell populations (loss of photoreceptors, microglial proliferation and macrophage infiltration) may account for the rise observed when analyzing whole retina extracts.

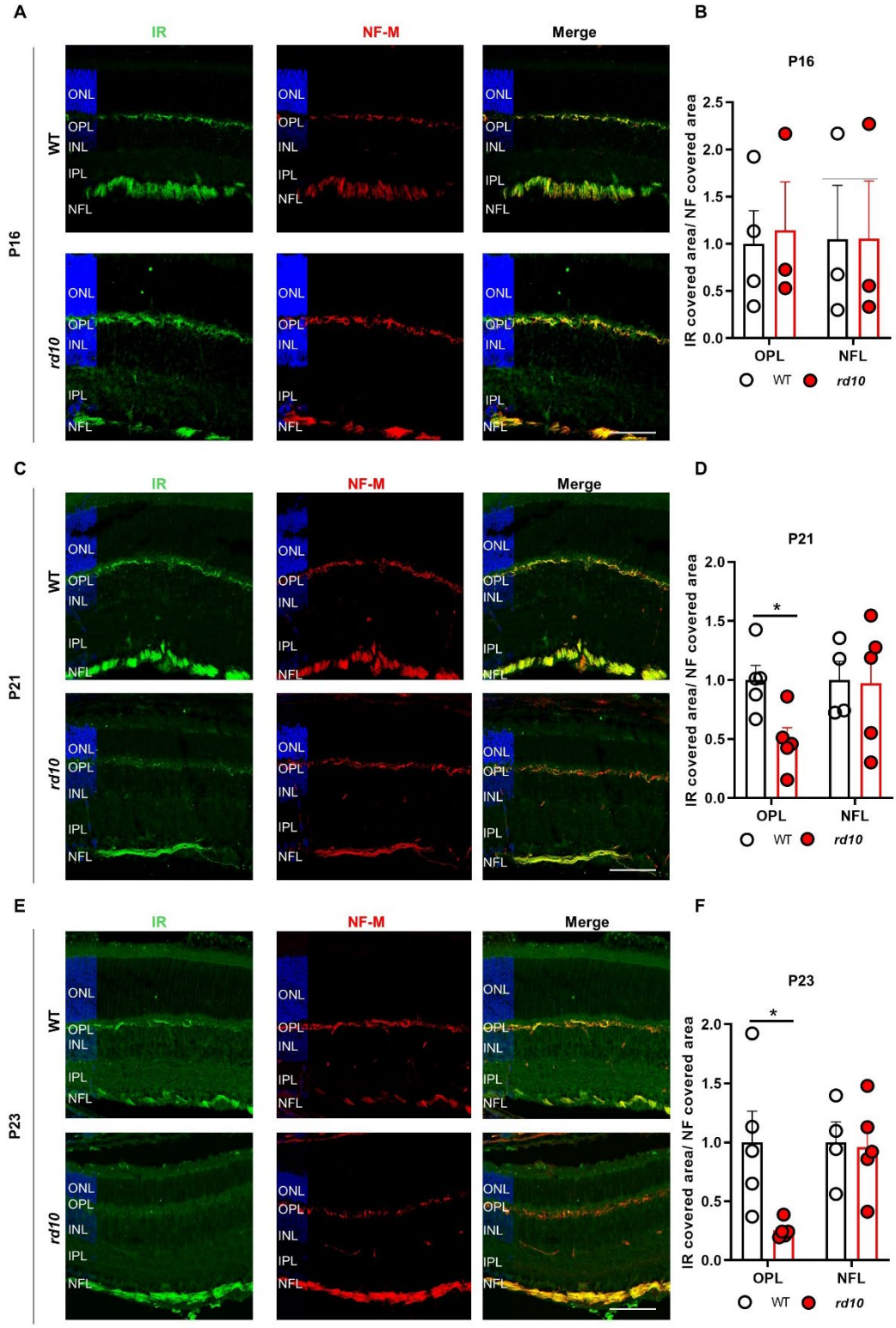

Figure 4.3. Insulin receptor expression in WT and *rd10* retinas. A, C and E. Representative images of P16 (A), P21 (C) and P23 (E) WT and *rd10* retinal sections immunostained for IR (green) and NF-M (red). Nuclei are stained with DAPI. ONL, outer nuclear layer; OPL, outer plexiform layer; INL, inner nuclear layer; GFL, ganglion fiber layer. Scale bars 65 µm. **B, D and F**: Quantification of the area covered with IR-staining of several retinal sections of P16, (B) P21 (D) and P23 (F) WT and *rd10* retinal sections. The area covered with IR-staining was normalized to that of Neurofilament-staining of the same region to correct for potential variation among retinal sections and relativized to that of WT (=1). Dots represent individual mice and bars represent the mean value for each experimental group (+SEM). n=3-5 mice, 4 images per retina. Unpaired t-test was applied for statistical analysis *$p < 0.05$.

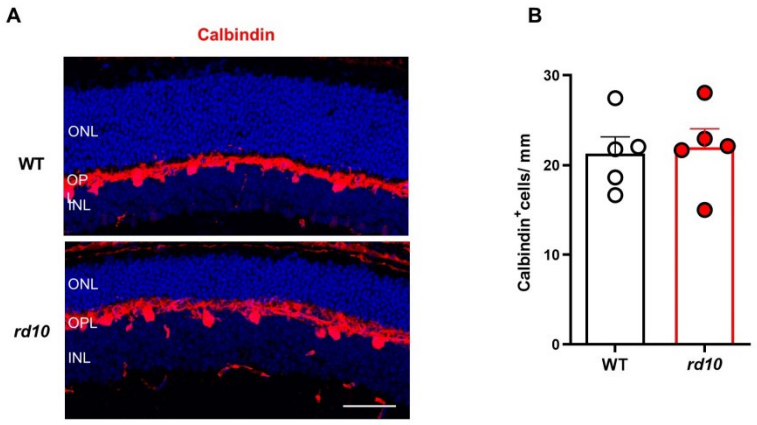

Figure 4.4. Comparison of the number of horizontal cells in WT and *rd10* retinas. A. Representative images of P23 retinal sections from WT and *rd10* mice, immunostained for calbindin to label horizontal cells (red). Nuclei are stained with DAPI (blue). **B.** The number of calbindin-positive cells was quantified in equatorial sections in the central areas of the retina (T3–T4; see section 3.9). The plots show the mean + SEM. Dots represent individual mice. n=5 mice, 10 images per retina. Statistical analysis was performed using unpaired t-test. Scale bar: 44 µm.

4.1.2. Insulin receptor signaling in WT and RP retinas

We next examined whether the selective decrease of IR levels in horizontal cell axons had consequences on the local IR signaling. Out of the multiple downstream effectors of IR signaling we focused on S6 ribosomal protein. A recent study (Agostinone et al., 2018) has shown robust pS6$^{Ser240/244}$ immunostaining in the retinal horizontal and ganglion cells, where we found prominent IR expression. Immunostaining of WT retinas for pS6$^{Ser240/244}$ confirmed the previously reported labeling at the horizontal and ganglion cell bodies (Figure 4.5A-C). Moreover, a closer examination of pS6$^{Ser240/244}$ staining in the OPL revealed profuse punctuate labeling in close apposition to the horizontal cell terminal tips (Figure 4.5A). Interestingly, pS6$^{Ser240/244}$ immunostaining in the *rd10* retina revealed a similar staining of horizontal cell bodies and ganglion cells but a dramatic decrease in the horizontal cell puncta labeling (Figure 4.5A-C). Double immunostaining for calbindin revealed diminished number of calbindin tips due to the horizontal cell terminal retraction as a consequence of photoreceptor loss (Cuenca et al., 2014), but more striking half of the remaining horizontal cell tips were devoid of pS6$^{Ser240/244}$ labeling in the *rd10* retina (Figure 4.5A and B).

The down-regulation of IR expression and signaling in the horizontal cell axons and terminal tips parallel to rod degeneration, together with the role of IR in synapse formation and maintenance (Chiu et al., 2008; Urwyler et al., 2019), prompted us to investigate whether the alteration of IR expression correlated with structural synaptic modifications in the OPL. We focused on the rod synapse analysis, since at early degenerative stage in the *rd10* retina cone survival is still not compromised.

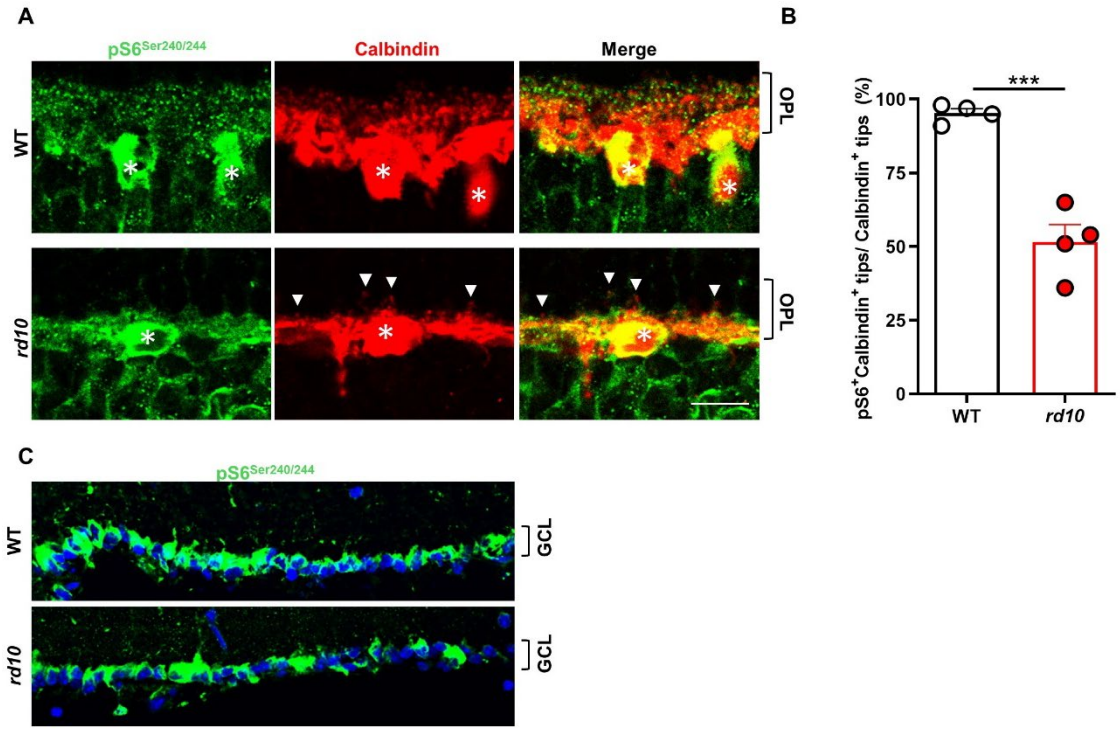

Figure 4.5. Levels of pS6$^{Ser240/244}$ associated to horizontal cell tips in *rd10* and WT. A. Representative images of the OPL of WT and *rd10* sections immunostained for pS6$^{Ser240/Ser444}$ (green) and calbindin (red) at P23. Arrowheads indicate calbindin^{+} tips without pS6$^{Ser240/244}$ staining. Asterisks indicate horizontal cell bodies. **B.** Quantification of the number of horizontal terminal tips (calbindin^{+} puncta) expressing pS6$^{Ser240/244}$. **C.** Representative images of the GCL of WT and rd10 retinas immunostained for pS6$^{Ser240/Ser444}$ (green) at P23. Nuclei were stained with DAPI (blue). Results represent the mean + SEM. n=4 mice, 4 images per retina, over 200 calbindin^{+} tips were scored per retina. Statistical analysis was done with unpaired t-test. **p<0.01. Scale bar: 12 µm in A and 31 µm in C.

4.1.3. Analysis of triad synapses in the OPL of WT and *rd10* retinas

As described in section 1.1, rod spherules form triad synapses with horizontal and bipolar terminals. We assessed rod synaptic connectivity by immunostaining with specific markers for the photoreceptor ribbon (Ribeye and c-terminal binding protein 2, CtBP2) and horizontal (GluA2, ionotropic glutamate receptor A2) and bipolar (mGluR6, metabotropic glutamate receptor 6) postsynaptic terminal tips.

As shown in Figure 4.6, almost all of the rod spherules are associated to horizontal and bipolar cell terminals. However, in the *rd10* mice we found rod ribbons that lack the postsynaptic horizontal or bipolar terminal. The further characterization of rod synaptic abnormalities was carried out by electron microscopy by Dr. C. Lillo (Universidad de Salamanca, Spain, see Appendix 1).

The aforementioned results showed that *rd10* mice display downregulation of the IR expression and signaling (by means of pS6$^{Ser240/244}$ levels), specifically at the horizontal cell axons and terminals, parallel to the synaptic disruption of rods and their postsynaptic partners

(horizontal and bipolar cells). Therefore, we hypothesized that the activation of IR signaling may result in a preservation of rod synaptic connectivity.

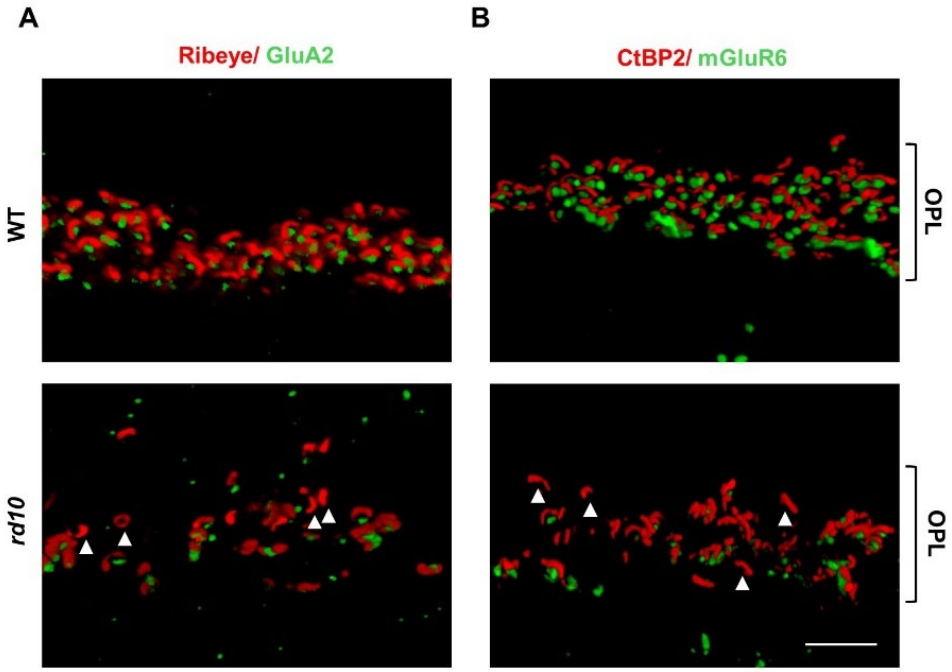

Figure 4.6. Synaptic connectivity of WT and *rd10* mice at the OPL. A, B. Representative 3D reconstruction images of WT and *rd10* synapses in the OPL. P23 retinal sections were immunostained for Ribeye (ribbon at presynaptic terminal, red) and the glutamate receptor subunit GluA2 (horizontal postsynaptic terminal, green) (A); or for CtBP2 (ribbon at presynaptic terminal, red) and the glutamate receptor mGluR6 (bipolar postsynaptic terminal, green) (B). Arrowheads indicate ribbons (rod presynaptic terminals) without post-synaptic partner. OPL, outer plexiform layer. Scale bar: 6 µm

4.1.4. Activation of insulin receptor in *rd10* animals employing human proinsulin

As mentioned in the introduction, proinsulin binds to and activates IR downstream signaling pathways. However, proinsulin has lower metabolic profile than insulin due to its low affinity for the IR-B isoform (EC_{50} for IR-A 4.5 nM versus EC_{50} for IR-B 31 nM) (Galloway et al., 1992; Malaguarnera et al., 2012). Interestingly, WT and *rd10* retinas predominantly express the IR-A isoform (assessed by RT-PCR, Hernández-Sánchez, personal communication). Considering the long-term administration required to treat human patients and that proinsulin has shown neuroprotective activity during retinal development and degeneration (Hernandez-Sanchez et al., 1995; Valenciano et al., 2006; Corrochano et al., 2008; Fernandez-Sanchez et al., 2012; Isiegas et al., 2016) we chose proinsulin administration to stimulate IR in the retina.

First, we confirmed that systemic proinsulin administration could stimulate IR signaling in the *rd10* retina. For that, human proinsulin (hPi) or vehicle was administered by intraperitoneal injection to P20 *rd10* and the retinas were collected 90 min post injection for Western blot assay.

As shown in Figure 4.7, hPi increased the phosphorylated levels of retinal ERK, a read-out of IR stimulation.

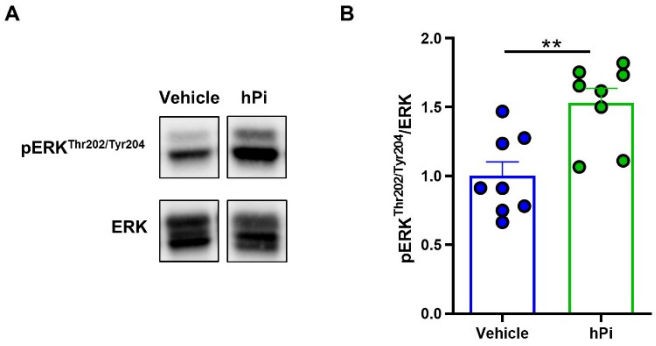

Figure 4.7. Effect of hPi administration in retinal insulin receptor signaling. A. Representative images of Western blots for pERK$^{Thr202/Tyr204}$ and total ERK in P20 *rd10* retinal extracts 90 minutes after the administration of vehicle or human proinsulin (hPi). **B.** Densitometric analysis of Western blot membranes as those shown in A. pERK$^{Thr202/Tyr204}$ levels were normalized by those of total ERK levels and relativized to vehicle (=1). Dots represent individual retinas and the bar represents the mean for each group (+SEM). n=8 retinas. The statistical analysis was done using unpaired t-test **p<0.01.

As a strategy to activate IR signaling during the course of *rd10* degeneration, we took advantage of previous experience with recombinant serotype 1 AAV expressing the human proinsulin coding region (AAV-hPi) (Fernandez-Sanchez et al., 2012; Corpas et al., 2017). The characterization of AAV-hPi was performed by other members of the group and is summarized in Appendix 1. Briefly, i) AAV-hPi treated *rd10* mice displayed hPi serum levels that were uniformly sustained within each individual mouse up to 5-months; ii) hPi was detected in the whole eye and retinal extracts already one week post-injection and up to 7 weeks post-injection; iii) the glycaemia and body weight of the AAV-hPi treated mice were not altered in comparison to those of the AAV-null treated animals.

To determine hPi effect on the dystrophic retina, we first examined whether hPi treatment was able to restore IR levels and signaling. Analysis of IR expression on horizontal cell axons, that selectively displayed decreased IR, did not provide evidence of differences between the AAV-hPi-treated and the control (AAV-null) *rd10* retinas (Figure 4.8A and B). On the contrary, AAV-hPi-treated *rd10* mouse retinas showed increased pS6$^{Ser240/244}$ puncta staining in the OPL in comparison with the untreated *rd10* mouse (AAV-null). Quantification of the number of pS6$^{Ser240/244}$ immunostained horizontal cell tips at P21 demonstrated that hPi treatment increased the proportion of double calbindin-pS6$^{Ser240/244}$ labelled tips to near 90%, close to the proportion of WT retinas, whereas in the control, untreated *rd10*, the fraction of horizontal cell tips positive for pS6$^{Ser240/244}$ labeling remained between 50-60% (Figure 4.8C and D).

Interestingly, hPi treatment also results in a preservation of the total number of calbindin tips (Figure 4.9A and B).

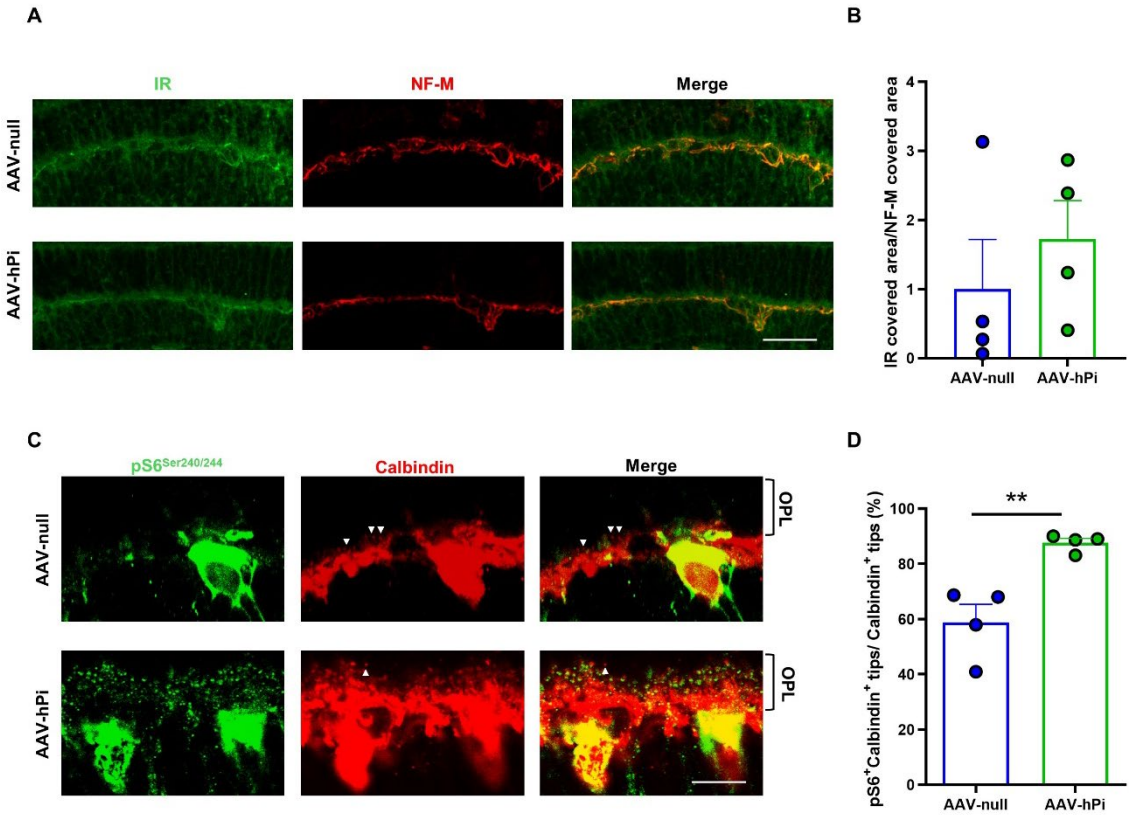

Figure 4.8. Effects of AAV-hPi administration in insulin receptor and insulin receptor signaling in *rd10*. *rd10* mice received a single intramuscular injection of either AAV-null or AAV-hPi at P12 and were analyzed at P21 for IR and pS6$^{Ser240/244}$ expression. **A, C.** Representative images of the OPL in P21 retinal sections co-immunostained for IR (green) and NF-M (red) (A) or pS6$^{Ser240/244}$ (green) and calbindin (red) (C). **B.** Quantification of IR covered area normalized to NF-M and relativized to that of AAV-null (=1) **D.** Quantification of the number of horizontal terminal tips (calbindin^{+} puncta) with associated pS6$^{Ser240/244}$ labeling. Dots represent individual mice, while bars show the mean of each group (+SEM). n=4 mice, 4 images per retina and over 200 calbindin^{+} tips per retina were examined. Unpaired t-test was applied for statistical analysis **p<0.01. Scale bars: 40 µm in A and 11 µm in C.

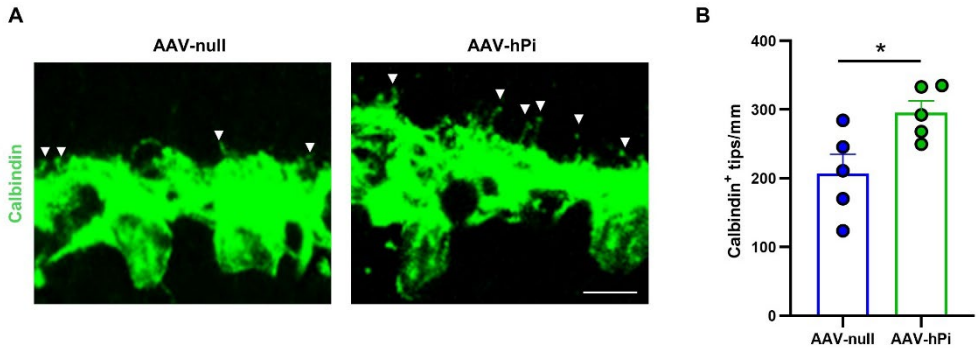

Figure 4.9. Analysis of horizontal cell tips in *rd10* after AAV-hPi administration. *rd10* mice received at P12 a single intramuscular AAV-null or AAV-hPi injection and were analyzed at P30 for calbindin labeling. **A.** Representative images of horizontal cells stained for calbindin (green). Arrowheads indicate calbindin$^+$ puncta. Scale bar: 7 µm **B.** Quantification of the number of calbindin$^+$ tips. n=5 mice, 4 images per animal. Dots represent individual mice and bars the mean of each group (+SEM). Unpaired t-test was applied for statistical analysis *p<0.05.

Then, we analyzed whether long-term AAV-hPi treatment was able to display a neuroprotective effect. To this aim, *rd10* mice were injected at P10-P12 and their retinas were analyzed at P30, when most of the photoreceptors have been lost. Two different histological aspects were evaluated, namely photoreceptor cell preservation and synapse maintenance. To assess photoreceptor preservation, the ratio ONL/INL thickness was analyzed in different retinal areas following a nasotemporal distribution as explained in section 3.9. Proinsulin treated *rd10* mice showed modest but statistically significant photoreceptor preservation that was more evident in the naso-periferal retina (T1; Figure 4.10A and B). This preservation of the photoreceptor cells by hPi treatment could result in the increase of horizontal cell tips observed in Figure 4.9. In parallel, the photoreceptor synaptic connectivity was determined by examining the rod-bipolar and rod-horizontal synapses by immunostaining. AAV-hPi treatment increased the number of rod postsynaptic terminals as expected from the better preservation of the ONL, but more significant, hPi reduced the proportion of disconnected rod postsynaptic terminals. The proportion of synaptic ribbons lacking either GluA2-positive horizontal (Figure 4.11A and C), or mGluR6-positive bipolar postsynaptic terminals (Figure 4.11B and D) was significantly decreased in AAV-hPi-treated animals. These results feature a novel function of proinsulin preserving rod synaptic connectivity with their postsynaptic second order neuronal partners, and suggest that hPi displays another distinct action, maybe partially independent, to that of photoreceptor survival revealed by previous studies (Corrochano et al., 2008; Fernandez-Sanchez et al., 2012; Isiegas et al., 2016).

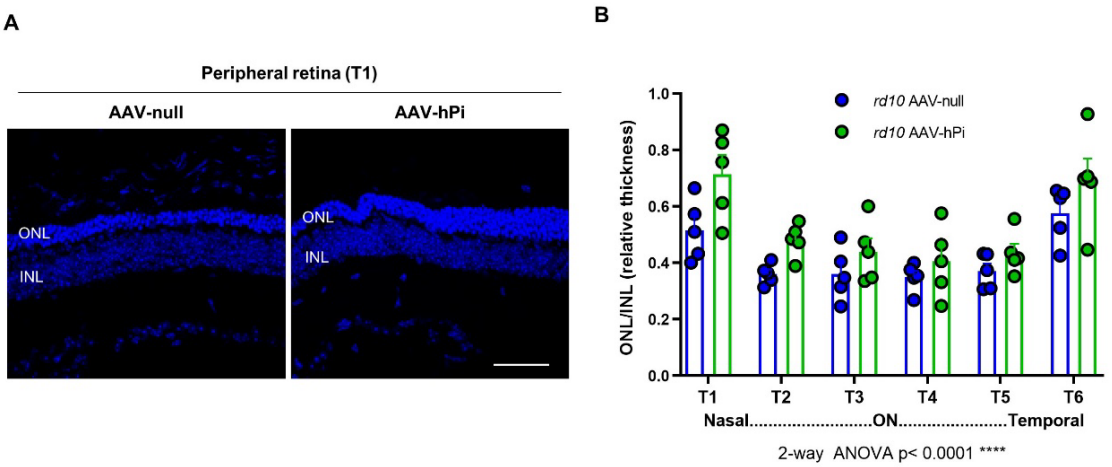

Figure 4.10. Effect of AAV-hPi administration on photoreceptor preservation. *rd10* mice received a single intramuscular injection of AAV-null or AVV-hPi at P12 and were analyzed at P30. **A**. Representative images of P30 retinal sections of the T1 region from AAV-null- and AVV-hPi-treated *rd10* mice stained with DAPI (blue). ONL, outer nuclear layer; INL, inner nuclear layer. Scale bar: 60 µm. **B.** ONL and INL thickness were measured in equatorial sections corresponding to 6 regions of the retina, following a nasotemporal sequence (T1–T6 as defined in materials and methods). Dots represent individual mice and bars show the mean + SEM. n=5 mice, 3 sections per retina, 6 regions and 3 measurements per region. ON, optic nerve. Two-way ANOVA was used for statistical analysis ****p <0.0001.

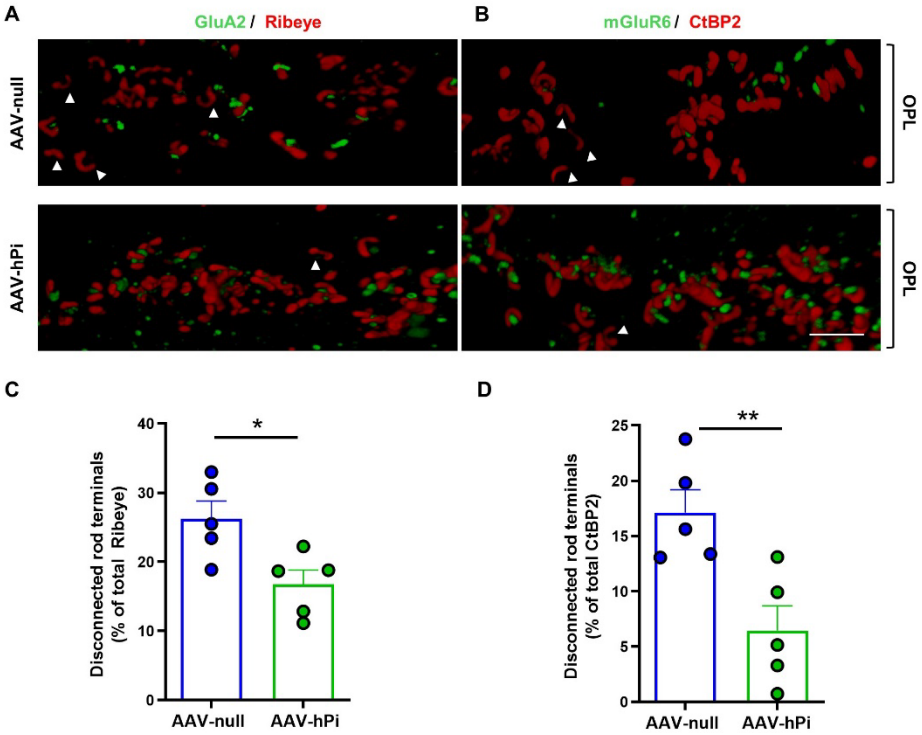

Figure 4.11. Effect of AAV-hPi administration on rod-horizontal and rod-bipolar synapses. *rd10* mice received a single intramuscular injection of AAV-null or AVV-hPi at P12 and were analyzed at P30. **A, B.** Representative 3D reconstructions of synapses at the OPL. Retinal sections were co-immunostained for Ribeye (ribbon at presynaptic terminal, red) and the glutamate receptor subunit GluA2 (horizontal postsynaptic terminal, green) (A) or for CtBP2 (ribbon at presynaptic terminal, red) and the glutamate receptor mGluR6 (bipolar postsynaptic terminal, green) (B). Arrowheads indicate ribbons (rod presynaptic terminals) without post-synaptic partner. OPL, outer plexiform layer; Scale bar: 3 µm. **C, D.** Quantification of the number of disconnected rod presynaptic terminals. Percentage of ribbons without associated GluA2 (C) or mGluR6 puncta staining (D). Dots represent individual mice and bars show the mean + SEM. *n* = 5 mice, over 200 ribbons were analyzed per retina. Statistical analysis was done applying unpaired t-test *p < 0.05; ** < 0.01.

Recent studies (Chitnis and Weiner, 2017; Rashid et al., 2019) suggest that neuroinflammation contribute to the progress of neurodegenerative diseases of the brain and retina. Our group has previously shown that proinsulin decreased the signs of brain inflammation while protecting against cognitive impairment (Corpas et al., 2017). To assess whether proinsulin had any effect on the retinal inflammatory response associated to RP (Silverman and Wong, 2018) we analyzed the expression of proinflammatory markers. As shown in Figure 4.12A, administration of AAV-hPi reduced the gene expression of proinflammatory cytokines and chemokines. hPi reduced by approximately 50% the gene expression of tumor necrosis factor α (*Tnf*), interleukin 1 beta (*Il1b*), alpha-2-macroglobulin (*A2m*) and C-C motif ligand 3 (*Ccl3*). In addition, the gene expression of microglial markers such as ionized calcium binding adaptor molecule (*Iba1*) and cluster of differentiation 68 (*Cd68*) showed a 20% decrease in AAV-hPi-treated animals. The reduction of the expression of microglial genes was confirmed in histological studies. Immunostaining for Iba1, a pan-microglial marker, showed statistically significant reduction in the number of microglial cells in AAV-hPi-treated retinas. The percentage of the decrease [(AAV-null -AAV-hPi)/AAV-null %] was more evident in the nuclear layers (30% decrease in the ONL and 35% in the INL), where microglia is not present in homeostatic conditions than in the plexiform layers, were microglia reside in physiological conditions (8% decrease in the OPL and 6% in the IPL) (Figure 4.12B and C). Similar results were obtained when the phagocytic marker CD68 was analyzed. The number of $CD68^{+}$ was decreased by 30% in the ONL and INL and by 15% by in the OPL and IPL (Figure 4.12D and E).

Overall, these data showed that hPi treatment had several beneficial effects on *rd10* retinas. Proinsulin increased photoreceptor survival, preserved rod synapses and decreased retinal inflammation and microglial reactivity. Moreover, functional experiments carried out in the laboratory of Dr. P. de la Villa (Universidad de Alcalá de Henares, Spain) showed that AAV-hPi-treated animals displayed delayed visual function loss. The amplitudes of the different ERG waves recorded were higher in the AAV-hPi treated mice than in the control mice (Appendix 1). In addition, the AAV-hPi treated *rd10* mice presented higher contrast sensitivity than the untreated *rd10* (Appendix 1). Collectively, these results suggest that proinsulin is a multifaceted neuroprotective factor and a potential therapy for retinitis pigmentosa.

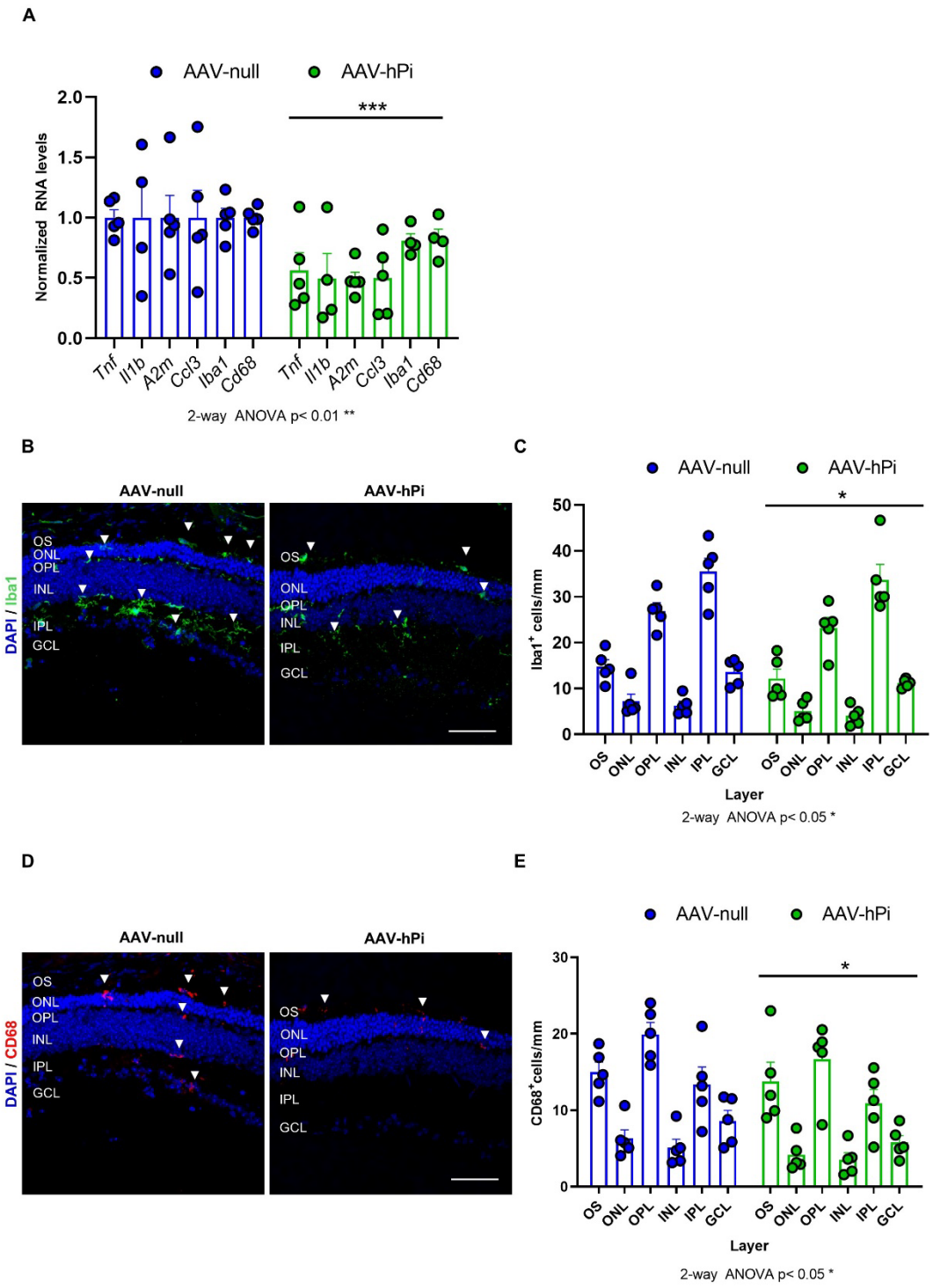

Figure 4.12. Effect of AAV-hPi administration on inflammatory status of *rd10* retina. *rd10* mice received a single intramuscular injection of AAV-null or AVV-hPi at P12 and were analyzed at P30**. A.** RT-qPCR for inflammatory cytokines and chemokines of AAV-null and AAV-hPi *rd10* retinas. The levels of the transcripts were normalized to the *Tbp* RNA and relativized to AAV-null levels (=1). **B, D.** Representative images of P30 retinal sections immunostained for Iba1(B, green) and CD68 (D, red). Nuclei were stained with DAPI (blue). Arrowheads indicate Iba1$^+$ cells (B) and CD68$^+$ cells (D). Scale bars: 50 µm. **C, E.** Quantification of the number of Iba1$^+$ (C) and CD68$^+$ (E) cells in retinal sections of AAV-null and AAV-hPi-treated animals. In all cases dots correspond to individual animals and bars represent the mean for each group. OS, outer segment; ONL, outer nuclear layer; OPL, outer plexiform layer; INL, inner nuclear layer; IPL, inner plexiform layer; GCL, ganglion cell layer. n=4-5 animals in A and 5 animals in C and E. Statistical analysis was carried out with 2-way ANOVA p *< 0.05; ** < 0.01.

4.2. Modulation of GSK-3 provides cellular and functional neuroprotection in the *rd10* mouse model of RP

As mentioned in section 1.7, GSK-3 is a multitask enzyme with over a 100 substrates that participates in a great variety of signaling pathways. IR signaling is one of the main GSK-3 regulatory pathways (Beurel et al., 2015). Since GSK-3 participates in the pathogenesis of many disorders, including neurodegenerative diseases (Mancinelli et al., 2017) we decided to study GSK-3 in the context of RP. We focused on GSK-3β the most abundant isoform in the CNS, including the retina (Kaidanovich-Beilin and Woodgett, 2011; Pardo et al., 2016).

4.2.1. GSK-3 expression and activation in WT and *rd10* retinas

We first analyzed *Gsk-3β* gene expression in WT and *rd10* retinas by RT-qPCR from P14, when the degenerative process has not yet started in *rd10*, until P21 when the photoreceptor loss is evident in these mice. No significant differences in *Gsk-3β* RNA levels were found between *rd10* and WT retinas at any of the studied ages (Figure 4.13A). Immunohistochemistry with a GSK-3β isoform-specific antibody showed a broad distribution expression pattern in both WT and *rd10* retinas. Moreover, despite the morphological differences between both genotypes caused by the degenerative process, no major changes in GSK-3β pattern were detected (Figure 4.13B).

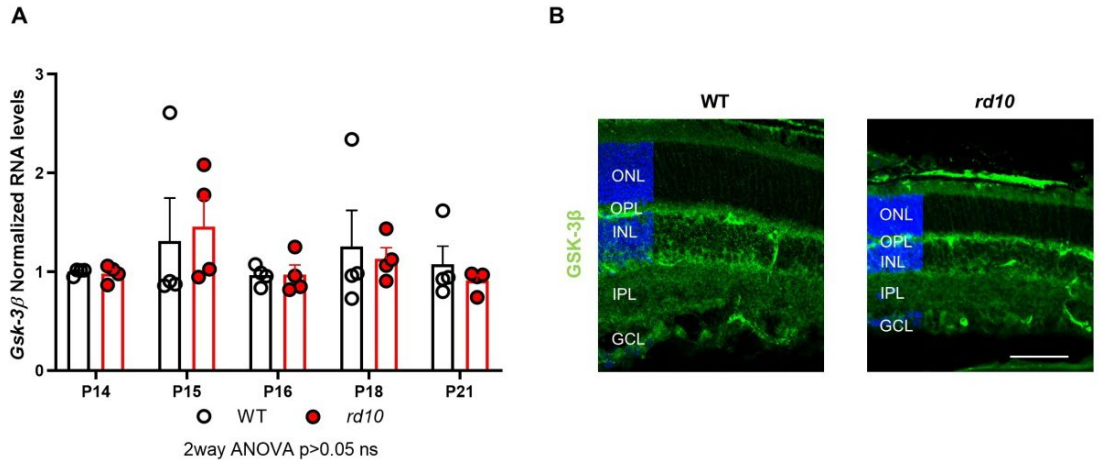

Figure 4.13. GSK-3 expression in WT and *rd10* retinas. A. *Gsk-3β* gene expression analysis by RT-qPCR in WT and *rd10* retinas from P14 to P21. Data are normalized to WT levels at P14 (=1). Dots represent individual mice and bars show the mean of each group (+SEM). Statistical analysis was done with 2-way ANOVA. n=4 mice. **B.** GSK-3β immunostaining (green) in WT and *rd10* retinal sections at P21. Nuclei were stained with DAPI (blue). ONL, outer nuclear layer; OPL, outer plexiform layer; INL, inner plexiform layer; IPL, inner plexiform layer; GCL, ganglion cell layer. Scale bar 60 µm.

As mentioned in the introduction, GSK-3 is an uncommon protein kinase because it is constitutively active but inhibited when phosphorylated in defined residues. One of the main regulatory mechanisms of GSK-3β activity is its inhibitory phosphorylation in serine 9 (pGSK-

3β^{Ser9}). We analyzed the levels of pGSK-3β^{Ser9} in WT and *rd10* retinas by Western blot. While the total amount of GSK-3β was similar between the WT and *rd10* retinas (Figure 4.14C and H), *rd10* retinas showed increased levels of pGSK-3β^{Ser9} in comparison with WT control retinas at P19 and P21, suggesting that GSK-3β is inhibited in *rd10* retinas (Figure 4.14A and F). On the contrary, the photoreceptor protein recoverin showed a trend to lower levels at P19 and was significantly decreased at P21 in the *rd10* retinas (Figure 4.14D and I) as a consequence of photoreceptor loss. These results suggest that the increased in pGSK-3β in *rd10* retinas takes place at early stages of degeneration. Since phosphorylation of GSK-3β in Ser9 is greatly due to AKT, we decided to analyze AKT activation. AKT phosphorylation in serine 473 (pAKT^{Ser473}), an indicator of AKT activation, increased in the *rd10* retinas at P19 and P21 relative to WT (Figure 4.14B and G). Remarkable at P17, when the degenerative process is barely present, the levels of both pGSK-3β^{Ser9} and pAKT^{Ser473} were similar between WT and *rd10* retinas (Figure 4.14E and J), suggesting that pGSK-3β^{Ser9} and pAKT^{Ser473} increase is disease-associated. These results were further confirmed by immunohistochemistry (Figure 4.15). pGSK-3β^{Ser9} and pAKT^{Ser473} staining was more intense in *rd10* retinas at P21 than in WT. The increase of pAKT^{Ser473} was more prominent in *rd10* bipolar cells, secondary neurons that directly contact photoreceptors. We interpret the inhibitory phosphorylation of GSK-3β coupled with the activation of AKT signaling cascade as a pro-survival response to photoreceptor cell death that occurs in the internal layers of the retina

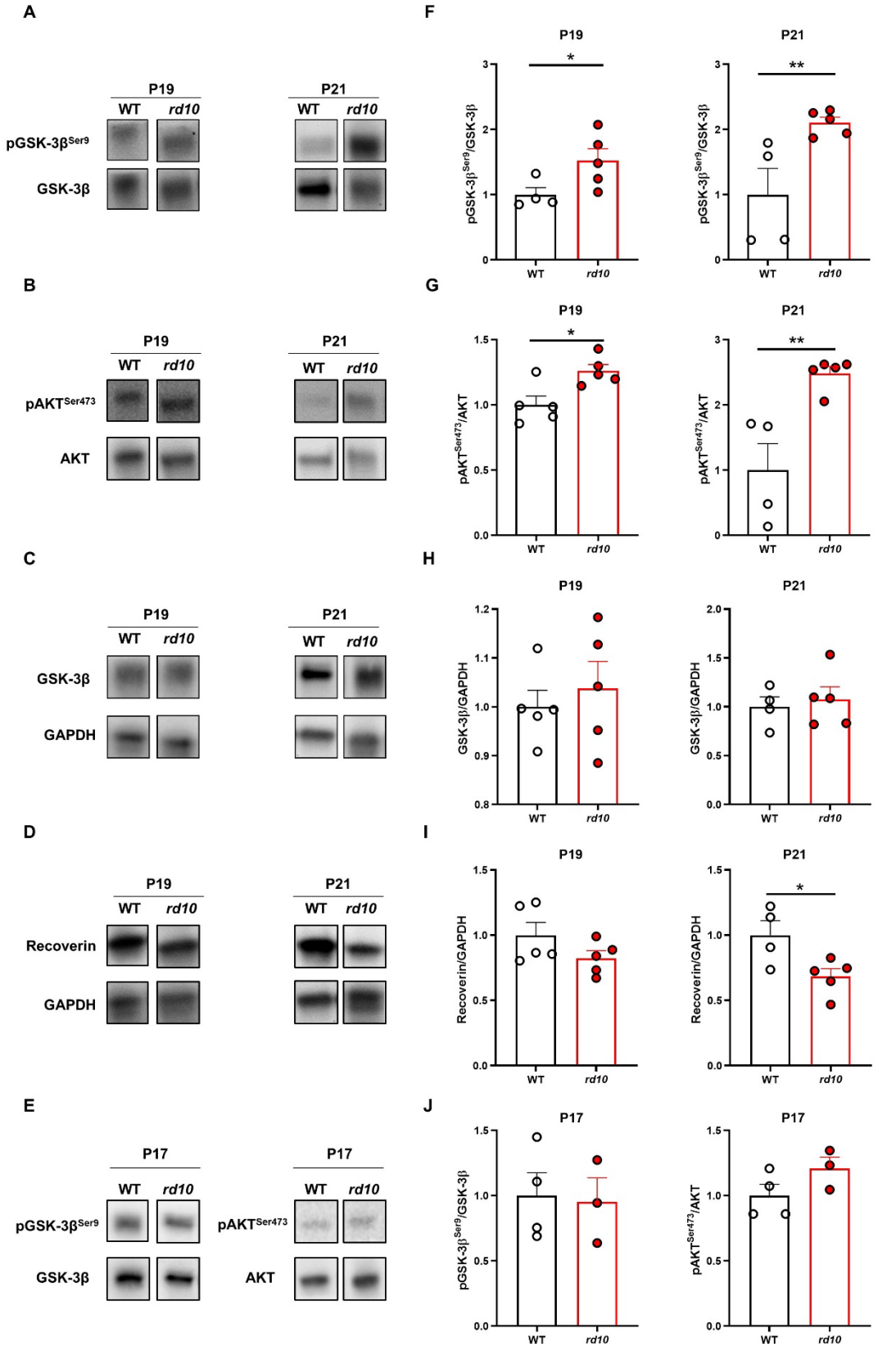

Figure 4.14. **GSK-3 and AKT activation in WT and *rd10* retinas. A-E**. Representative images showing Western blot for the indicated proteins and ages. **F-J.** Densitometric analysis of membranes as those in A-E. Levels of phosphorylated GSK-3β and AKT were normalized to those of total GSK-3β and AKT, respectively, and relativized to WT levels (=1). Levels of recoverin and GSK-3β were normalized to those of GAPDH and relativized to WT levels (=1). Dots represent individual animals and bars represent the mean (+SEM). n = 3–5 mice. Unpaired t-test was employed for statistical analysis *p < 0.05.

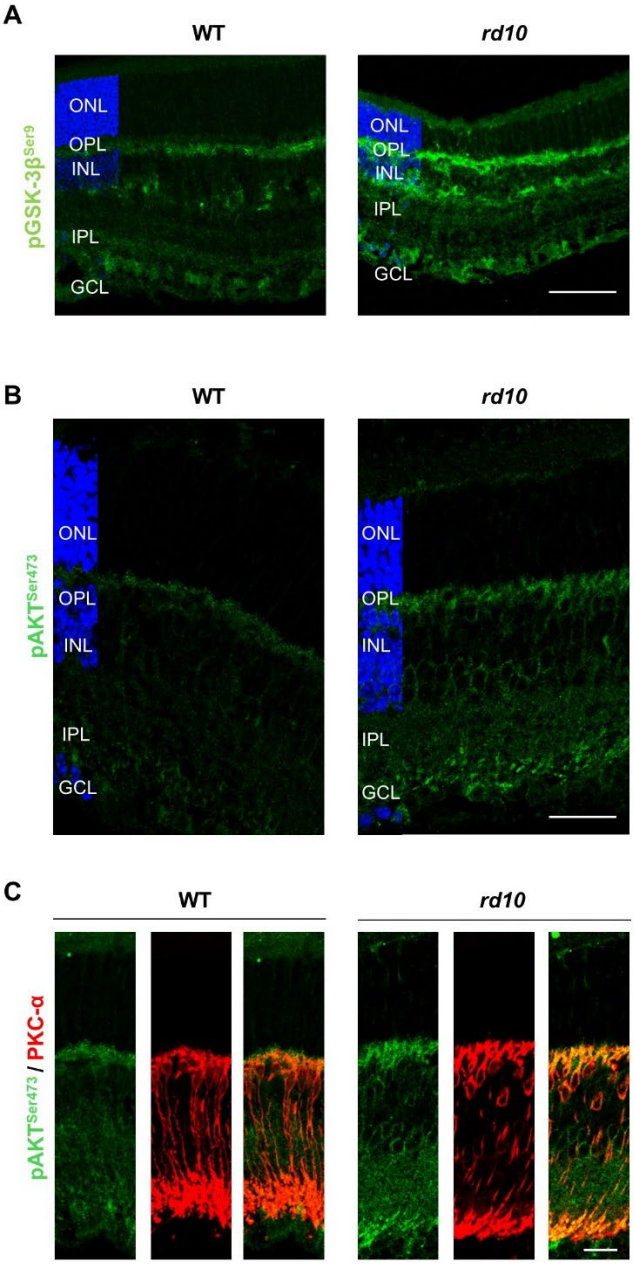

Figure 4.15. Expression pattern of pGSK-3^{Ser9} and pAKT^{Ser473} in WT and *rd10* retinas. **A, B.** Representative images of P21 WT and *rd10* retinal sections immunostained for pGSK-3βSer9 (green) (A) and pAKT^{Ser473} (green) (B). **C.** Representative images of P21 WT and *rd10* retinal sections co-immunostained for pAKT^{Ser473} (green) and PKC-α (red), magnification of B. Nuclei were stained with DAPI (blue). ONL, outer nuclear layer; OPL, outer plexiform layer; INL, inner nuclear layer; IPL, inner plexiform layer; GCL, ganglion cell layer. Scale bar: 60 µm in A, 31 µm in B and 20 µm in C.

4.2.2. Effect of inhibition of GSK-3 by administration of VP3.15

Previous studies of our group had shown pro-survival effects of several GSK-3 inhibitors in RP retinas *ex vivo* (Marchena et al., 2017). VP3.15 was selected for the following *in vivo* treatment, based on its favorable pharmacokinetic properties and IC_{50} (1.59 µM for GSK-3), as described in section 3.3.2. (Palomo et al., 2012). Importantly, VP3.15 crossed the blood-brain barrier after a single intraperitoneal injection (Medina-Rodríguez et al., 2017). In addition to its direct inhibitory effect on GSK-3, VP3.15 also acts as an allosteric inhibitor of cAMP-specific 3',5'-cyclic phosphodiesterease 7 (PDE7) (Redondo et al., 2012). However, PDE7 inhibition results in the increase of cAMP levels and protein kinase A (PKA) activation, which in turn converges on GSK-3 inhibition.

First, we examined the inhibitory capacity of VP3.15 on the GSK-3 activity. One of the *bona fide* GSK-3 substrates is β-catenin. GSK-3 phosphorylates β-catenin, targeting it to proteasomal degradation (Beurel et al., 2015). We assessed the effect of VP3.15 on β-catenin levels as a read-out of GSK-3 activity. As shown in Figure 4.16A and B, VP3.15 increased the amount of β-catenin in the microglia cell line N9 after 7 hours of exposure. This result confirms the GSK-3 inhibitory activity of VP3.15.

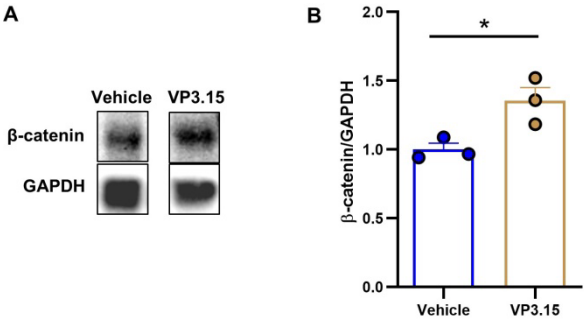

Figure 4.16. Effect of VP3.15 on β-catenin levels. N9 microglia cells were treated either with vehicle or with 10 µM VP3.15 for 7 h. **A.** Representative images of Western blots for β-catenin and GAPDH proteins. **B.** Densitometric analysis of membranes as those shown in A. Levels of β-catenin were normalized to those of GAPDH and relativized to vehicle levels (=1). Results represent the mean + SEM. $n = 3$. Statistical analysis was done with unpaired t test $*p < 0.05$.

We next analyzed the effect of GSK-3 inhibition on photoreceptor preservation. VP3.15 (10mg/kg) or vehicle were administrated to *rd10* mice by daily intraperitoneal injection from P15 to P32. Histological analysis of the retina at the end of the treatment displayed increased ONL/INL ratio of VP3.15-treated in comparison to control *rd10* mice, confirming the neuroprotective effect of VP3.15 over photoreceptors survival (Figure 4.17).

The pleiotropic activity of GSK-3 raised the question whether the administration of VP3.15 could be toxic to other retinal cells. To tackle this question, we analyzed the most internal layers of the retina, the INL and the GCL that are not affected in *rd10* mice at these degenerative stages (Barhoum et al., 2008). The number of bipolar cells, the most abundant cell type in the INL

(about 50% of the neurons), and that of ganglion cells, that account for 40% of the cells in the GCL (Jeon et al., 1998), were similar in the VP3.15 and vehicle-treated animals, ruling out toxic effects of the compound on those populations

These promising results prompted us to investigate whether longer treatment period preserved visual function in the *rd10* mouse model. *rd10* littermates received daily injection of either vehicle or VP3.15 from P15 to P46 inclusive. Visual function was assessed weekly by ERG between P25 and P46 in the laboratory of Dr. P. de la Villa (Universidad de Alcalá, Alcalá de Henares, Spain). The amplitude of ERG waves (a-mixed, b-mixed, b-photopic, and oscillatory potential [OP]) was significantly higher in VP3.15-treated than in vehicle-treated mice, indicating a prolongation of both rod- and cone-mediated vision function by VP3.15 (Appendix 2). Moreover, histological analysis of retinal cryosections at the end point of the study (P47) revealed a greater relative ONL thickness in VP3.15- versus vehicle-treated retinas (Figure 4.19A and B). Immunostaining for rhodopsin to label rod outer segments confirmed the partial preservation of rod outer segments in VP3.15-treated retinas, while they were barely present in vehicle-treated retinas (Figure 4.19A and B). Similarly, L/M-opsin immunostaining revealed longer cone outer segments in VP3.15- versus vehicle-treated *rd10* retinas (Figure 4.19A and B). These results provided further evidence for the VP3.15 neuroprotective properties.

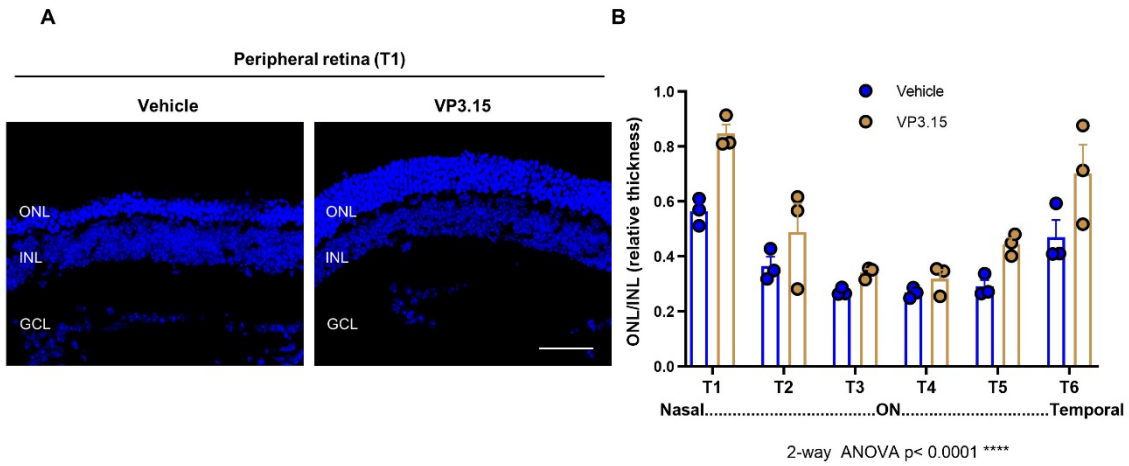

Figure 4.17. Effect of VP3.15 on photoreceptor preservation. *rd10* mice received daily an intraperitoneal injection of vehicle or VP3.15 from P15 to P32 and the retinas were analyzed one day after the last injection (P33). **A.** Representative images of P33 retinal sections from vehicle- and VP3.15-treated *rd10* mice. Nuclei were stained with DAPI (blue). ONL, outer nuclear layer; INL, inner nuclear layer. Scale bar: 45 µm. **B.** ONL and INL thickness were measured in equatorial sections corresponding to 6 regions of the retina, following a nasotemporal sequence (T1-T6; see material and methods). Dots represent individual mice and bars show the mean + SEM. *n* = 3 mice, 3 sections per retina, 3 measurements per region and section. ON, optic nerve. ****$p < 0.0001$ (2-way ANOVA)**.**

Given the role of GSK-3 in regulating the balance between pro- and anti-inflammatory signals (Jope et al., 2017), we analyzed whether GSK-3 inhibition may affect the retinal inflammatory

response associated to RP. NF-κB is a key regulator of the inflammatory response by enabling the transcription of the genes encoding many pro-inflammatory cytokines (Liu et al., 2017). We therefore evaluated the VP3.15 effect on NF-κB activation by Western blot. Phosphorylation of NF-κB in Ser 536 (pNF-κB^{Ser536}) is an indicator of activation (Christian et al., 2016). *rd10* retinal explants incubated with VP3.15 (10 µM) for 16 hours displayed decreased levels of pNF-κB^{Ser536} in comparison with those of *rd10* retinas incubated with vehicle (Figure 4.20A and B). The anti-inflammatory effect was confirmed in *in vivo* studies carried out by other members of the group (see Appendix 2). Briefly, VP3.15 treatment significantly decreased the expression of *Il1b*, *A2m* and *Gfap*. A similar trend was observed for *Tnf*.

All together, these results indicate that the GSK-3 inhibitor VP3.15 can delay RP progression in *rd10* mice and underscore the potential use of GSK-3 inhibitors in the treatment of retinal neurodegenerative diseases. Also, this study validates the strategy of repurposing drugs and targets that were studied in the context of other neurodegenerative diseases to search for novel RP therapies.

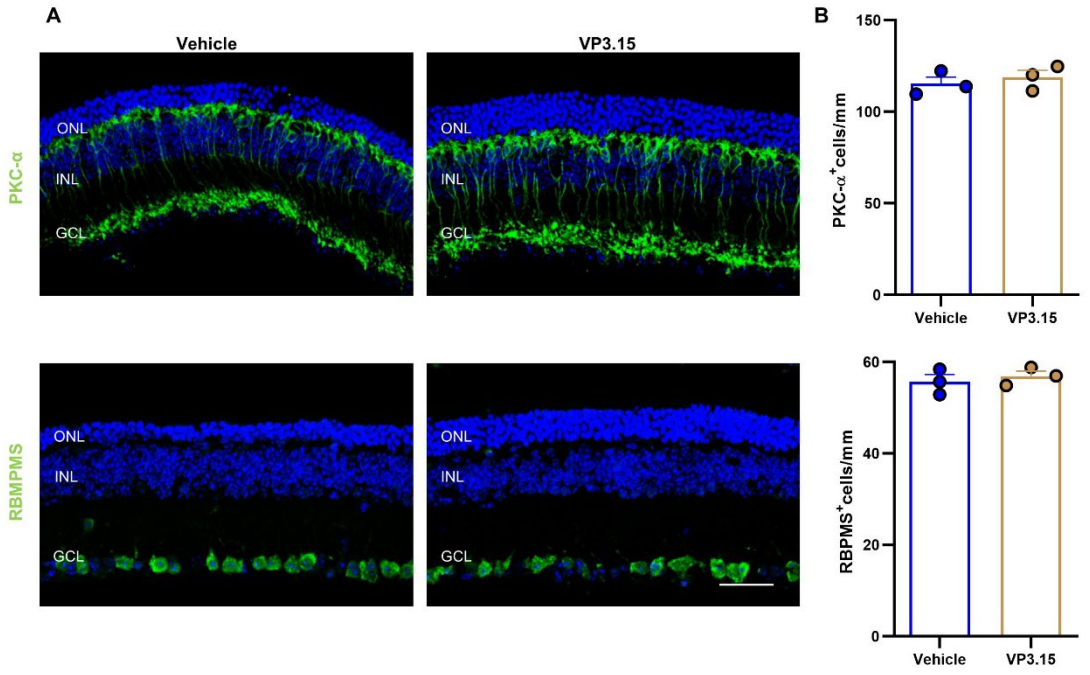

Figure 4.18. Effect of VP3.15 treatment on rod-bipolar and ganglion cells. *rd10* mice received daily an intraperitoneal injection of vehicle or VP3.15 from P15 to P32 and the retinas were analyzed one day after the last injection (P33). **A.** Representative images of P33 retinal sections from vehicle- and VP3.15-treated *rd10* mice, immunostained for PKC-α or RNA-binding protein with multiple splicing (RBPMS) to label rod-bipolar or ganglion cells respectively (green). Nuclei were stained with DAPI (blue). **B.** The number of PKCα- and RBPMS-positive cells were scored in equatorial sections corresponding to 6 regions of the retina, following a nasotemporal sequence (T1–T6; methods). The number of cells in these areas normalized by the quantified retinal section length is represented for each mouse. Dots represent individual mice and bars show the mean + SEM. n = 3 mice, 3 sections per retina, 3 measurements per region and section. ONL, outer nuclear layer; INL, inn nuclear layer; GCL, ganglion cell layer. Scale bar: 38 µm.

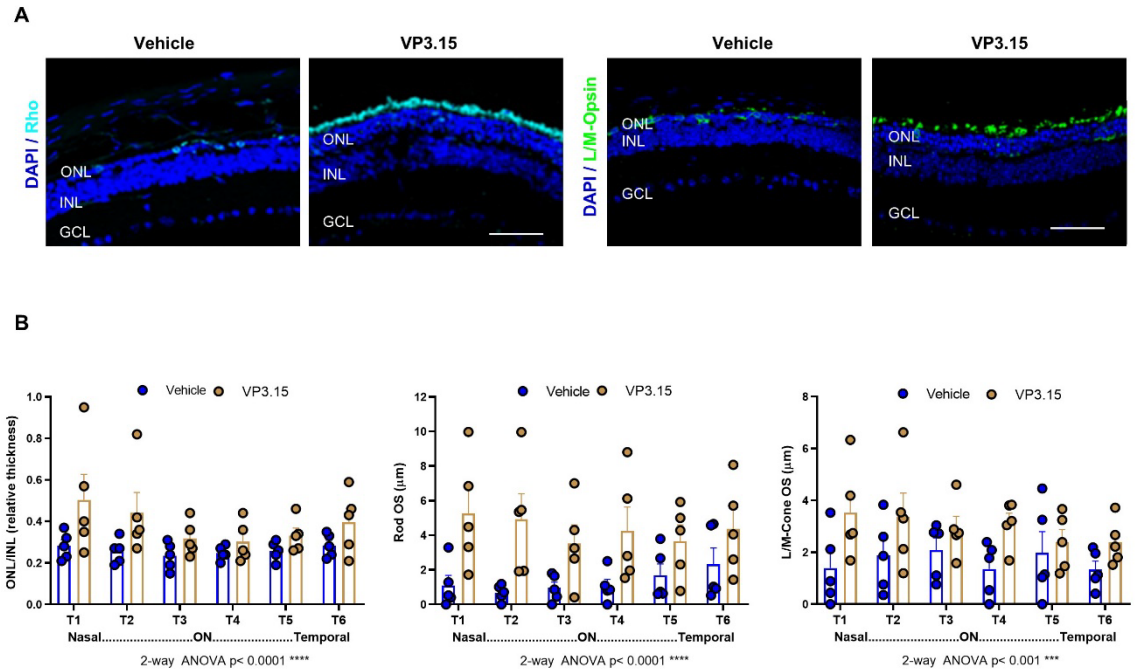

Figure 4.19. Effect of long-term VP3.15 administration on photoreceptor cell preservation. *rd10* mice received daily intraperitoneal injections of vehicle or VP3.15 from P15 to P45 and retinas of those animals were analyzed at P47. Retinal sections were immunostained to assess photoreceptor cell structure. **A.** Representative images of P47 retinal sections from vehicle- and VP3.15-treated rd10 mice immunostained for rhodopsin (cyan) and L/M-opsin (green). Nuclei were stained with DAPI (blue). OS, outer segments; ONL, outer nuclear layer; INL, inner nuclear layer; GCL, ganglion cell layer. Scale bar: 56 µm. **B.** ONL and INL thickness and the length of rod and cone outer segments were measured in equatorial sections corresponding to 6 regions of the retina, following a nasotemporal sequence (see methods section). Dots represent individual mice and bars display the mean for each group. n = 5 mice, 3 sections per retina, 3 measurements per region and section. ON, optic nerve. 2-way ANOVA was applied for statistical analysis ***p < 0.001, **** p < 0.0001.

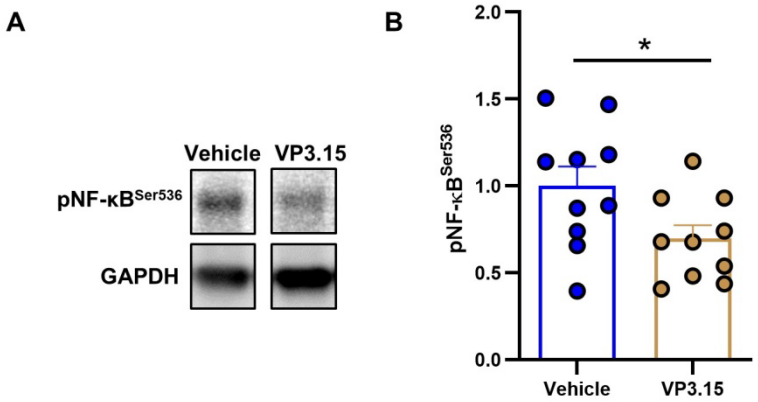

Figure 4.20. Effect of VP3.15 on NF-κB activation. Contralateral P22 *rd10* retinas were cultured either in the absence (vehicle) or in the presence of 3.2 µM VP3.15 for 16 h. **A.** Representative images showing Western blots of protein extracts of those retinal extracts for pNF-κB^{Ser536} and GAPDH**. B.** Densitometric analysis of membranes as those shown in A. Levels of pNF-κB^{Ser536} were normalized to those of GAPDH and relativized to vehicle levels (=1). Dots represent individual retinas and bars show the mean for each group (+SEM). n= 10 retina per group. Statistical analysis was performed applying paired t-test *p < 0.05.

4.3. Toll-like receptors in the context of animal models of RP

As explained in the introduction, besides being the first line of defense against pathogens, TLRs are sensors of tissue damage. Activation of TLRs by DAMPs triggers an inflammatory response that may affect the magnitude of the damage or the development of the disease. To tackle whether TLRs are involved in the progression of RP, we first analyzed *Tlr* gene expression in WT and *rd10* retinas along the course of the disease.

4.3.1. Expression of TLRs and TLR adaptor proteins in WT and RP retinas

We examined by qPCR the expression of *Tlr1* to *Tlr9,* the conserved *Tlr* genes between humans and mice (Kawai and Akira, 2009), from P14, prior to the onset of the degenerative process, to P21, when the photoreceptor loss is evident. In the WT retina, the expression of *Tlr2*, *Tlr3, Tlr4, Tlr5*, *Tlr7* and *Tlr9* did not change along the studied period. However, the levels of *Tlr1* and *Tlr6* expression decreased progressively from P14 to P21 (Figure 4.21A). In the *rd10* retina, all of the studied *Tlr* genes increased their expression at P21 in comparison to the expression in WT retinas at the same age. Nevertheless, this increase is different for each *Tlr* gene. In comparison to the expression of the WT at P21, the expression of *Tlr1*, *Tlr2* and *Tlr9* increased 30, 36 and 16 times respectively, the expression of *Tlr3*, *Tlr4, Tlr6* and *Tlr7* increased 5, 9, 6.5 and 8.5 times, while the expression of *Tlr5* only increased 2 times. *Tlr8* expression was below the limit of detection in WT animals but could be detected in *rd10* animals at P21 (data not shown), arguing that its expression is also increased in the *rd10* retina. In addition, it is worth mentioning that the increased expression of the different *Tlr* genes coincided with the increase of the gene expression of proinflammatory molecules such as TNF-α and IL-1β, *Tnf* and *Il1b* genes (Figure 4.21B).

We next analyzed the expression of the TLR adaptor protein genes (described in section 1.8). Similar to *Tlr1* and *Tlr6*, in the WT retina, the expression of *Tirap*, *Ticam1* (TRIF protein gene) and *Ticam2* (TRAM protein gene) significantly decreased with age from P14 to P18 (5-, 2- and 3-fold decrease respectively) and this decrease is maintained from P18 to P21 (Figure 4.22A and B). On the contrary, *Myd88* gene expression did not change with age in the WT retina at the analyzed time-points. In the *rd10* retina, the expression of the four adaptor proteins increased at P21 in comparison with the WT retina at the same age. The expression of *Myd88* and *Tirap* at P21 in the *rd10* retina is 4 times higher than their expression in the WT retina at the same age. In addition, *Ticam1* and *Ticam2* expression increased 3 and 9 times respectively in the *rd10* retina at P21 in comparison with the WT retina at P21.

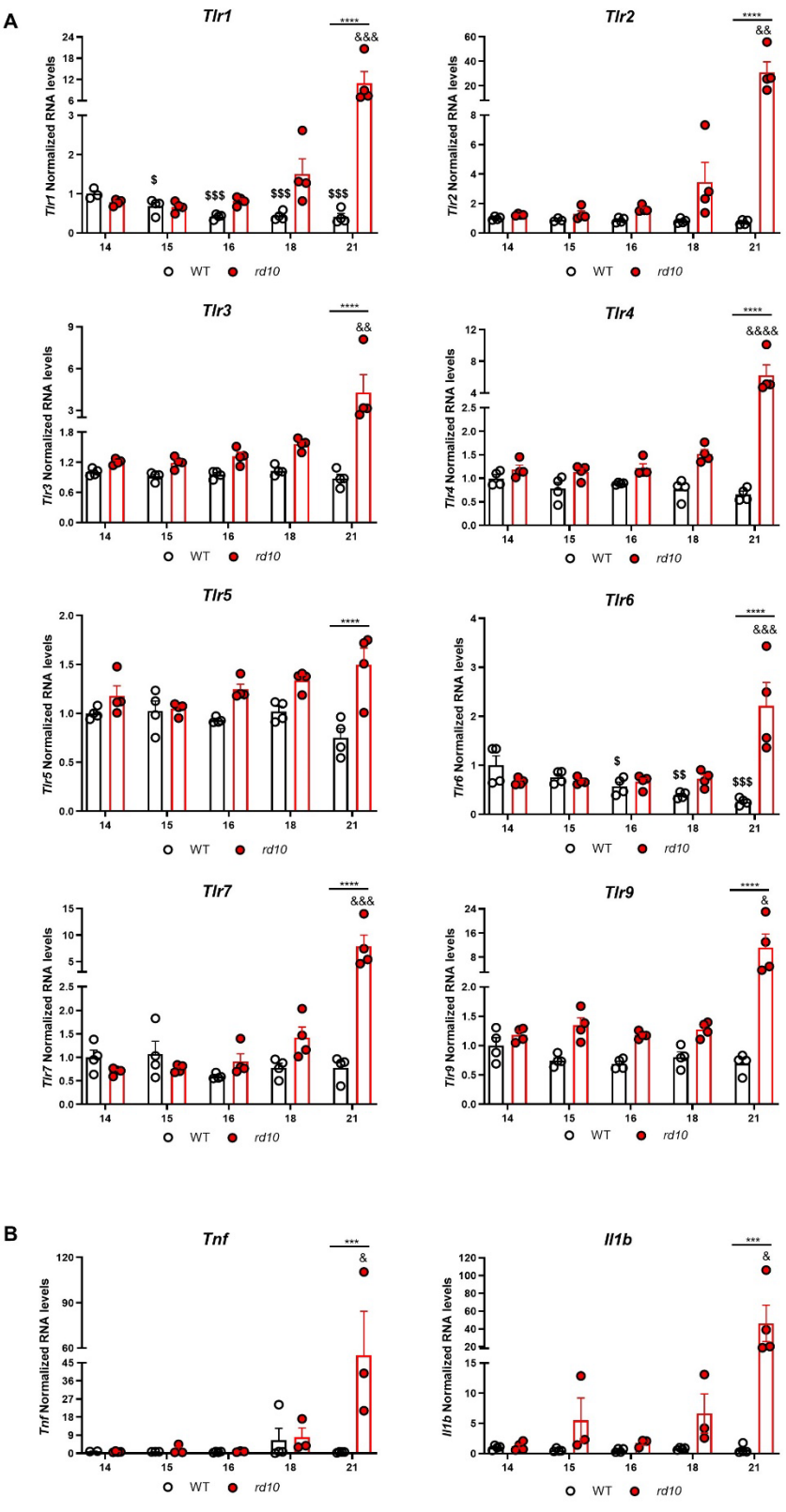

Figure 4.21. Expression of *Tlr* genes in WT and *rd10* retinas. The expression of *Tlr1*, *Tlr2*, *Tlr3*, *Tlr4*, *Tlr5*, *Tlr6*, *Tlr7*, and *Tlr9* genes (**A**) and that of the proinflammatory cytokines *Tnf* and *Il1b* (**B**) was analyzed by qPCR in WT and *rd10* retinas at the indicated ages. Dots represent individual animals, while bars represent the mean for each group (+SEM). n=3-4 animals per group. The levels of the transcripts were normalized to the *Tbp* RNA and relativized to WT P14 levels (=1). One-way ANOVA with Dunnett's post-test was applied to analyze differences in WT retinas between the *Tlr* expression at the different time points with the initial expression at P14 $$$ $p < 0.001$; $$ $p < 0.01$; $ $p < 0.05$. Similarly, one-way ANOVA with Dunnett's post-test was applied to analyze differences between the different time-points with P14 in *rd10* animals. &&&& $p < 0.0001$; &&& $p < 0.001$; && $p < 0.01$; & $p < 0.05$. 2-way ANOVA was used to compare *Tlr* expression between WT and *rd10* retinas along ages, followed by Sidak's multiple comparison test, as significant interactions were found between age and genotype of the mice. **** $p < 0.0001$; *** $p < 0.001$.

The results of the gene expression analysis showed upregulation of TLRs and adaptor proteins in the *rd10* retina associated to the retinal inflammatory response and photoreceptor degeneration. These results suggest that TLRs participate in the *rd10* degenerative process. To elucidate the role of TLRs in RP progression we focused on TLR2 and TLR4, two plasma membrane TLRs with prominent induction in the *rd10* retina. TLR2 was selected because it is the TLR with highest increase of expression (36-fold). TLR4 was selected because it is the most studied TLR in brain degenerative conditions (see section 1.8) and also shows a robust increase of expression (9-fold).

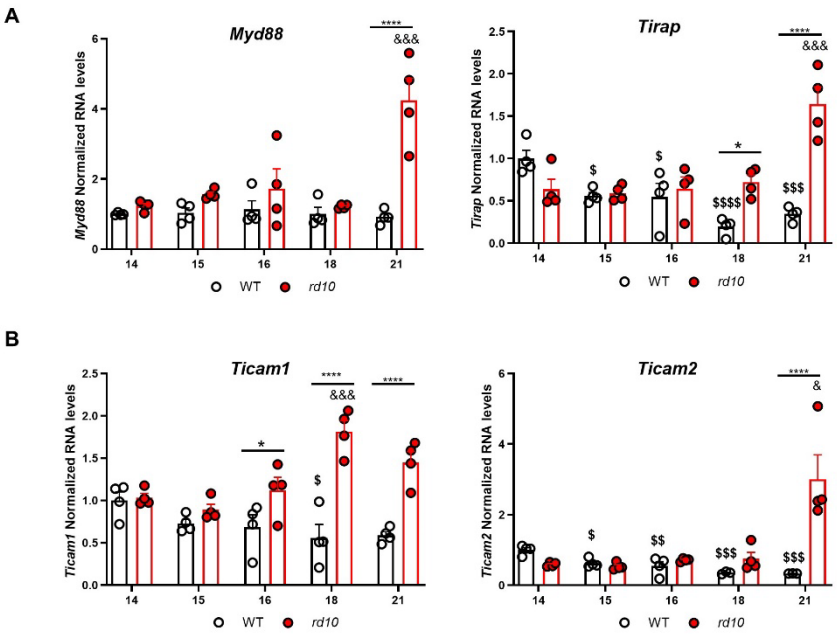

Figure 4.22. Expression of TLR adaptor genes in WT and *rd10* retinas. A, B. The expression of the adaptors of the MyD88-dependent pathway, *Myd88* and *Tirap* (A) and of the MyD88-independent pathway *Ticam1* (TRIF protein) and *Ticam2* (TRAM protein) (B) was analyzed by qPCR in WT and *rd10* retinas at the indicated ages (days). Dots represent individual animals, while bars represent the mean for each group (+SEM). n=3-4 animals per group. Data were normalized to the *Tbp* RNA and relativized to WT levels at P14 (=1). One-way ANOVA with Dunnett's post-test was applied to analyze differences in WT animals between the TLR expression at the different time points with the initial expression at P14 $$$$ p< 0.0001; $$$ p< 0.001; $$ p< 0.01; $ p< 0.05. Also, one-way ANOVA with Dunnett's post-test was applied to analyze differences between the different time-points with P14 in *rd10* animals. &&& p< 0.001; & p< 0.05. In order to compare TLR expression between WT and *rd10* animals at the different time-points 2-way ANOVA was applied. As significant interactions were found between age and genotype of the mice, Sidak's multiple comparison test was applied *p< 0.05; ***; p< 0.001; **** p< 0.0001.

We then analyzed whether the increase of expression of TLR2 and TLR4 and TLR adaptor proteins was restricted to *rd10* or if this increase could be observed in other RP mouse models. Therefore, we analyzed the expression of *Tlr2*, *Tlr4* and *Tlr* adaptor protein genes in WT versus P23H retinas at 3, 4 and 6 months (Figure 4.23). We observed that *Tlr2* and *Tlr4* expression increased in P23H respect to WT retinas. This increase was especially evident at 4 months: the expression of *Tlr2* and *Tlr4* was respectively 8 and 4 times higher in P23H respect to WT retinas. The gene expression of the *Tlr* adaptor proteins was also increased in P23H versus WT retinas,

particularly at 4 months when the expression was between 1.5 to 3 times higher. We did not observe gene expression changes in any case in WT retinas between the time-points. In a next step, we took advantage of the availability of *Tlr2* and *Tlr4* null mice and RP mouse models to generate double mutants and analyze their influence on RP progression.

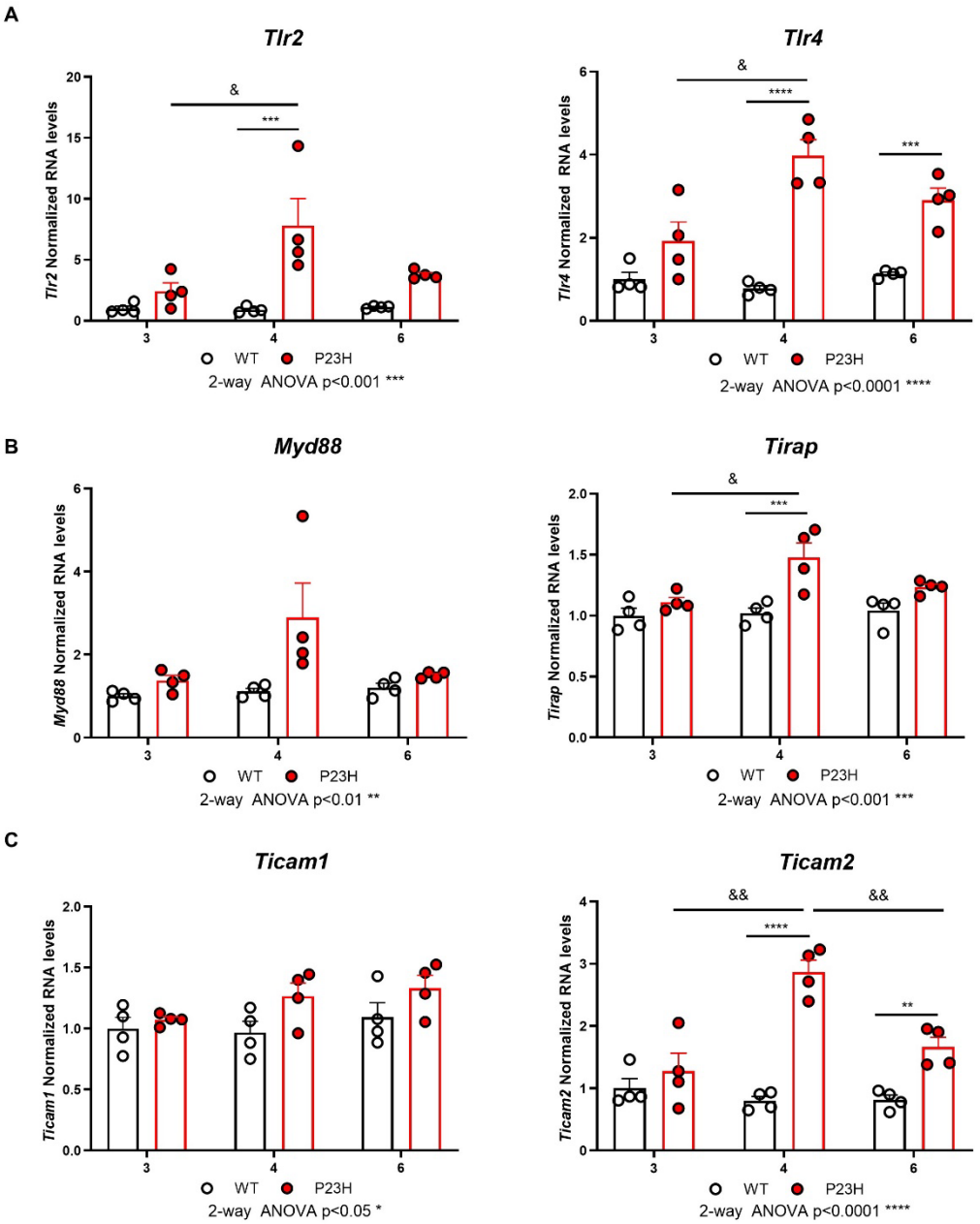

Figure 4.23. Expression of *Tlr2*, *Tlr4* and TLR adaptor genes in WT and P23H retinas. A, B, C. The expression of the *Tlr2* and *Tlr4* (A), of the adaptors of the MyD88-dependent pathway, *Myd88* and *Tirap* (B) and of the MyD88-independent pathway *Ticam1* (TRIF protein) and *Ticam2* (TRAM protein) (C) was analyzed by qPCR in WT and P23H retinas at the indicated ages (months). Dots represent individual animals, while bars represent the mean for each group (+SEM). n=4 animals per group. Data were normalized to the *Tbp* RNA and relativized to WT levels at 3 months (=1). One-way ANOVA with Tukey's post-test was applied to analyze differences in WT animals between the different time points. Also, one-way ANOVA with Tukey's post-test was applied to analyze differences between the different time-points. && $p< 0.01$; & $p< 0.05$. In order to compare TLR expression between WT and P23H animals at the different time-points 2-way ANOVA was applied. As significant interactions were found between age and genotype of the mice, Sidak's multiple comparison test was applied **$p< 0.01$; ***; $p< 0.001$; **** $p< 0.0001$.

4.3.2. Analysis of TLR4 deficiency in animal models of RP

Our first approach was to study the effect of a single *Tlr4* alelle deletion on the *rd10* mice (*rd10*:*Tlr4*$^{+/-}$) visual function. First, we confirmed a 50% reduction of *Tlr4* RNA levels in the *rd10*:*Tlr4*$^{+/-}$ respect to *rd10*:*Tlr4*$^{+/+}$ retinas (Figure 4.24). We then analyzed whether the deletion of a single *Tlr4* alelle had any effect on *rd10* visual function. ERG recordings in dark- and light-adapted conditions were performed at P25. *rd10*:*Tlr4*$^{+/-}$ mice displayed less prominent ERG waves than their *rd10*:*Tlr4*$^{+/+}$ littermates (Figure 4.25A and B). The amplitudes of the most relevant waves involving rod and cone responses (b-mixed) and cone-responses (b-photopic and flicker) were significantly decreased in the *rd10*:*Tlr4*$^{+/-}$. The analysis of the a-wave, that could only be quantified for the highest light intensity in scotopic conditions, did not show significant differences between genotypes. These results suggest that *Tlr4*-happloinsufficiency accelerates visual function loss in the *rd10* model.

We then examined whether the functional effects described above correlate with histological differences. Measurement of the ONL thickness did not show significant differences between the *rd10*:*Tlr4*$^{+/-}$ and the *rd10*:*Tlr4*$^{+/+}$ mice (Figure 4.26A and B). However, the length of rod and S-cone OS was decreased in *rd10*:*Tlr4*$^{+/-}$ respect to *rd10*:*Tlr4*$^{+/+}$ mice (Figure 4.26A and B). The length of the L/M-cone OS was similarly diminished although it did not reach statistical significance (p=0.12). These results showed that *Tlr4*-haploinsufficiency in *rd10* compromises photoreceptor integrity, although it does not affect their survival.

Altogether, these functional and histological studies suggest that *Tlr4*-haploinsufficiency is detrimental for RP progression in the *rd10* model and argue for a TLR4 protective role during the disease progression.

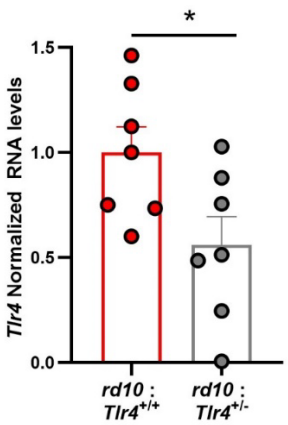

Figure 4.24. Expression of *Tlr4* in *rd10*:*Tlr4*$^{+/+}$ and *rd10*:*Tlr4*$^{+/-}$ retinas. RT-qPCR of *rd10*:*Tlr4*$^{+/+}$ and *rd10*:*Tlr4*$^{+/-}$ retinas at P26. The levels of *Tlr4* RNA were normalized to the *Tbp* RNA levels and relativized to *rd10*:*Tlr4*$^{+/+}$ levels (= 1). Dots represent individual mice and bars represent the mean for each group (+SEM). Unpaired t-test was applied for statistical analysis. *p<0.05.

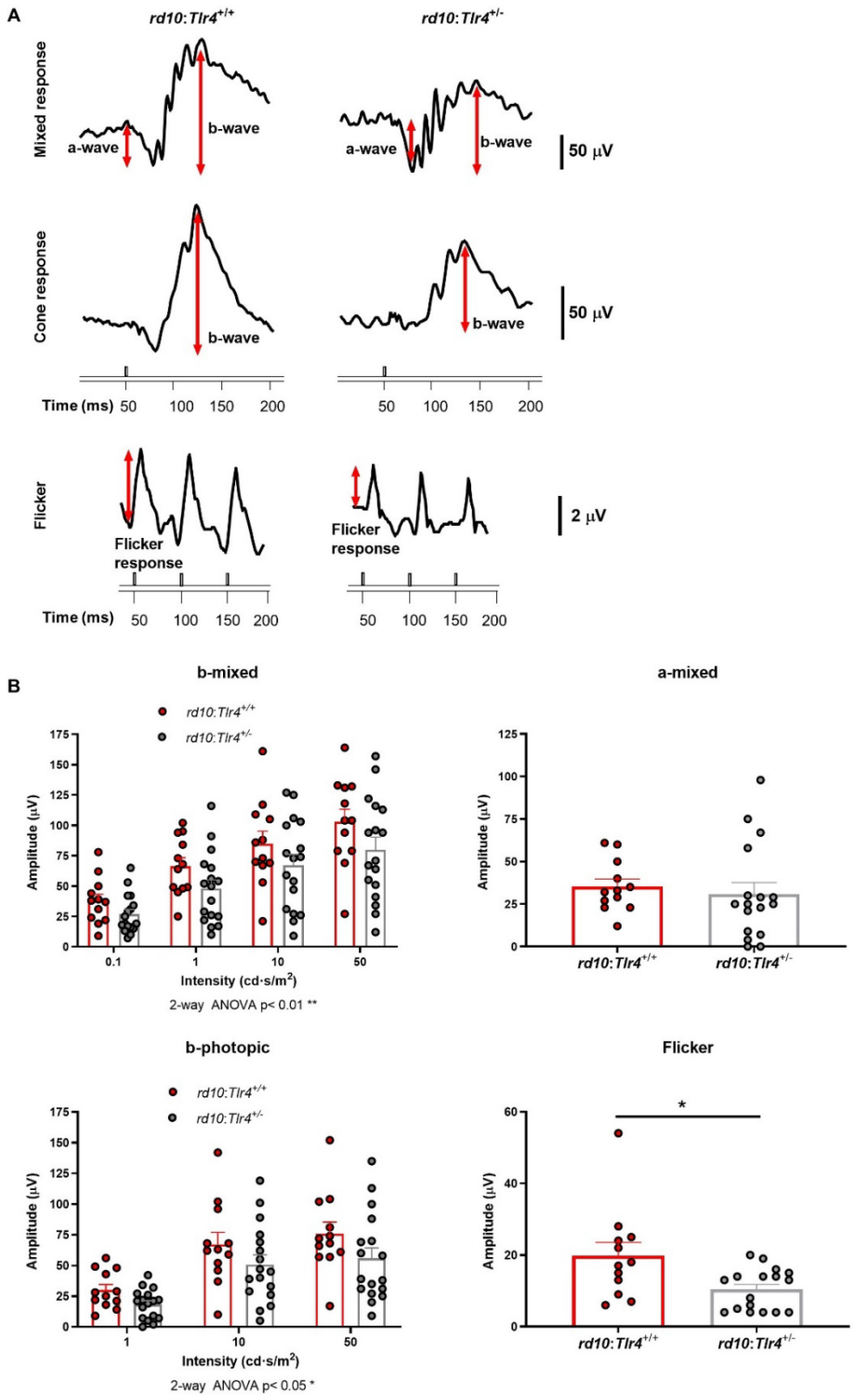

Figure 4.25. ERG response of *rd10*:*Tlr4*$^{+/+}$ and *rd10*:*Tlr4*$^{+/-}$ mice. A. Representative ERG trace recordings responses of *rd10*:*Tlr4*$^{+/+}$ and *rd10*:*Tlr4*$^{+/-}$ at P25 in response to a 50 cd·s/m^2 stimulus. Values of the scale bar are indicated in the figure. **B.** Graphs show averaged ERG wave amplitudes, plotted as a function of light stimuli. Amplitudes of the rod and cone mixed response (a- and b-mixed) were recorded under scotopic conditions after overnight adaptation to darkness. The b-mixed wave was measured for all of the light stimuli, while the mixed a-mixed wave could be measured only for the highest stimulus. Cone amplitudes (b-photopic and flicker) were recorded after 5 minutes of light-adaptation (30 cd/m^2 background light) under photopic conditions. Dots represent individual mice and bars represent the mean for each group (+SEM). n=12-17 mice per group. 2-way ANOVA was applied for statistical analysis of mixed and b-photopic waves, while unpaired t-test was applied for a-mixed wave and flicker response. **p<0.01; *p<0.05.

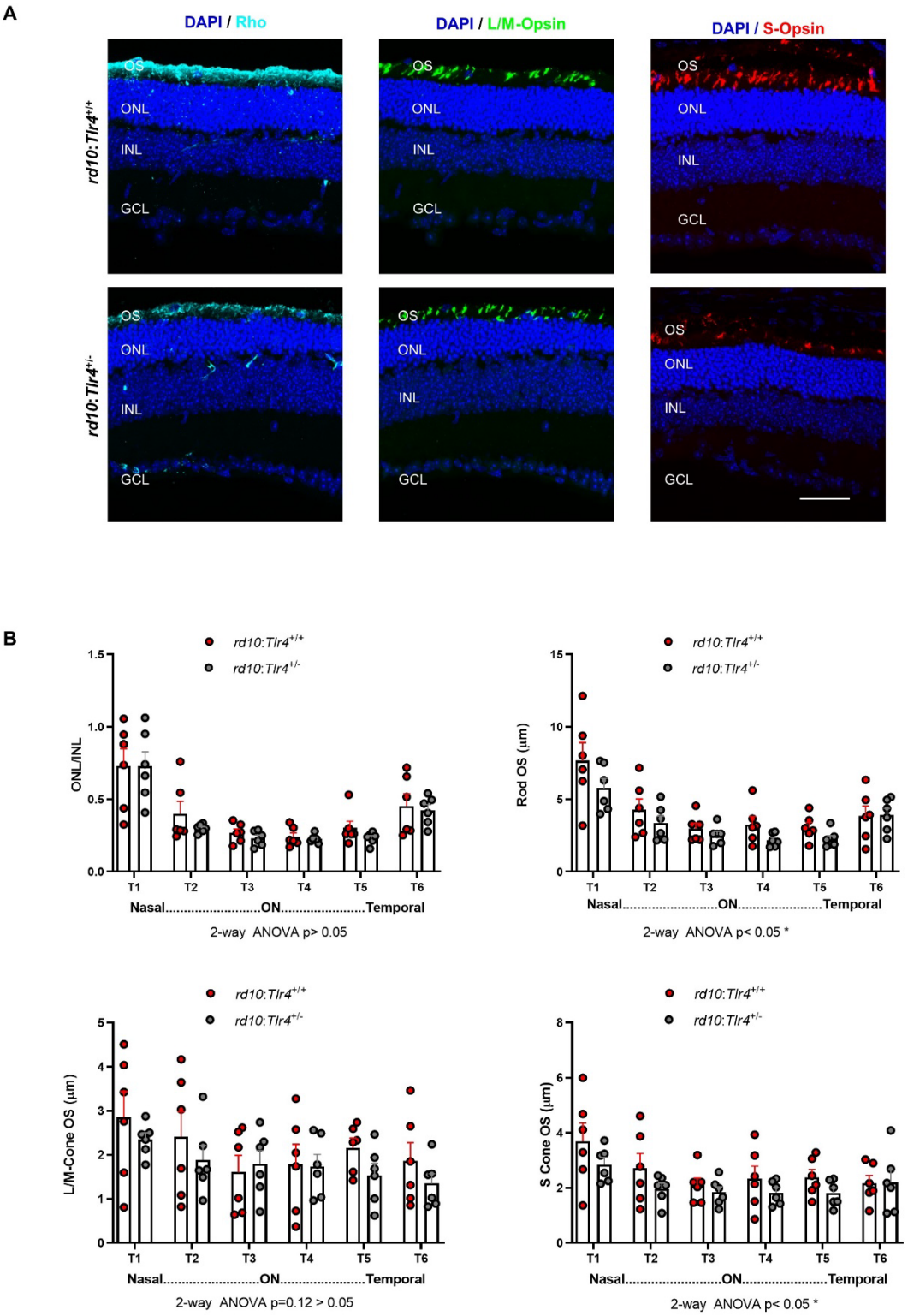

Figure 4.26. Analysis of the retinal structure of *rd10*:*Tlr4*$^{+/+}$ and *rd10*:*Tlr4*$^{+/-}$ mice. A. Representative images of P26 retinal cryosections (T1 area) from *rd10*:*Tlr4*$^{+/+}$ and *rd10*:*Tlr4*$^{+/-}$ immunostained for rhodopsin (cyan), S-opsin (red) and L/M-opsin (green). Nuclei were stained with DAPI (blue). OS, outer segment, ONL, outer nuclear layer; INL, inner nuclear layer and GCL, ganglion cell layer. Scale bar: 38 µm. **B.** ONL and INL thickness and the length of rod and cone outer segments were measured in equatorial sections corresponding to 6 regions of the retina, following a nasotemporal sequence (see methods section). Dots represent individual mice and bars display the mean for each group. n = 6 mice, 3 sections per retina, 3 measurements per region and section. ON, optic nerve. 2-way ANOVA was applied for statistical analysis. *p < 0.05.

To assess whether the *Tlr4*-haploinsuficency phenotype is aggravated by the complete deletion of *Tlr4*, we compared *rd10*:*Tlr4*$^{+/-}$ with *rd10*:*Tlr4*$^{-/-}$ littermates. ERG recordings in dark- and light-adapted conditions were performed at P39. The cone responses (b-photopic wave and flicker) were significantly lower in *rd10*:*Tlr4*$^{-/-}$ mice (Figure 4.27). In the same direction, a trend was also observed toward a reduction of the b-mixed amplitude in the *rd10*:*Tlr4*$^{-/-}$ mice (p=0.0961) (Figure 4.27). The amplitude of the a-mixed wave was similar for both genotypes. Analysis of the retinal structure showed no significant changes in the ONL thickness between the *rd10*:*Tlr4*$^{+/-}$ and the *rd10*:*Tlr4*$^{-/-}$ mice (Figure 4.28). However, the length of rod and L/M-cone was significantly decreased in *rd10*:*Tlr4*$^{-/-}$ in comparison with those of their *rd10*:*Tlr4*$^{+/-}$ counterparts (Figure 4.28). Likewise, a trend was also observed toward reduction of the S-cone OS length in the *rd10*:*Tlr4*$^{-/-}$ mice (p=0.067) (Figure 4.28).

These results demonstrate that complete elimination of TLR4 expression exacerbates the detrimental phenotype of TLR4 partial loss in the *rd10*. Overall, these studies suggest that TLR4 plays a protective role and hinders the progression of RP in the *rd10* model.

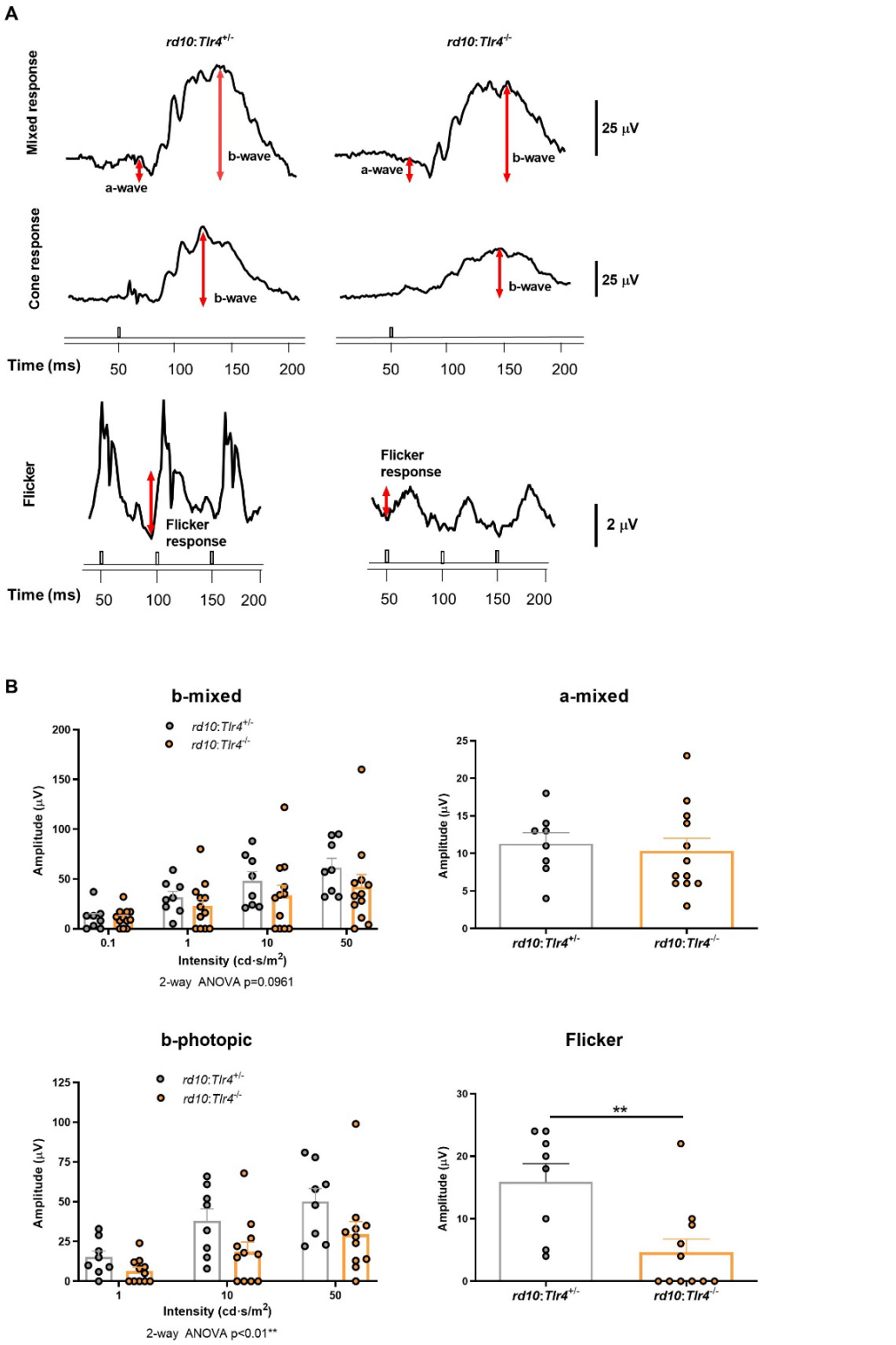

Figure 4.27. Analysis of ERG response of *rd10*:*Tlr4*$^{+/-}$ and *rd10*:*Tlr4*$^{-/-}$ mice. A. Representative ERG trace recordings responses of *rd10*:*Tlr4*$^{+/-}$ and *rd10*:*Tlr4*$^{-/-}$ at P39 in response to a 50 cd·s/m^2 light stimulus. The values of the scale bar are shown in the figure. **B.** Graphs show averaged ERG wave amplitudes, plotted as a function of light stimuli. Amplitudes of rod and cone mixed response (a- and b-mixed) were recorded under scotopic conditions after overnight adaptation to darkness. The mixed b-wave was measured for all of the light stimuli, while the mixed a-wave could be measured only for the highest stimulus. Cone amplitudes (b-photopic and flicker) were recorded after 5 minutes of light-adaptation (30 cd/m^2 background light) under photopic conditions. Dots represent individual mice and bars represent the mean for each group (+SEM). n=8-11 animals per group. 2-way ANOVA was applied for statistical analysis of mixed and b-photopic waves, while unpaired t-test was applied for a-mixed wave and flicker response. **p<0.01.

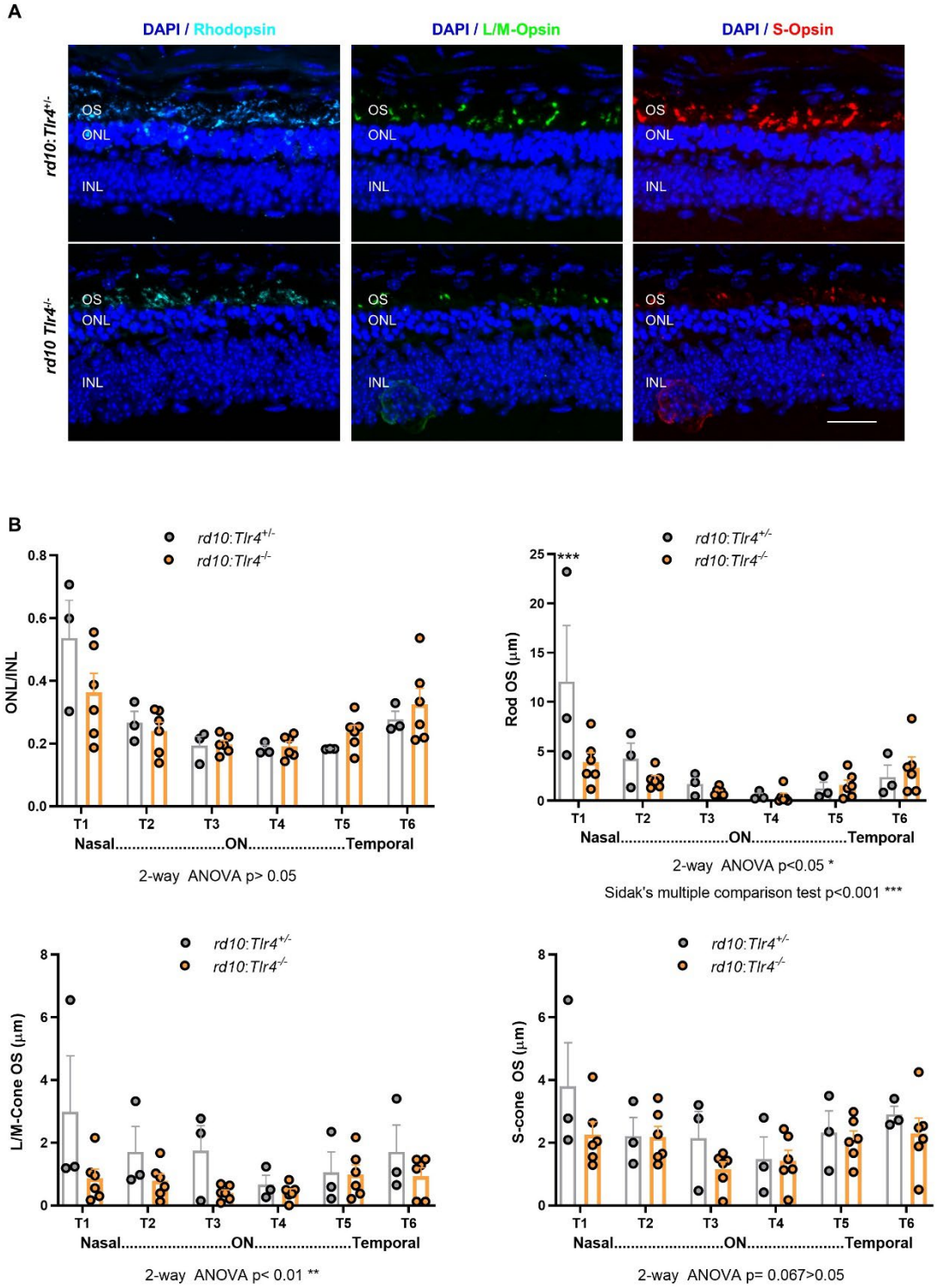

Figure 4.28. Retinal structure of *rd10*:*Tlr4*$^{+/-}$ and *rd10*:*Tlr4*$^{-/-}$ retinas. A. Representative images of retinal cryosections (T1 area) of *rd10*:*Tlr4*$^{+/-}$ and *rd10*:*Tlr4*$^{-/-}$ at P46 immunostained for rhodopsin (cyan), L/M opsin (green) and S-opsin (red). Nuclei were stained with DAPI (blue). OS, outer segment; ONL, outer nuclear layer; INL, inner nuclear layer and GCL, ganglion cell layer. Scale bar: 27 µm. **B.** ONL and INL thickness and the length of rod and cone outer segments were measured in equatorial sections corresponding to 6 regions of the retina, following a nasotemporal sequence (see methods section). Dots represent individual mice and bars display the mean for each group. n = 3-6 mice, 3 sections per retina, 3 measurements per region and section. ON, optic nerve. 2-way ANOVA was applied for statistical analysis and Sidak's multiple comparisons test was applied in the case of interaction between variables. ***p<0.001; ** p <0.01; *p <0.05.

To address whether TLR4 positive effects are restricted to the *rd10* mouse model or could be extrapolated to other RP models, we analyzed the effect of *Tlr4* deletions in a different RP model, the $Rho^{P23H/+}$ (P23H) mouse model. The P23H carries a dominant mutation in the rhodopsin gene that in heterozygosity causes a slow-pace photoreceptor degeneration, about half of the rods are lost at 4 months of age and cone retinal function is maintained for about a year (Sakami et al., 2011).

As a first approach, the electroretinographic response of P23H:*Tlr4*$^{+/-}$ and P23H:*Tlr4*$^{-/-}$ littermates was analyzed at 2 and 4 months. The amplitude of b-mixed wave (rod and cone response) of the P23H:*Tlr4*$^{-/-}$ mice was already lower at 2 months (early stage of the degeneration process) in comparison to P23H:*Tlr4*$^{+/-}$ mice. This decrease was accentuated at 4 months when approximately 50% of the rods are lost (Figure 4.29; Figure 4.30). Moreover, the amplitudes of the a-mixed (rod and cone response) and the b-photopic (cone response) waves were similar between the two genotypes at 2 months but significantly reduced in the P23H:*Tlr4*$^{-/-}$ at 4 months. No differences were observed in the flicker response at either analyzed ages. Histological analysis of those animals at 4 months showed greater loss of photoreceptors, as evidenced by the decrease of the ONL/INL ratio of the P23H:*Tlr4*$^{-/-}$ mice compared to that of P23H:*Tlr4*$^{+/-}$ mice (Figure 4.31). In addition, the length of the rod OS showed a trend ($p=0.08$) to shorten in the P23H:*Tlr4*$^{-/-}$. No differences were found in the length of the cone OS. These results showed that complete abolition of *Tlr4* expression increses photoreceptor demise and accelerates visual function loss in the P23H, and confirm our previous findings in the *rd10* mouse.

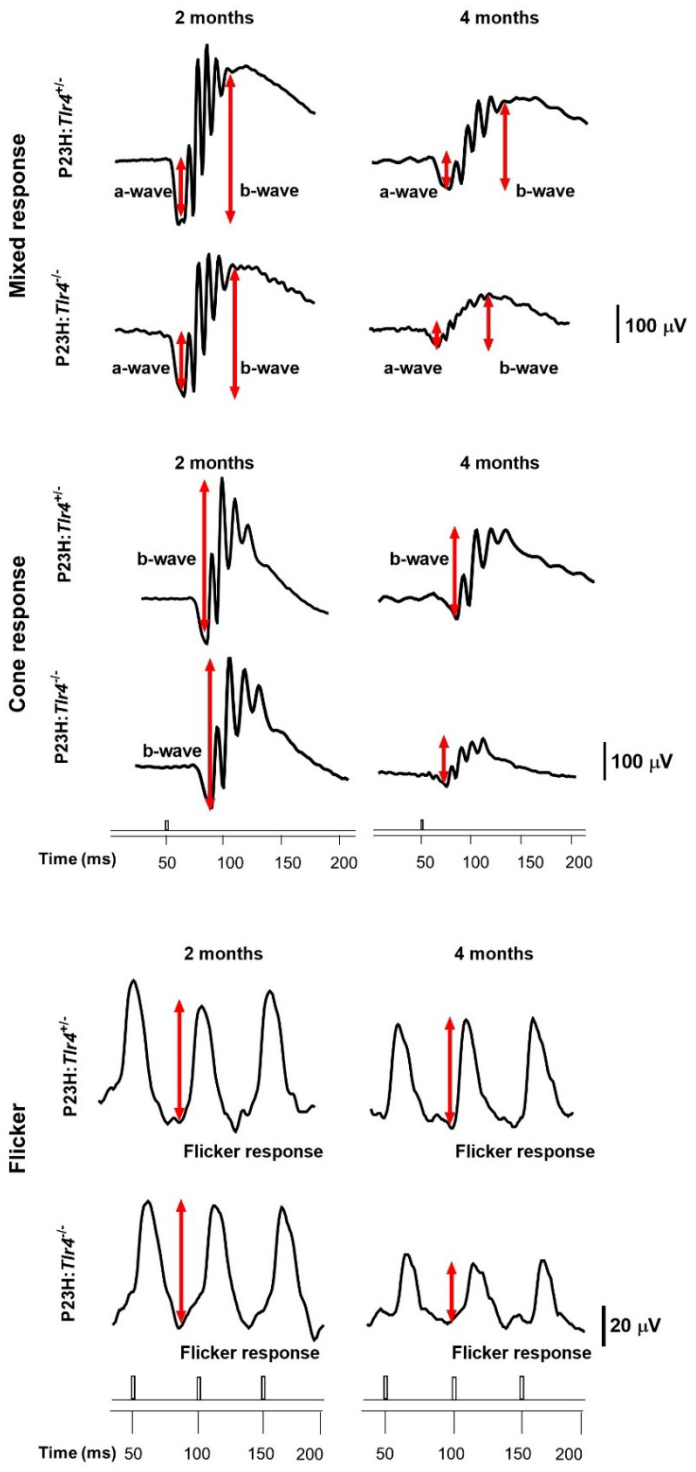

Figure 4.29. ERG recordings of P23H:*Tlr4*$^{+/-}$ and P23H:*Tlr4*$^{-/-}$ P23H mice. Representative ERG trace recordings of P23H:*Tlr4*$^{+/-}$ and P23H:*Tlr4*$^{-/-}$ at 2 and 4 months in response to stimuli of 50 cd·s/m^2 (a- and b-mixed responses) and 10 cd·s/m^2 (cone and flicker responses). The values of the scale bar are depicted in the figure.

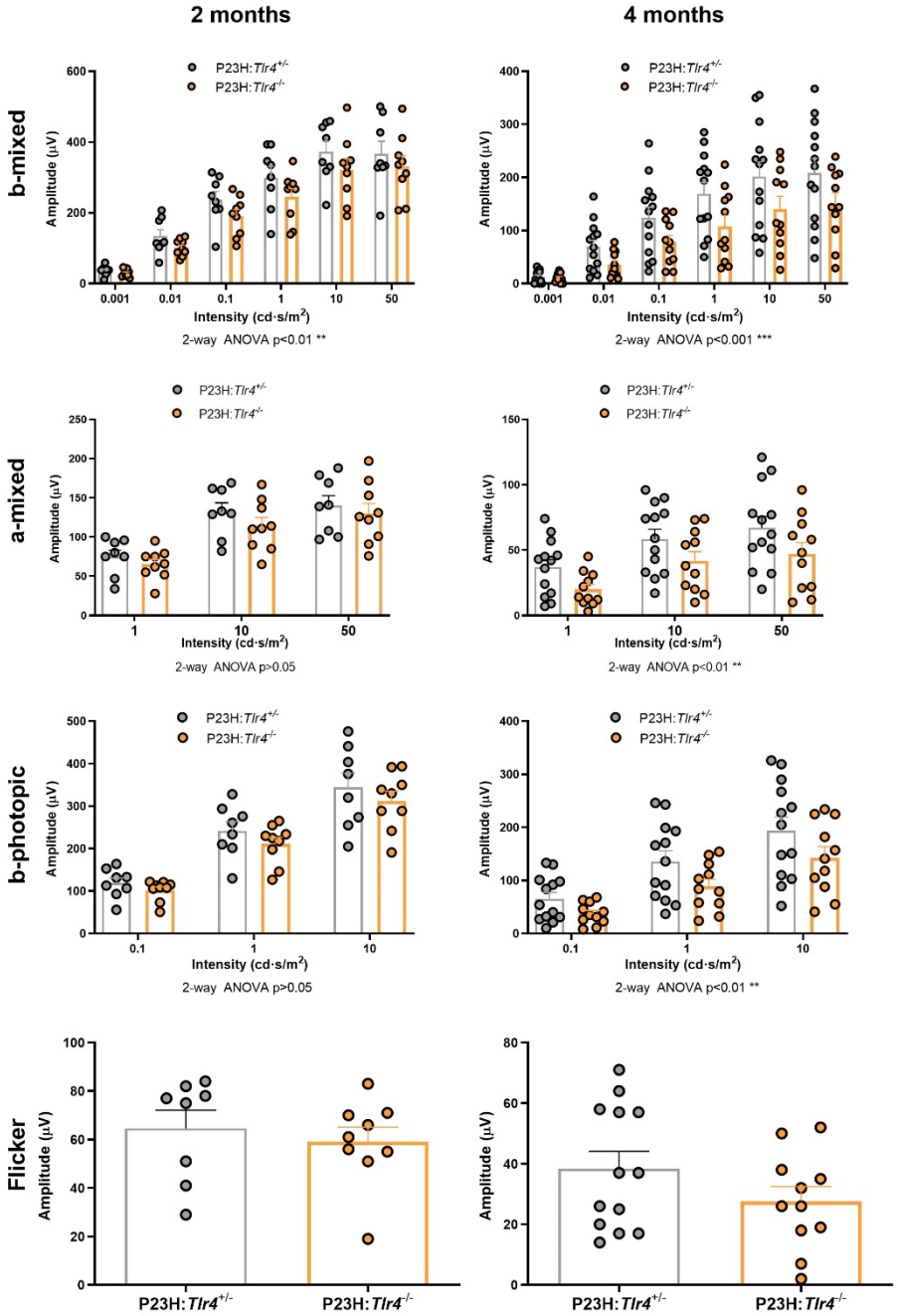

Figure 4.30. **Quantification of ERG recordings of P23H:*Tlr4*$^{+/-}$ and P23H:*Tlr4*$^{-/-}$ P23H mice at 2 and 4 months.** Graphs show averaged ERG wave amplitudes plotted as a function of light stimuli. Amplitudes of the rod and cone mixed response (a- and b-mixed) were recorded under scotopic conditions after overnight adaptation to darkness. The mixed b-wave was measured for all the applied light stimuli (see methods section), while the mixed a-wave could only be measured for the three highest stimuli. Cone amplitudes (b-photopic and flicker) were recorded after 5 minutes of light adaptation (30 cd/m^2 background light) under photopic conditions. Dots represent individual and bars represent the mean for each group (+SEM). n=8-11 mice. 2-way ANOVA was applied for statistical analysis of mixed and b-photopic wave and a-mixed wave, while unpaired t-test was applied for flicker response. ***p<0.001; **p<0.01.

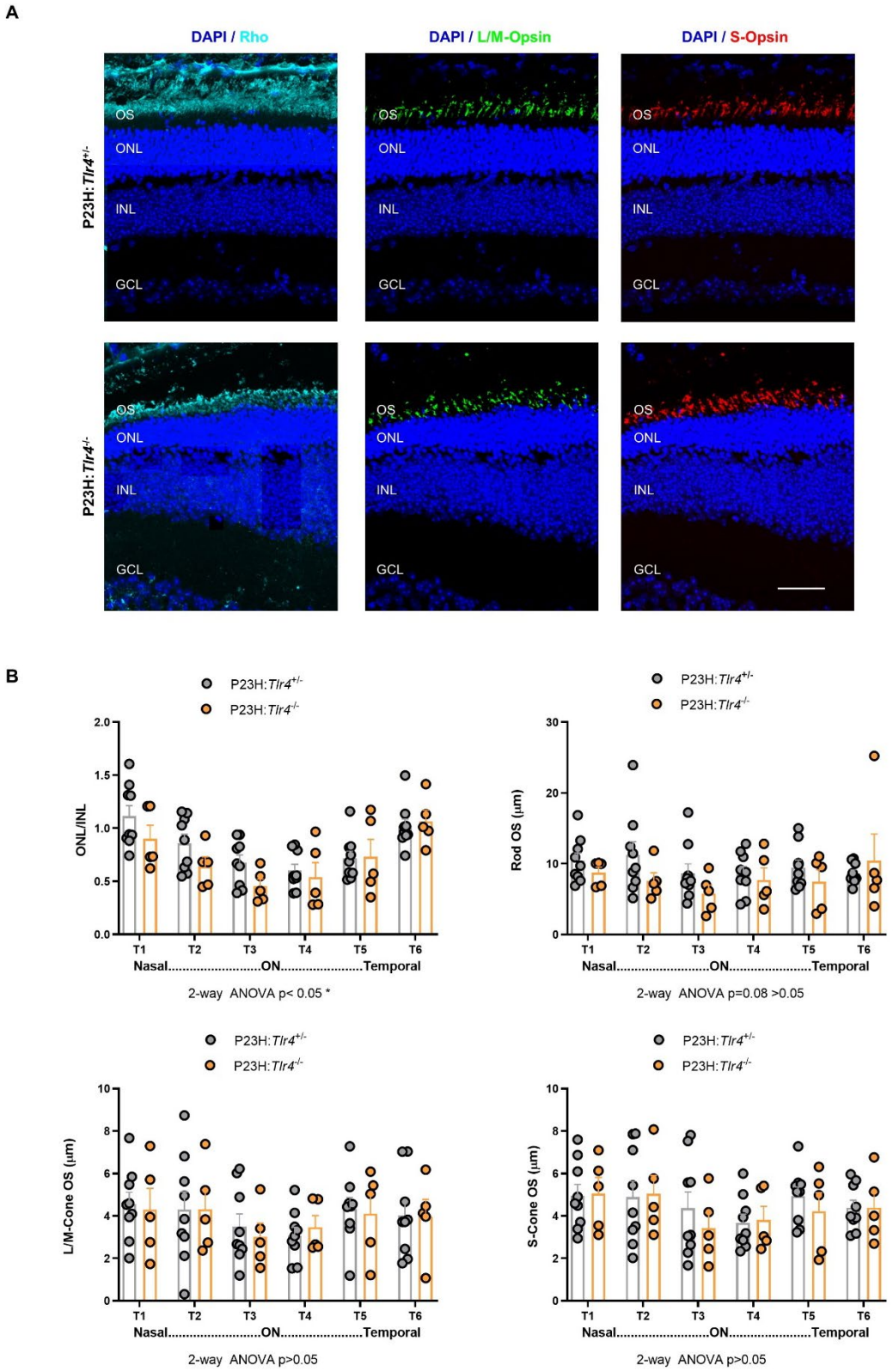

Figure 4.31. Retinal structure of P23H:*Tlr4*$^{+/-}$ and P23H:*Tlr4*$^{-/-}$ retinas. A. Representative images of retinal cryosections (T3 area) from P23H:*Tlr4*$^{+/-}$ and *P23H*:*Tlr4*$^{-/-}$ at 4 months immunostained for rhodopsin (cyan), L/M-opsin (green) and S-opsin (red). Nuclei were stained with DAPI (blue). OS, outer segment; ONL, outer nuclear layer; INL, inner nuclear layer and GCL, ganglion cell layer. Scale bar: 40 µm. **B.** ONL and INL thickness and the length of rod and cone outer segments were measured in equatorial sections corresponding to 6 regions of the retina, following a nasotemporal sequence (see methods section). Dots represent individual mice and bars display the mean for each group. n = 5-9 mice, 3 sections per retina, 3 measurements per region and section. ON, optic nerve. 2-way ANOVA was applied for statistical analysis. *p < 0.05.

The deleterious effect of TLR4 deficiency on RP progression made us hypothesize whether TLR4 loss could also affect retinal function under physiological conditions. In order to address this issue, we analyzed the ERG response of TLR4 null mice (*Tlr4*$^{-/-}$) in C57BL/6 background. ERG recordings were performed every 7 days between P34 and P48 and the following parameters were evaluated: scotopic threshold response (STR, measure of the activity of ganglion cells that reflects rod response), mixed b and a waves (to measure the response of rods and cones), oscillatory potential (OP, to measure the response of amacrine and ganglion cells) and the b-photopic wave and the flicker response (to assess cone function). As shown in Figure 4.32 and Figure 4.33, *Tlr4* deletion did not reduce the amplitude of any ERG recordings but rather an increment was observed for most of them. The a- and b-mixed and b-scotopic waves and the OP were increased in the *Tlr4*$^{-/-}$ respect to the *Tlr4*$^{+/+}$ mice. No significant changes were found in the STR, b-photopic and flicker responses, although the two latest show a trend for greater amplitude in the *Tlr4*$^{-/-}$ mice (p=0.09 and 0.05, respectively).

Retinal histological analysis of those mice did not show significant differences in the photoreceptor survival or integrity between *Tlr4*$^{-/-}$ and WT animals (Figure 4.34). Although further studies are needed to elucidate the reasons behind the higher amplitude of ERG responses in *Tlr4*$^{-/-}$ mice, our results indicate that *Tlr4* deletion is not disadvantageous under physiological conditions, but is detrimental under pathological situations arguing that TLR4 has a protective role during retinal degeneration, at least in the context of RP.

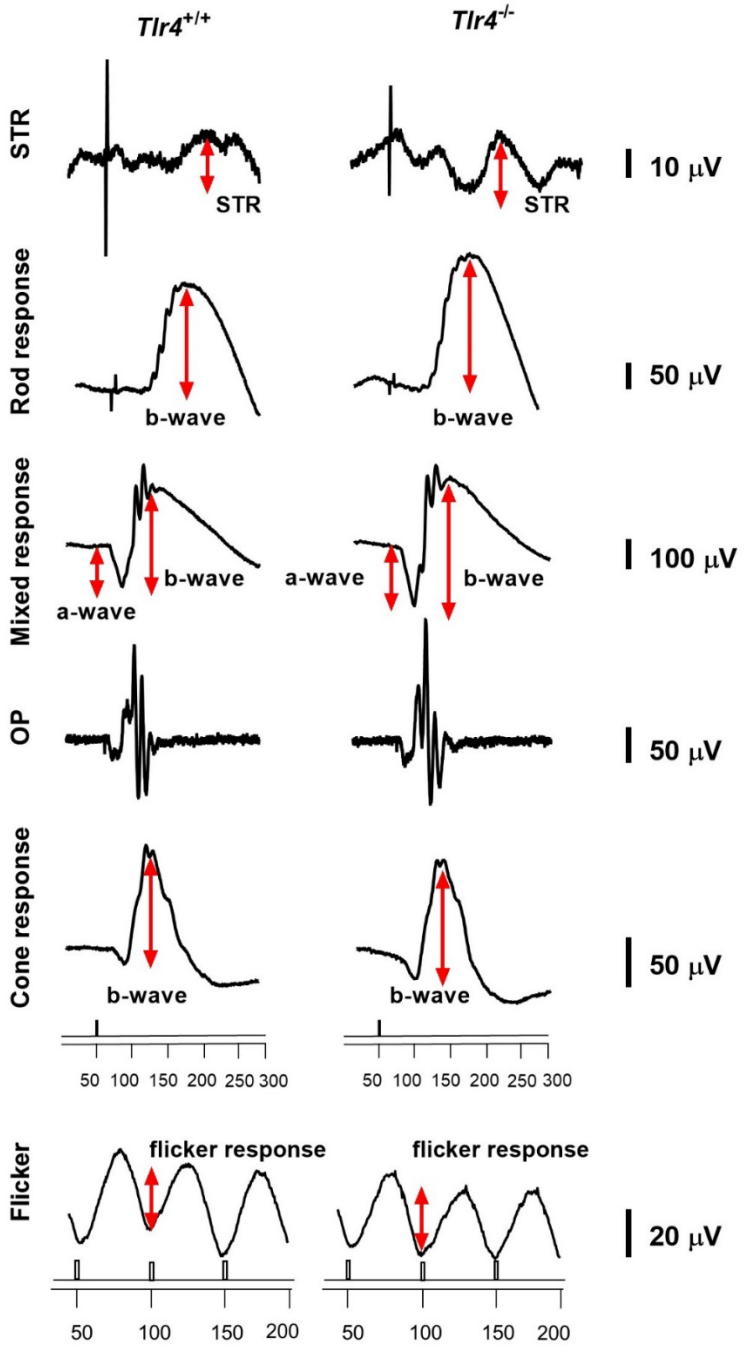

Figure 4.32. ERG recordings of *Tlr4*$^{+/+}$ and *Tlr4*$^{-/-}$ mice. Representative ERG trace recordings of *Tlr4*$^{+/+}$ and *Tlr4*$^{-/-}$ mice at P48. The response for each condition is shown (0.0001 cd·s/m^2 for STR; 0.0126 cd·s/m^2 for scotopic response and 8.3 cd·s/m^2 for mixed response, photopic response and flicker). Values of the scale bar are shown in the figure.

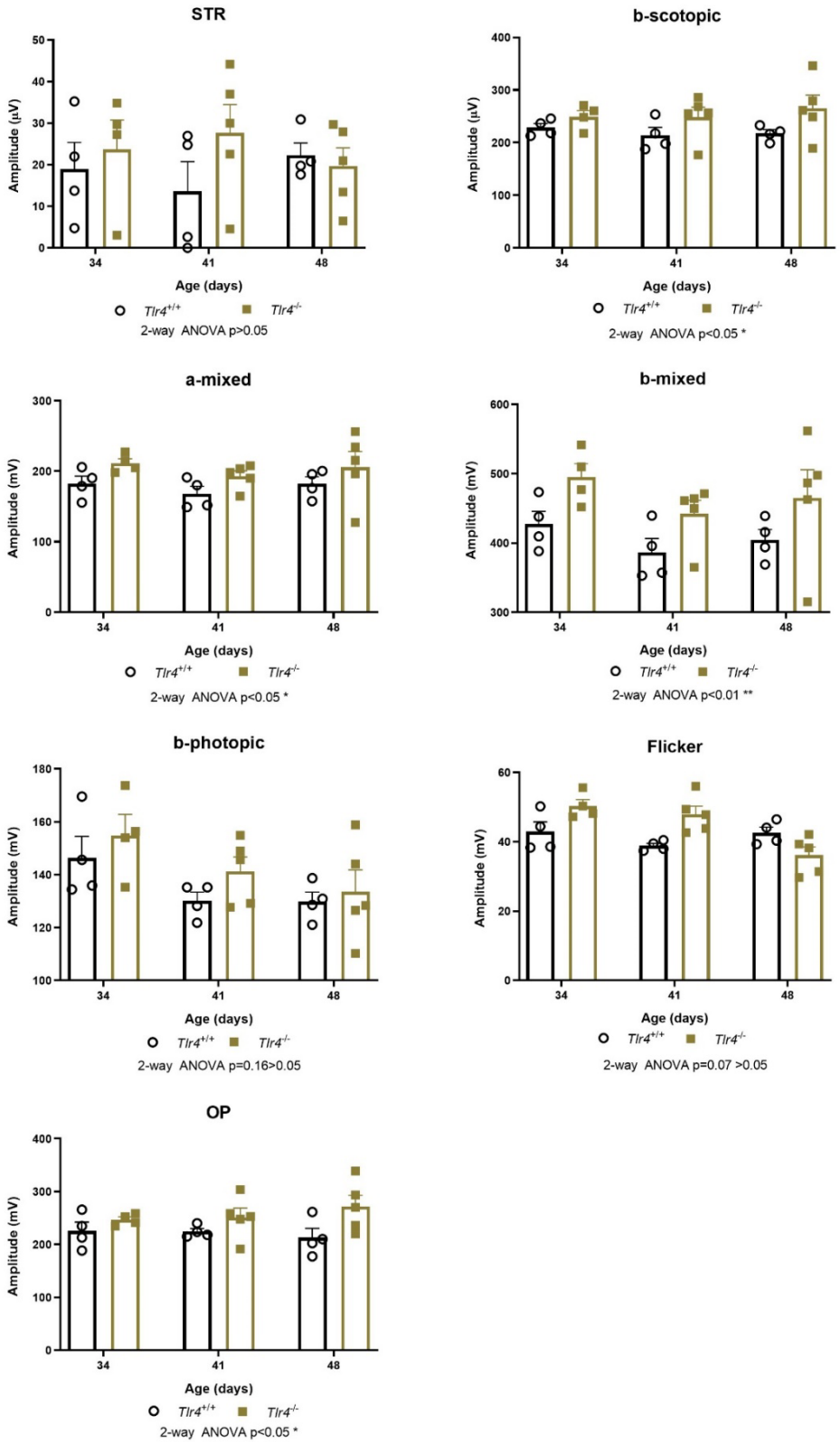

Figure 4.33. Quantification of retinal function of *Tlr4*$^{+/+}$ and *Tlr4*$^{-/-}$ mice. Graphs show averaged ERG wave amplitudes plotted as a function of animal age. Amplitudes of the rod (scotopic threshold response, STR; b-scotopic) and rod and cone mixed responses were recorded in scotopic conditions after overnight adaptation to darkness in response to: 0.0001 cd·s/m^2 for STR; 0.0126 cd·s/m^2 for scotopic response and 8.3 cd·s/m^2 for mixed response. Cone responses (b-photopic and flicker) were recorded after 5 minutes of light adaptation (30 cd/m^2 background light) under photopic conditions in response to 8.3 cd·s/m^2 for both photopic response and flicker. Dots represent individual mice and bars represent the mean for each group (+SEM). n=4-5 mice per group. 2-way ANOVA was applied for statistical analysis ** p<0.01; *p<0.05.

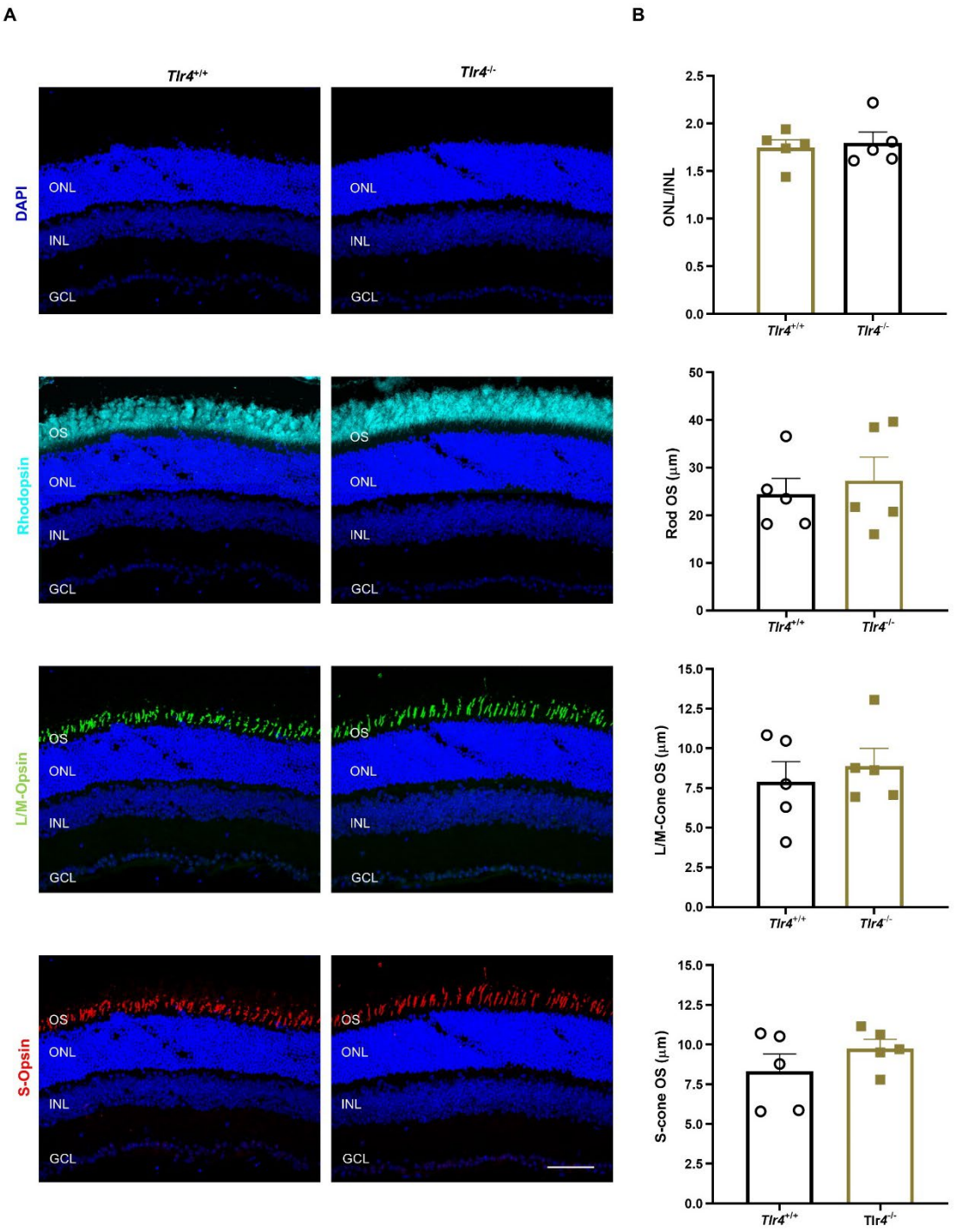

Figure 4.34. Retinal structure analysis of *Tlr4*$^{+/+}$ and *Tlr4*$^{-/-}$ mice. A. Representative images of retina (T3 area) cryosections from P23H:*Tlr4*$^{+/-}$ and P23H: *Tlr4*$^{-/-}$ at 4 months immunostained for rhodopsin (cyan) and L/M-opsin (green) and S-opsin (red). Nuclei were stained with DAPI (blue). OS, outer segment; ONL, outer nuclear layer; INL, inner nuclear layer and ganglion cell layer (GCL). Scale bar: 65 µm. **B.** ONL and INL thickness and the length of rod and cone outer segments were measured in equatorial sections corresponding to central retina (T3-T4 regions, see methods section). Dots represent individual mice and bars display the mean for each group. n=5 mice, 3 sections per retina, 3 measurements per region and section. Unpaired t-test was applied for statistical analysis.

To get insight into the TLR4-protective action on RP, we focused our attention on microglia. Microglia are a key component of the retina response to damage and microglia signature alterations have been shown to exacerbate retinal disease progression (Langmann, 2007; Silverman and Wong, 2018; Rashid et al., 2019). In addition, TLRs have been mainly associated to microglial cells in the CNS (Hanke and Kielian, 2011). To investigate whether *Tlr4* deficiency causes microglia alterations, we analyzed the microglial population on *rd10*:*Tlr4*$^{+/-}$ and *rd10*:*Tlr4*$^{-/-}$ mice. Flat-mounted retinas of both genotypes were co-stained for P2Y12 and CD68, and microglia were analyzed in the photoreceptor layers (ONL and OS) at P28. The purinergic receptor P2Y12 is a homeostatic microglia-specific marker, not expressed by macrophages or monocytes, which levels decrease as microglia go through reactive states (Okunuki et al., 2018). CD68 is a lysosomal protein, upregulated in phagocytic cells (Graeber et al., 1990; Zhao et al., 2015). According to the expression of both markers we classified microglia as: i) P2Y12^{+}CD68^{-} homeostatic microglia; ii) P2Y12^{+}CD68^{+} reactive microglia ; iii) P2Y12^{-}CD68^{+} phagocytic microglia plus infiltrating macrophages. As shown in (Figure 4.35A and B), the number of P2Y12^{+}CD68^{-} was significantly decreased in the OS of *rd10*:*Tlr4*$^{-/-}$ mice respect to that of *rd10*:*Tlr4*$^{+/-}$ mice. No differences were observed in the number of P2Y12^{+}CD68^{+} cells or P2Y12^{-}CD68^{+} cells. Similarly, a small reduction in the number of P2Y12^{+}CD68^{-} cells was found in the ONL of *rd10*:*Tlr4*$^{-/-}$ retinas, although it did not reach statistical significance (p=0.206). Conversely, the number of P2Y12^{-} CD68^{+} was significantly higher in the ONL of *rd10*:*Tlr4*$^{-/-}$, while that of P2Y12^{+}CD68^{+} was similar between both genotypes.

Overall, these data indicate that the *rd10*:*Tlr4*$^{-/-}$ retinas display reduced number of homeostatic microglia and an increase in the number of phagocytic microglia and/or infiltrating macrophages. These results suggest that *Tlr4* deletion shifted microglia to a more reactive/phagocytic state which may account, at least in part, for the accelerated retinal degeneration of the *rd10*:*Tlr4*$^{-/-}$ mice.

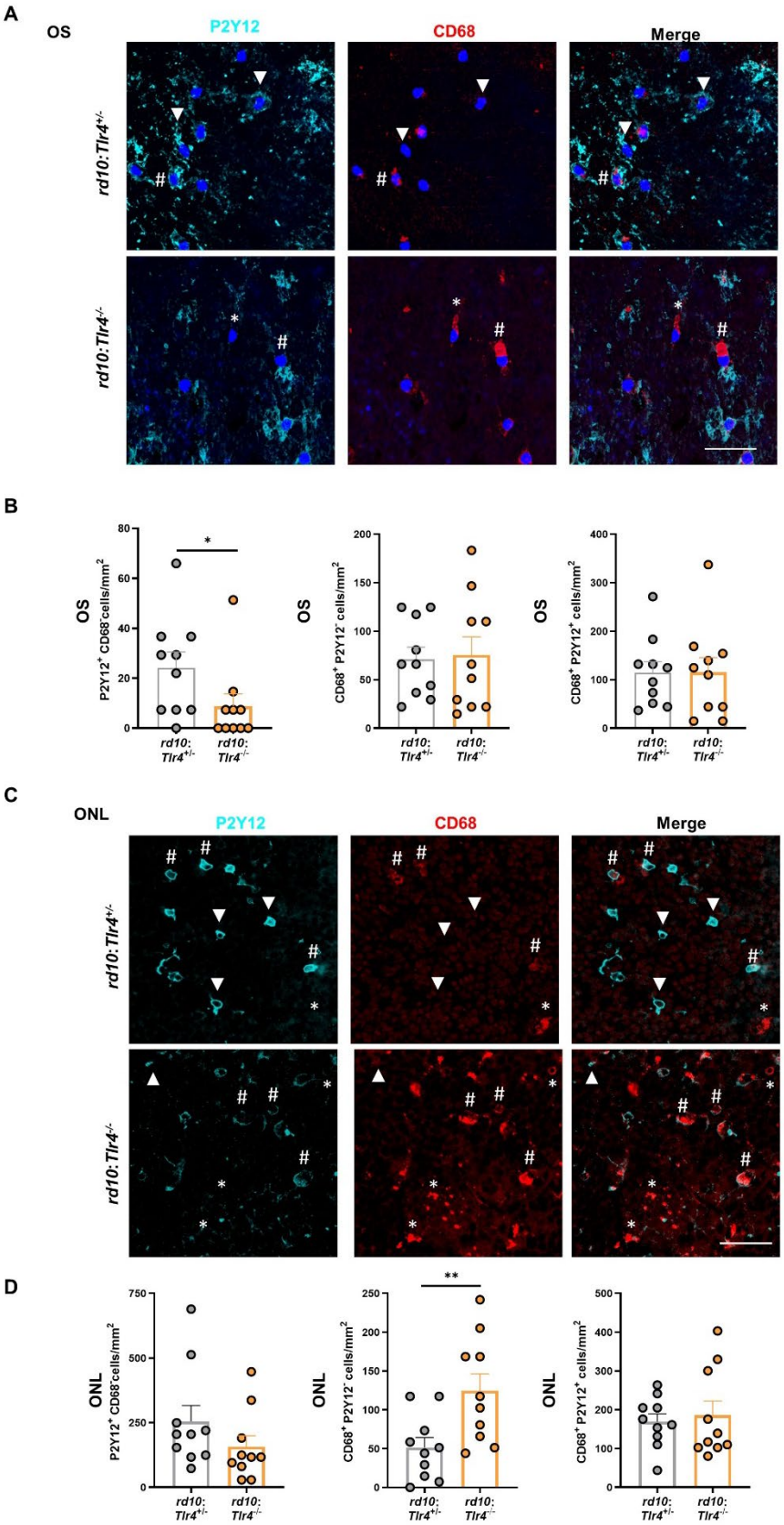

Figure 4.35 Microglia in the OS and the ONL of *rd10*:*Tlr4*$^{+/-}$ and *rd10*:*Tlr4*$^{-/-}$ at P28. A, C. Representative images of the OS (A) or the ONL (B) layers of flat-mounted retinas at P28 immunostained for P2Y12 (cyan) and CD68 (red). Arrowheads indicate P2Y12^{+}CD68^{-} cells, hash signs indicate P2Y12^{+}CD68^{+} cells and asterisks indicate P2Y12^{-}CD68^{+} cells. Scale bar corresponds to 37 µm. **B, D.** Quantification of the indicated populations in the OS (B) and ONL (D) layers. n=10 mice, four images at four areas adjacent to the optic nerve (see methods section, 3.9) per retina were quantified. Unpaired t-test was applied for statistical analysis. *p<0.05; **p<0.01.

4.3.3. Analysis of TLR2 deficiency in animal models of RP

As observed in Figure 4.21A, *Tlr2* underwent a dramatic increase (>35-fold) in the *rd10* retina. To assess the role of *Tlr2* in RP progression we followed the same strategy as for the TLR4 described above. As for *Tlr4*, we first studied the effect of *Tlr2* haploinsufficiency on *rd10* visual function. The ERG response was recorded for these animals at P25 in dark-adapted and light-adapted mice. No significant differences were found between the *rd10*:*Tlr2*$^{+/+}$ and *rd10*:*Tlr2*$^{+/-}$ mice at any of the analyzed parameters (Figure 4.36A and B). These results suggest that a single *Tlr2* allele deletion did not affect *rd10* vision loss.

We then study whether total *Tlr2* deletion have any impact on *rd10* visual function. ERG recordings in dark- and light-adapted conditions were performed at P35. The amplitudes of the most relevant waves involving rod and cone (b-mixed) and cone responses (b-photopic) were significantly increased in the *rd10*:*Tlr2*$^{-/-}$ respect to that of the *rd10*:*Tlr2*$^{+/-}$. The flicker response showed a mild trend to higher amplitude in the *rd10*:*Tlr2*$^{-/-}$ mice (p=0.11), while the a-mixed was similar for both genotypes (Figure 4.37). These results indicate that *Tlr2* deletion preserved visual function in *rd10* mice and suggest that TLR2 may be a therapeutic target for RP treatment.

The analysis of TLR2 depletion was further analyzed in P23H mice. The visual function was assessed at 4 months in P23H:*Tlr2*$^{+/-}$ and P23H:*Tlr2*$^{-/-}$ littermates (Figure 4.38). In dark-adapted mice the amplitude of the b-mixed wave was significantly higher in P23H:*Tlr2*$^{-/-}$. No clear differences were observed for the a-mixed wave between genotypes. In addition, after light adaptation the amplitude of the b-photopic wave was increased in P23H:*Tlr2*$^{-/-}$, although no clear differences were observed in the flicker response. These data suggest that *Tlr2* deletion results in a delay of visual function loss also in P23H mice.

In summary, our studies showed that the deficiency of *Tlr4*, both complete depletion or haploinsuffiency, results in accelerated retinal function loss and in faster photoreceptor degeneration in RP mouse models. On the contrary, the complete depletion of *Tlr2* results in a preservation of retinal function. Taken together these results suggest a dual role of TLRs in RP progression, beneficial in the case of *Tlr4* and detrimental in the case of *Tlr2*.

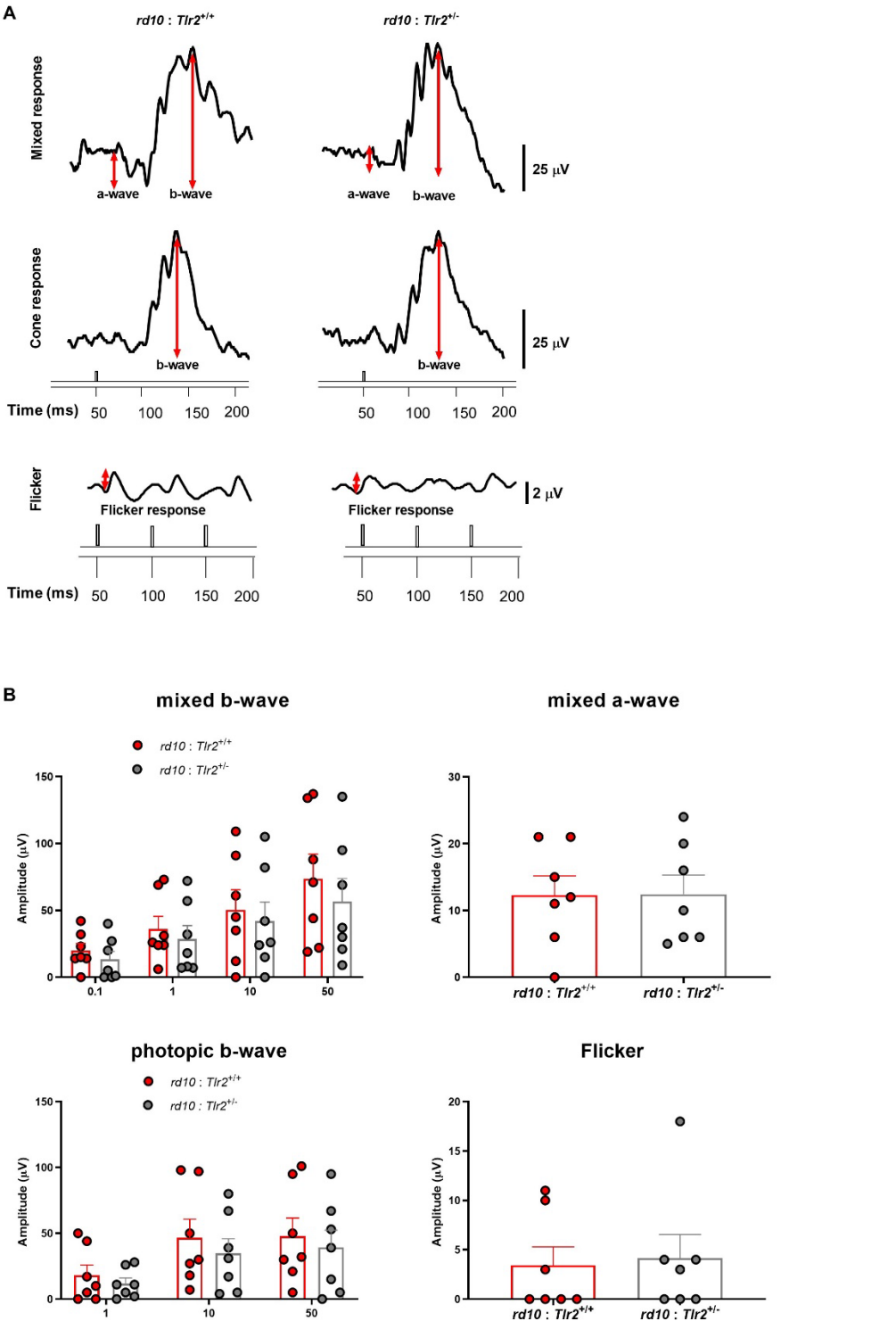

Figure 4.36. ERG response of *rd10*:*Tlr2*$^{+/+}$ and *rd10*:*Tlr2*$^{+/-}$ *rd10* mice. A. Representative ERG responses of *rd10*:*Tlr2*$^{+/+}$ and *rd10*:*Tlr2*$^{+/-}$ at P25 in response to 50 cd·s/m^2. Values of the scale bar are indicated in the figure. **B.** Graphs show averaged ERG waves amplitudes, plotted as a function of light stimuli. Amplitudes of rod and cone mixed response (a- and b- mixed) were recorded under scotopic conditions after overnight adaptation to darkness. The b-mixed wave was measured for all of the light stimuli (see methods section), while the a-mixed could be measured only for the highest stimulus. Cone amplitudes (b-photopic and flicker) were recorded after 5 minutes of light-adaptation (30 cd·s/m^2) under photopic conditions. Dots represent individual mice and bars represent the mean for each group (+SEM). n=7 animals per group. 2-way ANOVA was applied for statistical analysis of b-mixed and photopic waves, while unpaired t-test was applied for a-mixed wave and for flicker response.

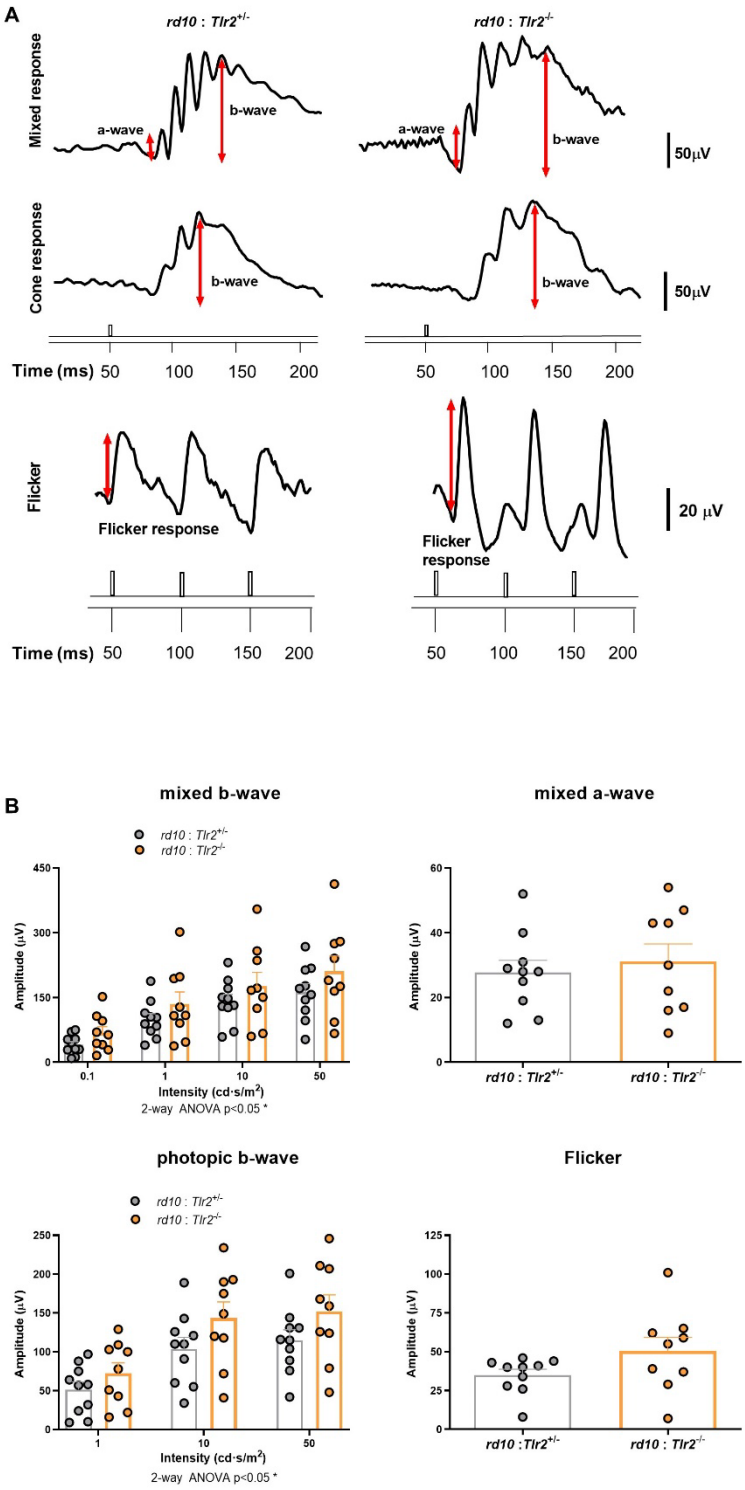

Figure 4.37. ERG response of *rd10*:*Tlr2*$^{+/-}$ and *rd10*:*Tlr2*$^{-/-}$ mice. A. Representative ERG responses of *rd10*:*Tlr2*$^{+/-}$ and *rd10*:*Tlr2*$^{-/-}$ at P35 in response to 50 cd·s/m^2. Values of the scale bar are indicated in the figure. **B.** Graphs show averaged ERG wave amplitudes, plotted as a function of light stimuli. Amplitudes of rod and cone mixed response (a- and b-mixed) were recorded under scotopic conditions after overnight adaptation to darkness. The b-mixed wave was measured for all of the light stimuli (see methods section), while the a-mixed wave could be measured only for the highest stimulus. Cone amplitudes (b-photopic and flicker) were recorded after 5 minutes of light adaptation (30 cd·s/m^2) under photopic conditions. Dots represent individual mice and bars represent the mean for each group (+SEM). n=9-10 animals per group. 2-way ANOVA was applied for statistical analysis of b-mixed and photopic waves, while unpaired t-test was applied for a-mixed wave and for the flicker response *p<0.05.

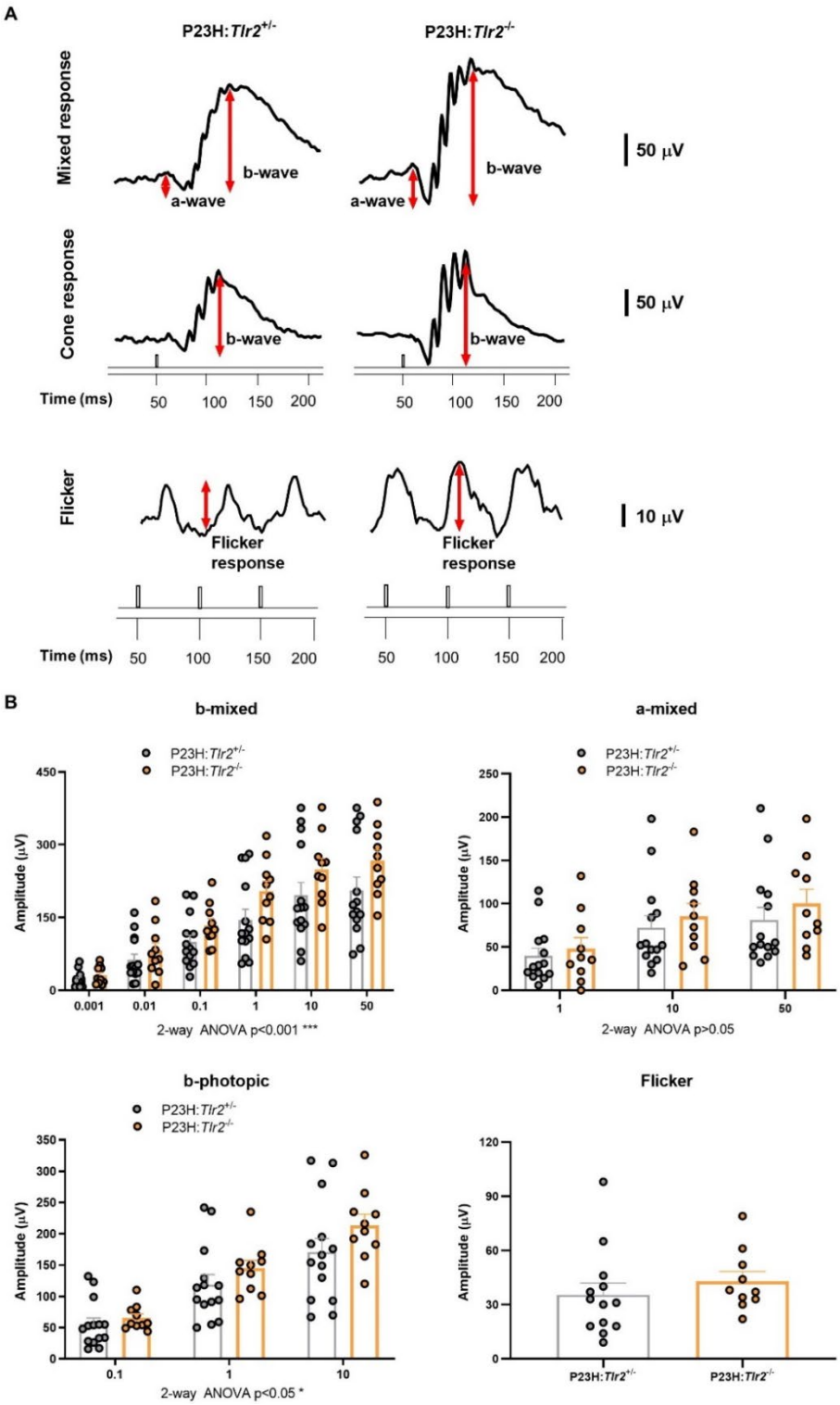

Figure 4.38. ERG response of P23H:*Tlr2*$^{+/-}$ and P23H:*Tlr2*$^{-/-}$ mice. A. Representative ERG responses of P23H:*Tlr2*$^{+/-}$ and P23H:*Tlr2*$^{-/-}$ at 4 months in response to stimuli of 50 cd·s/m^2 (a- and b-mixed responses) and 10 cd·s/m^2 (cone and flicker responses). Values of the scale bar are indicated in the figure. **B.** Graphs show averaged ERG wave amplitudes, plotted as a function of light stimuli. Amplitudes of rod and cone mixed response (a- and b-mixed) were recorded under scotopic conditions after overnight adaptation to darkness. The b-mixed wave was measured for all of the light stimuli (see methods), while the a-mixed wave could be measured only for three highest stimuli. Cone amplitudes (b-photopic and flicker) were recorded after 5 minutes of light adaptation (30 cd·s/m^2) under photopic conditions. Dots represent individual mice and bars represent the mean for each group (+SEM). n=10-14 animals per group. 2-way ANOVA was applied for statistical analysis of a-mixed and b-mixed and photopic waves, while unpaired t-test was applied for the flicker response. ***p<0.001; *p<0.05.

SECTION 5
DISCUSSION

5. DISCUSSION

5.1. Insulin receptor expression and activation in RP

The first objective of this thesis was to characterize the expression of IR and IR system in the context of RP, and analyze whether IR stimulation is a potential disease-modifying therapy.

IR expression was observed in all retinal cell layers, but remarkably enriched levels of IR are found in horizontal and ganglion cells fibers (Figure 4.1 and Figure 4.2). In *rd10*, IR expression and signaling (phosphorylation of ribosomal protein S6) were locally downregulated in horizontal cells (Figure 4.3 and Figure 4.5). This down-regulation was specific of horizontal cells, since IR and pS6 expression remained unchanged in ganglion cells (Figure 4.3 and Figure 4.5). Parallel to this local down-regulation, we found a disruption of the synapses of rods with their postsynaptic partners, horizontal and bipolar cell terminals (Figure 4.6; Appendix 1). The administration of hPi by a gene therapy approach to *rd10* mice restored IR signaling in horizontal cells (Figure 4.8). More importantly, hPi administration partially preserved photoreceptor cells (Figure 4.10) and maintained rod synaptic connectivity (Figure 4.11). These histological effects were accompanied by a decrease in the number of microglia cells as identified by Iba1 and CD68 markers, as well as in the expression of proinflammatory cytokines and chemokines (Figure 4.12).

IR expression was previously described to be broadly distributed in the mouse retina (Gosbell et al., 2000; Rajala et al., 2009), however in this thesis we show for the first time that IR expression is enriched in the axons of horizontal and ganglion cells. The finding that IR is enriched in axons is consistent with its function regulating the formation, maintenance and plasticity of synapses (Chiu et al., 2008; Chiu and Cline, 2010; Urwyler et al., 2019). In this regard, we showed that IR stimulation by hPi maintains photoreceptor synaptic connectivity with their postsynaptic partners (horizontal and bipolar cells), in agreement with previous studies in which insulin administration restores the number of dendrites and synapses in ganglion cells after axonal injury (Agostinone et al., 2018).

Interestingly, in the *rd10* retinas IR levels are selectively decreased in horizontal cell axons. This effect was not observed when IR expression was assessed in whole retina extracts (Figure 4.1), probably because this decrease gets diluted by the IR expression in the rest of the tissue. In addition, changes in retinal cell populations due to photoreceptor cell death, microglial proliferation and macrophage infiltration could alter the global expression of IR in the *rd10* retina. Our results highlight the necessity of analyzing each cell type independently and not

relying just on data of the whole retina, that could provide only incomplete information. The local decrease of IR expression in horizontal cells could be mechanistically related to the neuronal activity-dependent IR signaling variations observed in other models (Hori et al., 2005; Chiu et al., 2008). Chiu *et al* described that IR signaling in optic tectal neurons, in living tadpoles, varies in a neuronal activity-dependent manner. Similarly, in *rd10* mice, rod cell dysfunction and death cause altered horizontal cell input that could have an impact on IR expression. Consistently with the local decrease of IR expression in horizontal cells, a decrease of $pS6^{Ser240/244}$ levels was observed in horizontal cell tips in *rd10* mice, revealing that IR signaling is also locally decreased in these cells. On the contrary, IR expression and signaling is maintained in ganglion cells. These cells receive direct synaptic input only from cone bipolar cells and amacrine cells, whose activity is maintained in *rd10* for longer time (Mazzoni et al., 2008). In addition, the retinal inflammatory state could contribute to IR signaling impairment. Insulin resistance associated to AD is caused, in part, by the increased levels of TNF-α. Binding of TNF-α to its receptor leads to JNK activation that in turn phosphorylates IRS-1 inhibiting PI3K and AKT activation (Bloom et al., 2018). In *rd10* retinas, *Tnf* expression was dramatically increased (Figure 4.21), a fact that could contribute to the decrease of IR signaling in horizontal cells. Remarkably, tumor necrosis factor receptor 1 (TNF-R1) expression is enriched in horizontal cells but not in bipolar cells (where $pAKT^{473}$ levels are increased in the *rd10* retina, Figure 4.15), a fact that could explain why IR signaling is specifically decreased in horizontal cells (Fontaine et al., 2002; Gesslein et al., 2010). Moreover, the 50% decrease in *Tnf* gene expression that is observed upon hPi administration, may contribute to the preservation of IR signaling restoration that is observed in treated mice.

IR has been related with synaptic regulation for more than 20 years (Gralle, 2017). Knocking down IR expression using RNAi or IR signaling by the expression a dominant-negative form of the insulin receptor, results in a pronounced decrease in the number of synapses (Chiu et al., 2008; Urwyler et al., 2019). Here we show that IR signaling downregulation parallels photoreceptor disconnection and that hPi treatment restores $pS6^{Ser240/Ser244}$ levels and decreases photoreceptor disconnection. In light of our results and those aforementioned we postulate that IR local downregulation in horizontal cells causes, at least in part, the observed synaptic disconnection of rods from their postsynaptic partners, horizontal and bipolar cells. The determination of how IR signaling impairment leads to structural synaptic degeneration in *rd10* needs further investigations. The increased S6 phosphorylation has been associated to increased mRNA translation and therefore elevated protein production (Peterson and Schreiber, 1998). Remarkably, local protein synthesis is necessary for the maintenance of synaptic function and plasticity (Martin et al., 2000; Holt et al., 2019). Further experiments directed to analyze local

protein synthesis at horizontal cell processes, e.g. by the surface sensing of translation (SUnSet) method, could clarify this matter. The SUnSet method is based on the incorporation of puromycin to the novel-generated peptides (Briz et al., 2017), that could be visualized employing an anti-puromycin antibody and standard immunostaining techniques. In addition, selective IR deletion in horizontal cells by conditional knock-out mice technology will help to unravel the role of IR in triad synapse formation and maintenance.

Retinal synaptic alterations, as part of the retinal remodeling processes due to photoreceptor degeneration, have been acknowledged for more than two decades (Lewis et al., 1998; Strettoi et al., 2003; Jones et al., 2012; Pfeiffer et al., 2020). The degeneration of bipolar and horizontal cell processes has been typically described at advanced stages of degeneration as consequence of photoreceptor loss. However, here we illustrate early disconnection events among the apparently alive rods at the initial stages of the disease (Figure 4.6.; Appendix 1). Data obtained in Dr. C. Lillo laboratory (Universidad de Salamanca, Salamanca, Spain), suggest that synaptic disconnection is not just a previous step to photoreceptor cell death since both connected and disconnected rods were found to be degenerative. The triad rod synapse, besides horizontal terminals, also involves the participation of bipolar cells. The electron microscopy study carried by Dr. C. Lillo laboratory (Appendix 1), showed similar number of dyads (rod terminal plus bipolar or horizontal terminal) in WT and *rd10* retinas which are most likely caused by the misalignment of one of the postsynaptic elements with the plane of section (Wang et al., 2019). These results indicate that both horizontal and bipolar cells disconnect from rod synapse simultaneously or within a short time frame.

During retinal development, triad synapses are formed sequentially. First, rods and horizontal cells establish dyad synapses, and then bipolar cells are incorporated, resulting in the formation of triad synapses (Nemitz et al., 2019). Interestingly, rod-horizontal dyad formation is a mandatory step for the posterior bipolar cell connection. Moreover, the same authors described that in the absence of horizontal cells, the mGluR6 signaling complex is impaired in bipolar cells. Also, the ablation of horizontal cells in the adult mouse retina leads to the degeneration of rods and bipolar cells (Sonntag et al., 2012). In light of all these evidences we favor that there is a primary disconnection of horizontal cells with rods which leads to the posterior disconnection of bipolar cells. Nevertheless, further experiments are needed to support this hypothesis. For example, triple co-immunostaining for the photoreceptor ribbon, mGluR6 (marker of bipolar cell tip) and GluA2 (marker of horizontal cell tip) in *rd10* mice would help to clarify this matter. This approach could not be undertaken during this thesis due to the lack of suitable antibodies.

DISCUSSION

The observation of disconnected alive photoreceptors has direct implications for the development of novel neuroprotective therapies, suggesting that it is not sufficient to preserve the number of viable cells but also their synaptic connections. Here we show that hPi administration to *rd10* mice, besides partial preservation of photoreceptor survival, also results in a maintenance of rod synapses. These neuroprotective effects are accompanied by a decrease in the number of microglia cells identified by the pan-microglial marker Iba1, and the phagocytic marker CD68, and also by a reduction in the expression of proinflammatory cytokines and chemokines (*Tnf*, *Il1b*, *Ccl3* and *A2m*). As mentioned in the introduction, the retinal proinflammatory response has been related with the aggravation of RP progression (Zhao et al., 2015; Rashid et al., 2019). Moreover, strategies to lower the retinal inflammatory state associated to RP have rendered positive outcomes. Examples of which are the treatment with anti-TNF-α (adalimumab) (Martínez-Fernández de la Cámara et al., 2015) or the use of the anti-inflammatory compound minocycline (Peng et al., 2014). The photoreceptor prosurvival effect of hPi could be a consequence of the anti-inflammatory action of hPi. On the other hand, lower retinal inflammatory status could be due to the attenuation of photoreceptor death (Sochocka et al., 2017). Further studies are necessary to establish a hierarchy between these two hPi actions. Moreover, the observed decrease in retinal load of microglia cells as result of hPi administration suggests an attenuation of microglia reactivity which may contribute to photoreceptor survival (Zhao et al., 2015) and to synapse maintenance. It has been described that microglia participate in the over-pruning of synapses associated to neurodegenerative disorders like AD and psychiatric diseases like schizophrenia (Salter and Stevens, 2017). Therefore, the reduction of microglia reactivity by hPi could preserve synaptic connectivity.

IR signaling impairment has been observed in other neurodegenerative diseases. In the brain, IR signaling alterations have been described to be key players in the neurodegenerative process of AD (de la Monte and Wands, 2005; Steen et al., 2005; Talbot et al., 2012) and PD (Moroo et al., 1994). In the retina, alterations of insulin signaling have been predominantly studied in the context of diabetic retinopathy (Reiter et al., 2006), although IR signaling alterations have been observed in a model of glaucoma (Agostinone et al., 2018). Here, we described for the first time alterations in the IR and IR signaling in the RP retina, which most likely participate in the pathogenesis of the disease. We propose that IR local downregulation in horizontal cells contributes to retinal structural alterations (rod synaptic disconnection) and visual dysfunction in *rd10* animals, opening a new window into the much-anticipated treatment of RP.

The administration of hPi to *rd10* mice results in a restoration of IR signaling in horizontal cells and in a preservation of rod connectivity and of the number of photoreceptor cells. In parallel,

hPi administration reduces the retinal inflammatory response. Most likely, the retinal function preservation that is observed in *rd10* mice treated with hPi is probably a consequence of all these effects. The intervention of hPi at various levels makes it a good candidate for RP treatment, since RP is a heterogeneous disease. In addition, considering that dysregulation of IR and IR signaling seems to be a common feature of different neurodegenerative diseases, hPi could be a potential therapeutic candidate not only for RP but also for numerous neurodegenerative diseases of brain and retina.

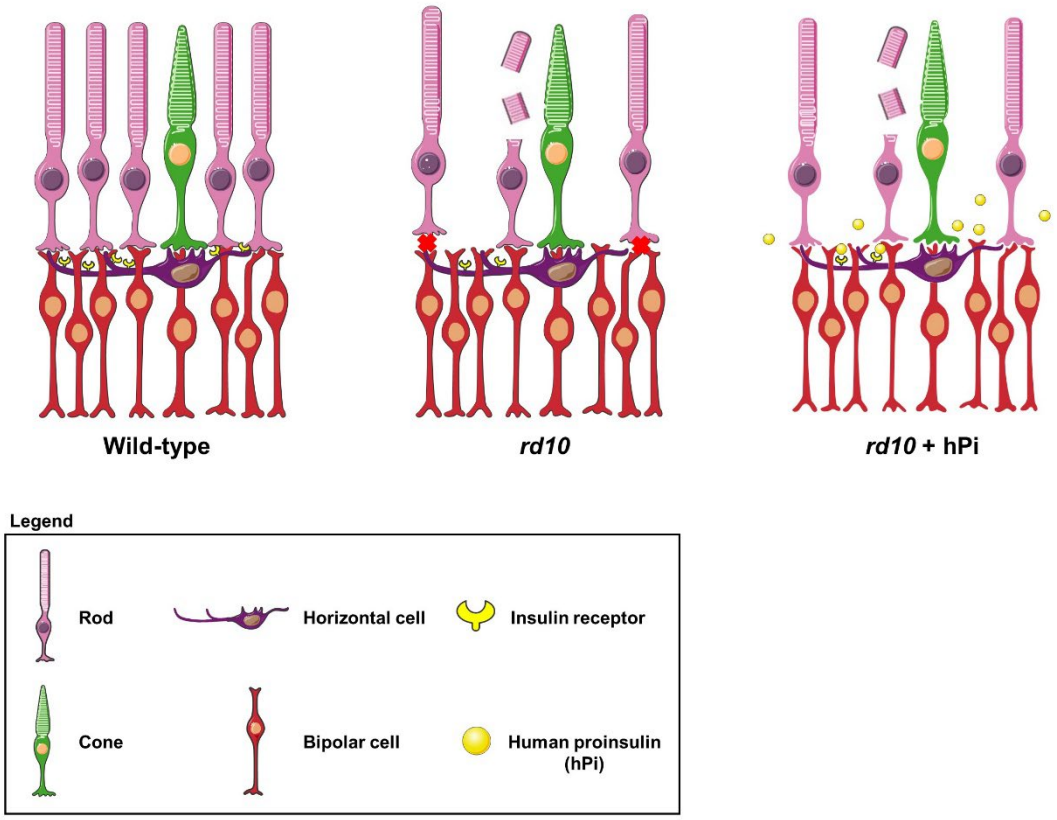

Figure 5.1. Graphical summary of IR role in *rd10* mice. In the WT retinas insulin receptor is present in the axons of horizontal cells and rods display a perfect connectivity with their postsynaptic partners, horizontal and bipolar cells. In *rd10* mice, rod cell death causes a decrease in the input that horizontal cells receive, causing the specific reduction of IR levels and of its signaling in horizontal cell fibers. This decrease results in the synaptic disconnection of rods from horizontal and bipolar cells. The exogenous administration of human proinsulin (hPi) to *rd10* mice restores IR signaling of the existent receptors, providing preservation of rod synaptic connectivity

5.2. GSK-3 inhibition in RP

In this second part of the thesis we aimed to characterize GSK-3β expression and activation in the *rd10* retina, and validate GSK-3 targeting as a potential therapeutic strategy for RP treatment. Our findings provide proof of concept of the neuroprotective effect of GSK-3 inhibition on photoreceptor integrity. *In vivo* administration of VP3.15, a small-molecule GSK-3 inhibitor, reduced photoreceptor cell loss and preserved retinal structure and function.

GSK-3 is a constitutively activated multitask enzyme, the activity of which is regulated by several inhibitory signaling pathways (Beurel et al., 2015). Inhibitory phosphorylation of GSK-3 is one of the main regulatory mechanisms. Our analysis of GSK-3β RNA and protein levels during the degenerative process in *rd10* retinas revealed no differences with respect to WT counterparts (Figure 4.13). However, at both P19 and P21, when the photoreceptor degeneration is well established, phosphorylation of GSK-3β at Ser9 and of its regulator AKT, were increased in the *rd10* retinas (Figure 4.14 and Figure 4.15). We interpret this endogenous activation of the AKT-GSK-3β pro-survival pathway as an attempt of the *rd10* retina to diminish photoreceptor cell death. The activation of AKT as intrinsic prosurvival response has been previously described in the photoreceptor cell line 661W after its exposition to a variety of insults (Finnegan et al., 2010), in retinas subjected to physical injury (Nakazawa et al., 2003) or in mice treated with methylnitrosourea (MNU) to induce photoreceptor cell death (Hamon et al., 2019). In our experiments, the administration of the GSK-3 inhibitor VP3.15 may have exogenously potentiated this prosurvival pathway, thus delaying photoreceptor cell death. In fact, several agents with neuroprotective effects in the retina exert stimulatory effects on the AKT-GSK-3 pathway. This is the case of Norgestrel, the synthetic progesterone, that has neuroprotective properties in RP animal models that have been proposed to be mediated by GSK-3 inhibition (Wyse Jackson and Cotter, 2016). Another result that relates GSK-3 inhibition to neuroprotection is that valproic acid, a compound that has been described to inhibit GSK-3 (Chen et al., 1999; De Sarno et al., 2002), has been linked with neuroprotection in both RP animal models and patients, although its clinical use is controversial (Chen et al., 2019). This fact underlines the importance of finding novel GSK-3 inhibitors with better neuroprotective properties. In this regard, due to vast quantity of GSK-3 substrates, modulators of GSK-3 activity that achieved mild GSK-3 inhibition are preferred rather than GSK-3 blockers (Martinez et al., 2013; Palomo et al., 2017). In addition, GSK-3 is a well-known downstream substrate of the IR (Beurel et al., 2015) and is therefore inhibited upon IR stimulation. Our group previously demonstrated that hPi stimulates AKT phosphorylation in retinal explants (Isiegas et al., 2016), providing a potential link between IR-AKT-GSK-3 pathway stimulation and photoreceptor

survival. Moreover, VP3.15 treatment reduced inflammation in the *rd10* retinas as hPi treatment does. While hPi anti-inflammatory mechanism remains unexplored, here we showed that VP3.15 attenuated NF-κB activation (Figure 4.20). NF-κB is a key regulator of the inflammatory response by enabling the transcription of the genes encoding many pro-inflammatory cytokines. Moreover, NF-κB expression and DNA-binding activity have been reported to be increased in the retinal microglia of RP mouse retinas (Zeng et al., 2008), suggesting that GSK-3 could regulate microglia inflammatory response. Nevertheless, GSK-3 is a versatile enzyme with over 100 described substrates (Beurel et al., 2015) and NF-κB may be one of its plethora of targets. As aforementioned, strategies to lower the retinal inflammatory state associated to RP have rendered positive outcomes (Peng et al., 2014; Martínez-Fernández de la Cámara et al., 2015). VP3.15 treatment reduced the expression levels of proinflammatory cytokines (*Tnf* and *Il1b*, Appendix 2), which could explain, at least in part, the attenuation of photoreceptor degeneration and loss. When VP3.15 was administered *in vivo* to *rd10* animals, we observed that the thickness of the photoreceptor cell layer was better preserved in VP3.15-treated *rd10* mice (Figure 4.17 and Figure 4.19). Interestingly, also both the cone and the rod outer segment were better preserved in VP3.15-treated mice (Figure 4.19). Importantly, the treatment with VP3.15 did not have deleterious effects on other retinal cells, such bipolar and ganglion cells (Figure 4.18). This retinal cytoarchitecture protection achieved by VP3.15 was accompanied by a delay in visual function loss. Studies carried out in the laboratory of Dr. P. de la Villa showed that the administration of VP.15 resulted in a better retinal electroretinographic response in the *rd10* mice (Appendix 2).

Moreover, it would be of interest to analyze which isoform of GSK-3 is responsible for the beneficial effects of VP3.15 since both GSK-3β and GSK-3α are inhibited by VP3.15. However, this may be a complicated task due to their frequent overlapping functions (Beurel et al., 2015). VP3.15 is also an allosteric inhibitor of PDE7 and it would be interesting to determine the contribution of PDE7 inhibition to the VP3.15 neuroprotective properties. However, PDE7 inhibition, via increasing cAMP levels and PKA activation, also converges on GSK-3 inhibition (Morales-Garcia et al., 2014). PKA is able to phosphorylate GSK-3β at Ser9 and, subsequently, to inactivate it (Morales-Garcia et al., 2014; Wyse Jackson and Cotter, 2016). Besides, previous findings by our group support that the prosurvival effect of VP3.15 in photoreceptors may be primarily due to GSK-3 inhibition, since the specific GSK-3 inhibitor tideglusib exerted an even more potent neuroprotective effect in photoreceptors (Marchena et al., 2017).

Overall, in this thesis we have shown that GSK-3 could be a good target for RP treatment. The administration of GSK-3 inhibitor VP3.15 to *rd10* mice provides a delay in the photoreceptor

death, in line with the observed ameliorated retinal function loss. VP3.15 was a compound designed to treat non-retinal neurodegenerative disorders like multiple sclerosis (Medina-Rodríguez et al., 2017). The successful use of VP3.15 in RP animal models emphasizes the importance of repurposing drugs that were designed to treat other neurodegenerative diseases to treat RP.

5.3. TLRs in the context of RP

The objective of the third part of this thesis was to characterize *Tlr* gene expression in *rd10* in comparison with WT retinas and to determine whether the depletion of *Tlr2* or *Tlr4* alters the course of RP.

The expression of *Tlr1-9* and their adaptor proteins (of both MyD88-dependent and MyD88-independent pathways) was increased in *rd10* in comparison with WT mice (Figure 4.21 and Figure 4.22). In parallel, *rd10* mice showed an increase in the gene expression of pro-inflammatory cytokines (*Tnf* and *Il1b*). Also, P23H retinas increased the expression of *Tlr2*, *Tlr4* and TLR adaptor protein genes (Figure 4.23). Interestingly, in the WT mice, the expression of most of the *Tlr* and TLR adaptor genes decreased between P14 to P21 (Figure 4.21 and Figure 4.22). In addition, we showed that the deficiency of *Tlr2* or *Tlr4* resulted in opposite effects in RP progression. The deficiency of *Tlr4* both in heterozygosity or homozygosity resulted in a faster retinal function loss in *rd10* mice (Figure 4.25 and Figure 4.27). Similarly, the deficiency of *Tlr4* resulted in an accelerated retinal function loss in P23H mice (Figure 4.29 and Figure 4.30). These results were associated to a decreased preservation of photoreceptor integrity in *Tlr4*-deficient RP mice (Figure 4.26, Figure 4.28 and Figure 4.31). The detrimental consequences of *Tlr4* deletion could be related to an alteration of the phenotype of the microglia that invade the photoreceptor layers (Figure 4.35). However, the absence of *Tlr4* did not decrease the ERG response or affect photoreceptor integrity in physiological conditions (Figure 4.32, Figure 4.33 and Figure 4.34). On the contrary, *Tlr2* deficiency in both *rd10* and P23H mice preserved retinal function loss (Figure 4.37 and Figure 4.38).

In this study we have shown that the expression of *Tlr* genes and their adaptor proteins is increased in the *rd10* retina at P21, when the inflammatory status of the retina is well established. Similar increase of TLR expression has been described in human brains in the context of neurodegenerative conditions like AD and PD (Dzamko et al., 2017; Fiebich et al., 2018). This net increase is likely contributed by an increment in expression levels per cell, by the proliferation of microglia cells, which present prominent expression of TLRs (Hanke and Kielian, 2011) and by the infiltration of circulating monocytes (Zhao et al., 2015).

Interestingly, in the WT retina, *Tlr* expression (particularly of *Tlr1* and *Tlr6*) and that of some adaptor proteins (Figure 4.21 and Figure 4.22) decreased from P14 to P21. This reduction was not observed in the *rd10* retinas, most probably because it was masked by the increased expression levels of *Tlr* and TLR adaptor proteins associated to disease progression. The changes of the expression of *Tlr* and TLR adaptor molecules during early post-natal age of the WT retina could be due to microglia maturation that is still taking place during post-natal development (Tian, 2004; Scheffel et al., 2012). Variations in *Tlr* expression have been reported associated to brain development and post-natal maturation (Barak et al., 2014). Some *Tlr* genes increased their expression during brain maturation (*Tlr* genes 1, 2, 4, 6 and 9), while others showed decreased levels at the last stages of brain maturation (*Tlr* genes 3, 7 and 8).

The role of TLRs, mainly of TLR4, has been studied in animal models of other ocular neurodegenerative conditions like glaucoma (Kilic et al., 2008) or AMD (Kohno et al., 2013). *Tlr4* deficiency results in a decreased ganglion cell death after *in vivo* axotomy as a model of glaucoma. In the same line, deletion of *Tlr4* in an AMD mouse leads to decreased photoreceptor cell death after light exposure. However, the role of TLRs in RP progression had not been specifically studied.

As previously mentioned, the influence of TLR4 in brain neurodegeneration has been studied in animal models of different neurodegenerative disorders with outcomes that vary in a disease-specific manner and even with controversial results. Tahara et al. (2006) showed that *Tlr4* heterozygosity leads to an aggravation of AD, effect that is further intensified by the complete depletion of *Tlr4*. In contrast, the presence of the TLR4 polymorphism Asp299Gly that results in a hypofunctional protein is considered to be protective in AD (Minoretti et al., 2006). The effect of TLR4 in the progression of α-synucleinopathies is also controversial, while some authors reported that *Tlr4* deletion has a beneficial role (Stefanova et al., 2011), others showed the opposite effect (Campolo et al., 2019). In stroke, *Tlr4* depletion or pharmacological inhibition showed beneficial outcomes in animal models, reducing the infarct volume (Cao et al., 2007; Caso et al., 2007; Fernández et al., 2018). However, it is known that TLR4 can be protective in stroke due to its participation in ischemic preconditioning. In this case, a short ischemic event results in a subsequent protection to a severe ischemia (Tasaki et al., 1997; Rosenzweig et al., 2007; Pradillo et al., 2009).

In the two RP models studied here, TLR4 exerts a protective role in the progression of the disease. Although more studies are needed to determine the mechanisms underlying this effect, our preliminary results indicate that TLR4 acts as molecular brake, preventing microglia of

entering in an over-reactive state. Interestingly, it has been proposed that TLR4 participate in ischemic preconditioning, a protective endogenous response triggered by a low-grade insult previous to a severe injury (Tasaki et al., 1997; Rosenzweig et al., 2007; Pradillo et al., 2009). This protective effect has been mimicked by pre-exposing the animals to low doses of the TLR4 agonist LPS (Rosenzweig, 2004) and is reduced in *Tlr4* deficient mice (Pradillo et al., 2009). In addition, the previous administration of small doses of LPS to mice can lead to a tolerized state, which prevents overproduction of pro-inflammatory cytokines and protects the mice to otherwise lethal doses of LPS, as reviewed in Biswas and Lopez-Collazo (2009). Tolerance can also be induced towards heterologous stimuli (Seeley and Ghosh, 2017). The acquisition of the tolerized state could be mediated by several mechanisms. It has been proposed to be regulated by a variety of epigenetic mechanisms (Foster et al., 2007; Novakovic et al., 2016) that include histone acetylation, methylation or phosphorylation in genes such as *Tnf* or *Il6*, as reviewed in Seeley and Ghosh (2017). In addition, the switch from TLR4 MyD88-dependent to MyD88-independent signaling pathway could lead to an attenuation of the inflammatory response and thus to the acquisition of the tolerized phenotype. It has been described that after a first stress the MyD88 pathway is activated, while the response to the second stress is mediated via the less inflammatory MyD88-independent pathway (Broad et al., 2006; Biswas and Lopez-Collazo, 2009; Leitner et al., 2019). In this regard, interferon regulatory factor 3 (IRF3), a crucial molecule in the MyD88-independent pathway has been shown to mediate the switch from inflammatory microglia to a less inflammatory phenotype (Tarassishin et al., 2011). Interestingly, type I IFNs have been shown to redirect microglia in an AMD animal model to a more neuroprotective phenotype, as reviewed in Rashid et al. (2019) and lead to the production of the anti-inflammatory cytokine IL-10 (Chang et al., 2007).

The beneficial effects of TLR4 in AD and PD have been related to the microglial clearance of β-amyloid plaques (Tahara et al., 2006) and α-synuclein deposits (Stefanova et al., 2011). In absence of TLR4, microglial phagocytic activity is decreased, aggravating the disease progression. Conversely, it has been shown that over-reactive microglia phagocyte alive neurons (Brown and Neher, 2014). In this line, Zhao *et al*, demonstrate that microglia engulf alive photoreceptors in an RP model (Zhao et al., 2015). In our study, *rd10* TLR4-deficient animals depict increase amount of phagocytic $P2Y12^{-}CD68^{+}$ cells and decrease of $P2Y12^{+}CD68^{-}$ homeostatic microglia. The higher number of phagocytic cells observed upon *Tlr4* depletion could compromise photoreceptor integrity and retinal function. Analysis of microglia isolated from RP animal models with or without TLR4 would facilitate the study of the role of TLR4 on microglia behavior. Thus, microglia phagocytic activity could be addressed by using assays based

on the engulfment of fluorescent beads as described in Lian et al. (2016). Also, the transcriptomic profile of the microglia of the different genotypes could be compared. Nevertheless, during RP progression, besides microglia activation, there is retinal infiltration of circulating monocyte-derived macrophages. Since both populations could have distinct functions in photoreceptor degeneration, as described in O'Koren et al. (2019), it would be interesting to assess both cell types independently.

However, TLRs actions in the retina could not be restricted to microglia since expression of TLRs has been associated to other retinal cells like Müller glia (Lin et al., 2013). In RP, Müller glia undergo a process of gliosis in response to damage, which can lead to the aggravation of the disease (Goldman, 2014; de Hoz et al., 2016). Therefore, it would be interesting to address whether the presence of TLRs in this cell type could participate in Müller glia gliosis. The RPE also expresses high levels of TLRs (Kindzelskii et al., 2004). The RPE participates in the homeostatic phagocytosis of photoreceptors allowing for the recycle of the retinal in the visual cycle, which has been suggested to be mediated by TLR4 (Kindzelskii et al., 2004). In addition, the RPE is an immunoprivileged layer with anti-inflammatory functions that secretes transforming growth factor β (TGF-β) (Griffith et al., 1995; Wenkel and Streilein, 2000; Levy et al., 2015). These immune properties could be altered in the absence of TLR4 and thus contribute to the inflammatory state associated to RP. The generation of cell-type conditional deletion of *Tlr4* would help to clarify the contribution of each cell type to the observed phenotype.

Of note, *Tlr4* deletion in WT mice did not have negative consequences but increased the animal ERG response (Figure 4.32 and Figure 4.33). Although, further studies are necessary to explain this result, it could be a consequence of the participation of microglia in the developmental pruning of synapses (Li et al., 2019), as well as of compensatory mechanisms of *Tlr4* deficient mice. Again, conditional knock out animal models that allow for age- and cell-type specific deletion may help to address this point. These results are in discrepancy with the study by Noailles et al. (2019), that found mild attenuation of ERG response upon *Tlr4* deletion in WT mice. We do not know the reason for this disagreement but different light housing conditions have major impact in the age-dependent visual function loss because excessive light can aggravate phototoxicity. In that case, *Tlr4* deletion may accelerate the deleterious effect of excessive light as shown in Kohno et al. (2013).

The influence of TLR2 in neurodegenerative disorders has been less studied, although its participation in the progression of AD, PD and stroke has been reported, with controversial results in some cases. In the context of AD, the activity of TLR2 has been reported to be beneficial

(Richard et al., 2008) or detrimental (McDonald et al., 2016). In PD and stroke, TLR2 has been reported to be detrimental (Tang et al., 2007; Kim et al., 2018). Our results show that contrary to *Tlr4*, the absence of *Tlr2* delays disease progression in two RP models. TLR2 only signals through the MyD88-dependent pathway that leads to the activation of NF-κB, among other proinflammatory regulators, resulting in the expression of pro-inflammatory cytokines, such as *Tnf* and *Il1b* (Kawai and Akira, 2007). In this direction, *Myd88* genetic ablation or pharmacological inhibition results in a delayed RP progression in mice (Syeda et al., 2015; Garces et al., 2020). In this regard, since TLR4 shares several DAMPs with TLR2 and other TLRs (Fadakar et al., 2014), the absence of TLR4 could lead to increased signaling through the MyD88-dependent pathway resulting in a more exacerbated inflammatory response.

Given that the genetic ablation provides protection in RP progression, TLR2 inhibition could be a good pharmacological target for the treatment of RP. Pharmacological inhibitors of TLR2 have been developed and are commercially available, although their use for the treatment of neurodegenerative diseases has been scarce. One of these molecules is CUCPT22 (Tocris, Bristol, UK). Remarkably, this molecule could reduce the activation of primary mouse microglia when α-synuclein was administered *ex vivo* (Daniele et al., 2015). However, CUCPT22 only inhibits TLR1/TLR2 interaction and has no antagonist activity toward TLR2/TLR6 signaling. In addition, antibodies that target TLR2 have been employed with good results in PD animal models (Kim et al., 2018). In addition, another TLR2 neutralizing antibody (OPN-305) is being studied in clinical trials for the treatment of a subtype of blood cell neoplasias without showing toxicity (Garcia-Manero et al., 2016). Pharmacological interference studies would validate TLR2 as a target for RP treatment.

To sum up, we have shown that the expression of TLRs is upregulated in the context of RP. Genetic deletion of TLR4 and TLR2 resulted in opposite outcomes on RP progression. While TLR4 has a protective function, TLR2 has a detrimental role. In light of these results, we propose that TLR2 could be a potential therapeutic target for the RP. However, the pharmacological inhibition of TLR4 in RP should be questioned since in our models TLR4 deficiency leads to an aggravation of the disease.

5.4. Concluding remarks

In this thesis we have explored several targets that provide novel perspectives for RP treatment. On the one hand, we used two pharmacological drugs aimed to confer neuroprotection on RP mice. Administration of hPi and the GSK-3 inhibitor VP3.15 could be potential therapeutic approaches for RP treatment. In addition, we characterized the physio-

pathological status of both IR and GSK-3 and showed that IR expression and signaling at horizontal cells were damped in the RP retina, which could participate in the RP retinal structural and functional decline. On the contrary, the AKT-GSK3 pathway was activated in the RP retina. Both hPi and VP3.15 treatments modulated the inflammatory response of RP retinas. In addition, we carried out genetic deletion strategies to analyze the role of TLR4 and TLR2 on RP progression. While *Tlr4* deficiency was detrimental for RP progression, *Tlr2* deletion preserved visual function. These results indicate that TLR2 could be a potential therapeutic target for RP treatment, but caution should be taken respect to TLR4 inhibition in the context of RP.

In this thesis, we have emphasized the importance of repurposing therapeutic targets and drugs that were previously described in the context of other neurodegenerative conditions to treat RP. The retina is part of the CNS and therefore it shares many traits and characteristics with the brain (de la Rosa and Hernández-Sánchez, 2018). The accessibility of the retina to non-invasive quantitative diagnostic techniques, such as ERG and OCT, allows an easier evaluation of the efficacy of candidate therapies in clinical trials. The evaluation of these drugs provides important clues not only to the treatment of devastating conditions caused by retinal degeneration, but also to their potential efficacy in the brain. In summary, the devastating effects of neurodegenerative diseases of both the retina and the brain on patients, their families, and society as a whole can be better fought by taking advantage of the large body of knowledge obtained in the search for novel treatments for neurodegenerative conditions of the brain and by exploiting the unique physiological features of the eye that provide us with a window into the CNS.

SECTION 6
CONCLUSIONS

6. CONCLUSIONS

1. In physiological conditions, IR is prominently expressed in the horizontal and ganglion cell axons.

2. IR and IR signaling ($pS6^{Ser240/Ser244}$) are selectively downregulated in the horizontal cells in the *rd10* retinas. In parallel with this alteration, there is a disconnection of rods with their post-synaptic partners, horizontal and bipolar cells.

3. The administration of hPi to *rd10* mice results in a) restoration of IR signaling in horizontal cells, b) preservation of photoreceptors, c) maintenance of rod synaptic connectivity and d) decrease of retinal inflammation.

4. The AKT-GSK-3 pathway is endogenously activated in the *rd10* retina.

5. The *in vivo* administration of the GSK-3 inhibitor VP3.15 to *rd10* mice results in a delay of the photoreceptor cell death and in a better preservation of photoreceptor outer segments.

6. The expression of *Tlr1-9* genes and TLR-adaptor protein genes is increased in *rd10* mice at early stages of degeneration. In P23H the gene expression of *Tlr2*, *Tlr4* and TLR adaptor proteins is also increased.

7. *Tlr4* haploinsufficiency accelerates visual function loss and photoreceptor degeneration in the *rd10* mice. Complete elimination of *Tlr4* aggravates this deleterious phenotype in both *rd10* and P23H RP models.

8. *Tlr4* deletion does not produce retinal function loss or affect retinal cytoarchitecture in physiological conditions.

9. Deletion of *Tlr4* alters the reactivity state of microglia occupying the photoreceptor layers. Increase proportion of phagocytic microglia and decrease of that of homeostatic microglia was observed in the *rd10*:$Tlr4^{-/-}$ respect to the *rd10*:$Tlr4^{+/-}$ retinas.

10. The depletion of *Tlr2* results in an extension of visual function in *rd10* and P23H mice.

SECTION 7
REFERENCES

7. REFERENCES

Agostinone, J., Alarcon-Martinez, L., Gamlin, C., Yu, W.Q., Wong, R.O.L., and Di Polo, A. (2018). Insulin signalling promotes dendrite and synapse regeneration and restores circuit function after axonal injury. Brain : a journal of neurology *141*, 1963-1980.

Aguirre, G.D. (2017). Concepts and Strategies in Retinal Gene Therapy. Invest Ophthalmol Vis Sci *58*, 5399-5411.

Ajami, B., Bennett, J.L., Krieger, C., Tetzlaff, W., and Rossi, F.M. (2007). Local self-renewal can sustain CNS microglia maintenance and function throughout adult life. Nature neuroscience *10*, 1538-1543.

Akiyama, M., Ikeda, Y., Yoshida, N., Notomi, S., Murakami, Y., Hisatomi, T., Enaida, H., and Ishibashi, T. (2014). Therapeutic efficacy of topical unoprostone isopropyl in retinitis pigmentosa. Acta ophthalmologica *92*, e229-234.

Ali, R.R., Sarra, G.M., Stephens, C., Alwis, M.D., Bainbridge, J.W., Munro, P.M., Fauser, S., Reichel, M.B., Kinnon, C., Hunt, D.M., Bhattacharya, S.S., and Thrasher, A.J. (2000). Restoration of photoreceptor ultrastructure and function in retinal degeneration slow mice by gene therapy. Nature genetics *25*, 306-310.

Anderson, B., Jr. (1968). Ocular effects of changes in oxygen and carbon dioxide tension. Trans Am Ophthalmol Soc *66*, 423-474.

Andrieu-Soler, C., Aubert-Pouessel, A., Doat, M., Picaud, S., Halhal, M., Simonutti, M., Venier-Julienne, M.C., Benoit, J.P., and Behar-Cohen, F. (2005). Intravitreous injection of PLGA microspheres encapsulating GDNF promotes the survival of photoreceptors in the rd1/rd1 mouse. Molecular vision *11*, 1002-1011.

Arroba, A.I., Álvarez-Lindo, N., van Rooijen, N., and de la Rosa, E.J. (2011). Microglia-Mediated IGF-I Neuroprotection in the rd10 Mouse Model of Retinitis Pigmentosa. Investigative Ophthalmology & Visual Science *52*, 9124-9130.

Athauda, D., and Foltynie, T. (2016). Insulin resistance and Parkinson's disease: A new target for disease modification? Progress in neurobiology *145-146*, 98-120.

Bahrami, H., Melia, M., and Dagnelie, G. (2006). Lutein supplementation in retinitis pigmentosa: PC-based vision assessment in a randomized double-masked placebo-controlled clinical trial [NCT00029289]. BMC Ophthalmol *6*, 23.

Baki, A., Bielik, A., Molnár, L., Szendrei, G., and Keserü, G.M. (2007). A high throughput luminescent assay for glycogen synthase kinase-3beta inhibitors. Assay Drug Dev Technol. *5*, 75-83.

Bakondi, B., Lv, W., Lu, B., Jones, M.K., Tsai, Y., Kim, K.J., Levy, R., Akhtar, A.A., Breunig, J.J., Svendsen, C.N., and Wang, S. (2016). In Vivo CRISPR/Cas9 Gene Editing Corrects Retinal Dystrophy in the S334ter-3 Rat Model of Autosomal Dominant Retinitis Pigmentosa. Molecular therapy : the journal of the American Society of Gene Therapy *24*, 556-563.

Barak, B., Feldman, N., and Okun, E. (2014). Toll-like receptors as developmental tools that regulate neurogenesis during development: an update. Frontiers in neuroscience *8*, 272.

Barhoum, R., Martinez-Navarrete, G., Corrochano, S., Germain, F., Fernandez-Sanchez, L., de la Rosa, E.J., de la Villa, P., and Cuenca, N. (2008). Functional and structural modifications during retinal degeneration in the rd10 mouse. Neuroscience *155*, 698-713.

Belfiore, A., Malaguarnera, R., Vella, V., Lawrence, M.C., Sciacca, L., Frasca, F., Morrione, A., and Vigneri, R. (2017). Insulin receptor isoforms in physiology and disease: an updated view. Endocrine reviews *38*, 379-431.

Berson, E.L., Rosner, B., Sandberg, M.A., Hayes, K.C., Nicholson, B.W., Weigel-DiFranco, C., and Willett, W. (1993). A randomized trial of vitamin A and vitamin E supplementation for retinitis pigmentosa. Archives of Ophthalmology *111*, 761-772.

Berson, E.L., Rosner, B., Sandberg, M.A., Weigel-DiFranco, C., Brockhurst, R.J., Hayes, K.C., Johnson, E.J., Anderson, E.J., Johnson, C.A., Gaudio, A.R., Willett, W.C., and Schaefer, E.J. (2010). Clinical trial of lutein in patients with retinitis pigmentosa receiving vitamin A. Archives of ophthalmology (Chicago, Ill : 1960) *128*, 403-411.

Beurel, E., Grieco, S.F., and Jope, R.S. (2015). Glycogen synthase kinase-3 (GSK3): regulation, actions, and diseases. Pharmacology & therapeutics *148*, 114-131.

Beurel, E., and Jope, R.S. (2006). The paradoxical pro- and anti-apoptotic actions of GSK3 in the intrinsic and extrinsic apoptosis signaling pathways. Progress in neurobiology *79*, 173-189.

Beurel, E., Kaidanovich-Beilin, O., Yeh, W.I., Song, L., Palomo, V., Michalek, S.M., Woodgett, J.R., Harrington, L.E., Eldar-Finkelman, H., Martinez, A., and Jope, R.S. (2013). Regulation of Th1 cells and experimental autoimmune encephalomyelitis by glycogen synthase kinase-3. Journal of immunology (Baltimore, Md : 1950) *190*, 5000-5011.

Bhalla, S., Joshi, D., Bhullar, S., Kasuga, D., Park, Y., and Kay, C.N. (2013). Long-term follow-up for efficacy and safety of treatment of retinitis pigmentosa with valproic acid. The British journal of ophthalmology *97*, 895-899.

Birch, D.G., Bernstein, P.S., Iannacone, A., Pennesi, M.E., Lam, B.L., Heckenlively, J., Csaky, K., Hartnett, M.E., Winthrop, K.L., Jayasundera, T., Hughbanks-Wheaton, D.K., Warner, J., Yang, P., Fish, G.E., Teske, M.P., Sklaver, N.L., Erker, L., Chegarnov, E., Smith, T., Wahle, A., VanVeldhuisen, P.C., McCormack, J., Lindblad, R., Bramer, S., Rose, S., Zilliox, P., Francis, P.J., and Weleber, R.G. (2018). Effect of oral valproic acid vs placebo for vision loss in patients with autosomal dominant retinitis pigmentosa: a randomized phase 2 multicenter placebo-controlled clinical trial. JAMA ophthalmology *136*, 849-856.

Birch, D.G., Weleber, R.G., Duncan, J.L., Jaffe, G.J., and Tao, W. (2013). Randomized trial of ciliary neurotrophic factor delivered by encapsulated cell intraocular implants for retinitis pigmentosa. Am J Ophthalmol *156*, 283-292.e281.

Biswas, S.K., and Lopez-Collazo, E. (2009). Endotoxin tolerance: new mechanisms, molecules and clinical significance. Trends in immunology *30*, 475-487.

Blázquez, E., Velázquez, E., Hurtado-Carneiro, V., and Ruiz-Albusac, J.M. (2014). Insulin in the brain: its pathophysiological implications for states related with central insulin resistance, type 2 diabetes and Alzheimer's disease. Frontiers in endocrinology *5*, 161.

Bloom, G.S., Lazo, J.S., and Norambuena, A. (2018). Reduced brain insulin signaling: A seminal process in Alzheimer's disease pathogenesis. Neuropharmacology *136*, 192-195.

Boatright, J.H., Moring, A.G., McElroy, C., Phillips, M.J., Do, V.T., Chang, B., Hawes, N.L., Boyd, A.P., Sidney, S.S., Stewart, R.E., Minear, S.C., Chaudhury, R., Ciavatta, V.T., Rodrigues, C.M., Steer, C.J., Nickerson, J.M., and Pardue, M.T. (2006). Tool from ancient pharmacopoeia prevents vision loss. Molecular vision *12*, 1706-1714.

Botta, S., Marrocco, E., de Prisco, N., Curion, F., Renda, M., Sofia, M., Lupo, M., Carissimo, A., Bacci, M.L., Gesualdo, C., Rossi, S., Simonelli, F., and Surace, E.M. (2016). Rhodopsin targeted transcriptional silencing by DNA-binding. Elife *5*, e12242.

Bradley, C.A., Peineau, S., Taghibiglou, C., Nicolas, C.S., Whitcomb, D.J., Bortolotto, Z.A., Kaang, B.K., Cho, K., Wang, Y.T., and Collingridge, G.L. (2012). A pivotal role of GSK-3 in synaptic plasticity. Frontiers in molecular neuroscience *5*, 13.

Bravo-Gil, N., Mendez-Vidal, C., Romero-Perez, L., Gonzalez-del Pozo, M., Rodriguez-de la Rua, E., Dopazo, J., Borrego, S., and Antinolo, G. (2016). Improving the management of Inherited Retinal Dystrophies by targeted sequencing of a population-specific gene panel. Sci Rep *6*, 23910.

Brito-Garcia, N., Del Pino-Sedeno, T., Trujillo-Martin, M.M., Coco, R.M., Rodriguez de la Rua, E., Del Cura-Gonzalez, I., and Serrano-Aguilar, P. (2017). Effectiveness and safety of nutritional supplements in the treatment of hereditary retinal dystrophies: a systematic review. Eye (Lond) *31*, 273-285.

Briz, V., Restivo, L., Pasciuto, E., Juczewski, K., Mercaldo, V., Lo, A.C., Baatsen, P., Gounko, N.V., Borreca, A., Girardi, T., Luca, R., Nys, J., Poorthuis, R.B., Mansvelder, H.D., Fisone, G., Ammassari-Teule, M., Arckens, L., Krieger, P., Meredith, R., and Bagni, C. (2017). The non-coding RNA BC1 regulates experience-dependent structural plasticity and learning. Nature communications *8*, 293.

Broad, A., Jones, D.E., and Kirby, J.A. (2006). Toll-like receptor (TLR) response tolerance: a key physiological "damage limitation" effect and an important potential opportunity for therapy. Current medicinal chemistry *13*, 2487-2502.

Brown, G.C., and Neher, J.J. (2014). Microglial phagocytosis of live neurons. Nature reviews Neuroscience *15*, 209-216.

Bruning, J.C., Gautam, D., Burks, D.J., Gillette, J., Schubert, M., Orban, P.C., Klein, R., Krone, W., Muller-Wieland, D., and Kahn, C.R. (2000). Role of brain insulin receptor in control of body weight and reproduction. Science (New York, NY) *289*, 2122-2125.

Bsibsi, M., Ravid, R., Gveric, D., and van Noort, J.M. (2002). Broad expression of Toll-like receptors in the human central nervous system. Journal of neuropathology and experimental neurology *61*, 1013-1021.

Cai, X., Conley, S.M., Nash, Z., Fliesler, S.J., Cooper, M.J., and Naash, M.I. (2010). Gene delivery to mitotic and postmitotic photoreceptors via compacted DNA nanoparticles results in improved phenotype in a mouse model of retinitis pigmentosa. FASEB journal : official publication of the Federation of American Societies for Experimental Biology *24*, 1178-1191.

Cajal, S.R. (1892). La retina de los teleósteos y algunas observaciones sobre la de los vertebrados superiores. An Soc Españ d Hist Nat *21*, 1-29.

Callejas, D., Mann, C.J., Ayuso, E., Lage, R., Grifoll, I., Roca, C., Andaluz, A., Ruiz-de Gopegui, R., Montané, J., Muñoz, S., Ferre, T., Haurigot, V., Zhou, S., Ruberte, J., Mingozzi, F., A High, K., Garcia, F. and Bosch, F. (2013) Treatment of diabetes and long-term survival after insulin and glucokinase gene therapy. Diabetes *62*, 1718-1729.

Campolo, M., Paterniti, I., Siracusa, R., Filippone, A., Esposito, E., and Cuzzocrea, S. (2019). TLR4 absence reduces neuroinflammation and inflammasome activation in Parkinson's diseases in vivo model. Brain, behavior, and immunity *76*, 236-247.

Cao, C.X., Yang, Q.W., Lv, F.L., Cui, J., Fu, H.B., and Wang, J.Z. (2007). Reduced cerebral ischemia-reperfusion injury in Toll-like receptor 4 deficient mice. Biochemical and biophysical research communications *353*, 509-514.

Caso, J.R., Pradillo, J.M., Hurtado, O., Lorenzo, P., Moro, M.A., and Lizasoain, I. (2007). Toll-like receptor 4 is involved in brain damage and inflammation after experimental stroke. Circulation *115*, 1599-1608.

Castro, A.A., Ghisoni, K., Latini, A., Quevedo, J., Tasca, C.I., and Prediger, R.D. (2012). Lithium and valproate prevent olfactory discrimination and short-term memory impairments in the intranasal 1-methyl-4-phenyl-1,2,3,6-tetrahydropyridine (MPTP) rat model of Parkinson's disease. Behavioural brain research *229*, 208-215.

Cayouette, M., Behn, D., Sendtner, M., Lachapelle, P., and Gravel, C. (1998). Intraocular gene transfer of ciliary neurotrophic factor prevents death and increases responsiveness of rod photoreceptors in the retinal degeneration slow mouse. The Journal of neuroscience : the official journal of the Society for Neuroscience *18*, 9282-9293.

Cayouette, M., and Gravel, C. (1997). Adenovirus-mediated gene transfer of ciliary neurotrophic factor can prevent photoreceptor degeneration in the retinal degeneration (rd) mouse. Human gene therapy *8*, 423-430.

Cayouette, M., Smith, S.B., Becerra, S.P., and Gravel, C. (1999). Pigment Epithelium-Derived Factor delays the death of photoreceptors in mouse models of inherited retinal degenerations. Neurobiology of Disease *6*, 523-532.

Chakravarty, S., and Herkenham, M. (2005). Toll-like receptor 4 on nonhematopoietic cells sustains CNS inflammation during endotoxemia, independent of systemic cytokines. The Journal of neuroscience : the official journal of the Society for Neuroscience *25*, 1788-1796.

Chang, E.Y., Guo, B., Doyle, S.E., and Cheng, G. (2007). Cutting Edge: Involvement of the type I IFN production and signaling pathway in lipopolysaccharide-induced IL-10 production. *178*, 6705-6709.

Chapman, C.D., Schiöth, H.B., Grillo, C.A., and Benedict, C. (2018). Intranasal insulin in Alzheimer's disease: Food for thought. Neuropharmacology *136*, 196-201.

Chapot, C.A., Euler, T., and Schubert, T. (2017). How do horizontal cells 'talk' to cone photoreceptors? Different levels of complexity at the cone-horizontal cell synapse. The Journal of physiology *595*, 5495-5506.

Chen, G., Huang, L.D., Jiang, Y.M., and Manji, H.K. (1999). The mood-stabilizing agent valproate inhibits the activity of glycogen synthase kinase-3. Journal of neurochemistry *72*, 1327-1330.

Chen, G.Y., and Nuñez, G. (2010). Sterile inflammation: sensing and reacting to damage. Nature reviews Immunology *10*, 826-837.

Chen, W.J., Ma, L., Li, M.S., and Ma, X. (2019). Valproic acid's effects on visual acuity in retinitis pigmentosa: a systemic review and Meta-analysis. International journal of ophthalmology *12*, 129-134.

Chitnis, T., and Weiner, H.L. (2017). CNS inflammation and neurodegeneration. The Journal of clinical investigation *127*, 3577-3587.

Chiu, S.L., Chen, C.M., and Cline, H.T. (2008). Insulin receptor signaling regulates synapse number, dendritic plasticity, and circuit function in vivo. Neuron *58*, 708-719.

Chiu, S.L., and Cline, H.T. (2010). Insulin receptor signaling in the development of neuronal structure and function. Neural development *5*, 7.

Choi, J., Ko, J., Racz, B., Burette, A., Lee, J.R., Kim, S., Na, M., Lee, H.W., Kim, K., Weinberg, R.J., and Kim, E. (2005). Regulation of dendritic spine morphogenesis by insulin receptor substrate 53, a downstream effector of Rac1 and Cdc42 small GTPases. The Journal of neuroscience : the official journal of the Society for Neuroscience *25*, 869-879.

Christian, F., Smith, E.L., and Carmody, R.J. (2016). The Regulation of NF-κB Subunits by Phosphorylation. Cells *5*.

Cideciyan, A.V., Sudharsan, R., Dufour, V.L., Massengill, M.T., Iwabe, S., Swider, M., Lisi, B., Sumaroka, A., Marinho, L.F., Appelbaum, T., Rossmiller, B., Hauswirth, W.W., Jacobson, S.G., Lewin, A.S., Aguirre, G.D., and Beltran, W.A. (2018). Mutation-independent rhodopsin gene therapy by knockdown and replacement with a single AAV vector. Proceedings of the National Academy of Sciences of the United States of America *115*, E8547-e8556.

Claxton, A., Baker, L.D., Wilkinson, C.W., Trittschuh, E.H., Chapman, D., Watson, G.S., Cholerton, B., Plymate, S.R., Arbuckle, M., and Craft, S. (2013). Sex and ApoE genotype differences in treatment response to two doses of intranasal insulin in adults with mild cognitive impairment or Alzheimer's disease. Journal of Alzheimer's disease : JAD *35*, 789-797.

Clemson, C.M., Tzekov, R., Krebs, M., Checchi, J.M., Bigelow, C., and Kaushal, S. (2011). Therapeutic potential of valproic acid for retinitis pigmentosa. The British journal of ophthalmology *95*, 89-93.

Corpas, R., Hernandez-Pinto, A.M., Porquet, D., Hernandez-Sanchez, C., Bosch, F., Ortega-Aznar, A., Comellas, F., de la Rosa, E.J., and Sanfeliu, C. (2017). Proinsulin protects against age-related cognitive loss through anti-inflammatory convergent pathways. Neuropharmacology *123*, 221-232.

Corrochano, S., Barhoum, R., Boya, P., Arroba, A.I., Rodriguez-Muela, N., Gomez-Vicente, V., Bosch, F., de Pablo, F., de la Villa, P., and de la Rosa, E.J. (2008). Attenuation of vision loss and delay in apoptosis of photoreceptors induced by proinsulin in a mouse model of retinitis pigmentosa. Invest Ophthalmol Vis Sci *49*, 4188-4194.

Craft, S., Baker, L.D., Montine, T.J., Minoshima, S., Watson, G.S., Claxton, A., Arbuckle, M., Callaghan, M., Tsai, E., Plymate, S.R., Green, P.S., Leverenz, J., Cross, D., and Gerton, B. (2012). Intranasal insulin therapy for alzheimer disease and amnestic mild cognitive impairment: a pilot clinical trial. Archives of Neurology *69*, 29-38.

Craft, S., Claxton, A., Baker, L.D., Hanson, A.J., Cholerton, B., Trittschuh, E.H., Dahl, D., Caulder, E., Neth, B., Montine, T.J., Jung, Y., Maldjian, J., Whitlow, C., and Friedman, S. (2017). Effects of regular and long-acting insulin on cognition and Alzheimer's disease biomarkers: a pilot clinical trial. Journal of Alzheimer's disease : JAD *57*, 1325-1334.

Cuenca, N., Fernandez-Sanchez, L., Campello, L., Maneu, V., De la Villa, P., Lax, P., and Pinilla, I. (2014). Cellular responses following retinal injuries and therapeutic approaches for neurodegenerative diseases. Prog Retin Eye Res *43*, 17-75.

Daniele, S.G., Béraud, D., Davenport, C., Cheng, K., Yin, H., and Maguire-Zeiss, K.A. (2015). Activation of MyD88-dependent TLR1/2 signaling by misfolded α-synuclein, a protein linked to neurodegenerative disorders. Science signaling *8*, ra45.

de Hoz, R., Rojas, B., Ramirez, A.I., Salazar, J.J., Gallego, B.I., Trivino, A., and Ramirez, J.M. (2016). Retinal macroglial responses in health and disease. Biomed Res Int *2016*, 2954721.

de la Monte, S.M., and Wands, J.R. (2005). Review of insulin and insulin-like growth factor expression, signaling, and malfunction in the central nervous system: relevance to Alzheimer's disease. Journal of Alzheimer's disease : JAD *7*, 45-61.

de la Rosa, E.J., and Hernández-Sánchez, C. (2018). CNS targets for the treatment of retinal dystrophies: a win-win strategy. Therapies for retinal degeneration, 61-75.

De Sarno, P., Axtell, R.C., Raman, C., Roth, K.A., Alessi, D.R., and Jope, R.S. (2008). Lithium prevents and ameliorates experimental autoimmune encephalomyelitis. Journal of immunology (Baltimore, Md : 1950) *181*, 338-345.

De Sarno, P., Li, X., and Jope, R.S. (2002). Regulation of Akt and glycogen synthase kinase-3 beta phosphorylation by sodium valproate and lithium. Neuropharmacology *43*, 1158-1164.

del Ser, T., Steinwachs, K.C., Gertz, H.J., Andres, M.V., Gomez-Carrillo, B., Medina, M., Vericat, J.A., Redondo, P., Fleet, D., and Leon, T. (2013). Treatment of Alzheimer's disease with the GSK-3 inhibitor tideglusib: a pilot study. Journal of Alzheimer's disease : JAD *33*, 205-215.

Diakatou, M., Manes, G., Bocquet, B., Meunier, I., and Kalatzis, V. (2019). Genome editing as a treatment for the most prevalent causative genes of autosomal dominant retinitis pigmentosa. Int J Mol Sci *20*.

Dixon-Salazar, T.J., Fourgeaud, L., Tyler, C.M., Poole, J.R., Park, J.J., and Boulanger, L.M. (2014). MHC class I limits hippocampal synapse density by inhibiting neuronal insulin receptor signaling. The Journal of neuroscience : the official journal of the Society for Neuroscience *34*, 11844-11856.

Doonan, F., Donovan, M., and Cotter, T.G. (2005). Activation of multiple pathways during photoreceptor apoptosis in the rd mouse. Invest Ophthalmol Vis Sci *46*, 3530-3538.

Doonan, F., O'Driscoll, C., Kenna, P., and Cotter, T.G. (2011). Enhancing survival of photoreceptor cells in vivo using the synthetic progestin Norgestrel. Journal of neurochemistry *118*, 915-927.

Doroudchi, M.M., Greenberg, K.P., Liu, J., Silka, K.A., Boyden, E.S., Lockridge, J.A., Arman, A.C., Janani, R., Boye, S.E., Boye, S.L., Gordon, G.M., Matteo, B.C., Sampath, A.P., Hauswirth, W.W., and Horsager, A. (2011). Virally delivered channelrhodopsin-2 safely and effectively restores visual function in multiple mouse models of blindness. Molecular therapy : the journal of the American Society of Gene Therapy *19*, 1220-1229.

Dou, J.T., Chen, M., Dufour, F., Alkon, D.L., and Zhao, W.Q. (2005). Insulin receptor signaling in long-term memory consolidation following spatial learning. Learning & memory (Cold Spring Harbor, NY) *12*, 646-655.

Drack, A.V., Dumitrescu, A.V., Bhattarai, S., Gratie, D., Stone, E.M., Mullins, R., and Sheffield, V.C. (2012). TUDCA slows retinal degeneration in two different mouse models of retinitis pigmentosa and prevents obesity in Bardet-Biedl syndrome type 1 mice. Investigative Ophthalmology & Visual Science *53*, 100-106.

Drenser, K.A., Timmers, A.M., Hauswirth, W.W., and Lewin, A.S. (1998). Ribozyme-targeted destruction of RNA associated with autosomal-dominant retinitis pigmentosa. Invest Ophthalmol Vis Sci *39*, 681-689.

Dryja, T.P., McGee, T.L., Hahn, L.B., Cowley, G.S., Olsson, J.E., Reichel, E., Sandberg, M.A., and Berson, E.L. (1990). Mutations within the rhodopsin gene in patients with autosomal dominant retinitis pigmentosa. N Engl J Med *323*, 1302-1307.

Dutta, S., and Sengupta, P. (2016). Men and mice: Relating their ages. Life sciences *152*, 244-248.

Dzamko, N., Gysbers, A., Perera, G., Bahar, A., Shankar, A., Gao, J., Fu, Y., and Halliday, G.M. (2017). Toll-like receptor 2 is increased in neurons in Parkinson's disease brain and may contribute to alpha-synuclein pathology. Acta neuropathologica *133*, 303-319.

Eigeldinger-Berthou, S., Meier, C., Zulliger, R., Lecaude, S., Enzmann, V., and Sarra, G.M. (2012). Rasagiline interferes with neurodegeneration in the Prph2/rds mouse. Retina (Philadelphia, Pa) *32*, 617-628.

Eldar-Finkelman, H., and Martinez, A. (2011). GSK-3 Inhibitors: Preclinical and clinical focus on CNS. Frontiers in molecular neuroscience *4*, 32.

Fadakar, K., Dadkhahfar, S., Esmaeili, A., and Rezaei, N. (2014). The role of Toll-like receptors (TLRs) in stroke. Reviews in the neurosciences *25*, 699-712.

Faktorovich, E.G., Steinberg, R.H., Yasumura, D., Matthes, M.T., and LaVail, M.M. (1990). Photoreceptor degeneration in inherited retinal dystrophy delayed by basic fibroblast growth factor. Nature *347*, 83-86.

Falsini, B., Iarossi, G., Chiaretti, A., Ruggiero, A., Manni, L., Galli-Resta, L., Corbo, G., and Abed, E. (2016). NGF eye-drops topical administration in patients with retinitis pigmentosa, a pilot study. Journal of translational medicine *14*, 8.

Feigenspan, A., and Babai, N. (2015). Functional properties of spontaneous excitatory currents and encoding of light/dark transitions in horizontal cells of the mouse retina. The European journal of neuroscience *42*, 2615-2632.

Fernandez-Sanchez, L., Lax, P., Isiegas, C., Ayuso, E., Ruiz, J.M., de la Villa, P., Bosch, F., de la Rosa, E.J., and Cuenca, N. (2012). Proinsulin slows retinal degeneration and vision loss in the P23H rat model of retinitis pigmentosa. Human gene therapy *23*, 1290-1300.

Fernández, G., Moraga, A., Cuartero, M.I., García-Culebras, A., Peña-Martínez, C., Pradillo, J.M., Hernández-Jiménez, M., Sacristán, S., Ayuso, M.I., Gonzalo-Gobernado, R., Fernández-López, D., Martín, M.E., Moro, M.A., González, V.M., and Lizasoain, I. (2018). TLR4-Binding DNA aptamers show a protective effect against acute stroke in animal models. Molecular therapy : the journal of the American Society of Gene Therapy *26*, 2047-2059.

Ferrari, S., Di Iorio, E., Barbaro, V., Ponzin, D., Sorrentino, F.S., and Parmeggiani, F. (2011). Retinitis pigmentosa: genes and disease mechanisms. Current genomics *12*, 238-249.

Fiebich, B.L., Batista, C.R.A., Saliba, S.W., Yousif, N.M., and de Oliveira, A.C.P. (2018). Role of Microglia TLRs in Neurodegeneration. *12*.

Finnegan, S., Mackey, A.M., and Cotter, T.G. (2010). A stress survival response in retinal cells mediated through inhibition of the serine/threonine phosphatase PP2A. The European journal of neuroscience *32*, 322-334.

Flores-Rodríguez, P.L.-S., E.; Gili P.; Carracedo, G. (2013). Retinitis pigmentosa. Gaceta de Optometría y óptica oftálmica *481*, 1-7.

Fontaine, V., Mohand-Said, S., Hanoteau, N., Fuchs, C., Pfizenmaier, K., and Eisel, U. (2002). Neurodegenerative and neuroprotective effects of tumor Necrosis factor (TNF) in retinal ischemia: opposite roles of TNF receptor 1 and TNF receptor 2. The Journal of neuroscience : the official journal of the Society for Neuroscience *22*, Rc216.

Foster, S.L., Hargreaves, D.C., and Medzhitov, R. (2007). Gene-specific control of inflammation by TLR-induced chromatin modifications. Nature *447*, 972-978.

Frasson, M., Picaud, S., Leveillard, T., Simonutti, M., Mohand-Said, S., Dreyfus, H., Hicks, D., and Sabel, J. (1999). Glial cell line-derived neurotrophic factor induces histologic and functional protection of rod photoreceptors in the rd/rd mouse. Invest Ophthalmol Vis Sci *40*, 2724-2734.

Freland, L., and Beaulieu, J.M. (2012). Inhibition of GSK3 by lithium, from single molecules to signaling networks. Frontiers in molecular neuroscience *5*, 14.

Galan, A., Jmaeff, S., Barcelona, P.F., Brahimi, F., Sarunic, M.V., and Saragovi, H.U. (2017). In retinitis pigmentosa TrkC.T1-dependent vectorial ERK activity upregulates glial TNF-alpha, causing selective neuronal death. Cell death & disease *8*, 3222.

Galloway, J.A., Hooper, S.A., Spradlin, C.T., Howey, D.C., Frank, B.H., Bowsher, R.R., and Anderson, J.H. (1992). Biosynthetic human proinsulin. Review of chemistry, in vitro and in vivo receptor binding, animal and human pharmacology studies, and clinical trial experience. Diabetes care *15*, 666-692.

Garces, K., Carmy, T., Illiano, P., Brambilla, R., and Hackam, A.S. (2020). Increased neuroprotective microglia and photoreceptor survival in the retina from a peptide inhibitor of myeloid differentiation factor 88 (MyD88). Journal of molecular neuroscience *70*, 968-980.

Garcia-Delgado, A.B., Valdes-Sanchez, L., Calado, S.M., Diaz-Corrales, F.J., and Bhattacharya, S.S. (2018). Rasagiline delays retinal degeneration in a mouse model of retinitis pigmentosa via modulation of Bax/Bcl-2 expression. CNS neuroscience & therapeutics *24*, 448-455.

Garcia-Manero, G., Montalban-Bravo, G., Yang, H., Wei, Y., Alvarado, Y., DiNardo, C.D., Daver, N.G., Konopleva, M., Hearn, K.P., Miller, R., Arbe-Barnes, S., Mc Guirk, P., Kearney, T., Keogh, B., Kantarjian, H.M., and Reilly, M. (2016). A clinical study of OPN-305, a Toll-like receptor 2 (TLR-2) antibody, in patients with lower risk myelodysplastic syndromes (MDS) that have received prior hypomethylating agent (HMA) therapy. Blood *128*, 227-227.

Gasparini, S.J., Llonch, S., Borsch, O., and Ader, M. (2019). Transplantation of photoreceptors into the degenerative retina: Current state and future perspectives. Prog Retin Eye Res *69*, 1-37.

Gesslein, B., Håkansson, G., Gustafsson, L., Ekström, P., and Malmsjö, M. (2010). Tumor necrosis factor and its receptors in the neuroretina and retinal vasculature after ischemia-reperfusion injury in the pig retina. Molecular vision *16*, 2317-2327.

Ghazi, N.G., Abboud, E.B., Nowilaty, S.R., Alkuraya, H., Alhommadi, A., Cai, H., Hou, R., Deng, W.T., Boye, S.L., Almaghamsi, A., Al Saikhan, F., Al-Dhibi, H., Birch, D., Chung, C., Colak, D., LaVail, M.M., Vollrath, D., Erger, K., Wang, W., Conlon, T., Zhang, K., Hauswirth, W., and Alkuraya, F.S. (2016). Treatment of retinitis pigmentosa due to MERTK mutations by ocular subretinal injection of adeno-associated virus gene vector: results of a phase I trial. Hum Genet *135*, 327-343.

Ghosal, K., Vogt, D.L., Liang, M., Shen, Y., Lamb, B.T., and Pimplikar, S.W. (2009). Alzheimer's disease-like pathological features in transgenic mice expressing the APP intracellular domain. Proceedings of the National Academy of Sciences of the United States of America *106*, 18367-18372.

Ginhoux, F., Greter, M., Leboeuf, M., Nandi, S., See, P., Gokhan, S., Mehler, M.F., Conway, S.J., Ng, L.G., Stanley, E.R., Samokhvalov, I.M., and Merad, M. (2010). Fate mapping analysis reveals that adult microglia derive from primitive macrophages. Science (New York, NY) *330*, 841-845.

Glybina, I.V., Kennedy, A., Ashton, P., Abrams, G.W., and Iezzi, R. (2010). Intravitreous delivery of the corticosteroid fluocinolone acetonide attenuates retinal degeneration in S334ter-4 rats. Invest Ophthalmol Vis Sci *51*, 4243-4252.

Goldman, D. (2014). Muller glial cell reprogramming and retina regeneration. Nature reviews Neuroscience *15*, 431-442.

Gorbatyuk, M.S., Pang, J.J., Thomas, J., Jr., Hauswirth, W.W., and Lewin, A.S. (2005). Knockdown of wild-type mouse rhodopsin using an AAV vectored ribozyme as part of an RNA replacement approach. Molecular vision *11*, 648-656.

Gosbell, A., Favilla, I., Baxter, K., and Jablonski, P. (2000). Insulin receptor and insulin receptor substrate-1 in rat retinae. *28*, 212-215.

Graeber, M.B., Streit, W.J., Kiefer, R., Schoen, S.W., and Kreutzberg, G.W. (1990). New expression of myelomonocytic antigens by microglia and perivascular cells following lethal motor neuron injury. Journal of neuroimmunology *27*, 121-132.

Gralle, M. (2017). The neuronal insulin receptor in its environment. Journal of neurochemistry *140*, 359-367.

Griffith, T.S., Brunner, T., Fletcher, S.M., Green, D.R., and Ferguson, T.A. (1995). Fas Ligand-Induced Apoptosis as a Mechanism of Immune Privilege. *270*, 1189-1192.

Guadagni, V., Biagioni, M., Novelli, E., Aretini, P., Mazzanti, C.M., and Strettoi, E. (2019). Rescuing cones and daylight vision in retinitis pigmentosa mice. FASEB journal : official publication of the Federation of American Societies for Experimental Biology *33*, 10177-10192.

Guadagni, V., Novelli, E., Piano, I., Gargini, C., and Strettoi, E. (2015). Pharmacological approaches to retinitis pigmentosa: A laboratory perspective. Prog Retin Eye Res *48*, 62-81.

Gupta, N., Brown, K.E., and Milam, A.H. (2003). Activated microglia in human retinitis pigmentosa, late-onset retinal degeneration, and age-related macular degeneration. Experimental Eye Research *76*, 463-471.

Hamer, J.A., Testani, D., Mansur, R.B., Lee, Y., Subramaniapillai, M., and McIntyre, R.S. (2019). Brain insulin resistance: A treatment target for cognitive impairment and anhedonia in depression. Experimental neurology *315*, 1-8.

Hamon, A., Garcia-Garcia, D., Ail, D., Bitard, J., Chesneau, A., Dalkara, D., Locker, M., Roger, J.E., and Perron, M. (2019). Linking YAP to muller glia quiescence exit in the degenerative retina. Cell reports *27*, 1712-1725.e1716.

Hampel, H., Ewers, M., Burger, K., Annas, P., Mortberg, A., Bogstedt, A., Frolich, L., Schroder, J., Schonknecht, P., Riepe, M.W., Kraft, I., Gasser, T., Leyhe, T., Moller, H.J., Kurz, A., and Basun, H. (2009). Lithium trial in Alzheimer's disease: a randomized, single-blind, placebo-controlled, multicenter 10-week study. The Journal of clinical psychiatry *70*, 922-931.

Hanger, D.P., Hughes, K., Woodgett, J.R., Brion, J.-P., and Anderton, B.H. (1992). Glycogen synthase kinase-3 induces Alzheimer's disease-like phosphorylation of tau: generation of paired helical filament epitopes and neuronal localisation of the kinase. Neuroscience Letters *147*, 58-62.

Hanke, M.L., and Kielian, T. (2011). Toll-like receptors in health and disease in the brain: mechanisms and therapeutic potential. Clinical science (London, England : 1979) *121*, 367-387.

Hartong, D.T., Berson, E.L., and Dryja, T.P. (2006). Retinitis pigmentosa. Lancet *368*, 1795-1809.

Havrankova, J., Roth, J., and Brownstein, M. (1978). Insulin receptors are widely distributed in the central nervous system of the rat. Nature *272*, 827-829.

Hayakawa, M., Fujiki, K., Kanai, A., Matsumura, M., Honda, Y., Sakaue, H., Tamai, M., Sakuma, T., Tokoro, T., Yura, T., Kubota, N., Kawano, S., Matsui, M., Yuzawa, M., Oguchi, Y., Akeo, K., Adachi, E., Kimura, T., Miyake, Y., Horiguchi, M., Wakabayashi, K., Ishizaka, N., Koizumi, K.,

Uyama, M., Ohba, N., and et al. (1997). Multicenter genetic study of retinitis pigmentosa in Japan: I. Genetic heterogeneity in typical retinitis pigmentosa. Japanese journal of ophthalmology *41*, 1-6.

Hernandez-Pinto, A., Polato, F., Subramanian, P., Rocha-Munoz, A., Vitale, S., de la Rosa, E.J., and Becerra, S.P. (2019). PEDF peptides promote photoreceptor survival in rd10 retina models. Exp Eye Res *184*, 24-29.

Hernandez-Sanchez, C., Lopez-Carranza, A., Alarcon, C., de La Rosa, E.J., and de Pablo, F. (1995). Autocrine/paracrine role of insulin-related growth factors in neurogenesis: local expression and effects on cell proliferation and differentiation in retina. Proceedings of the National Academy of Sciences of the United States of America *92*, 9834-9838.

Hirami, Y., Osakada, F., Takahashi, K., Okita, K., Yamanaka, S., Ikeda, H., Yoshimura, N., and Takahashi, M. (2009). Generation of retinal cells from mouse and human induced pluripotent stem cells. Neurosci Lett *458*, 126-131.

Hoang, M.V., Smith, L.E., and Senger, D.R. (2010). Moderate GSK-3beta inhibition improves neovascular architecture, reduces vascular leakage, and reduces retinal hypoxia in a model of ischemic retinopathy. Angiogenesis *13*, 269-277.

Hoeflich, K.P., Luo, J., Rubie, E.A., Tsao, M.S., Jin, O., and Woodgett, J.R. (2000). Requirement for glycogen synthase kinase-3beta in cell survival and NF-kappaB activation. Nature *406*, 86-90.

Hoglinger, G.U., Huppertz, H.J., Wagenpfeil, S., Andres, M.V., Belloch, V., Leon, T., and Del Ser, T. (2014). Tideglusib reduces progression of brain atrophy in progressive supranuclear palsy in a randomized trial. Movement disorders : official journal of the Movement Disorder Society *29*, 479-487.

Holt, C.E., Martin, K.C., and Schuman, E.M. (2019). Local translation in neurons: visualization and function. Nature structural & molecular biology *26*, 557-566.

Hori, K., Yasuda, H., Konno, D., Maruoka, H., Tsumoto, T., and Sobue, K. (2005). NMDA receptor-dependent synaptic translocation of insulin receptor substrate p53 via protein kinase C signaling. The Journal of neuroscience : the official journal of the Society for Neuroscience *25*, 2670-2681.

Huang, Q., Chen, R., Lin, X., and Xiang, Z. (2017). Efficacy of carbonic anhydrase inhibitors in management of cystoid macular edema in retinitis pigmentosa: A meta-analysis. PloS one *12*, e0186180.

Iraha, S., Hirami, Y., Ota, S., Sunagawa, G.A., Mandai, M., Tanihara, H., Takahashi, M., and Kurimoto, Y. (2016). Efficacy of valproic acid for retinitis pigmentosa patients: a pilot study. Clinical ophthalmology (Auckland, NZ) *10*, 1375-1384.

Isiegas, C., Marinich-Madzarevich, J.A., Marchena, M., Ruiz, J.M., Cano, M.J., de la Villa, P., Hernandez-Sanchez, C., de la Rosa, E.J., and de Pablo, F. (2016). Intravitreal injection of proinsulin-loaded microspheres delays photoreceptor cell death and vision loss in the rd10 mouse model of retinitis pigmentosa. Invest Ophthalmol Vis Sci *57*, 3610-3618.

Jeon, C.J., Strettoi, E., and Masland, R.H. (1998). The major cell populations of the mouse retina. The Journal of neuroscience : the official journal of the Society for Neuroscience *18*, 8936-8946.

Jiang, H., Guo, W., Liang, X., and Rao, Y. (2005). Both the establishment and the maintenance of neuronal polarity require active mechanisms: critical roles of GSK-3beta and its upstream regulators. Cell *120*, 123-135.

Jones, B.W., Kondo, M., Terasaki, H., Lin, Y., McCall, M., and Marc, R.E. (2012). Retinal remodeling. Japanese journal of ophthalmology *56*, 289-306.

Jope, R.S., Cheng, Y., Lowell, J.A., Worthen, R.J., Sitbon, Y.H., and Beurel, E. (2017). Stressed and inflamed, can GSK3 be blamed? Trends in biochemical sciences *42*, 180-192.

Jou, I., Lee, J.H., Park, S.Y., Yoon, H.J., Joe, E.H., and Park, E.J. (2006). Gangliosides trigger inflammatory responses via TLR4 in brain glia. The American journal of pathology *168*, 1619-1630.

Kaidanovich-Beilin, O., and Woodgett, J.R. (2011). GSK-3: functional insights from cell biology and animal models. Frontiers in molecular neuroscience *4*, 40.

Kaplan, H.J., Tezel, T.H., Berger, A.S., Wolf, M.L., and Del Priore, L.V. (1997). Human photoreceptor transplantation in retinitis pigmentosa. A safety study. Archives of ophthalmology (Chicago, Ill : 1960) *115*, 1168-1172.

Karlstetter, M., Scholz, R., Rutar, M., Wong, W.T., Provis, J.M., and Langmann, T. (2015). Retinal microglia: just bystander or target for therapy? Prog Retin Eye Res *45*, 30-57.

Kawai, T., and Akira, S. (2007). Signaling to NF-kappaB by Toll-like receptors. Trends in molecular medicine *13*, 460-469.

Kawai, T., and Akira, S. (2009). The roles of TLRs, RLRs and NLRs in pathogen recognition. International immunology *21*, 317-337.

Kessing, L.V., Forman, J.L., and Andersen, P.K. (2010). Does lithium protect against dementia? Bipolar disorders *12*, 87-94.

Kigerl, K.A., Lai, W., Rivest, S., Hart, R.P., Satoskar, A.R., and Popovich, P.G. (2007). Toll-like receptor (TLR)-2 and TLR-4 regulate inflammation, gliosis, and myelin sparing after spinal cord injury. *102*, 37-50.

Kilic, U., Kilic, E., Matter, C.M., Bassetti, C.L., and Hermann, D.M. (2008). TLR-4 deficiency protects against focal cerebral ischemia and axotomy-induced neurodegeneration. Neurobiol Dis *31*, 33-40.

Kim, C., Spencer, B., Rockenstein, E., Yamakado, H., Mante, M., Adame, A., Fields, J.A., Masliah, D., Iba, M., Lee, H.J., Rissman, R.A., Lee, S.J., and Masliah, E. (2018). Immunotherapy targeting toll-like receptor 2 alleviates neurodegeneration in models of synucleinopathy by modulating alpha-synuclein transmission and neuroinflammation. Molecular neurodegeneration *13*, 43.

Kindzelskii, A.L., Elner, V.M., Elner, S.G., Yang, D., Hughes, B.A., and Petty, H.R. (2004). Toll-like receptor 4 (TLR4) of retinal pigment epithelial cells participates in transmembrane signaling in response to photoreceptor outer segments. The Journal of general physiology *124*, 139-149.

Klein, P.S., and Melton, D.A. (1996). A molecular mechanism for the effect of lithium on development. Proceedings of the National Academy of Sciences of the United States of America *93*, 8455-8459.

Kohno, H., Chen, Y., Kevany, B.M., Pearlman, E., Miyagi, M., Maeda, T., Palczewski, K., and Maeda, A. (2013). Photoreceptor proteins initiate microglial activation via Toll-like receptor 4 in retinal degeneration mediated by all-trans-retinal. The Journal of biological chemistry *288*, 15326-15341.

Kolb, H. (1970). Organization of the outer plexiform layer of the primate retina: electron microscopy of Golgi-impregnated cells. Philosophical transactions of the Royal Society of London Series B, Biological sciences *258*, 261-283.

Kolb, H. (1974). The connections between horizontal cells and photoreceptors in the retina of the cat: Electron microscopy of Golgi preparations. *155*, 1-14.

Komeima, K., Rogers, B.S., and Campochiaro, P.A. (2007). Antioxidants slow photoreceptor cell death in mouse models of retinitis pigmentosa. Journal of cellular physiology *213*, 809-815.

Komeima, K., Rogers, B.S., Lu, L., and Campochiaro, P.A. (2006). Antioxidants reduce cone cell death in a model of retinitis pigmentosa. Proceedings of the National Academy of Sciences of the United States of America *103*, 11300-11305.

Lagali, P.S., Balya, D., Awatramani, G.B., Munch, T.A., Kim, D.S., Busskamp, V., Cepko, C.L., and Roska, B. (2008). Light-activated channels targeted to ON bipolar cells restore visual function in retinal degeneration. Nature neuroscience *11*, 667-675.

Lambiase, A., and Aloe, L. (1996). Nerve growth factor delays retinal degeneration in C3H mice. Graefe's archive for clinical and experimental ophthalmology (Albrecht von Graefes Archiv fur klinische und experimentelle Ophthalmologie) *234 Suppl 1*, S96-100.

Langmann, T. (2007). Microglia activation in retinal degeneration. Journal of leukocyte biology *81*, 1345-1351.

Lau, D., McGee, L.H., Zhou, S., Rendahl, K.G., Manning, W.C., Escobedo, J.A., and Flannery, J.G. (2000). Retinal degeneration is slowed in transgenic rats by AAV-mediated delivery of FGF-2. Invest Ophthalmol Vis Sci *41*, 3622-3633.

LaVail, M.M., Yasumura, D., Matthes, M.T., Lau-Villacorta, C., Unoki, K., Sung, C.H., and Steinberg, R.H. (1998). Protection of mouse photoreceptors by survival factors in retinal degenerations. Investigative Ophthalmology & Visual Science *39*, 592-602.

Lazarus, N.R., Penhos, J.C., Tanese, T., Michaels, L., Gutman, R., and Recant, L. (1970). Studies on the biological activity of porcine proinsulin. The Journal of clinical investigation *49*, 487-496.

Lehnardt, S., Massillon, L., Follett, P., Jensen, F.E., Ratan, R., Rosenberg, P.A., Volpe, J.J., and Vartanian, T. (2003). Activation of innate immunity in the CNS triggers neurodegeneration through a Toll-like receptor 4-dependent pathway. *100*, 8514-8519.

Leitner, G.R., Wenzel, T.J., Marshall, N., Gates, E.J., and Klegeris, A. (2019). Targeting toll-like receptor 4 to modulate neuroinflammation in central nervous system disorders. Expert opinion on therapeutic targets *23*, 865-882.

Leveillard, T., Mohand-Said, S., Lorentz, O., Hicks, D., Fintz, A.C., Clerin, E., Simonutti, M., Forster, V., Cavusoglu, N., Chalmel, F., Dolle, P., Poch, O., Lambrou, G., and Sahel, J.A. (2004). Identification and characterization of rod-derived cone viability factor. Nature genetics *36*, 755-759.

Levy, O., Lavalette, S., Hu, S.J., Housset, M., Raoul, W., Eandi, C., Sahel, J.A., Sullivan, P.M., Guillonneau, X., and Sennlaub, F. (2015). APOE isoforms control pathogenic subretinal inflammation in age-related macular degeneration. The Journal of neuroscience : the official journal of the Society for Neuroscience *35*, 13568-13576.

Lewis, G.P., Linberg, K.A., and Fisher, S.K. (1998). Neurite outgrowth from bipolar and horizontal cells after experimental retinal detachment. Invest Ophthalmol Vis Sci *39*, 424-434.

Li, F., Jiang, D., and Samuel, M.A. (2019). Microglia in the developing retina. Neural development *14*, 12.

Lian, H., Roy, E., and Zheng, H. (2016). Microglial Phagocytosis Assay. Bio-protocol *6*.

Lim, J.E., Kou, J., Song, M., Pattanayak, A., Jin, J., Lalonde, R., and Fukuchi, K. (2011). MyD88 deficiency ameliorates beta-amyloidosis in an animal model of Alzheimer's disease. The American journal of pathology *179*, 1095-1103.

Lin, B., Koizumi, A., Tanaka, N., Panda, S., and Masland, R.H. (2008). Restoration of visual function in retinal degeneration mice by ectopic expression of melanopsin. Proceedings of the National Academy of Sciences of the United States of America *105*, 16009-16014.

Lin, X., Fang, D., Zhou, H., and Su, S.B. (2013). The expression of Toll-like receptors in murine Müller cells, the glial cells in retina. Neurological sciences : official journal of the Italian Neurological Society and of the Italian Society of Clinical Neurophysiology *34*, 1339-1346.

Linding, R., Jensen, L.J., Ostheimer, G.J., van Vugt, M.A., Jorgensen, C., Miron, I.M., Diella, F., Colwill, K., Taylor, L., Elder, K., Metalnikov, P., Nguyen, V., Pasculescu, A., Jin, J., Park, J.G., Samson, L.D., Woodgett, J.R., Russell, R.B., Bork, P., Yaffe, M.B., and Pawson, T. (2007). Systematic discovery of in vivo phosphorylation networks. Cell *129*, 1415-1426.

Liu, T., Zhang, L., Joo, D., and Sun, S.-C. (2017). NF-κB signaling in inflammation. Signal transduction and targeted therapy *2*, 17023.

Lovestone, S., Boada, M., Dubois, B., Hull, M., Rinne, J.O., Huppertz, H.J., Calero, M., Andres, M.V., Gomez-Carrillo, B., Leon, T., and del Ser, T. (2015). A phase II trial of tideglusib in Alzheimer's disease. Journal of Alzheimer's disease : JAD *45*, 75-88.

Lovestone, S., Davis, D.R., Webster, M.T., Kaech, S., Brion, J.P., Matus, A., and Anderton, B.H. (1999). Lithium reduces tau phosphorylation: effects in living cells and in neurons at therapeutic concentrations. Biological psychiatry *45*, 995-1003.

Lu, L., Oveson, B.C., Jo, Y.J., Lauer, T.W., Usui, S., Komeima, K., Xie, B., and Campochiaro, P.A. (2009). Increased expression of glutathione peroxidase 4 strongly protects retina from oxidative damage. Antioxidants & redox signaling *11*, 715-724.

MacLaren, R.E., Pearson, R.A., MacNeil, A., Douglas, R.H., Salt, T.E., Akimoto, M., Swaroop, A., Sowden, J.C., and Ali, R.R. (2006). Retinal repair by transplantation of photoreceptor precursors. Nature *444*, 203-207.

Maguire, A.M., Russell, S., Wellman, J.A., Chung, D.C., Yu, Z.F., Tillman, A., Wittes, J., Pappas, J., Elci, O., Marshall, K.A., McCague, S., Reichert, H., Davis, M., Simonelli, F., Leroy, B.P., Wright, J.F., High, K.A., and Bennett, J. (2019). Efficacy, safety, and durability of voretigene neparvovec-rzyl in RPE65 mutation-associated inherited retinal dystrophy: results of phase 1 and 3 trials. Ophthalmology *126*, 1273-1285.

Malaguarnera, R., Sacco, A., Voci, C., Pandini, G., Vigneri, R., and Belfiore, A. (2012). Proinsulin binds with high affinity the insulin receptor isoform A and predominantly activates the mitogenic pathway. Endocrinology *153*, 2152-2163.

Mancinelli, R., Carpino, G., Petrungaro, S., Mammola, C.L., Tomaipitinca, L., Filippini, A., Facchiano, A., Ziparo, E., and Giampietri, C. (2017). Multifaceted roles of GSK-3 in cancer and autophagy-related diseases. Oxidative medicine and cellular longevity *2017*, 4629495.

Mao, H., James, T., Jr., Schwein, A., Shabashvili, A.E., Hauswirth, W.W., Gorbatyuk, M.S., and Lewin, A.S. (2011). AAV delivery of wild-type rhodopsin preserves retinal function in a mouse model of autosomal dominant retinitis pigmentosa. Human gene therapy *22*, 567-575.

Marchena, M., Villarejo-Zori, B., Zaldivar-Diez, J., Palomo, V., Gil, C., Hernández-Sánchez, C., Martínez, A., and de la Rosa, E.J. (2017). Small molecules targeting glycogen synthase kinase 3 as potential drug candidates for the treatment of retinitis pigmentosa. Journal of enzyme inhibition and medicinal chemistry *32*, 522-526.

Marks, J.L., Porte, D., Jr., Stahl, W.L., and Baskin, D.G. (1990). Localization of insulin receptor mRNA in rat brain by in situ hybridization. Endocrinology *127*, 3234-3236.

Martin, K.C., Barad, M., and Kandel, E.R. (2000). Local protein synthesis and its role in synapse-specific plasticity. Current opinion in neurobiology *10*, 587-592.

Martínez-Fernández de la Cámara, C., Hernández-Pinto, A.M., Olivares-González, L., Cuevas-Martín, C., Sánchez-Aragó, M., Hervás, D., Salom, D., Cuezva, J.M., de la Rosa, E.J., Millán, J.M.,

and Rodrigo, R. (2015). Adalimumab reduces photoreceptor cell death in a mouse model of retinal degeneration. Sci Rep *5*, 11764.

Martinez, A., Perez, D.I., and Gil, C. (2013). Lessons learnt from glycogen synthase kinase 3 inhibitors development for Alzheimer's disease. Current topics in medicinal chemistry *13*, 1808-1819.

Mayer, G., Nitsch, R., and Hoyer, S. (1990). Effects of changes in peripheral and cerebral glucose metabolism on locomotor activity, learning and memory in adult male rats. Brain research *532*, 95-100.

Mazzoni, F., Novelli, E., and Strettoi, E. (2008). Retinal ganglion cells survive and maintain normal dendritic morphology in a mouse model of inherited photoreceptor degeneration. The Journal of neuroscience : the official journal of the Society for Neuroscience *28*, 14282-14292.

McDonald, C.L., Hennessy, E., Rubio-Araiz, A., Keogh, B., McCormack, W., McGuirk, P., Reilly, M., and Lynch, M.A. (2016). Inhibiting TLR2 activation attenuates amyloid accumulation and glial activation in a mouse model of Alzheimer's disease. Brain, behavior, and immunity *58*, 191-200.

McGee Sanftner, L.H., Abel, H., Hauswirth, W.W., and Flannery, J.G. (2001). Glial cell line derived neurotrophic factor delays photoreceptor degeneration in a transgenic rat model of retinitis pigmentosa. Molecular therapy : the journal of the American Society of Gene Therapy *4*, 622-629.

Medina-Rodríguez, E.M., Bribián, A., Boyd, A., Palomo, V., Pastor, J., Lagares, A., Gil, C., Martínez, A., Williams, A., and de Castro, F. (2017). Promoting in vivo remyelination with small molecules: a neuroreparative pharmacological treatment for Multiple Sclerosis. Scientific Reports *7*, 43545.

Mehran, A.E., Templeman, N.M., Brigidi, G.S., Lim, G.E., Chu, K.Y., Hu, X., Botezelli, J.D., Asadi, A., Hoffman, B.G., Kieffer, T.J., Bamji, S.X., Clee, S.M., and Johnson, J.D. (2012). Hyperinsulinemia drives diet-induced obesity independently of brain insulin production. Cell metabolism *16*, 723-737.

Michaud, J.P., Richard, K.L., and Rivest, S. (2011). MyD88-adaptor protein acts as a preventive mechanism for memory deficits in a mouse model of Alzheimer's disease. Molecular neurodegeneration *6*, 5.

Mines, M.A., Beurel, E., and Jope, R.S. (2011). Regulation of cell survival mechanisms in Alzheimer's disease by glycogen synthase kinase-3. International journal of Alzheimer's disease *2011*, 861072.

Minoretti, P., Gazzaruso, C., Vito, C.D., Emanuele, E., Bianchi, M., Coen, E., Reino, M., and Geroldi, D. (2006). Effect of the functional toll-like receptor 4 Asp299Gly polymorphism on susceptibility to late-onset Alzheimer's disease. Neurosci Lett *391*, 147-149.

Morales-Garcia, J.A., Palomo, V., Redondo, M., Alonso-Gil, S., Gil, C., Martinez, A., and Perez-Castillo, A. (2014). Crosstalk between phosphodiesterase 7 and glycogen synthase kinase-3: two relevant therapeutic targets for neurological disorders. ACS chemical neuroscience *5*, 194-204.

Moroo, I., Yamada, T., Makino, H., Tooyama, I., McGeer, P.L., McGeer, E.G., and Hirayama, K. (1994). Loss of insulin receptor immunoreactivity from the substantia nigra pars compacta neurons in Parkinson's disease. Acta neuropathologica *87*, 343-348.

Mowat, F.M., Occelli, L.M., Bartoe, J.T., Gervais, K.J., Bruewer, A.R., Querubin, J., Dinculescu, A., Boye, S.L., Hauswirth, W.W., and Petersen-Jones, S.M. (2017). Gene therapy in a large animal model of PDE6A-retinitis pigmentosa. Frontiers in neuroscience *11*, 342.

Murray, S.F., Jazayeri, A., Matthes, M.T., Yasumura, D., Yang, H., Peralta, R., Watt, A., Freier, S., Hung, G., Adamson, P.S., Guo, S., Monia, B.P., LaVail, M.M., and McCaleb, M.L. (2015). Allele-specific inhibition of rhodopsin with an antisense oligonucleotide slows photoreceptor cell degeneration. Invest Ophthalmol Vis Sci *56*, 6362-6375.

Mussolino, C., Sanges, D., Marrocco, E., Bonetti, C., Di Vicino, U., Marigo, V., Auricchio, A., Meroni, G., and Surace, E.M. (2011). Zinc-finger-based transcriptional repression of rhodopsin in a model of dominant retinitis pigmentosa. EMBO molecular medicine *3*, 118-128.

Mustafi, D., Engel, A.H., and Palczewski, K. (2009). Structure of cone photoreceptors. Prog Retin Eye Res *28*, 289-302.

Nakano, T., Ando, S., Takata, N., Kawada, M., Muguruma, K., Sekiguchi, K., Saito, K., Yonemura, S., Eiraku, M., and Sasai, Y. (2012). Self-formation of optic cups and storable stratified neural retina from human ESCs. Cell Stem Cell *10*, 771-785.

Nakazawa, T., Shimura, M., Tomita, H., Akiyama, H., Yoshioka, Y., Kudou, H., and Tamai, M. (2003). Intrinsic activation of PI3K/Akt signaling pathway and its neuroprotective effect against retinal injury. Current eye research *26*, 55-63.

Nemitz, L., Dedek, K., and Janssen-Bienhold, U. (2019). Rod bipolar cells require horizontal cells for invagination into the terminals of rod photoreceptors. Frontiers in cellular neuroscience *13*, 423.

Neveling, K., Collin, R.W., Gilissen, C., van Huet, R.A., Visser, L., Kwint, M.P., Gijsen, S.J., Zonneveld, M.N., Wieskamp, N., de Ligt, J., Siemiatkowska, A.M., Hoefsloot, L.H., Buckley, M.F., Kellner, U., Branham, K.E., den Hollander, A.I., Hoischen, A., Hoyng, C., Klevering, B.J., van den Born, L.I., Veltman, J.A., Cremers, F.P., and Scheffer, H. (2012). Next-generation genetic testing for retinitis pigmentosa. Hum Mutat *33*, 963-972.

Noailles, A., Kutsyr, O., Maneu, V., Ortuño-Lizarán, I., Campello, L., de Juan, E., Gómez-Vicente, V., Cuenca, N., and Lax, P. (2019). The absence of toll-like receptor 4 mildly affects the structure and function in the adult mouse retina. Frontiers in cellular neuroscience *13*, 59.

Novak, P., Pimentel Maldonado, D.A., and Novak, V. (2019). Safety and preliminary efficacy of intranasal insulin for cognitive impairment in Parkinson disease and multiple system atrophy: A double-blinded placebo-controlled pilot study. PloS one *14*, e0214364.

Novakovic, B., Habibi, E., Wang, S.Y., Arts, R.J.W., Davar, R., Megchelenbrink, W., Kim, B., Kuznetsova, T., Kox, M., Zwaag, J., Matarese, F., van Heeringen, S.J., Janssen-Megens, E.M., Sharifi, N., Wang, C., Keramati, F., Schoonenberg, V., Flicek, P., Clarke, L., Pickkers, P., Heath, S., Gut, I., Netea, M.G., Martens, J.H.A., Logie, C., and Stunnenberg, H.G. (2016). β-Glucan reverses the epigenetic state of LPS-induced immunological tolerance. Cell *167*, 1354-1368.e1314.

Nunes, M.A., Viel, T.A., and Buck, H.S. (2013). Microdose lithium treatment stabilized cognitive impairment in patients with Alzheimer's disease. Current Alzheimer research *10*, 104-107.

O'Koren, E.G., Yu, C., Klingeborn, M., Wong, A.Y.W., Prigge, C.L., Mathew, R., Kalnitsky, J., Msallam, R.A., Silvin, A., Kay, J.N., Bowes Rickman, C., Arshavsky, V.Y., Ginhoux, F., Merad, M., and Saban, D.R. (2019). Microglial function is distinct in different anatomical locations during retinal homeostasis and degeneration. Immunity *50*, 723-737.e727.

O'Neill, L.A., Golenbock, D., and Bowie, A.G. (2013). The history of Toll-like receptors - redefining innate immunity. Nature reviews Immunology *13*, 453-460.

Okunuki, Y., Mukai, R., Pearsall, E.A., Klokman, G., Husain, D., Park, D.-H., Korobkina, E., Weiner, H.L., Butovsky, O., Ksander, B.R., Miller, J.W., and Connor, K.M. (2018). Microglia inhibit photoreceptor cell death and regulate immune cell infiltration in response to retinal detachment. *115*, E6264-E6273.

Olson, J.K., and Miller, S.D. (2004). Microglia initiate central nervous system innate and adaptive immune responses through multiple TLRs. Journal of Immunology *173*, 3916-3924.

Ortin-Martinez, A., Tsai, E.L., Nickerson, P.E., Bergeret, M., Lu, Y., Smiley, S., Comanita, L., and Wallace, V.A. (2017). A reinterpretation of cell transplantation: GFP transfer from donor to host photoreceptors. Stem cells (Dayton, Ohio) *35*, 932-939.

Osakada, F., Ikeda, H., Mandai, M., Wataya, T., Watanabe, K., Yoshimura, N., Akaike, A., Sasai, Y., and Takahashi, M. (2008). Toward the generation of rod and cone photoreceptors from mouse, monkey and human embryonic stem cells. Nat Biotechnol *26*, 215-224.

Ozinsky, A., Underhill, D.M., Fontenot, J.D., Hajjar, A.M., Smith, K.D., Wilson, C.B., Schroeder, L., and Aderem, A. (2000). The repertoire for pattern recognition of pathogens by the innate immune system is defined by cooperation between Toll-like receptors. *97*, 13766-13771.

Pagon, R.A. (1988). Retinitis pigmentosa. Surv Ophthalmol *33*, 137-177.

Palomo, V., and Martinez, A. (2017). Glycogen synthase kinase 3 (GSK-3) inhibitors: a patent update (2014-2015). Expert opinion on therapeutic patents *27*, 657-666.

Palomo, V., Perez, D.I., Perez, C., Morales-Garcia, J.A., Soteras, I., Alonso-Gil, S., Encinas, A., Castro, A., Campillo, N.E., Perez-Castillo, A., Gil, C., and Martinez, A. (2012). 5-imino-1,2,4-thiadiazoles: first small molecules as substrate competitive inhibitors of glycogen synthase kinase 3. Journal of medicinal chemistry *55*, 1645-1661.

Palomo, V., Perez, D.I., Roca, C., Anderson, C., Rodriguez-Muela, N., Perez, C., Morales-Garcia, J.A., Reyes, J.A., Campillo, N.E., Perez-Castillo, A.M., Rubin, L.L., Timchenko, L., Gil, C., and Martinez, A. (2017). Subtly modulating glycogen synthase kinase 3 beta: allosteric inhibitor development and their potential for the treatment of chronic diseases. Journal of medicinal chemistry *60*, 4983-5001.

Pang, J.J., Boye, S.L., Kumar, A., Dinculescu, A., Deng, W., Li, J., Li, Q., Rani, A., Foster, T.C., Chang, B., Hawes, N.L., Boatright, J.H., and Hauswirth, W.W. (2008). AAV-mediated gene therapy for retinal degeneration in the rd10 mouse containing a recessive PDEbeta mutation. Invest Ophthalmol Vis Sci *49*, 4278-4283.

Pardo, M., Abrial, E., Jope, R.S., and Beurel, E. (2016). GSK3beta isoform-selective regulation of depression, memory and hippocampal cell proliferation. Genes, brain, and behavior *15*, 348-355.

Peichl, L., and Gonzalez-Soriano, J. (1993). Unexpected presence of neurofilaments in axon-bearing horizontal cells of the mammalian retina. The Journal of neuroscience : the official journal of the Society for Neuroscience *13*, 4091-4100.

Peichl, L., and Gonzalez-Soriano, J. (1994). Morphological types of horizontal cell in rodent retinae: a comparison of rat, mouse, gerbil, and guinea pig. Visual neuroscience *11*, 501-517.

Peng, B., Xiao, J., Wang, K., So, K.-F., Tipoe, G.L., and Lin, B. (2014). Suppression of Microglial Activation Is Neuroprotective in a Mouse Model of Human Retinitis Pigmentosa. *34*, 8139-8150.

Perlmuter, L.C., Hakami, M.K., Hodgson-Harrington, C., Ginsberg, J., Katz, J., Singer, D.E., and Nathan, D.M. (1984). Decreased cognitive function in aging non-insulin-dependent diabetic patients. The American journal of medicine *77*, 1043-1048.

Peterson, R.T., and Schreiber, S.L. (1998). Translation control: connecting mitogens and the ribosome. Current biology : CB *8*, R248-250.

Pfeiffer, R.L., Marc, R.E., and Jones, B.W. (2020). Persistent remodeling and neurodegeneration in late-stage retinal degeneration. Prog Retin Eye Res *74*, 100771.

Phiel, C.J., Wilson, C.A., Lee, V.M., and Klein, P.S. (2003). GSK-3alpha regulates production of Alzheimer's disease amyloid-beta peptides. Nature *423*, 435-439.

Phillips, M.J., Walker, T.A., Choi, H.-Y., Faulkner, A.E., Kim, M.K., Sidney, S.S., Boyd, A.P., Nickerson, J.M., Boatright, J.H., and Pardue, M.T. (2008). Tauroursodeoxycholic Acid Preservation of Photoreceptor Structure and Function in the rd10 Mouse through Postnatal Day 30. Investigative Ophthalmology & Visual Science *49*, 2148-2155.

Piano, I., Novelli, E., Gasco, P., Ghidoni, R., Strettoi, E., and Gargini, C. (2013). Cone survival and preservation of visual acuity in an animal model of retinal degeneration. The European journal of neuroscience *37*, 1853-1862.

Poltorak, A., He, X., Smirnova, I., Liu, M.Y., Van Huffel, C., Du, X., Birdwell, D., Alejos, E., Silva, M., Galanos, C., Freudenberg, M., Ricciardi-Castagnoli, P., Layton, B., and Beutler, B. (1998). Defective LPS signaling in C3H/HeJ and C57BL/10ScCr mice: mutations in Tlr4 gene. Science (New York, NY) *282*, 2085-2088.

Pradillo, J.M., Fernandez-Lopez, D., Garcia-Yebenes, I., Sobrado, M., Hurtado, O., Moro, M.A., and Lizasoain, I. (2009). Toll-like receptor 4 is involved in neuroprotection afforded by ischemic preconditioning. Journal of neurochemistry *109*, 287-294.

Price, B.A., Sandoval, I.M., Chan, F., Nichols, R., Roman-Sanchez, R., Wensel, T.G., and Wilson, J.H. (2012). Rhodopsin gene expression determines rod outer segment size and rod cell resistance to a dominant-negative neurodegeneration mutant. PloS one *7*, e49889.

Punzo, C., Kornacker, K., and Cepko, C.L. (2009). Stimulation of the insulin/mTOR pathway delays cone death in a mouse model of retinitis pigmentosa. Nature neuroscience *12*, 44-52.

Qin, Y., Liu, Y., Hao, W., Decker, Y., Tomic, I., Menger, M.D., Liu, C., and Fassbender, K. (2016). Stimulation of TLR4 attenuates Alzheimer's disease–related symptoms and pathology in tau-Transgenic Mice. *197*, 3281-3292.

Radtke, N.D., Aramant, R.B., Petry, H.M., Green, P.T., Pidwell, D.J., and Seiler, M.J. (2008). Vision improvement in retinal degeneration patients by implantation of retina together with retinal pigment epithelium. American Journal of Ophthalmology *146*, 172-182.e171.

Radtke, N.D., Aramant, R.B., Seiler, M., and Petry, H.M. (1999). Preliminary report: indications of improved visual function after retinal sheet transplantation in retinitis pigmentosa patients. American Journal of Ophthalmology *128*, 384-387.

Radtke, N.D., Aramant, R.B., Seiler, M.J., Petry, H.M., and Pidwell, D. (2004). Vision change after sheet transplant of fetal retina with retinal pigment epithelium to a patient with retinitis pigmentosa. Archives of ophthalmology (Chicago, Ill : 1960) *122*, 1159-1165.

Rajala, R.V., Wiskur, B., Tanito, M., Callegan, M., and Rajala, A. (2009). Diabetes reduces autophosphorylation of retinal insulin receptor and increases protein-tyrosine phosphatase-1B activity. Invest Ophthalmol Vis Sci *50*, 1033-1040.

Ramachandran, R., Zhao, X.F., and Goldman, D. (2011). Ascl1a/Dkk/beta-catenin signaling pathway is necessary and glycogen synthase kinase-3beta inhibition is sufficient for zebrafish retina regeneration. Proceedings of the National Academy of Sciences of the United States of America *108*, 15858-15863.

Ramos-Rodriguez, J.J., Ortiz, O., Jimenez-Palomares, M., Kay, K.R., Berrocoso, E., Murillo-Carretero, M.I., Perdomo, G., Spires-Jones, T., Cozar-Castellano, I., Lechuga-Sancho, A.M., and Garcia-Alloza, M. (2013). Differential central pathology and cognitive impairment in pre-diabetic and diabetic mice. Psychoneuroendocrinology *38*, 2462-2475.

Rashid, K., Akhtar-Schaefer, I., and Langmann, T. (2019). Microglia in retinal degeneration. Frontiers in immunology *10*, 1975.

Rayapudi, S., Schwartz, S.G., Wang, X., and Chavis, P. (2013). Vitamin A and fish oils for retinitis pigmentosa. Cochrane Database Syst Rev *12*, Cd008428.

Recio-Pinto, E., Lang, F.F., and Ishii, D.N. (1984). Insulin and insulin-like growth factor II permit nerve growth factor binding and the neurite formation response in cultured human neuroblastoma cells. Proceedings of the National Academy of Sciences of the United States of America *81*, 2562-2566.

Redondo, M., Palomo, V., Brea, J., Pérez, D.I., Martín-Álvarez, R., Pérez, C., Paúl-Fernández, N., Conde, S., Cadavid, M.I., Loza, M.I., Mengod, G., Martínez, A., Gil, C., and Campillo, N.E. (2012). Identification in silico and experimental validation of novel phosphodiesterase 7 inhibitors with efficacy in experimental autoimmune encephalomyelitis mice. ACS chemical neuroscience *3*, 793-803.

Reger, M.A., Watson, G.S., Frey, W.H., Baker, L.D., Cholerton, B., Keeling, M.L., Belongia, D.A., Fishel, M.A., Plymate, S.R., Schellenberg, G.D., Cherrier, M.M., and Craft, S. (2006). Effects of intranasal insulin on cognition in memory-impaired older adults: Modulation by APOE genotype. Neurobiology of Aging *27*, 451-458.

Reger, M.A., Watson, G.S., Green, P.S., Baker, L.D., Cholerton, B., Fishel, M.A., Plymate, S.R., Cherrier, M.M., Schellenberg, G.D., Frey, W.H., 2nd, and Craft, S. (2008). Intranasal insulin administration dose-dependently modulates verbal memory and plasma amyloid-beta in memory-impaired older adults. Journal of Alzheimer's disease : JAD *13*, 323-331.

Reiter, C.E., Wu, X., Sandirasegarane, L., Nakamura, M., Gilbert, K.A., Singh, R.S., Fort, P.E., Antonetti, D.A., and Gardner, T.W. (2006). Diabetes reduces basal retinal insulin receptor signaling: reversal with systemic and local insulin. Diabetes *55*, 1148-1156.

Richard, K.L., Filali, M., Prefontaine, P., and Rivest, S. (2008). Toll-like receptor 2 acts as a natural innate immune receptor to clear amyloid beta 1-42 and delay the cognitive decline in a mouse model of Alzheimer's disease. The Journal of neuroscience : the official journal of the Society for Neuroscience *28*, 5784-5793.

Roche, S.L., Kutsyr, O., Cuenca, N., and Cotter, T.G. (2019). Norgestrel, a progesterone analogue, promotes significant long-term neuroprotection of cone photoreceptors in a mouse model of retinal disease. Invest Ophthalmol Vis Sci *60*, 3221-3235.

Rodrigues, M., Waldbillig, R.J., Rajagopalan, S., Hackett, J., LeRoith, D., and Chader, G.J. (1988). Retinal insulin receptors: localization using a polyclonal anti-insulin receptor antibody. Brain research *443*, 389-394.

Roque, R.S., Imperial, C.J., and Caldwell, R.B. (1996). Microglial cells invade the outer retina as photoreceptors degenerate in Royal College of Surgeons rats. Invest Ophthalmol Vis Sci *37*, 196-203.

Rosenbloom, M.H., Barclay, T.R., Pyle, M., Owens, B.L., Cagan, A.B., Anderson, C.P., Frey, W.H., 2nd, and Hanson, L.R. (2014). A single-dose pilot trial of intranasal rapid-acting insulin in apolipoprotein E4 carriers with mild-moderate Alzheimer's disease. CNS drugs *28*, 1185-1189.

Rosenzweig, H.L., Minami, M., Lessov, N.S., Coste, S.C., Stevens, S.L., Henshall, D.C., Meller, R., Simon, R.P., and Stenzel-Poore, M.P. (2007). Endotoxin preconditioning protects against the cytotoxic effects of TNFalpha after stroke: a novel role for TNFalpha in LPS-ischemic tolerance. Journal of cerebral blood flow and metabolism : official journal of the International Society of Cerebral Blood Flow and Metabolism *27*, 1663-1674.

Rotenstreich, Y., Belkin, M., Sadetzki, S., Chetrit, A., Ferman-Attar, G., Sher, I., Harari, A., Shaish, A., and Harats, D. (2013). Treatment with 9-cis beta-carotene-rich powder in patients with retinitis pigmentosa: a randomized crossover trial. JAMA ophthalmology *131*, 985-992.

Rui, Y., Myers, K.R., Yu, K., Wise, A., De Blas, A.L., Hartzell, H.C., and Zheng, J.Q. (2013). Activity-dependent regulation of dendritic growth and maintenance by glycogen synthase kinase 3beta. Nature communications *4*, 2628.

Russo, R., Adornetto, A., Cavaliere, F., Varano, G.P., Rusciano, D., Morrone, L.A., Corasaniti, M.T., Bagetta, G., and Nucci, C. (2015). Intravitreal injection of forskolin, homotaurine, and L-carnosine affords neuroprotection to retinal ganglion cells following retinal ischemic injury. Molecular vision *21*, 718-729.

Sahel, J.-A., and Roska, B. (2013). Gene Therapy for Blindness. *36*, 467-488.

Sahni, J.N., Angi, M., Irigoyen, C., Semeraro, F., Romano, M.R., and Parmeggiani, F. (2011). Therapeutic challenges to retinitis pigmentosa: from neuroprotection to gene therapy. Current genomics *12*, 276-284.

Sakami, S., Maeda, T., Bereta, G., Okano, K., Golczak, M., Sumaroka, A., Roman, A.J., Cideciyan, A.V., Jacobson, S.G., and Palczewski, K. (2011). Probing mechanisms of photoreceptor degeneration in a new mouse model of the common form of autosomal dominant retinitis pigmentosa due to P23H opsin mutations. The Journal of biological chemistry *286*, 10551-10567.

Salter, M.W., and Stevens, B. (2017). Microglia emerge as central players in brain disease. Nature medicine *23*, 1018-1027.

Saragovi, H.U., Sidorova, Y., Saarma, M., and Jmaeff, S. (2014). Retinal neuroprotection using small molecule GDNF mimetics. Investigative Ophthalmology & Visual Science *55*, 5754-5754.

Sauter, A., Goldstein, M., Engel, J., and Ueta, K. (1983). Effect of insulin on central catecholamines. Brain research *260*, 330-333.

Scheffel, J., Regen, T., Van Rossum, D., Seifert, S., Ribes, S., Nau, R., Parsa, R., Harris, R.A., Boddeke, H.W., Chuang, H.N., Pukrop, T., Wessels, J.T., Jurgens, T., Merkler, D., Bruck, W., Schnaars, M., Simons, M., Kettenmann, H., and Hanisch, U.K. (2012). Toll-like receptor activation reveals developmental reorganization and unmasks responder subsets of microglia. Glia *60*, 1930-1943.

Schon, C., Biel, M., and Michalakis, S. (2015). Retinal gene delivery by adeno-associated virus (AAV) vectors: Strategies and applications. Eur J Pharm Biopharm *95*, 343-352.

Seeley, J.J., and Ghosh, S. (2017). Molecular mechanisms of innate memory and tolerance to LPS. Journal of leukocyte biology *101*, 107-119.

Sieving, P.A., Caruso, R.C., Tao, W., Coleman, H.R., Thompson, D.J., Fullmer, K.R., and Bush, R.A. (2006). Ciliary neurotrophic factor (CNTF) for human retinal degeneration: phase I trial of CNTF delivered by encapsulated cell intraocular implants. Proceedings of the National Academy of Sciences of the United States of America *103*, 3896-3901.

Silverman, S.M., and Wong, W.T. (2018). Microglia in the retina: roles in development, maturity, and disease. Annual review of vision science *4*, 45-77.

Simunovic, M.P., Shen, W., Lin, J.Y., Protti, D.A., Lisowski, L., and Gillies, M.C. (2019). Optogenetic approaches to vision restoration. Experimental Eye Research *178*, 15-26.

Singh, M.S., Aslam, S.A., Duncan, I.L., Cramer, A.O., Barnard, A.R., and MacLaren, R.E. (2014). Cell fusion following photoreceptor transplantation into the non-degenerate retina. Investigative Ophthalmology & Visual Science *55*, 3989-3989.

Sisk, R.A. (2012). Valproic acid treatment may be harmful in non-dominant forms of retinitis pigmentosa. The British journal of ophthalmology *96*, 1154-1155.

Sochocka, M., Diniz, B.S., and Leszek, J. (2017). Inflammatory response in the CNS: friend or foe? Molecular neurobiology *54*, 8071-8089.

Song, B.J., Aiello, L.P., and Pasquale, L.R. (2016). Presence and Risk Factors for Glaucoma in Patients with Diabetes. Current diabetes reports *16*, 124.

Sonntag, S., Dedek, K., Dorgau, B., Schultz, K., Schmidt, K.F., Cimiotti, K., Weiler, R., Lowel, S., Willecke, K., and Janssen-Bienhold, U. (2012). Ablation of retinal horizontal cells from adult mice leads to rod degeneration and remodeling in the outer retina. The Journal of neuroscience : the official journal of the Society for Neuroscience *32*, 10713-10724.

Spitzer, J.H., Visintin, A., Mazzoni, A., Kennedy, M.N., and Segal, D.M. (2002). Toll-like receptor 1 inhibits Toll-like receptor 4 signaling in endothelial cells. *32*, 1182-1187.

Steen, E., Terry, B.M., Rivera, E.J., Cannon, J.L., Neely, T.R., Tavares, R., Xu, X.J., Wands, J.R., and de la Monte, S.M. (2005). Impaired insulin and insulin-like growth factor expression and signaling mechanisms in Alzheimer's disease--is this type 3 diabetes? Journal of Alzheimer's disease : JAD *7*, 63-80.

Stefanova, N., Fellner, L., Reindl, M., Masliah, E., Poewe, W., and Wenning, G.K. (2011). Toll-like receptor 4 promotes α-synuclein clearance and survival of nigral dopaminergic neurons. The American journal of pathology *179*, 954-963.

Strauss, O. (2005). The retinal pigment epithelium in visual function. Physiol Rev *85*, 845-881.

Strettoi, E., Gargini, C., Novelli, E., Sala, G., Piano, I., Gasco, P., and Ghidoni, R. (2010). Inhibition of ceramide biosynthesis preserves photoreceptor structure and function in a mouse model of retinitis pigmentosa. Proceedings of the National Academy of Sciences of the United States of America *107*, 18706-18711.

Strettoi, E., Pignatelli, V., Rossi, C., Porciatti, V., and Falsini, B. (2003). Remodeling of second-order neurons in the retina of rd/rd mutant mice. Vision research *43*, 867-877.

Sudduth, T.L., Wilson, J.G., Everhart, A., Colton, C.A., and Wilcock, D.M. (2012). Lithium treatment of APPSwDI/NOS2-/- mice leads to reduced hyperphosphorylated tau, increased amyloid deposition and altered inflammatory phenotype. PloS one *7*, e31993.

Sudharsan, R., Beiting, D.P., Aguirre, G.D., and Beltran, W.A. (2017). Involvement of innate immune system in late stages of inherited photoreceptor degeneration. Sci Rep *7*, 17897.

Sun, X.B., Lu, H.E., Chen, Y., Fan, X.H., and Tong, B. (2014). Effect of lithium chloride on endoplasmic reticulum stress-related PERK/ROCK signaling in a rat model of glaucoma. Die Pharmazie *69*, 889-893.

Sutherland, C. (2011). What Are the bona fide GSK3 Substrates? International journal of Alzheimer's disease *2011*, 505607.

Syeda, S., Patel, A.K., Lee, T., and Hackam, A.S. (2015). Reduced photoreceptor death and improved retinal function during retinal degeneration in mice lacking innate immunity adaptor protein MyD88. Experimental neurology *267*, 1-12.

Tahara, K., Kim, H.D., Jin, J.J., Maxwell, J.A., Li, L., and Fukuchi, K. (2006). Role of toll-like receptor signalling in Abeta uptake and clearance. Brain : a journal of neurology *129*, 3006-3019.

Takeuchi, O., Hoshino, K., Kawai, T., Sanjo, H., Takada, H., Ogawa, T., Takeda, K., and Akira, S. (1999). Differential roles of TLR2 and TLR4 in recognition of gram-negative and gram-positive bacterial cell wall components. Immunity *11*, 443-451.

Talbot, K., Wang, H.Y., Kazi, H., Han, L.Y., Bakshi, K.P., Stucky, A., Fuino, R.L., Kawaguchi, K.R., Samoyedny, A.J., Wilson, R.S., Arvanitakis, Z., Schneider, J.A., Wolf, B.A., Bennett, D.A., Trojanowski, J.Q., and Arnold, S.E. (2012). Demonstrated brain insulin resistance in Alzheimer's disease patients is associated with IGF-1 resistance, IRS-1 dysregulation, and cognitive decline. The Journal of clinical investigation *122*, 1316-1338.

Tang, S.C., Arumugam, T.V., Xu, X., Cheng, A., Mughal, M.R., Jo, D.G., Lathia, J.D., Siler, D.A., Chigurupati, S., Ouyang, X., Magnus, T., Camandola, S., and Mattson, M.P. (2007). Pivotal role for neuronal Toll-like receptors in ischemic brain injury and functional deficits. Proceedings of the National Academy of Sciences of the United States of America *104*, 13798-13803.

Tarassishin, L., Suh, H.S., and Lee, S.C. (2011). Interferon regulatory factor 3 plays an anti-inflammatory role in microglia by activating the PI3K/Akt pathway. Journal of neuroinflammation *8*, 187.

Tasaki, K., Ruetzler, C.A., Ohtsuki, T., Martin, D., Nawashiro, H., and Hallenbeck, J.M. (1997). Lipopolysaccharide pre-treatment induces resistance against subsequent focal cerebral ischemic damage in spontaneously hypertensive rats. Brain research *748*, 267-270.

Tian, N. (2004). Visual experience and maturation of retinal synaptic pathways. Vision research *44*, 3307-3316.

Tolosa, E., Litvan, I., Hoglinger, G.U., Burn, D., Lees, A., Andres, M.V., Gomez-Carrillo, B., Leon, T., and Del Ser, T. (2014). A phase 2 trial of the GSK-3 inhibitor tideglusib in progressive supranuclear palsy. Movement disorders : official journal of the Movement Disorder Society *29*, 470-478.

Trapani, I., and Auricchio, A. (2019). Has retinal gene therapy come of age? From bench to bedside and back to bench. Human molecular genetics *28*, R108-R118.

Tsai, Y.T., Wu, W.H., Lee, T.T., Wu, W.P., Xu, C.L., Park, K.S., Cui, X., Justus, S., Lin, C.S., Jauregui, R., Su, P.Y., and Tsang, S.H. (2018). Clustered regularly interspaced short palindromic repeats-based genome surgery for the treatment of autosomal dominant retinitis pigmentosa. Ophthalmology *125*, 1421-1430.

Tsuruma, K., Tanaka, Y., Shimazawa, M., Mashima, Y., and Hara, H. (2011). Unoprostone reduces oxidative stress- and light-induced retinal cell death, and phagocytotic dysfunction, by activating BK channels. Molecular vision *17*, 3556-3565.

Urwyler, O., Izadifar, A., Vandenbogaerde, S., Sachse, S., Misbaer, A., and Schmucker, D. (2019). Branch-restricted localization of phosphatase Prl-1 specifies axonal synaptogenesis domains. Science (New York, NY) *364*.

Usui, S., Komeima, K., Lee, S.Y., Jo, Y.J., Ueno, S., Rogers, B.S., Wu, Z., Shen, J., Lu, L., Oveson, B.C., Rabinovitch, P.S., and Campochiaro, P.A. (2009). Increased expression of catalase and superoxide dismutase 2 reduces cone cell death in retinitis pigmentosa. Molecular therapy : the journal of the American Society of Gene Therapy *17*, 778-786.

Valenciano, A.I., Corrochano, S., de Pablo, F., de la Villa, P., and de la Rosa, E.J. (2006). Proinsulin/insulin is synthesized locally and prevents caspase- and cathepsin-mediated cell death in the embryonic mouse retina. Journal of neurochemistry *99*, 524-536.

van der Heide, L.P., Kamal, A., Artola, A., Gispen, W.H., and Ramakers, G.M. (2005). Insulin modulates hippocampal activity-dependent synaptic plasticity in a N-methyl-d-aspartate receptor and phosphatidyl-inositol-3-kinase-dependent manner. Journal of neurochemistry *94*, 1158-1166.

Vecino, E., Rodriguez, F.D., Ruzafa, N., Pereiro, X., and Sharma, S.C. (2016). Glia-neuron interactions in the mammalian retina. Prog Retin Eye Res *51*, 1-40.

Vent-Schmidt, R.Y.J., Wen, R.H., Zong, Z., Chiu, C.N., Tam, B.M., May, C.G., and Moritz, O.L. (2017). Opposing effects of valproic acid treatment mediated by histone deacetylase inhibitor activity in four transgenic X. laevis models of retinitis pigmentosa. The Journal of neuroscience : the official journal of the Society for Neuroscience *37*, 1039-1054.

Verbakel, S.K., van Huet, R.A.C., Boon, C.J.F., den Hollander, A.I., Collin, R.W.J., Klaver, C.C.W., Hoyng, C.B., Roepman, R., and Klevering, B.J. (2018). Non-syndromic retinitis pigmentosa. Prog Retin Eye Res *66*, 157-186.

Vollrath, D., Feng, W., Duncan, J.L., Yasumura, D., D'Cruz, P.M., Chappelow, A., Matthes, M.T., Kay, M.A., and LaVail, M.M. (2001). Correction of the retinal dystrophy phenotype of the RCS rat by viral gene transfer of Mertk. Proceedings of the National Academy of Sciences of the United States of America *98*, 12584-12589.

Wang, T., Pahlberg, J., Cafaro, J., Frederiksen, R., Cooper, A.J., Sampath, A.P., Field, G.D., and Chen, J. (2019). Activation of rod input in a model of retinal degeneration reverses retinal remodeling and induces formation of functional synapses and recovery of visual signaling in the adult retina. The Journal of neuroscience : the official journal of the Society for Neuroscience *39*, 6798-6810.

Wang, T., Reingruber, J., Woodruff, M.L., Majumder, A., Camarena, A., Artemyev, N.O., Fain, G.L., and Chen, J. (2018). The PDE6 mutation in the rd10 retinal degeneration mouse model causes protein mislocalization and instability and promotes cell death through increased ion influx. The Journal of biological chemistry *293*, 15332-15346.

Wang, X., Zhao, L., Zhang, J., Fariss, R.N., Ma, W., Kretschmer, F., Wang, M., Qian, H.H., Badea, T.C., Diamond, J.S., Gan, W.B., Roger, J.E., and Wong, W.T. (2016). Requirement for microglia for the maintenance of synaptic function and integrity in the mature retina. The Journal of neuroscience : the official journal of the Society for Neuroscience *36*, 2827-2842.

Weitz, T.M., Gate, D., Rezai-Zadeh, K., and Town, T. (2014). MyD88 is dispensable for cerebral amyloidosis and neuroinflammation in APP/PS1 transgenic mice. The American journal of pathology *184*, 2855-2861.

Wenkel, H., and Streilein, J.W. (2000). Evidence that retinal pigment epithelium functions as an immune-privileged tissue. Invest Ophthalmol Vis Sci *41*, 3467-3473.

Wingo, A.P., Wingo, T.S., Harvey, P.D., and Baldessarini, R.J. (2009). Effects of lithium on cognitive performance: a meta-analysis. The Journal of clinical psychiatry *70*, 1588-1597.

Wyse Jackson, A.C., and Cotter, T.G. (2016). The synthetic progesterone Norgestrel is neuroprotective in stressed photoreceptor-like cells and retinal explants, mediating its effects via basic fibroblast growth factor, protein kinase A and glycogen synthase kinase 3beta signalling. The European journal of neuroscience *43*, 899-911.

Yamamoto, S., Sugawara, T., Murakami, A., Nakazawa, M., Nao, I.N., Machida, S., Wada, Y., Mashima, Y., and Myake, Y. (2012). Topical isopropyl unoprostone for retinitis pigmentosa: microperimetric results of the phase 2 clinical study. Ophthalmology and therapy *1*, 5.

Yang, Y., Mohand-Said, S., Danan, A., Simonutti, M., Fontaine, V., Clerin, E., Picaud, S., Léveillard, T., and Sahel, J.-A. (2009). Functional cone rescue by rdcvf protein in a dominant model of retinitis pigmentosa. Molecular Therapy *17*, 787-795.

Yao, K., Qiu, S., Tian, L., Snider, W.D., Flannery, J.G., Schaffer, D.V., and Chen, B. (2016). Wnt regulates proliferation and neurogenic potential of muller glial cells via a Lin28/let-7 miRNA-dependent pathway in adult mammalian retinas. Cell reports *17*, 165-178.

Yoshida, N., Ikeda, Y., Murakami, Y., Nakatake, S., Fujiwara, K., Notomi, S., Hisatomi, T., and Ishibashi, T. (2015). Factors affecting visual acuity after cataract surgery in patients with retinitis pigmentosa. Ophthalmology *122*, 903-908.

Yoshida, N., Ikeda, Y., Notomi, S., Ishikawa, K., Murakami, Y., Hisatomi, T., Enaida, H., and Ishibashi, T. (2013a). Clinical evidence of sustained chronic inflammatory reaction in retinitis pigmentosa. Ophthalmology *120*, 100-105.

Yoshida, N., Ikeda, Y., Notomi, S., Ishikawa, K., Murakami, Y., Hisatomi, T., Enaida, H., and Ishibashi, T. (2013b). Laboratory evidence of sustained chronic inflammatory reaction in retinitis pigmentosa. Ophthalmology *120*, e5-12.

Yu, D.Y., Cringle, S., Valter, K., Walsh, N., Lee, D., and Stone, J. (2004). Photoreceptor death, trophic factor expression, retinal oxygen status, and photoreceptor function in the P23H rat. Invest Ophthalmol Vis Sci *45*, 2013-2019.

Yu, D.Y., and Cringle, S.J. (2001). Oxygen distribution and consumption within the retina in vascularised and avascular retinas and in animal models of retinal disease. Prog Retin Eye Res *20*, 175-208.

Zareparsi, S., Buraczynska, M., Branham, K.E., Shah, S., Eng, D., Li, M., Pawar, H., Yashar, B.M., Moroi, S.E., Lichter, P.R., Petty, H.R., Richards, J.E., Abecasis, G.R., Elner, V.M., and Swaroop, A. (2005). Toll-like receptor 4 variant D299G is associated with susceptibility to age-related macular degeneration. Human molecular genetics *14*, 1449-1455.

Zein, W.M., Jeffrey, B.G., Wiley, H.E., Turriff, A.E., Tumminia, S.J., Tao, W., Bush, R.A., Marangoni, D., Wen, R., Wei, L.L., and Sieving, P.A. (2014). CNGB3-Achromatopsia clinical trial with CNTF: diminished rod pathway responses with no evidence of improvement in cone function. Investigative Ophthalmology & Visual Science *55*, 6301-6308.

Zeiss, C.J., and Johnson, E.A. (2004). Proliferation of microglia, but not photoreceptors, in the outer nuclear layer of the rd-1 mouse. Investigative Ophthalmology & Visual Science *45*, 971-976.

Zeng, H.-y., Zhu, X.-a., Zhang, C., Yang, L.-P., Wu, L.-m., and Tso, M.O.M. (2005). Identification of sequential events and factors associated with microglial activation, migration, and cytotoxicity in retinal degeneration in rd mice. Investigative Ophthalmology & Visual Science *46*, 2992-2999.

Zeng, H.Y., Tso, M.O., Lai, S., and Lai, H. (2008). Activation of nuclear factor-kappaB during retinal degeneration in rd mice. Molecular vision *14*, 1075-1080.

Zhao, L., Zabel, M.K., Wang, X., Ma, W., Shah, P., Fariss, R.N., Qian, H., Parkhurst, C.N., Gan, W.B., and Wong, W.T. (2015). Microglial phagocytosis of living photoreceptors contributes to inherited retinal degeneration. EMBO molecular medicine *7*, 1179-1197.

Zhao, W., Chen, H., Xu, H., Moore, E., Meiri, N., Quon, M.J., and Alkon, D.L. (1999). Brain insulin receptors and spatial memory. Correlated changes in gene expression, tyrosine phosphorylation, and signaling molecules in the hippocampus of water maze trained rats. The Journal of biological chemistry *274*, 34893-34902.

Zhao, W.Q., De Felice, F.G., Fernandez, S., Chen, H., Lambert, M.P., Quon, M.J., Krafft, G.A., and Klein, W.L. (2008). Amyloid beta oligomers induce impairment of neuronal insulin receptors. FASEB journal : official publication of the Federation of American Societies for Experimental Biology *22*, 246-260.

APPENDICES

APPENDICES

Appendix 1: Insulin receptor activation by proinsulin preserves synapses and vision in retinitis pigmentosa (2020). **Alonso Sánchez-Cruz**, Alberto Hernández-Pinto, Concepción Lillo, Carolina Isiegas, Miguel Marchena, Ignacio Lizasoain, Fátima Bosch, Pedro de la Villa, Catalina Hernández-Sánchez and Enrique J. de la Rosa.
Submitted for publication. bioRxiv preprint doi: https://doi.org/10.1101/2020.05.13.092833

Appendix 2: Modulation of GSK-3 provides cellular and functional neuroprotection in the *rd10* mouse model of retinitis pigmentosa (2018). **Alonso Sánchez-Cruz**, Beatriz Villarejo-Zori, Miguel Marchena, Josefa Zaldivar-Díez, Valle Palomo, Carmen Gil, Ignacio Lizasoain, Pedro de la Villa, Ana Martínez, Enrique J. de la Rosa and Catalina Hernández-Sánchez.
Mol Neurodegener; 13: 19.

Insulin receptor activation by proinsulin preserves synapses and vision in retinitis pigmentosa

Alonso Sánchez-Cruz[1,2], Alberto Hernández-Pinto[1], Concepción Lillo[3], Carolina Isiegas[1], Miguel Marchena[1], Ignacio Lizasoain[2], Fátima Bosch[4,5], Pedro de la Villa[6,7], Catalina Hernández-Sánchez[1,5]* and Enrique J. de la Rosa[1]*.

[1]Department of Molecular Biomedicine, Centro de Investigaciones Biológicas Margarita Salas (CSIC), C/ Ramiro de Maeztu 9, 28040 Madrid, Spain.

[2]Neurovascular Research Unit, Department of Pharmacology and Toxicology and Instituto Universitario de Investigación en Neuroquímica, Facultad de Medicina, Universidad Complutense de Madrid, Ciudad Universitaria, 28040 Madrid, Spain; Instituto de Investigación Hospital 12 de Octubre (IMAS12), 28041 Madrid, Spain.

[3]Cell Biology and Pathology Department, University of Salamanca, Institute for Biomedical Research of Salamanca (IBSAL), Institute of Neurosciences of Castilla y León (INCYL), C/ Pintor Fernando Gallego,1, 37007 Salamanca, Spain.

[4]Center of Animal Biotechnology and Gene Therapy and Department of Biochemistry and Molecular Biology, School of Veterinary Medicine, Universitat Autònoma de Barcelona, 08193 Bellaterra, Spain.

[5]Centro de Investigación Biomédica en Red de Diabetes y Enfermedades Metabólicas Asociadas (CIBERDEM), ISCIII, 28034 Madrid, Spain.

[6]Department of Systems Biology, Facultad de Medicina, Universidad de Alcalá, 28805 Alcalá de Henares, Spain.

[7]Instituto Ramón y Cajal de Investigación Sanitaria, ISCIII, 28034, Madrid, Spain.

*Corresponding authors: Catalina Hernández-Sánchez and Enrique J. de la Rosa, CIB Margarita Salas-CSIC, Madrid, Spain; chernandez@cib.csic.es, ejdelarosa@cib.csic.es

Running title: Insulin receptor in retinitis pigmentosa.

Keywords: Insulin receptor, pS6, neurodegeneration, synapses, retina.

ABSTRACT

Synaptic loss, neuronal death, and circuit remodeling are common features of central nervous system neurodegenerative disorders. Retinitis pigmentosa (RP), the leading cause of inherited blindness, is a group of retinal dystrophies characterized by photoreceptor dysfunction and death. The insulin receptor, a key controller of metabolism, also regulates neuronal survival and synaptic formation, maintenance, and activity. Indeed, deficient insulin receptor signaling has been implicated in several brain neurodegenerative pathologies. We present evidence linking impaired insulin receptor signaling with RP. We describe a selective decrease in the levels of the insulin receptor and its downstream effector phospho-S6 in retinal horizontal cell axons in the rd10 mouse model of RP, as well as aberrant synapses between rod photoreceptors and the postsynaptic terminals of horizontal and bipolar cells. A gene therapy strategy to induce sustained proinsulin production restored retinal insulin receptor signaling, by increasing S6 phosphorylation, without peripheral metabolic consequences. Moreover, proinsulin preserved photoreceptor synaptic connectivity and prolonged visual function in electroretinogram and optomotor tests. These findings support the therapeutic potential of proinsulin in RP.

INTRODUCTION

Neurodegenerative disorders are complex pathological conditions that involve, among other processes, synaptic loss and neuronal cell death leading to deterioration of neuronal structure and function. According to the 2017 Global Burden of Disease report (Collaborators, 2019), neurodegenerative diseases are the second leading cause of death and a major cause of disability. The development of strategies to cure or at least delay the progression of neurodegenerative diseases has been hindered by their diverse etiology and complex nature, and by the limited regenerative capacity of neurons. There is thus an urgent need for effective medical interventions. As part of the central nervous system (CNS), the retina shares multiple pathophysiological features with the brain (de La Rosa & Hernandez-Sanchez, 2018). Despite their diverse etiology, retinal neurodegenerative diseases, like those affecting the brain, are characterized by synaptic failure and neuronal cell death (Pfeiffer, Marc et al., 2020). Retinitis pigmentosa (RP) comprises a group of hereditary retinal neurodegenerative conditions with a complex genetic etiology. To date more than 60 genes and 3,000 mutations have been implicated in RP, and over 300 genes associated with inherited retinal dystrophies (https://sph.uth.edu/retnet/disease.htm) have been identified. RP is characterized by primary dysfunction and death of photoreceptor cells followed by reactive gliosis and remodeling of the retinal structure, resulting in vision loss and eventual blindness (Cuenca, Fernandez-Sanchez et al., 2014, Pfeiffer et al., 2020). RP is categorized as a rare disease (prevalence 1/3,500-4,000), but accounts for most cases of hereditary blindness. Gene therapy would be the ideal definitive treatment, and one such therapy has been recently approved for a related retinal dystrophy (Russell, Bennett et al., 2017). However, the complexity and diversity of the mutations underlying RP necessitate the development of alternative therapeutic approaches, particularly those independent of the causative

mutation, as well as palliative treatments. The insulin receptor (INSR), traditionally considered a key peripheral metabolic regulator, is increasingly viewed as an important modulator of neuronal cell survival, and synaptic formation, maintenance, and activity (Arnold, Arvanitakis et al., 2018, Banks, Owen et al., 2012, Chiu & Cline, 2010). Since initial reports described widespread INSR expression in the CNS, including the retina (de la Rosa, Bondy et al., 1994, Havrankova, Roth et al., 1978, Marks, Porte et al., 1990, Rodrigues, Waldbillig et al., 1988, Unger, McNeill et al., 1989), INSR signaling has been implicated in a growing number of CNS functions. In addition to regulating feeding behavior and peripheral metabolism, central INSR signaling is involved in memory formation and cognitive functions (Arnold et al., 2018, Banks et al., 2012, Gralle, 2017). The mechanisms underpinning the non-metabolic actions of INSR are being gradually unraveled. At the neuronal level, INSR is involved in the control of synaptic function, through regulation of neurotransmitter receptor trafficking, and in synapse maintenance and dendritic arbor formation (Chiu & Cline, 2010, Lee, Huang et al., 2011). Downregulation of INSR signaling has been implicated in several neurodegenerative diseases (Arnold et al., 2018), particularly Alzheimer's disease (Moloney, Griffin et al., 2010, Rivera, Goldin et al., 2005, Steen, Terry et al., 2005, Talbot, Wang et al., 2012), and INSR stimulation proposed as a potential treatment for neurodegenerative disorders (Chapman, Schioth et al., 2018).

We previously showed that INSR stimulation in the embryonic retina promotes neuronal differentiation and downregulates developmental cell death (Hernandez-Sanchez, Lopez-Carranza et al., 1995, Valenciano, Corrochano et al., 2006), and that the insulin precursor proinsulin (Pi) can slow RP progression (Corrochano, Barhoum et al., 2008, Fernandez-Sanchez, Lax et al., 2012, Isiegas, Marinich-Madzarevich et al., 2016). In the present study, we investigated the role of INSR in retinal neurodegeneration and

sought to characterize the neuroprotective role of Pi as a putative INSR ligand. We present the first evidence linking impaired INSR signaling with retinal neurodegeneration, and provide insight into the multifaceted neuroprotective role of INSR. We employed a gene therapy strategy to produce sustained increases in systemic Pi levels without peripheral metabolic consequences. Pi treatment restored INSR signaling as measured by S6 phosphorylation, preserved photoreceptor synaptic connectivity, and more importantly, extended visual function in a murine model of RP.

RESULTS

Insulin receptor expression and signaling in WT and rd10 retinas

The insulin receptor gene (*Insr*) is expressed in mammals as two differentially spliced mRNA isoforms that differ by the presence of a small exon (exon 11) encoding 12 amino acids at the C-terminal of the α-subunit (Belfiore, Malaguarnera et al., 2017, Hernandez-Sanchez, Mansilla et al., 2008). The two isoforms (INSR-A and INSR-B) have distinct biochemical and functional properties and tissue distributions (Belfiore et al., 2017). To first characterize the possible role of INSR signaling in the dystrophic retina, we evaluated the retinal expression of each isoform in both physiological and pathological conditions: retinal *Insr-a* and *Insr-b* expression was analyzed by reverse transcriptase polymerase chain reaction (RT-PCR) in wild type (WT) mice and in the *Pde6b*$^{rd10/rd10}$ (*rd10*) mouse model of RP (Chang, Hawes et al., 2007). Retinal RNA extracts were obtained at different stages from postnatal day 15 (P15) (i.e. before the appearance of evident retinal degeneration) up to P60 (after rod loss) (Fig. 1A). The *Insr-a* isoform, which lacks exon 11, was the only isoform detected in both WT and *rd10* retinas at all stages analyzed, as well as in the three adult WT brain areas analyzed (cerebellum, brainstem, remainder of the telencephalon-diencephalon and olfactory bulb). Conversely, key glucoregulatory tissues, such as the liver and adipose tissue, preferentially expressed the *Insr-b* isoform, which contains exon 11.

INSR tissue distribution was visualized by immunofluorescence using the anti-INSR β-subunit antibody C19 (see Table 1). The specificity of this antibody in neural tissue has been previously confirmed in *Insr*-knockout mice (Bruning, Gautam et al., 2000, Dixon-Salazar, Fourgeaud et al., 2014). We found that INSR was widely distributed in the WT retina, in accordance with its versatile role in the CNS. Interestingly, we observed prominent expression in the outer plexiform layer (OPL) and the retinal nerve

fiber layer (NFL) (Fig. 1B). The OPL is a synaptic layer in which photoreceptor, horizontal, and bipolar cell axons and dendrites connect. Double immunostaining for INSR and calbindin, a marker of horizontal cells, revealed that INSR expression in the OPL was restricted to a subset of calbindin-positive fibers (Fig. 1C). By contrast, we observed no colocalization of INSR and PKC-α, which labels the dendrites of ON-bipolar cells (Suppl. Fig. 1A). To determine the type (axon or dendrite) of INSR-positive horizontal cell processes, we performed immunostaining for neurofilament M (NF-M), which is selectively expressed by the axons (Peichl & Gonzalez-Soriano, 1993, Peichl & Gonzalez-Soriano, 1994) (Fig. 1E). INSR expression in the OPL was restricted to NF-M-positive horizontal cell axons (Fig. 1D). NF-M-positive ganglion cell axons also showed robust INSR expression (Suppl. Fig. 1B). Horizontal cells receive rod and cone inputs separately; while their axon terminals receive inputs from rods, their dendrites collect input from cone pedicles (Feigenspan & Babai, 2015, Kolb, 1970, Kolb, 1974, Peichl & Gonzalez-Soriano, 1994). Therefore, our results indicate preferential expression of INSR in the horizontal cell axons that synapse with rod spherules.

Next, we sought to characterize the pattern of INSR expression associated with retinal dystrophy. In early disease stages, before the onset of any significant disturbances in rod cells (P16), comparable global patterns of INSR immunostaining were observed in WT and *rd10* retinas (Suppl. Fig. 2A). However, during the course of rod degeneration (P21–P23) we observed a selective and progressive decrease in INSR immunostaining in horizontal cell axons in the *rd10* retina (Fig. 2). This decrease was not due to the loss of horizontal cells, since similar numbers of calbindin-positive cells were observed in WT and *rd10* retinas at these ages (Suppl. Fig. 3), nor due to degeneration of horizontal cell axons, as evidenced by the preservation of NF-M immunostaining (Fig. 2). Moreover,

INSR downregulation was specific to horizontal cell axons; we observed no significant changes in INSR immunostaining in ganglion cell axons (Fig. 2).

We next investigated whether the selective decrease in INSR expression in horizontal cell axons had consequences at the level of local INSR signaling. Of the multiple downstream effectors of INSR signaling, we specifically focused on ribosomal protein S6. A recent study (Agostinone, Alarcon-Martinez et al., 2018) reported robust pS6$^{Ser240/244}$ immunostaining in retinal horizontal and ganglion cells, where we observed prominent INSR expression. Immunostaining of WT retinas for pS6$^{Ser240/244}$ corroborated the aforementioned labeling of horizontal and ganglion cell bodies (Fig. 3A, upper panels and Suppl. Fig. 4). Moreover, a closer examination of pS6$^{Ser240/244}$ staining in the OPL revealed profuse punctate labeling in close apposition to the horizontal cell terminal tips (Fig. 3). Interestingly, pS6$^{Ser240/244}$ immunostaining in the *rd10* retina revealed similar staining of horizontal cell bodies, but a dramatic decrease in punctate labeling (Fig. 3A). Double immunostaining for pS6$^{Ser240/244}$ and calbindin showed a decrease in the number of calbindin-positive tips due to retraction of horizontal terminal fibers caused by photoreceptor loss (Cuenca et al., 2014, Pfeiffer et al., 2020). Moreover, in the *rd10* retina half of the remaining horizontal cell terminal tips were devoid of pS6$^{Ser240/244}$ labeling (Fig. 3A, lower panels and Fig. 3B).

Taken together, our results indicate that in parallel with the degeneration of rod photoreceptors, the terminals of their post-synaptic horizontal cell partners undergo a putative process of insulin resistance, as evidenced by the decreases in INSR levels and pS6$^{Ser240/244}$ signaling. This process may resemble the central and peripheral insulin resistance that occurs in brain neurodegenerative conditions and in type 2 diabetes (Arnold et al., 2018, Holscher, 2020).

Analysis of synaptic ultrastructure in the OPL of WT and rd10 retinas

Given the marked downregulation of INSR expression and signaling in horizontal cell axons and terminal tips that accompanies rod degeneration, together with the role of INSR in synapse formation and maintenance (Chiu & Cline, 2010, Gralle, 2017, Lee et al., 2011), we next investigated whether changes in INSR expression coincided with alterations in synaptic structure in the OPL. Our analyses focused on rod synapses, since cone survival remains uncompromised in the early stages of degeneration in the *rd10* retina (Zhao, Zabel et al., 2015). The OPL contains so-called triad synapses, formed by the presynaptic rod spherule, two lateral horizontal, and one or two central bipolar postsynaptic terminals invaginating in close apposition to the synaptic ribbon (Fig. 4A and C). Using electron microscopy, we examined WT and *rd10* retinas in the early stages of degeneration (P21), when a large proportion of rod photoreceptor cells persist but signs of degeneration are also evident (Suppl. Fig. 5). In WT retinas, most of the rod synapses (70%) corresponded to characteristic triad synapses (Fig. 4A and D). Conversely, in *rd10* retinas at the same timepoint, triad synapses accounted for less than 20% of all synapses (Fig. 4D). Moreover, in *rd10* retinas more than 40% of rod terminals lacked any postsynaptic element while in WT retinas this was observed in only 8% of rod terminals (Fig. 4B and D). Despite the absence of postsynaptic partners, disconnected rod spherules had a viable appearance, as evidenced by intact mitochondria and electro-lucent content. In these disconnected spherules the synaptic ribbon, when present, was attached to an unusually flat cell membrane with no signs of any postsynaptic invagination (Fig. 4B). By contrast, the degenerative rod spherules (accounting for 20% and 3% of rod terminals in *rd10* and WT retinas, respectively) were highly vacuolated, with electro-dense content and aberrant mitochondria (Fig. 4B and D). Among the degenerated rod spherules we observed both disconnected terminals and triad synapses (Fig. 4B), suggesting that disconnection is not a necessary step before degeneration. Furthermore, both genotypes

showed similar numbers of dyads (Suppl. Fig. 6), most likely due to the misalignment of one of the postsynaptic elements with the plane of section (Wang, Pahlberg et al., 2019).

Immunostaining using specific markers for photoreceptor ribbon (Ribeye and Ctbp2) and horizontal (GluA2) and bipolar (mGluR6) postsynaptic terminal tips also revealed synaptic disconnection of rod photoreceptors (Suppl. Fig. 7).

Systemic proinsulin reaches the retina and exerts no metabolic effect

The results described above suggest a possible link between deficient INSR signaling, synaptic disconnection in rod photoreceptors, and the visual impairment characteristic of RP. To determine whether deficient INSR signaling is a disease-modifying factor in RP, and therefore a potential therapeutic target, we employed a gene therapy strategy to enhance INSR signaling. Proinsulin, the insulin precursor, is an INSR-A selective ligand (Malaguarnera, Sacco et al., 2012) with a low metabolic profile, likely due to its poor affinity for the INSR-B isoform (Belfiore et al., 2017, Malaguarnera et al., 2012). We have previously demonstrated the neuroprotective potential of Pi during retinal development and degeneration (Corrochano et al., 2008, Fernandez-Sanchez et al., 2012, Hernandez-Sanchez, Mansilla et al., 2006, Isiegas et al., 2016). Given that treatment of RP in humans would entail long-term administration, we selected Pi to activate INSR-A, the predominant INSR isoform expressed in the retina (Fig. 1A).

To achieve sustained production of Pi, we built upon our previous experience with a recombinant AAV2/1 expressing the human proinsulin (hPi) coding region (Fig. 5; AAV-hPi) (Corpas, Hernandez-Pinto et al., 2017, Fernandez-Sanchez et al., 2012). We first evaluated hPi production following intramuscular administration of AAV-hPi. *rd10* mice received a single injection of AAV-hPi into the gastrocnemius muscle at P10 to induce hPi production before the onset of degeneration (around P18). In AAV-hPi-treated *rd10* mice hPi serum levels were uniformly sustained within each individual mouse for

up to 5 months (the maximum follow-up period) (Fig. 5B). Moreover, hPi was detected in whole eye and in retinal extracts as early as 1 week post-injection and up to 7 weeks post-injection (the maximum follow-up period) (Suppl. Fig. 8A). Conversely, hPi was not detected at any timepoint in serum samples, whole eye, or retinal extracts from mice injected with the control vector (AAV-null). Moreover, mature human insulin was absent in serum samples from AAV-hPi-treated WT mice, in agreement with our previous findings (Corpas et al., 2017, Fernandez-Sanchez et al., 2012). Therefore, Pi produced from AAV-hPi remained mainly, if not completely, unprocessed. Importantly, we observed no differences in glycaemia or body weight in AAV-hPi- versus AAV-null-treated mice (Fig. 5C and D), confirming an absence of significant metabolic effects of systemic hPi production, in line with previous studies (Corrochano et al., 2008; Fernández-Sánchez et al., 2012; Corpas et al. 2017).

AAV-hPi treatment in rd10 mice preserves photoreceptors and photoreceptor synaptic connectivity

To determine the effect of hPi on the dystrophic retina, we first examined whether hPi treatment could restore INSR signaling. AAV-hPi treated *rd10* retinas exhibited higher levels of punctate pS6$^{Ser240/244}$ staining in the OPL than control (AAV-null-treated) *rd10* retinas (Fig. 6). Quantification of the number of pS6$^{Ser240/244}$-positive horizontal cell tips at P21 showed that hPi treatment increased the proportion of calbindin-pS6$^{Ser240/244}$-positive tips to near 90%, close to the proportion observed in WT retinas (Fig. 3). By contrast, in control (AAV-null-treated) *rd10* retinas the proportion of pS6$^{Ser240/244}$-positive horizontal cell tips remained in the range of 50–60% (Fig. 6B). In addition, we observed a greater abundance of total calbindin-positive tips in the AAV-hPi-treated than in the control retinas, most likely a consequence of photoreceptor preservation caused by hPi treatment (Fig. 7).

We next investigated whether long-term hPi treatment exerted a neuroprotective effect. To this end, we injected *rd10* mice with AAV-null or AAV-hPi at P10–P12 and analyzed the corresponding retinas at P30, at which point most photoreceptor cells have been lost in this mouse model. Two distinct histological parameters were evaluated: photoreceptor cell preservation and synapse maintenance. AAV-hPi-treated *rd10* retinas showed modest but significant photoreceptor preservation, as determined by measuring the relative increase in thickness of the outer nuclear layer (ONL), an effect that was more evident in the nasal peripheral retina (T1; Fig. 7). In parallel, the synaptic connectivity of photoreceptors was assessed by immunostaining rod-bipolar and rod-horizontal synapses. As expected, photoreceptor preservation in AAV-hPi-treated retinas led to an increase in the number of ribbons. Moreover, hPi reduced the proportion of disconnected postsynaptic terminals of rod cells (i.e. those lacking either a GluA2-positive horizontal postsynaptic terminal [Fig, 8A and C] or a mGluR6-positive bipolar postsynaptic terminal [Fig. 8B and D]). These results reveal a novel effect of proinsulin: preservation of the synaptic connectivity of rod cells with their postsynaptic second-order neuronal partners. This observation suggests a second distinct role of hPi that may be partially independent of its effects on photoreceptor cell survival revealed in our previous studies (Corrochano et al., 2008, Fernandez-Sanchez et al., 2012, Isiegas et al., 2016). Moreover, the increase in the number of photoreceptor synapses induced by proinsulin treatment that we previously observed in the P23H rat model of RP (Fernandez-Sanchez et al., 2012) is most likely a consequence of the rescue of photoreceptor cells as well as preservation of their synaptic contacts, as described here.

AAV-hPi treatment in rd10 mice preserves visual function

Finally, in AAV-hPi-treated *rd10* mice we assessed whether hPi preserved visual function, which is the most clinically relevant outcome for a potential RP treatment.

Electroretinographic (ERG) recordings were performed in dim and daylight conditions every 10 days between P30 and P60 to evaluate rod- and cone-mediated light responses (Fig 9). AAV-hPi-treated *rd10* mice displayed better defined and more prominent ERG waves than their AAV-null-treated counterparts (Fig 9B). Waves corresponding to rods (b-scotopic wave), cones (b-photopic wave), and both photoreceptors (a-mixed and b-mixed waves) were of a significantly greater amplitude in AAV-hPi-treated than AAV-null-treated *rd10* mice (Fig. 9C). ERG recordings thus confirmed that hPi treatment preserved visual function, consistent with the aforementioned preservation of photoreceptor cells and their synapses. Optokinetic testing further confirmed partial preservation of the light response in AAV-hPi-treated *rd10* retinas. In addition to measuring the retinal response to light, this visual behavior test evaluates the function of other components of the visual system, namely optic nerve transmission and visual integration in the brain (Abdeljalil, Hamid et al., 2005). Mice instinctively respond to rotating vertical bars with characteristic movement of their heads in the same direction as the rotation of the bar (Fig. 10A and B). AAV-hPi-treated *rd10* mice showed greater contrast sensitivity than AAV-null-treated counterparts at the two ages studied (P40 and P50; Fig. 10C and D). Together, our results support the disease-modifying potential of Pi, which can prolong visual function in an animal model of RP and therefore constitutes a viable candidate therapy for retinal dystrophies.

DISCUSSION

This study describes the downregulation of retinal INSR levels and local signaling during the early stages of retinal neurodegeneration in the *rd10* mouse model of RP, together with concomitant disruption of photoreceptor triad synapses. These findings suggest that deterioration of INSR signaling contributes to the structural and functional degeneration of the retina in *rd10* mice. We provide proof of concept of the neuroprotective effect of INSR stimulation with the insulin precursor Pi, which is selective for the INSR-A isoform found in the retina. Gene therapy using an AAV induced sustained production of circulating Pi, which reached the retina, restored local INSR signaling, and exerted neuroprotective effects on retinal structure and visual function, without affecting peripheral metabolic parameters. Proinsulin treatment attenuated both photoreceptor cell loss and synaptic disconnection, and prolonged visual function, highlighting the potential of Pi as a candidate therapy for RP.

Studies over the past two decades have broadened the scope of INSR activity far beyond the peripheral metabolic role initially ascribed to this receptor. The versatility of this receptor is also implied by its widespread expression in the CNS. At the neuronal level, INSR has been implicated in synaptic plasticity, dendritic outgrowth, and cell survival (Chiu & Cline, 2010, Gralle, 2017, Lee et al., 2011). The *Insr-a* splice variant, which is predominantly expressed in different areas of the brain as well as the retina, is the most ancient and promiscuous isoform, and participates in insulin, Pi, and IGF-II signaling (Hernandez-Sanchez et al., 2008, Malaguarnera et al., 2012). Interestingly, many of the signaling pathways in which INSR-A is involved are similar to those mediated by growth factor receptors, and in some ways this isoform resembles the ancestral INSR expressed in invertebrates and low vertebrates (Banks et al., 2012, Belfiore, Frasca et al., 2009, Chan & Steiner, 2000). The present findings confirm the

previously described wide distribution of INSR in the WT retina (Gosbell, Favilla et al., 2000, Rajala, Wiskur et al., 2009). However, we also describe for the first time more intense INSR immunostaining in horizontal and ganglion cell axons than in other retinal structures. Interestingly, analysis of INSR expression during retinal degeneration in the rd10 mouse revealed local downregulation of INSR, specifically in horizontal cell axons. This was accompanied by a decrease in the phosphorylation of ribosomal protein S6 in horizontal cell terminals, indicating impaired INSR signaling. Notably, horizontal cell axon terminals receive input from the rod photoreceptors, the main targets of degeneration in RP. A recent study by Agostinone et al. (Agostinone et al., 2018) reported specific decreases in $pS6^{Ser240/244}$ in ganglion cells following transection of their axons, but no alterations in $pS6^{Ser240/244}$ in horizontal cells. In the present study, we observed selective downregulation of INSR expression and impaired signaling in the horizontal cells with which the damaged rod photoreceptors synapse. It remains unclear whether this finding is mechanistically linked to the decreases in $pS6^{Ser240/244}$ described by Agostinone et al (Agostinone et al., 2018). However, our results are consistent with the proposals by other authors that INSR signaling may vary in a neuronal activity-dependent manner (Chiu & Cline, 2010, Clarke, Mudd et al., 1986, Hori, Yasuda et al., 2005), and suggest that INSR expression and signaling in horizontal cells may depend on rod input.

Interestingly, in *rd10* retinas INSR downregulation and consequent impairment of INSR signaling coincided with the presence of disconnected but otherwise apparently viable rod terminals. Alterations in retinal synaptic circuitry as part of retinal remodeling during photoreceptor degeneration have been acknowledged for more than two decades (Jones, Kondo et al., 2012, Lewis, Linberg et al., 1998, Pfeiffer et al., 2020, Strettoi, Pignatelli et al., 2003). De-afferentiation of second-order neurons has typically been described in advanced stages of degeneration as a consequence of photoreceptor loss

(Jones et al., 2012, Lewis et al., 1998, Pfeiffer et al., 2020, Strettoi et al., 2003). However, here we describe early disconnection events affecting up to 50% of apparently viable rod spherules during the initial stages of degeneration. Although further studies will be required to clarify the consequences of this disconnection, it does not appear to necessarily precede rod death, as we detected degenerative triads containing the presynaptic rod spherule and horizontal and bipolar terminals. These observations have direct implications for the development of neuroprotective therapies and could open a new line of research into interventions aimed at preserving rod connectivity.

Our findings demonstrate the potential of Pi as a synaptoprotective factor. In *rd10* mice treated with AAV-hPi, systemically produced Pi reached the retina and restored INSR signaling, as determined by measuring $pS6^{Ser240/244}$ levels. Concomitantly, Pi treatment reduced the number of disconnected rod presynaptic terminals, supporting a role of INSR signaling in photoreceptor synaptic connectivity. Our results are in line with those of the seminal study by Chiu et al. 2008 (Chiu & Cline, 2010), who used optic tectal neurons in living *Xenopus* tadpoles to demonstrate that INSR signaling maintains both synaptic contacts and the branches on which they lie. Moreover, in the aforementioned study by Agostinone et al. (Agostinone et al., 2018) stimulation of INSR signaling with insulin promoted regeneration of the dendritic arbors of retinal ganglion cells after axonal injury.

Deficient local INSR signaling associated with RP may be a general feature of neurodegenerative diseases, irrespective of peripheral insulin resistance [reviewed in (Arnold et al., 2018)]. Several studies have described decreased INSR expression and/or attenuation of the activation states of INSR signaling molecules in affected brain regions in patients with Alzheimer's (Rivera et al., 2005, Steen et al., 2005, Talbot et al., 2012) and Parkinson's (Moroo, Yamada et al., 1994, Takahashi, Yamada et al., 1996, Timmons,

Coakley et al., 2009) diseases. We show that pharmacological stimulation of INSR signaling with Pi has a disease-modifying effect over the course of retinal degeneration, in line with the beneficial effects of INSR stimulation with insulin reported in other neurodegenerative diseases of the brain and retina (Agostinone et al., 2018, Arnold et al., 2018, Holscher, 2020). Moreover, the widespread expression of INSR in the retina suggests that synaptic maintenance promoted by INSR signaling is only one of several retinal processes regulated by INSR. Indeed, we and others have demonstrated the neuroprotective effects of INSR signaling molecules on photoreceptor survival (Punzo, Kornacker et al., 2009, Rajala, Tanito et al., 2008, Sanchez-Cruz, Villarejo-Zori et al., 2018).

Our results provide a novel mechanism to account for our previous descriptions of the neuroprotective effects of Pi on retinal dystrophy (Corrochano et al., 2008, Fernandez-Sanchez et al., 2012, Isiegas et al., 2016) and cognitive impairment (Corpas et al., 2017), and further support the validity of Pi-mediated stimulation of INSR as a candidate therapy for neurodegenerative conditions of the CNS.

MATERIALS AND METHODS

Animals

The *rd10* mouse is an autosomal recessive homozygous mutant for phosphodiesterase 6b (*Pde6b*$^{rd10/rd10}$) on a C57BL/6J background (Chang et al., 2007). Both *rd10* and WT control mice of the same background were obtained from The Jackson Laboratory (Bar Harbor, ME, USA). All animals were housed and handled in accordance with the ARVO statement for the Use of Animals in Ophthalmic and Vision Research, European Union guidelines, and those of the local ethics committees of the CSIC and the Comunidad de Madrid (Spain). Mice were bred in the CIB core facilities on a 12/12-h light/dark cycle. Light intensity was maintained at 3–5 lx.

Generation and administration of adeno-associated viral vectors

Recombinant AAV serotype 2/1 viral vectors bearing cDNA from the human proinsulin (hPi) gene under control of the cytomegalovirus promoter (AAV-hPi) or without hPi cDNA (AAV-null) were generated in the Center for Animal Biotechnology and Gene Therapy at the Universitat Autònoma de Barcelona, as previously described (Corpas et al., 2017). *rd10* mice received a single intramuscular injection of 7.2×10^{11} vector genomes/kg body weight of AAV-hPi or AAV-null at P10–12. The total vector dose was distributed equally between the gastrocnemius muscles of both hindlimbs.

Measurement of proinsulin, insulin, and glycaemia

Serum, eye, and retinal levels of human Pi and serum levels of human insulin were measured using human Pi and human insulin ELISA kits (EZHPI-15K and EZHI-14K, respectively; Millipore, Darmstadt, Germany) according to the manufacturer's instructions and as described previously (Isiegas et al., 2016). Glycaemia was directly measured in blood samples using the Glucocart™ Gmeter kit (A. Menarini Diagnostics Ltd., Berkshire, UK).

RNA isolation and RT-PCR

Total RNA from tissues was isolated using Trizol reagent (Invitrogen). The reverse transcriptase reaction (RT) was typically performed with 2 µg RNA, the Superscript III Kit, and random primers (all from ThermoFisher Scientific, Waltham, MA), followed by amplification with the 2X PANGEA-Long PCR Master Mix (Canvax Biotech, Córdoba, Spain). Mouse *Insr* was amplified using the following primers: sense, 5'-GGCCAGTGAGTGCTGCTCATGC-3' (inside exon 10); antisense, 5'-TGTGGTGGCTGTCACATTCC-3' (inside exon 12). Mouse β-actin was amplified using the following primers: sense, 5'-AAGGCCAACCGTGAAAAGAT-3'; antisense, 5'-GTGGTACGACCAGAGGCATAC-3'.

Immunofluorescence and image analysis

Animals were euthanized and their eyes enucleated and fixed for 50 minutes in freshly prepared 4% paraformaldehyde in Sörensen's phosphate buffer (SPB) (0.1 M, pH 7.4), and then cryoprotected by incubation in increasing concentrations of sucrose (final concentration, 50% in SPB). The eyes were then embedded in Tissue-Tek OCT (Sakura Finetec, Torrance, CA, USA) and snap frozen in dry-ice cold isopentane. Equatorial sections (12 µm) were cut on a cryostat and mounted on Superfrost Plus slides (Thermo Scientific, Massachusetts, USA), dried at room temperature, and stored at -20ºC until the day of the assay.

Before performing further analyses, slides were dried at room temperature. After rinsing in PBS and permeation with 0.2% (w/v) Triton X-100 in PBS, sections were incubated with blocking buffer (5% normal goat serum, 1% Tween-20, 1 M glycine in PBS) for 1 h and then incubated overnight at 4ºC with primary antibodies (Table 1) diluted in blocking buffer. Sections incubated in the absence of primary antibody were used as specificity controls. After rinsing in PBS and incubation with the appropriate

secondary antibodies (Table 1), sections were stained with DAPI (4´,6-diamidino-2-phenylindole; Sigma-Aldrich Corp., St. Louis, MO, USA) and cover slipped with Fluoromont-G. For GluA2 and mGluR6 immunostaining, an antigen retrieval step was performed prior to incubation in blocking buffer. To this end, sections were incubated in citrate buffer (10 mM sodium citrate, 0.05% Tween-20, pH 6.0) in boiling water for 10 minutes. After cooling to room temperature, sections were rinsed with PBS and then incubated in freshly prepared 0.2% sodium borohydride in PBS before continuing with the blocking reaction described above.

Table 1

Antibody against	**Host species**	**Dilution**	**Manufacturer**	**Catalog number**
Calbindin	Mouse	1:500	Sigma	C9848
Ctbp2	Mouse	1:300	BD Biosciences	612044
GluA2	Mouse	1:300	Neuromab	75-002
Insulin receptor (INSR)	Rabbit	1:200	Santa Cruz	C19; SC-711
mGluR6	Guinea Pig	1:200	Acris GmBh	AP20134SU-N
Neurofilament Medium (NF-M)	Mouse	1:500	Developmental Studies Hybridoma Bank	DH-3
PKC-α	Mouse	1:500	Abcam	AB11723

$pS6^{(Ser240/Ser244)}$	Rabbit	1:200	Cell Signaling	5364
Ribeye	Rabbit	1:400	Synaptic Systems	192103

Sections were analyzed using a laser confocal microscope (TCS SP5 and TCS SP8; Leica Microsystems, Wetzlar, Germany). In all cases, retinal sections to be compared were stained and imaged under identical conditions. To measure the area occupied by INSR and NF-M immunostaining, images were converted to black and white and analyzed with Fiji software. To quantify the number of horizontal cell tips with associated $pS6^{Ser240/244}$ punctate staining, over 200 horizontal cell tips per animal in 4 retinal areas were analyzed. Similarly, for synapse quantification, over 200 rod ribbons per animal in 4 retinal areas were assessed for associated GluA2 (horizontal cell postsynaptic terminal) or mGluR6 (horizontal cell postsynaptic terminal) punctate immunostaining. To evaluate photoreceptor preservation, three sections per retina were analyzed: for each section, six areas in a nasotemporal sequence were photographed (Fig. 7A). ONL and INL thickness were measured in three random positions for each image.

Transmission electron microscopy

Animals were euthanized and their eyes enucleated and fixed overnight in freshly prepared 2% paraformaldehyde and 2% glutaraldehyde in sodium cacodylate buffer (0.1 M, pH 7.4). After dissection of the cornea and lens, optic cups were post-fixed for 1 hour with 1% OsO_4 (v/v) and 1% $K_3Fe(CN)_6$ (v/v) in ultrapure water, dehydrated through a graded series of ethanol solutions and embedded in Epoxy EMbed-812 resin (EMS, Electron Microscopy Sciences). Semi-thin (0.5 μm) and ultra-thin sections were obtained using an Ultracut E ultramicrotome (Leica). Semi-thin sections were stained with Toluidine Blue and mounted with Entellan and images were obtained using a light microscope (Axio Observer Z1, Zeiss) with 20× and 100× oil immersion objectives.

Ultra-thin sections were contrasted with uranyl acetate and lead citrate, and analyzed at the NUCLEUS electron microscopy facility at the University of Salamanca using a Tecnai Spirit Twin 120 kv electron microscope with a CCD Gatan Orius SC200D camera with DigitalMicrograph™ software. The proportions of the different types of synapses were quantified in ultra-thin sections from 3 mice of each genotype by analyzing over 60 synapses per mouse.

ERG recordings and optomotor tests

Mice were handled and ERGs performed as previously described (Corrochano et al., 2008). Measurements were performed by an observer blind to experimental condition. ERG signals were amplified and band filtered between 0.3 and 1000 Hz (CP511 Preamplifier, Grass Instruments, Quincy, MA, USA) and digitized to 10 kHz using a PowerLab acquisition data card (AD Instruments Ltd., Oxfordshire, UK). Graphical representations of the signals recorded and luminous stimuli control were performed with Scope v6.4 PowerLab software (AD Instruments, Oxford, UK). ERG wave amplitudes were measured off-line and the results averaged. Wave amplitude analysis was performed using the MATLAB application.

An optomotor device was built based on the design proposed by Prusky et al. (Prusky, Alam et al., 2004). Mice were placed in the center of a square array of computer monitors that displayed stimulus gratings, and then monitored using an overhead infrared television camera placed above the testing chamber. The test started with the most easily visible stimulus, with a spatial frequency of 0.088 cycles/degree, a temporal frequency of 0.88 Hz, and a normalized contrast of 1. Contrast sensitivity was calculated as the inverse of contrast threshold, and was measured at distinct spatial frequencies ranging from 0.022–0.355 cycles/degree (Fig. 10B). The Vision Egg tool was used for light stimulation. Stimuli consisted of vertical black/white bars (gratings) moving through the screens.

Statistical analysis

Statistical analysis was performed with GraphPad Prism software 8.0 (GraphPad Software Inc., La Jolla, CA, USA).

To compare two groups, normality was assessed for each group using the Shapiro-Wilk normality test. Normally distributed data were analyzed using an unpaired T-test, and non-normally distributed data using a Mann Whitney U-test. Homocedasticity for all data sets was assessed employing F test. When variance between data sets was significantly different Welch's correction was applied to the T-test. Unpaired T-tests were used to compare insulin receptor and $pS6^{Ser240/244}$ levels between WT and *rd10* animals, and to assess rod-horizontal and rod-bipolar connectivity in AAV-null and AAV-hPi mice.

Analysis of variables over time was achieved using a 1-way ANOVA. Dunnett's multiple comparison test was used to compare values at different time points with those at a specific time point. Accordingly, serum, eye and retinal hPi levels at different time points were compared with initials values using Dunnett's multiple comparison test.

Comparisons of two variables were performed using a 2-way ANOVA, followed by Sidak's multiple comparison test where a significant interaction was detected. Sidak's multiple comparison test was thus used to compare the different synaptic morphologies between WT and *rd10* animals. Differences in histological parameters (ONL/INL ratio), ERG wave amplitude, and optomotor test results between AAV-null mice and AAV-hPi mice were assessed using a 2-way ANOVA.

In all cases, statistical significance was set at $p \leq 0.05$.

FIGURE LEGENDS

Figure 1. Insulin receptor expression in the retina.

A. RT-PCR of WT and *rd10* mouse retinas at the indicated ages, and WT adult brain regions and peripheral tissues. Forward and reverse PCR primers corresponded to exons 10 and 12, respectively, of *Insr*. CB, cerebellum; BS, brain stem; TE, remainder of telencephalon and diencephalon; OB, olfactory bulb; M, muscle; L, liver; A, adipose tissue. ß-actin was used as a loading control.

B-E. Representative images of P21 retinal sections from WT mice. B, Image of a retinal section immunostained for INSR (green). Nuclei are stained with DAPI (blue). **C-E**, Magnified image of the OPL showing double immunostaining for the indicated markers. ONL, outer nuclear layer; OPL, outer plexiform layer; INL, inner nuclear layer; IPL, inner plexiform layer; NFL, nerve fiber layer. Scale bars: 90 μm (B) and 45 μm (C–E).

Figure 2. Downregulation of insulin receptor expression in the *rd10* retina.

A, C. Representative images of P21 (A) and P23 (C) retinal sections from WT and *rd10* mice co-immunostained for INSR (green) and neurofilament-M (NF-M, red). Nuclei are stained with DAPI (blue). ONL, outer nuclear layer; OPL, outer plexiform layer; INL, inner nuclear layer; IPL, inner plexiform layer; NFL, nerve fiber layer. Scale bar: 66 μm.

B, D. Quantification of the area of INSR-positive staining in P21 (B) and P23 (D) WT and *rd10* retinal sections. The area corresponding to INSR immunostaining was normalized to that of neurofilament-M within the same region to correct for potential variations among retinal sections, and to *INSR* immunostaining in corresponding WT sections (=1.0). Data are presented as the mean + SEM. n=4-5 mice, 4 images per retina. *$p \leq 0.05$ (unpaired-T test in B and unpaired-T test with Welch's correction in D).

Figure 3. Downregulation of insulin receptor signaling in the *rd10* retina.

A. Representative images of the OPL of P23 retinal sections from WT and *rd10* mice co-immunostained for $pS6^{Ser240/244}$ (green) and calbindin (red). Arrows indicate horizontal cell terminal tips ($calbindin^{+}$ puncta) without apposite $pS6^{Ser240/244}$ labeling. Asterisks indicate horizontal cell bodies. Brackets delimit the OPL. Scale bar: 12 μm.

B. Quantification of the number of horizontal terminal tips ($calbindin^{+}$ puncta) with apposite $pS6^{Ser240/244}$ labeling. Data are presented as the mean + SEM. n=4 mice, 4 images. Over 200 $calbindin^{+}$ tips were scored per retina. ***$p \leq 0.001$ versus WT (unpaired T-test).

Figure 4. Ultrastructural analysis of rod photoreceptor synapses.

A, B. Representative electron microscopy images of P21 WT (A) and *rd10* (B) rod synapses. Synapses were categorized as follows: *Triad*, rod spherule with horizontal and bipolar invaginating postsynaptic terminals; *Disconnected*, viable rod spherule without postsynaptic elements; *Degenerative disconnected spherule*, rod spherule lacking postsynaptic profiles with characteristic signs of degeneration; *Degenerative triad*, rod spherule containing postsynaptic profiles but showing characteristic signs of degeneration. Scale bar: 500 nm.

C. Schematic diagram showing the structure of a rod triad synapse. The rod spherule (grey) consists of the synaptic ribbon (dark red) and a scaffold structure containing presynaptic vesicles (orange circles). Horizontal cell postsynaptic terminals (blue) and bipolar dendrites (green) invaginate into the rod presynaptic terminal (spherule).

D. Quantification of the proportions of the different synaptic types. Results are expressed as the mean + SEM. n=3 mice. Over 60 synapses were scored per mouse. ****p ≤0.0001, *p≤0.05 (2-way ANOVA followed by Sidak's multiple comparison test).

Figure 5. AAV-hPi treatment results in sustained hPi production.

A. *rd10* mice received a single intramuscular injection of AAV-hPi or AAV-null at P10 and were analyzed at different timepoints post-injection.

B. Long-term monitoring of serum hPi levels as determined by ELISA in individual *rd10* mice injected with AAV-hPi.

C, D. Long-term monitoring of glucose levels (C) and body weight (D) in AAV-hPi or AAV-null injected *rd10* mice. Data are presented as the mean + SEM. n=4 mice in B and 4–6 mice per group in C and D.

Figure 6. Effect of AAV-hPi administration on insulin receptor signaling. *rd10* mice received a single intramuscular injection of AAV-null or AAV-hPi at P12 and $pS6^{Ser240/244}$ expression was analyzed at P21.

A. Representative images of the OPL in P21 retinal sections co-immunostained for $pS6^{Ser240/244}$ (green) and calbindin (red). Arrows indicate horizontal cell terminal tips ($calbindin^{+}$ puncta) without apposite $pS6^{Ser240/244}$ labeling. Asterisks indicate horizontal cell bodies. Brackets delimit the OPL. Scale bar: 11 μm.

B. Quantification of the number of horizontal terminal tips ($calbindin^{+}$ puncta) with apposite $pS6^{Ser240/244}$ labeling. Data are presented as the mean + SEM. n=4 mice, 4 images. Over 200 $calbindin^{+}$ tips per retina were analyzed. *p≤0.05 versus AAV-null (unpaired T-test with Welch's correction).

Figure 7. Effect of AAV-hPi administration on photoreceptor preservation. *rd10* mice received a single intramuscular injection of AAV-null or AAV-hPi at P12 and were analyzed at P30.

A. Schematic depicting retinal sections. The 6 retinal zones in which quantification was performed (T1, T2, T3, T4, T5 and T6) are indicated. ON, optic nerve.

B. Representative images of P30 retinal sections showing the T1 region from AAV-null- and AAV-hPi-treated *rd10* mice. Blue color corresponds to DAPI staining. ONL, outer nuclear layer; INL, inner nuclear layer. Scale bar: 70 μm.

C. ONL and INL thickness were measured in equatorial sections corresponding to 6 retinal areas, following a nasotemporal sequence (T1–T6 as defined in panel A). Plot shows the mean + SEM. n=5 mice, 3 sections per retina, 6 regions, 3 measurements per region. ON, optic nerve. ****$p \leq 0.0001$ (2-way ANOVA).

Figure 8. Effect of AAV-hPi administration on rod horizontal and rod bipolar synapses. *rd10* mice received a single intramuscular injection of AAV-null or AAV-hPi at P12 and were analyzed at P30.

A, B. Representative 3D reconstructions of synapses in the OPL. Retinal sections were co-immunostained for Ribeye (ribbon at presynaptic terminal, red) and the glutamate receptor subunit GluA2 (horizontal postsynaptic terminal, green) (A), or for Ctbp2 (ribbon at presynaptic terminal, red) and the glutamate receptor mGluR6 (bipolar postsynaptic terminal, green) (B). Arrowheads indicate ribbons (rod presynaptic terminals) without post-synaptic partners. OPL, outer plexiform layer. Scale bar: 3 μm.

C, D. Quantification of the number of disconnected rod presynaptic terminals. Percentage of ribbons without associated GluA2 (C) or mGluR6 (D) punctate staining.

Plots show the mean + SEM. $n = 5$ mice. Over 200 ribbons were analyzed per retina. *$p \leq 0.05$ (unpaired T-test).

Figure 9. Effect of AAV-hPi administration on retinal response to light. *rd10* mice received a single intramuscular injection of AAV-null or AAV-hPi at P10. ERG recordings were performed at the indicated ages.

A. Schematic diagram depicting the ERG recording method.

B. Standard ERG representative trace recordings of the mixed response obtained from 1 AAV-null- and 1 AAV-hPi-treated mouse over the course of the study (P30–P60) in response to a light stimulus of 1.5 cd·s/m^2. Note the differences in the traced amplitudes between the 2 animals.

C. Graphs show averaged ERG wave amplitudes, plotted as a function of animal age. Amplitudes of the rod response (b-scotopic; light intensity = -2 log cd·s/m^2) and rod and cone mixed response (a-mixed and b-mixed; light intensity = 2 log cd·s/m^2) were recorded under scotopic conditions after overnight adaptation to darkness. Cone amplitudes (b-photopic; light intensity = 2 log cd·s/m^2) were recorded after 5 minutes of light-adaptation (30 cd/m^2 background light) under photopic conditions. Results are expressed as the mean + SEM. n=4–13. Significant differences between AAV-null- and AAV-hPi-treated mice were observed for b-scotopic, a-mixed, b-mixed, and b-photopic responses ($p \leq 0.05$) (2-way ANOVA).

Figure 10. Effect of AAV-hPi administration on optokinetic response. *rd10* mice received a single intramuscular injection of AAV-null or AAV-hPi at P10. The optomotor test was performed at the indicated ages.

A, B. Schematic depicting the optomotor test (A); 5 different spatial frequencies were tested (0.022–0.355 cycles/degree). The contrast of the moving bars was adjusted (from 100% to 5%) to determine contrast sensitivity (B).

C, D. Optokinetic responses recorded at the indicated ages in AAV-null- and AAV-hPi treated *rd10* mice. Contrast sensitivity is represented as a function of spatial frequency. Data are presented as the mean + SEM. n=6. Significant differences were observed between AAV-null- and AAV-hPi treated mice at P40 ($p \leq 0.05$) and P50 ($p \leq 0.0001$) (2-way ANOVA).

Supplementary Figure 1. Analysis of insulin receptor expression. Representative retinal sections collected from WT mice at P21.

A, B. Magnified image showing the OPL (A) and NFL (B) after co-immunostaining for the indicated markers. Nuclei are stained with DAPI (blue). OPL, outer plexiform layer; NFL, nerve fiber layer. Scale bar: 21 μm.

Supplementary Figure 2. Analysis of insulin receptor expression in WT and *rd10* retinas at P16.

A. Representative images of P16 retinal sections from WT and *rd10* mice co-immunostained for INSR (green) and neurofilament-M (NF-M, red). Nuclei are stained with DAPI (blue). ONL, outer nuclear layer; OPL, outer plexiform layer; INL, inner nuclear layer; IPL, inner plexiform layer; NFL, nerve fiber layer. Scale bar: 58 μm.

B. Quantification of the area of INSR-positive immunostaining at P16 in retinal sections from WT and *rd10* mice. The area of INSR-positive immunostaining was normalized to that of neurofilament-staining of the same region to correct for potential variation among retinal sections, and to *INSR* immunostaining in WT sections (=1.0). Data are presented as the mean + SEM. n=3 mice, 4 images per retina.

Supplementary Figure 3. Comparison of the number of horizontal cells in WT and *rd10* retinas.

A. Representative images of P23 retinal sections from WT and *rd10* mice, immunostained for calbindin to label horizontal cells (red). Nuclei are stained with DAPI (blue).

B. The number of calbindin^{+} cells was scored in equatorial sections in the central regions of the retina (T3–T4; see Methods and Figure 7A). Plots show the mean + SEM. n=5 mice, 10 images per retina. ONL, outer nuclear layer; OPL, outer plexiform layer; INL, inner nuclear layer. Scale bar: 38 μm.

Supplementary Figure 4. Analysis of pS6$^{Ser240/244}$ expression in ganglion cells in WT and *rd10* retinas.

Representative images of the GCL of P23 retinal sections from WT and *rd10* mice immunostained for pS6$^{Ser240/244}$ (green). Nuclei are stained with DAPI (blue). Brackets delimit the GCL. GCL, ganglion cell layer. Scale bar: 41 μm.

Supplementary Figure 5. Representative semi-thin retinal sections.

A. Semi-thin retinal sections collected at P21 from WT and *rd10* mice were prepared for electron microscopy analysis (Fig. 4D). Scale bar: 50 μm.

B. Magnification of the indicated region. Arrows indicate photoreceptor presynaptic terminals. Asterisks indicate degenerating photoreceptors, as evidenced by the condensed nucleus. ONL, outer nuclear layer; OPL, outer plexiform layer; IPL, inner plexiform layer; INL, inner nuclear layer; NFL, nerve fiber layer. Scale bar: 100 μm.

Supplementary Figure 6. Quantification of the proportion of dyads. Data are presented as the mean + SEM. n=3 mice, ≥60 synapses per mouse.

Supplementary Figure 7. Representative 3D reconstructions of P23 WT and *rd10* synapses in the OPL.

A, B. Retinal sections were co-immunostained for Ribeye (ribbon at presynaptic terminal, red) and the glutamate receptor subunit GluA2 (horizontal postsynaptic terminal, green) (A), or for Ctbp2 (ribbon at presynaptic terminal, red) and the glutamate receptor mGluR6 (bipolar postsynaptic terminal, green) (B). Arrowheads indicate ribbons (rod presynaptic terminals) without a post-synaptic partner. Scale bar: 6 μm.

Supplementary Figure 8. Determination of hPi levels after AAV-hPi treatment. *rd10* mice received a single intramuscular injection of AAV-hPi or AAV-null at P10.

A, B. ELISA was performed to measure hPi in retinal and eye extracts (A) and in serum (B) at the indicated times. Data are presented as the mean + SEM. n=3 mice. $*p \leq 0.05$ (1-way ANOVA with Dunnett's multiple comparison test).

ACKNOWLEDGEMENTS

The authors thank Cayetana Murillo, María D. Hernández-Fuentes, the staff at the CIB animal facility and CIB and UCM microscopy facilities for technical support; Nuria Forns and Ryan Steel for setting the conditions for the optomotor test and for synapse immunostaining; Noemi Alvarez Lindo for designing the diagrams; and José A. Esteban for supplying the anti-Glu2A antibody. This work was supported by grants from the Spanish MINECO (SAF2013-41059-R and SAF2016-75681-R to EJdlR, PI13-02098 to PdlV), the Instituto de Salud Carlos III and co-financed by the European Development Regional Fund ‘‘*A way to make Europe"/"Investing in your future*’’ (ERDF/ESF) (PI17/01601 to IL and PI18/01536 to CL), the Instituto de Salud Carlos III RETICS RD16/0019/0009 and the Madrid Regional Government B2017/BMD-3688 to IL. ASC is recipient of a UCM predoctoral fellowship (CT45/15).

AUTHOR CONTRIBUTION

ASC, AHP, CI and MM performed experimental procedures. CL carried out and analyzed the electron microscopy studies. PdlV designed the functional studies and analyzed the data. FB designed and generated the AAV vectors. EJdlR and CHS designed and supervised the biological experiments. EJdlR and CHS analyzed and discussed the results. ASC, CL, CI, IL, PdlV, FB, EJdlR and CHS contributed to the writing and editing of the manuscript. All authors read and approved the final manuscript.

CONFLICT OF INTEREST

The authors have no conflicts of interest to report.

THE PAPER EXPLAINED

Problem

Retinitis pigmentosa is a hereditary retinal neurodegenerative condition that accounts for the majority of cases of congenital blindness. It is considered a rare disease, with a worldwide incidence of 1 per 3500 people. Although gene therapy interventions are considered the definitive therapeutic strategy, their application is hindered by the wide range of genes and mutations implicated in RP. Therefore, there is an urgent social and medical need to develop effective treatments that are independent of the causative mutation.

Results

The insulin receptor is essential for the control of metabolism and glucose homeostasis. We show that the insulin receptor is predominantly expressed in the axons of retinal horizontal neurons. Moreover, the *rd10* mouse model of RP shows deficient insulin receptor signaling in horizontal neurons and aberrant synaptic contacts between rod photoreceptors and horizontal and bipolar cells. A gene therapy strategy to produce sustained systemic levels of proinsulin restored retinal insulin receptor signaling in *rd10* mice without affecting peripheral metabolism. Importantly, proinsulin treatment preserved photoreceptor synaptic connectivity and prolonged visual function.

Impact

This study underscores the role of insulin receptor signaling in retinal dystrophies. Our results support gene therapy as a feasible therapeutic strategy to induce sustained

proinsulin production. More importantly, they provide proof of concept of the therapeutic potential of proinsulin for the treatment of RP.

REFERENCE LIST

Abdeljalil J, Hamid M, Abdel-Mouttalib O, Stephane R, Raymond R, Johan A, Jose S, Pierre C, Serge P (2005) The optomotor response: a robust first-line visual screening method for mice. Vision Res 45: 1439-46

Agostinone J, Alarcon-Martinez L, Gamlin C, Yu WQ, Wong ROL, Di Polo A (2018) Insulin signalling promotes dendrite and synapse regeneration and restores circuit function after axonal injury. Brain 141: 1963-1980

Arnold SE, Arvanitakis Z, Macauley-Rambach SL, Koenig AM, Wang HY, Ahima RS, Craft S, Gandy S, Buettner C, Stoeckel LE, Holtzman DM, Nathan DM (2018) Brain insulin resistance in type 2 diabetes and Alzheimer disease: concepts and conundrums. Nat Rev Neurol 14: 168-181

Banks WA, Owen JB, Erickson MA (2012) Insulin in the brain: there and back again. Pharmacol Ther 136: 82-93

Belfiore A, Frasca F, Pandini G, Sciacca L, Vigneri R (2009) Insulin receptor isoforms and insulin receptor/insulin-like growth factor receptor hybrids in physiology and disease. Endocr Rev 30: 586-623

Belfiore A, Malaguarnera R, Vella V, Lawrence MC, Sciacca L, Frasca F, Morrione A, Vigneri R (2017) Insulin Receptor Isoforms in Physiology and Disease: An Updated View. Endocr Rev 38: 379-431

Bruning JC, Gautam D, Burks DJ, Gillette J, Schubert M, Orban PC, Klein R, Krone W, Muller-Wieland D, Kahn CR (2000) Role of brain insulin receptor in control of body weight and reproduction. Science 289: 2122-5

Chan SJ, Steiner DF (2000) Insulin Through the Ages: Phylogeny of a Growth Promoting and Metabolic Regulatory Hormone 1. American Zoologist, Volume 40, Issue 2, April 2000, Pages 213–222 40: 213-222

Chang B, Hawes NL, Pardue MT, German AM, Hurd RE, Davisson MT, Nusinowitz S, Rengarajan K, Boyd AP, Sidney SS, Phillips MJ, Stewart RE, Chaudhury R, Nickerson JM, Heckenlively JR, Boatright JH (2007) Two mouse retinal degenerations caused by missense mutations in the beta-subunit of rod cGMP phosphodiesterase gene. Vision Res 47: 624-33

Chapman CD, Schioth HB, Grillo CA, Benedict C (2018) Intranasal insulin in Alzheimer's disease: Food for thought. Neuropharmacology 136: 196-201

Chiu SL, Cline HT (2010) Insulin receptor signaling in the development of neuronal structure and function. Neural Dev 5: 7

Clarke DW, Mudd L, Boyd FT, Jr., Fields M, Raizada MK (1986) Insulin is released from rat brain neuronal cells in culture. J Neurochem 47: 831-6

Collaborators GBDN (2019) Global, regional, and national burden of neurological disorders, 1990-2016: a systematic analysis for the Global Burden of Disease Study 2016. Lancet Neurol 18: 459-480

Corpas R, Hernandez-Pinto AM, Porquet D, Hernandez-Sanchez C, Bosch F, Ortega-Aznar A, Comellas F, de la Rosa EJ, Sanfeliu C (2017) Proinsulin protects against age-related cognitive loss through anti-inflammatory convergent pathways. Neuropharmacology 123: 221-232

Corrochano S, Barhoum R, Boya P, Arroba AI, Rodriguez-Muela N, Gomez-Vicente V, Bosch F, de Pablo F, de la Villa P, de la Rosa EJ (2008) Attenuation of vision loss and delay in apoptosis of photoreceptors induced by proinsulin in a mouse model of retinitis pigmentosa. Invest Ophthalmol Vis Sci 49: 4188-94

Cuenca N, Fernandez-Sanchez L, Campello L, Maneu V, De la Villa P, Lax P, Pinilla I (2014) Cellular responses following retinal injuries and therapeutic approaches for neurodegenerative diseases. Prog Retin Eye Res 43: 17-75

de la Rosa EJ, Bondy CA, Hernandez-Sanchez C, Wu X, Zhou J, Lopez-Carranza A, Scavo LM, de Pablo F (1994) Insulin and insulin-like growth factor system components gene expression in the chicken retina from early neurogenesis until late development and their effect on neuroepithelial cells. Eur J Neurosci 6: 1801-10

de La Rosa EJ, Hernandez-Sanchez C (2018) CNS Targets for the Treatment of Retinal Dystrophies: A Win–Win Strategy. Therapies for retinal degeneration : targeting common processes. Royal Society of Chemistry,

Dixon-Salazar TJ, Fourgeaud L, Tyler CM, Poole JR, Park JJ, Boulanger LM (2014) MHC class I limits hippocampal synapse density by inhibiting neuronal insulin receptor signaling. J Neurosci 34: 11844-56

Feigenspan A, Babai N (2015) Functional properties of spontaneous excitatory currents and encoding of light/dark transitions in horizontal cells of the mouse retina. Eur J Neurosci 42: 2615-32

Fernandez-Sanchez L, Lax P, Isiegas C, Ayuso E, Ruiz JM, de la Villa P, Bosch F, de la Rosa EJ, Cuenca N (2012) Proinsulin slows retinal degeneration and vision loss in the P23H rat model of retinitis pigmentosa. Hum Gene Ther 23: 1290-300

Gosbell AD, Favilla I, Baxter KM, Jablonski P (2000) Insulin receptor and insulin receptor substrate-I in rat retinae. Clin Exp Ophthalmol 28: 212-5

Gralle M (2017) The neuronal insulin receptor in its environment. J Neurochem 140: 359-367

Havrankova J, Roth J, Brownstein M (1978) Insulin receptors are widely distributed in the central nervous system of the rat. Nature 272: 827-9

Hernandez-Sanchez C, Lopez-Carranza A, Alarcon C, de La Rosa EJ, de Pablo F (1995) Autocrine/paracrine role of insulin-related growth factors in neurogenesis: local expression and effects on cell proliferation and differentiation in retina. Proc Natl Acad Sci U S A 92: 9834-8

Hernandez-Sanchez C, Mansilla A, de la Rosa EJ, de Pablo F (2006) Proinsulin in development: New roles for an ancient prohormone. Diabetologia 49: 1142-50

Hernandez-Sanchez C, Mansilla A, de Pablo F, Zardoya R (2008) Evolution of the insulin receptor family and receptor isoform expression in vertebrates. Mol Biol Evol 25: 1043-53

Holscher C (2020) Brain insulin resistance: role in neurodegenerative disease and potential for targeting. Expert Opin Investig Drugs 29: 333-348

Hori K, Yasuda H, Konno D, Maruoka H, Tsumoto T, Sobue K (2005) NMDA receptor-dependent synaptic translocation of insulin receptor substrate p53 via protein kinase C signaling. J Neurosci 25: 2670-81

Isiegas C, Marinich-Madzarevich JA, Marchena M, Ruiz JM, Cano MJ, de la Villa P, Hernandez-Sanchez C, de la Rosa EJ, de Pablo F (2016) Intravitreal Injection of Proinsulin-Loaded Microspheres Delays Photoreceptor Cell Death and Vision Loss in the rd10 Mouse Model of Retinitis Pigmentosa. Invest Ophthalmol Vis Sci 57: 3610-8

Jones BW, Kondo M, Terasaki H, Lin Y, McCall M, Marc RE (2012) Retinal remodeling. Jpn J Ophthalmol 56: 289-306

Kolb H (1970) Organization of the outer plexiform layer of the primate retina: electron microscopy of Golgi-impregnated cells. Philos Trans R Soc Lond B Biol Sci 258: 261-83

Kolb H (1974) The connections between horizontal cells and photoreceptors in the retina of the cat: electron microscopy of Golgi preparations. J Comp Neurol 155: 1-14

Lee CC, Huang CC, Hsu KS (2011) Insulin promotes dendritic spine and synapse formation by the PI3K/Akt/mTOR and Rac1 signaling pathways. Neuropharmacology 61: 867-79

Lewis GP, Linberg KA, Fisher SK (1998) Neurite outgrowth from bipolar and horizontal cells after experimental retinal detachment. Invest Ophthalmol Vis Sci 39: 424-34

Malaguarnera R, Sacco A, Voci C, Pandini G, Vigneri R, Belfiore A (2012) Proinsulin binds with high affinity the insulin receptor isoform A and predominantly activates the mitogenic pathway. Endocrinology 153: 2152-63

Marks JL, Porte D, Jr., Stahl WL, Baskin DG (1990) Localization of insulin receptor mRNA in rat brain by in situ hybridization. Endocrinology 127: 3234-6

Moloney AM, Griffin RJ, Timmons S, O'Connor R, Ravid R, O'Neill C (2010) Defects in IGF-1 receptor, insulin receptor and IRS-1/2 in Alzheimer's disease indicate possible resistance to IGF-1 and insulin signalling. Neurobiol Aging 31: 224-43

Moroo I, Yamada T, Makino H, Tooyama I, McGeer PL, McGeer EG, Hirayama K (1994) Loss of insulin receptor immunoreactivity from the substantia nigra pars compacta neurons in Parkinson's disease. Acta Neuropathol 87: 343-8

Peichl L, Gonzalez-Soriano J (1993) Unexpected presence of neurofilaments in axon-bearing horizontal cells of the mammalian retina. J Neurosci 13: 4091-100

Peichl L, Gonzalez-Soriano J (1994) Morphological types of horizontal cell in rodent retinae: a comparison of rat, mouse, gerbil, and guinea pig. Vis Neurosci 11: 501-17

Pfeiffer RL, Marc RE, Jones BW (2020) Persistent remodeling and neurodegeneration in late-stage retinal degeneration. Prog Retin Eye Res 74: 100771

Prusky GT, Alam NM, Beekman S, Douglas RM (2004) Rapid quantification of adult and developing mouse spatial vision using a virtual optomotor system. Invest Ophthalmol Vis Sci 45: 4611-6

Punzo C, Kornacker K, Cepko CL (2009) Stimulation of the insulin/mTOR pathway delays cone death in a mouse model of retinitis pigmentosa. Nat Neurosci 12: 44-52

Rajala A, Tanito M, Le YZ, Kahn CR, Rajala RV (2008) Loss of neuroprotective survival signal in mice lacking insulin receptor gene in rod photoreceptor cells. J Biol Chem 283: 19781-92

Rajala RV, Wiskur B, Tanito M, Callegan M, Rajala A (2009) Diabetes reduces autophosphorylation of retinal insulin receptor and increases protein-tyrosine phosphatase-1B activity. Invest Ophthalmol Vis Sci 50: 1033-40

Rivera EJ, Goldin A, Fulmer N, Tavares R, Wands JR, de la Monte SM (2005) Insulin and insulin-like growth factor expression and function deteriorate with progression of Alzheimer's disease: link to brain reductions in acetylcholine. J Alzheimers Dis 8: 247-68

Rodrigues M, Waldbillig RJ, Rajagopalan S, Hackett J, LeRoith D, Chader GJ (1988) Retinal insulin receptors: localization using a polyclonal anti-insulin receptor antibody. Brain Res 443: 389-94

Russell S, Bennett J, Wellman JA, Chung DC, Yu ZF, Tillman A, Wittes J, Pappas J, Elci O, McCague S, Cross D, Marshall KA, Walshire J, Kehoe TL, Reichert H, Davis M, Raffini L, George LA, Hudson FP, Dingfield L et al. (2017) Efficacy and safety of voretigene neparvovec (AAV2-hRPE65v2) in patients with RPE65-mediated inherited retinal dystrophy: a randomised, controlled, open-label, phase 3 trial. Lancet 390: 849-860

Sanchez-Cruz A, Villarejo-Zori B, Marchena M, Zaldivar-Diez J, Palomo V, Gil C, Lizasoain I, de la Villa P, Martinez A, de la Rosa EJ, Hernandez-Sanchez C (2018) Modulation of GSK-3 provides cellular and functional neuroprotection in the rd10 mouse model of retinitis pigmentosa. Mol Neurodegener 13: 19

Steen E, Terry BM, Rivera EJ, Cannon JL, Neely TR, Tavares R, Xu XJ, Wands JR, de la Monte SM (2005) Impaired insulin and insulin-like growth factor expression and signaling mechanisms in Alzheimer's disease--is this type 3 diabetes? J Alzheimers Dis 7: 63-80

Strettoi E, Pignatelli V, Rossi C, Porciatti V, Falsini B (2003) Remodeling of second-order neurons in the retina of rd/rd mutant mice. Vision Res 43: 867-77

Takahashi M, Yamada T, Tooyama I, Moroo I, Kimura H, Yamamoto T, Okada H (1996) Insulin receptor mRNA in the substantia nigra in Parkinson's disease. Neurosci Lett 204: 201-4

Talbot K, Wang HY, Kazi H, Han LY, Bakshi KP, Stucky A, Fuino RL, Kawaguchi KR, Samoyedny AJ, Wilson RS, Arvanitakis Z, Schneider JA, Wolf BA, Bennett DA, Trojanowski JQ, Arnold SE (2012) Demonstrated brain insulin resistance in Alzheimer's disease patients is associated with IGF-1 resistance, IRS-1 dysregulation, and cognitive decline. J Clin Invest 122: 1316-38

Timmons S, Coakley MF, Moloney AM, C ON (2009) Akt signal transduction dysfunction in Parkinson's disease. Neurosci Lett 467: 30-5

Unger J, McNeill TH, Moxley RT, 3rd, White M, Moss A, Livingston JN (1989) Distribution of insulin receptor-like immunoreactivity in the rat forebrain. Neuroscience 31: 143-57

Valenciano AI, Corrochano S, de Pablo F, de la Villa P, de la Rosa EJ (2006) Proinsulin/insulin is synthesized locally and prevents caspase- and cathepsin-mediated cell death in the embryonic mouse retina. J Neurochem 99: 524-36

Wang T, Pahlberg J, Cafaro J, Frederiksen R, Cooper AJ, Sampath AP, Field GD, Chen J (2019) Activation of Rod Input in a Model of Retinal Degeneration Reverses Retinal Remodeling and Induces Formation of Functional Synapses and Recovery of Visual Signaling in the Adult Retina. J Neurosci 39: 6798-6810

Zhao L, Zabel MK, Wang X, Ma W, Shah P, Fariss RN, Qian H, Parkhurst CN, Gan WB, Wong WT (2015) Microglial phagocytosis of living photoreceptors contributes to inherited retinal degeneration. EMBO Mol Med 7: 1179-97

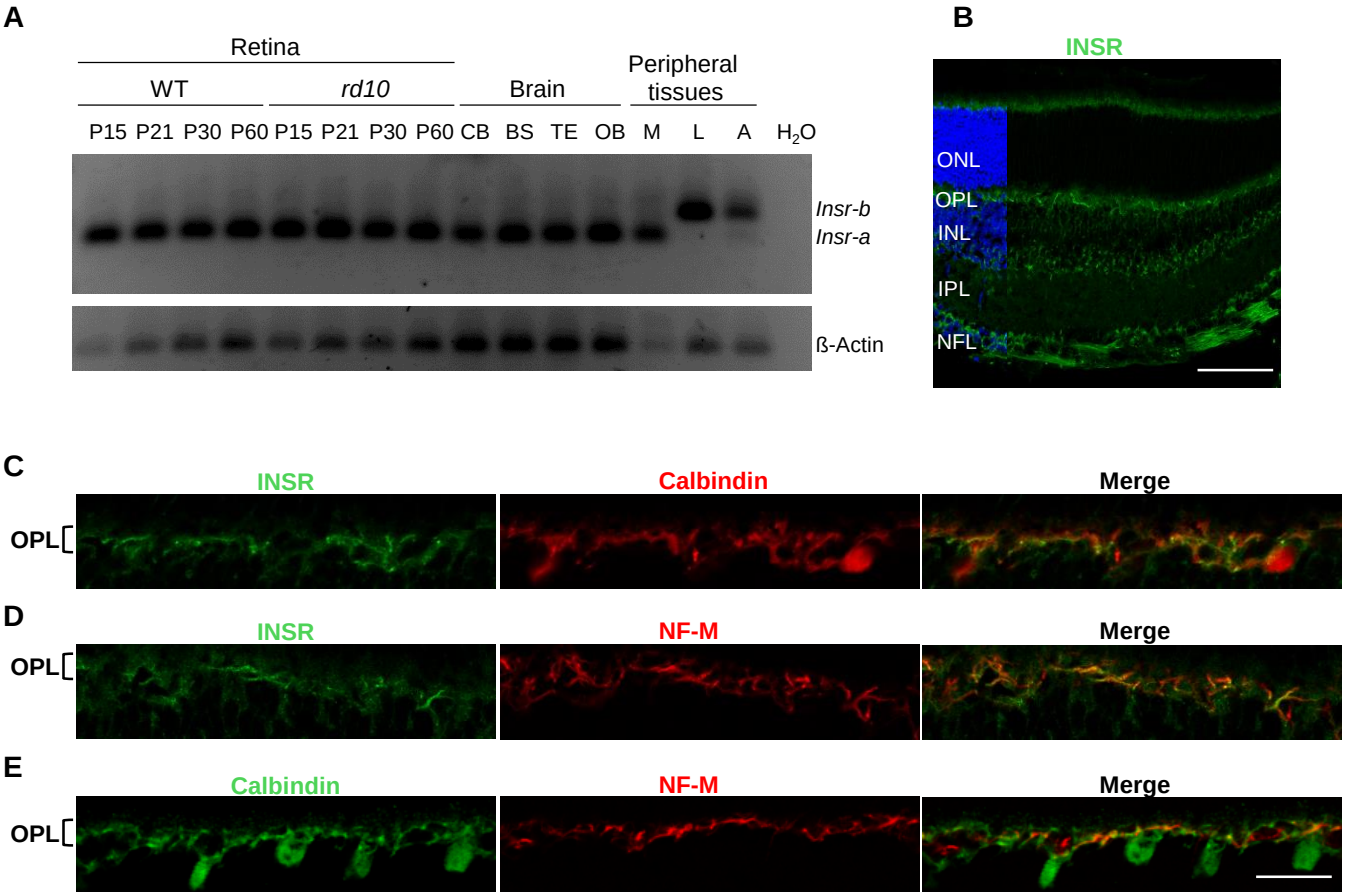
A
Retina
WT
rd10
Brain
Peripheral tissues
P15 P21 P30 P60 P15 P21 P30 P60 CB BS TE OB M L A H2O
Insr-b
Insr-a
ß-Actin
B
INSR
ONL
OPL
INL
IPL
NFL
C
INSR
Calbindin
Merge
OPL
D
INSR
NF-M
Merge
OPL
E
Calbindin
NF-M
Merge
OPL

Figure 1

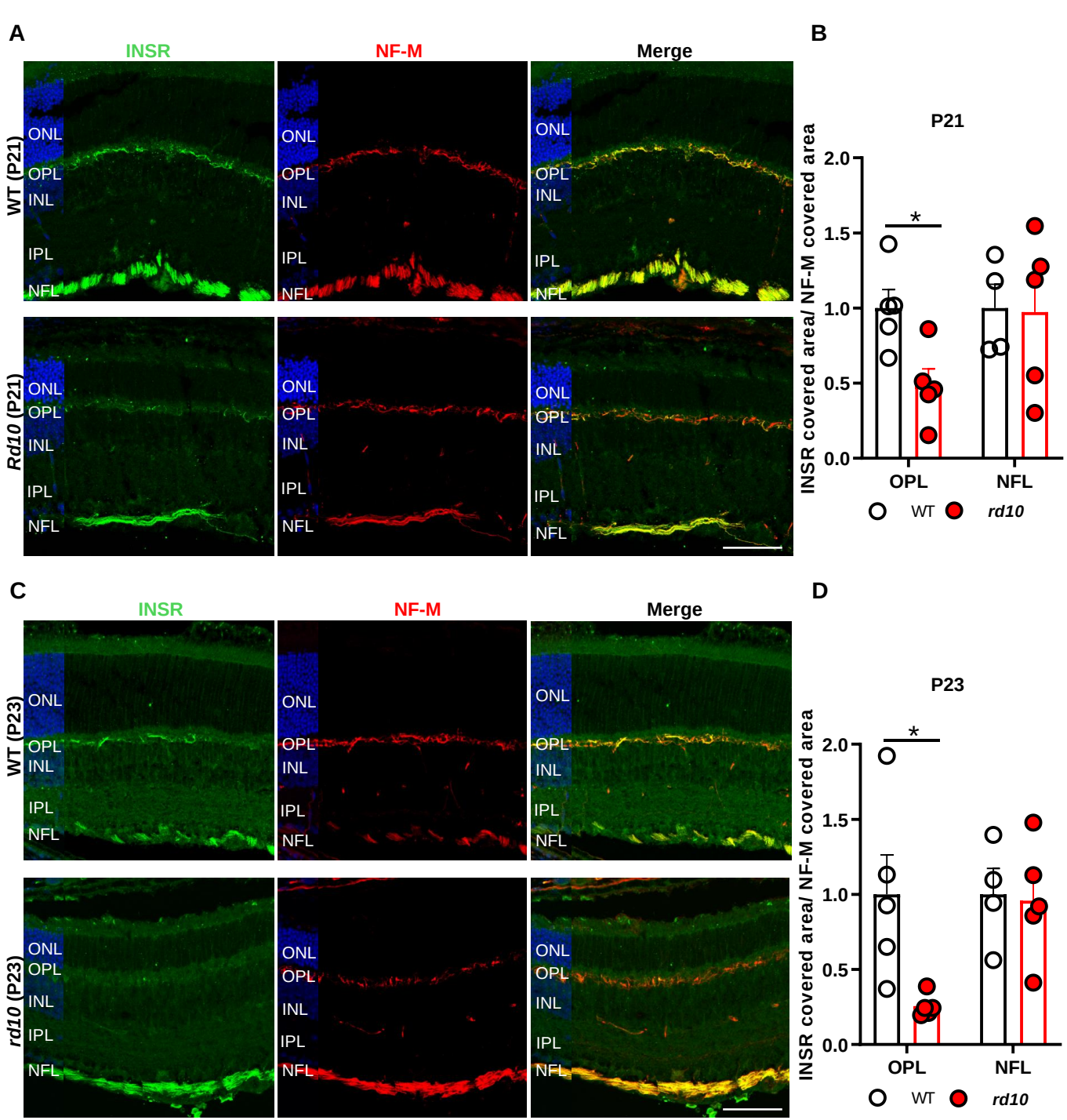
A
INSR
NF-M
Merge
WT (P21)
Rd10 (P21)
ONL
OPL
INL
IPL
NFL
B
P21
INSR covered area/ NF-M covered area
2.0
1.5
1.0
0.5
0.0
*
OPL
NFL
WT
rd10
C
INSR
NF-M
Merge
WT (P23)
rd10 (P23)
D
P23
INSR covered area/ NF-M covered area
2.0
1.5
1.0
0.5
0.0
*
OPL
NFL
WT
rd10

Figure 2

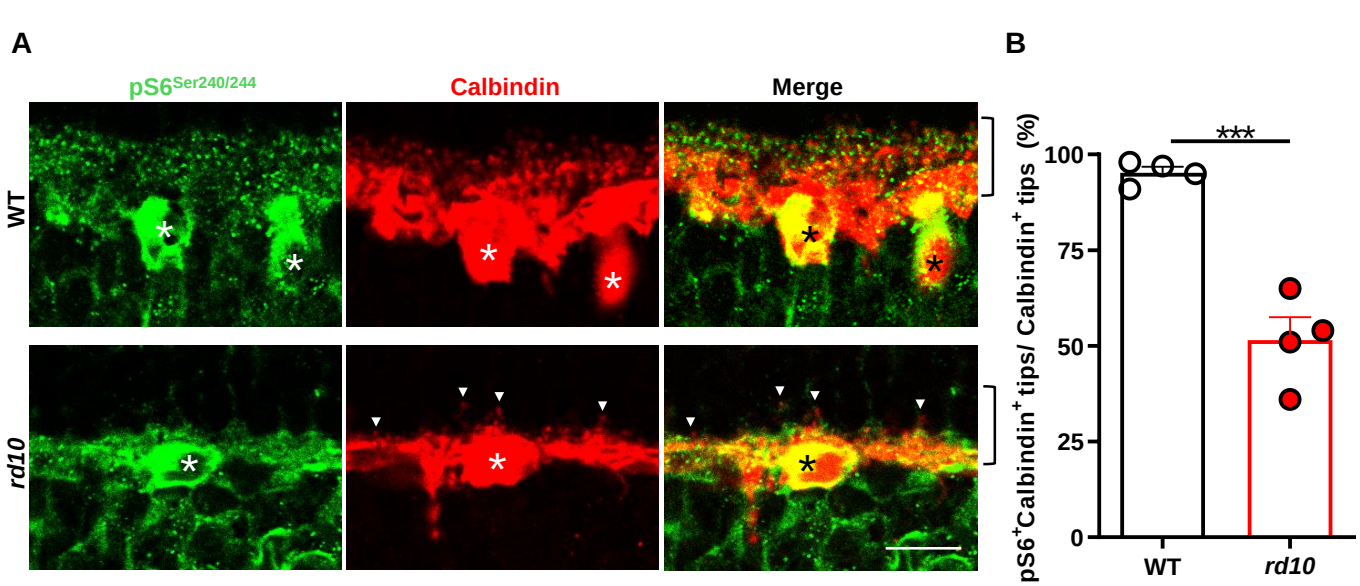
A
pS6Ser240/244
Calbindin
Merge
WT
rd10
B
***
pS6+Calbindin+ tips/ Calbindin+ tips (%)
100
75
50
25
0
WT
rd10

Figure 3

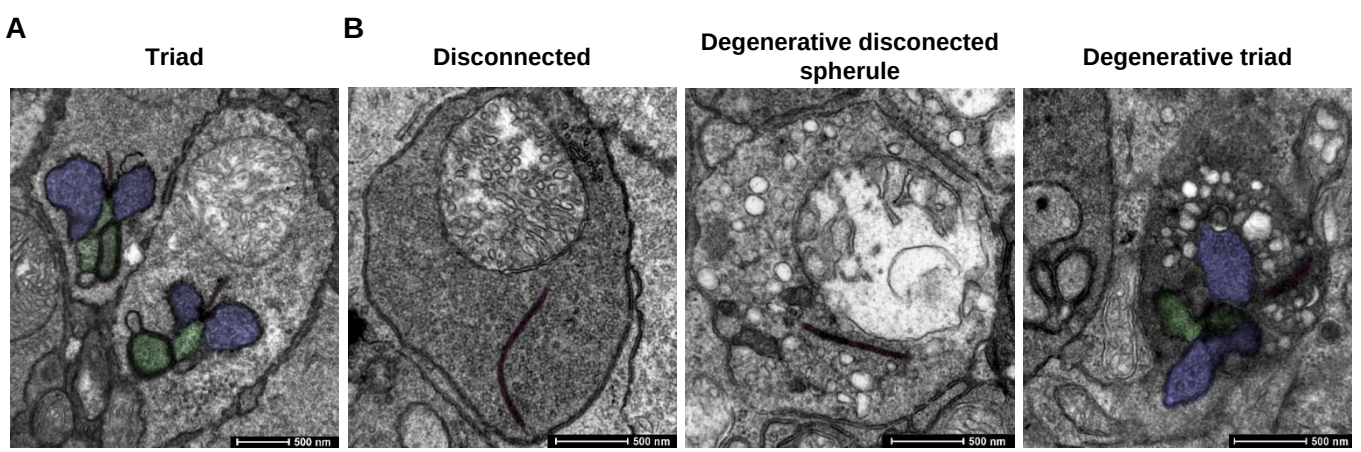
A
Triad
B
Disconnected
Degenerative disconected spherule
Degenerative triad
500 nm
500 nm
500 nm
500 nm

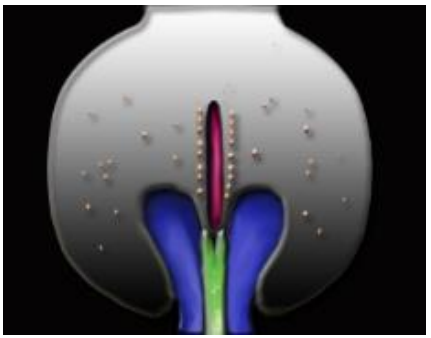
C

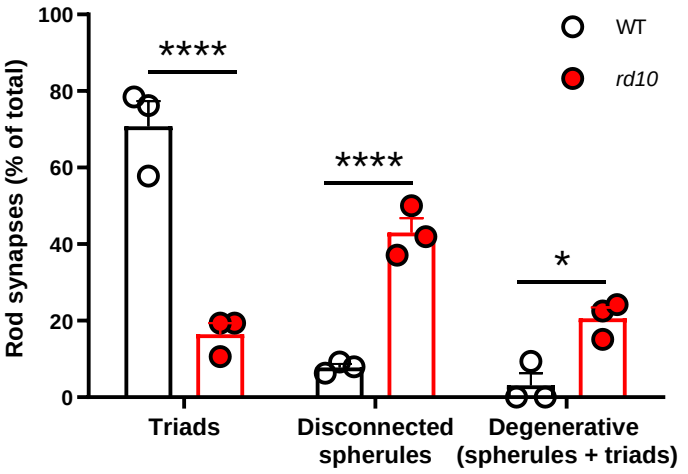
D
Rod synapses (% of total)
100
80
60
40
20
0
****
****
*
WT
rd10
Triads
Disconnected spherules
Degenerative (spherules + triads)

Figure 4

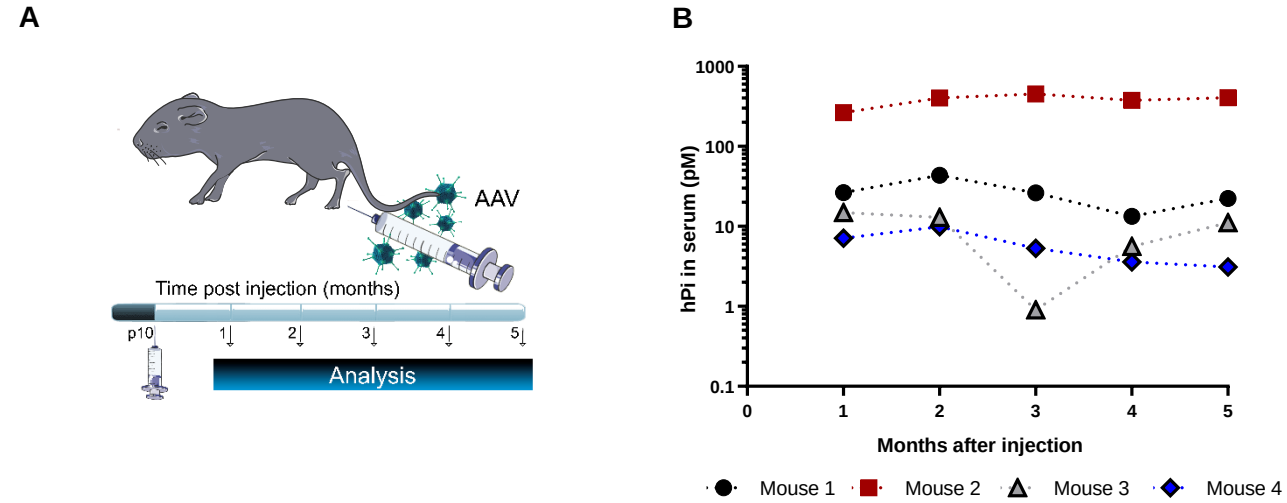
A
AAV
Time post injection (months)
p10
1
2
3
4
5
Analysis
B
hPi in serum (pM)
1000
100
10
1
0.1
0
1
2
3
4
5
Months after injection
Mouse 1
Mouse 2
Mouse 3
Mouse 4
C
Glucose levels in blood (mg/dL)
150
100
50
0
AAV-null
AAV-hPi
2
3
4
5
Months after injection
D
Corporal weight (g)
30
20
10
0
AAV-null
AAV-hPi
2
3
4
5
Months after injection

Figure 5

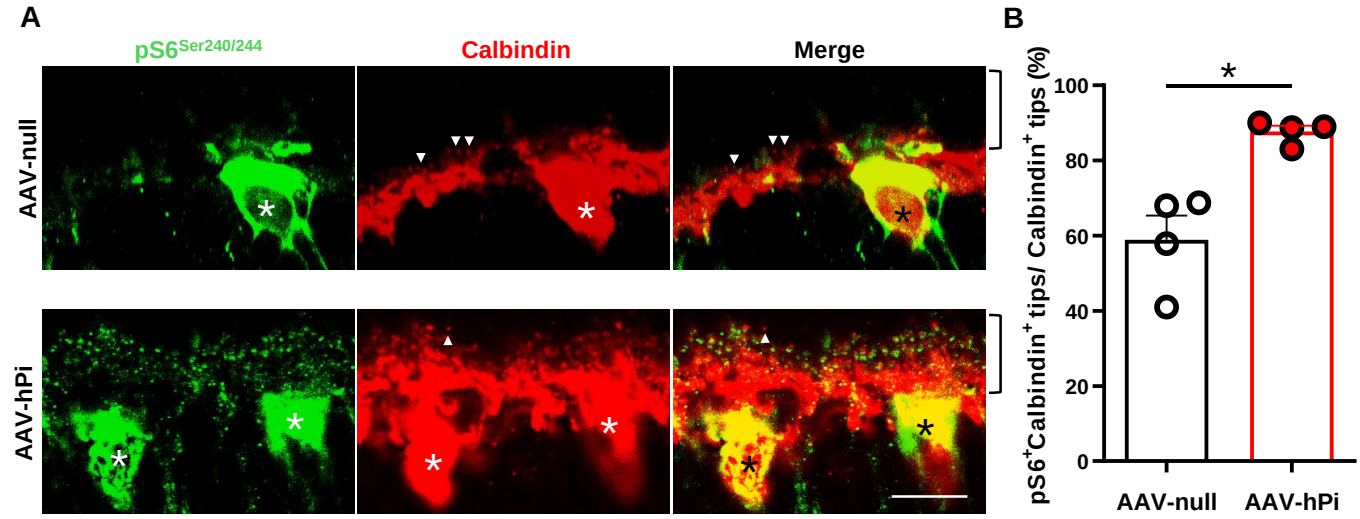
A
pS6Ser240/244
Calbindin
Merge
AAV-null
AAV-hPi
B
pS6+Calbindin+ tips/ Calbindin+ tips (%)
100
80
60
40
20
0
*
AAV-null
AAV-hPi

Figure 6

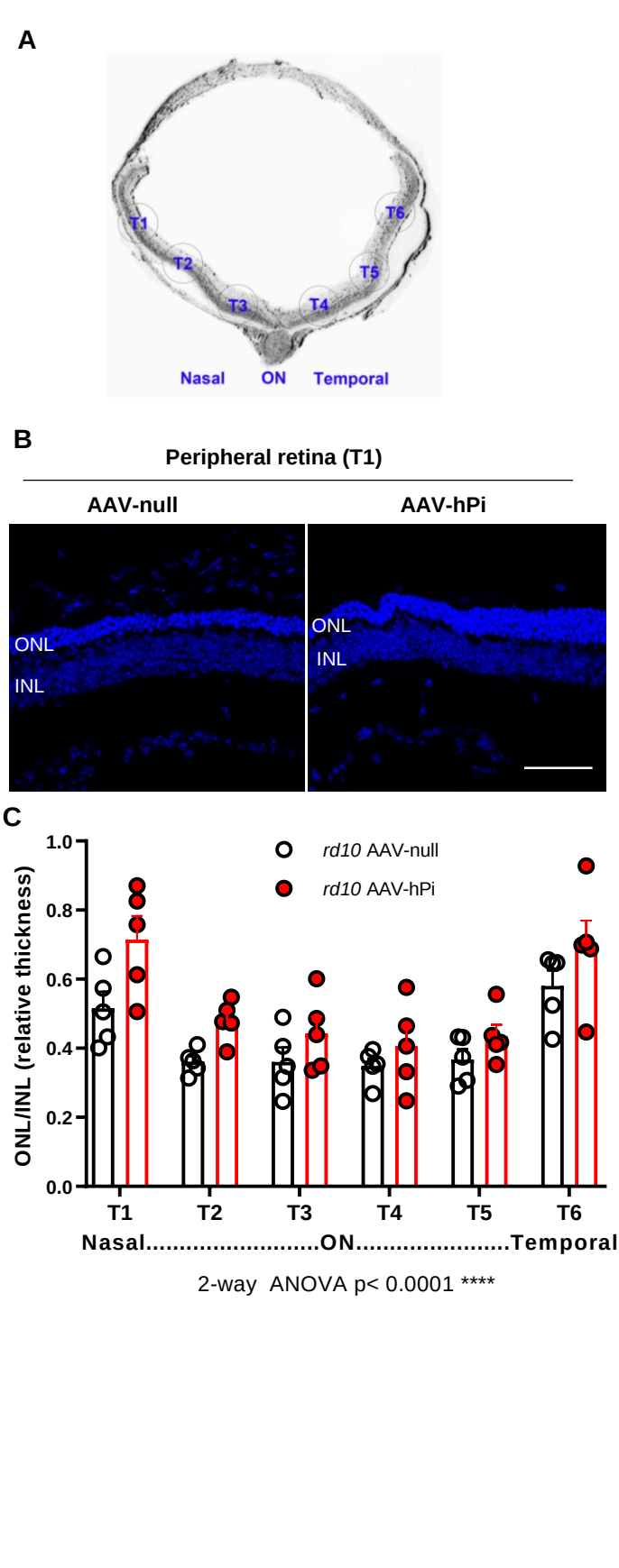
A
T1
T2
T3
T4
T5
T6
Nasal
ON
Temporal
B
Peripheral retina (T1)
AAV-null
AAV-hPi
ONL
INL
ONL
INL
C
rd10 AAV-null
rd10 AAV-hPi
ONL/INL (relative thickness)
1.0
0.8
0.6
0.4
0.2
0.0
T1
T2
T3
T4
T5
T6
Nasal.....ON.....Temporal
2-way ANOVA p< 0.0001 ****

Figure 7

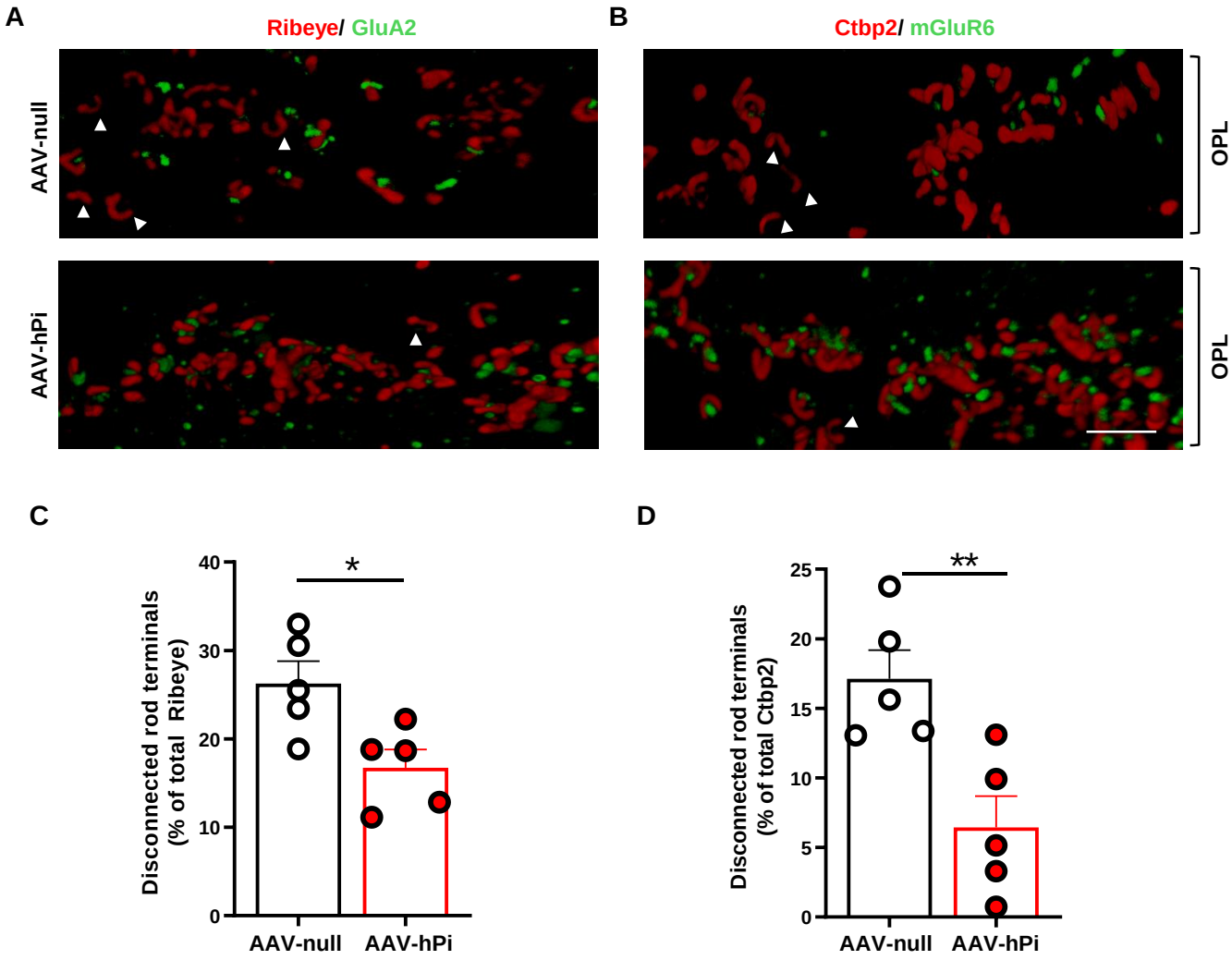
A
Ribeye/ GluA2
AAV-null
AAV-hPi
B
Ctbp2/ mGluR6
OPL
OPL
C
Disconnected rod terminals
(% of total Ribeye)
40
30
20
10
0
*
AAV-null
AAV-hPi
D
Disconnected rod terminals
(% of total Ctbp2)
25
20
15
10
5
0
**
AAV-null
AAV-hPi

Figure 8

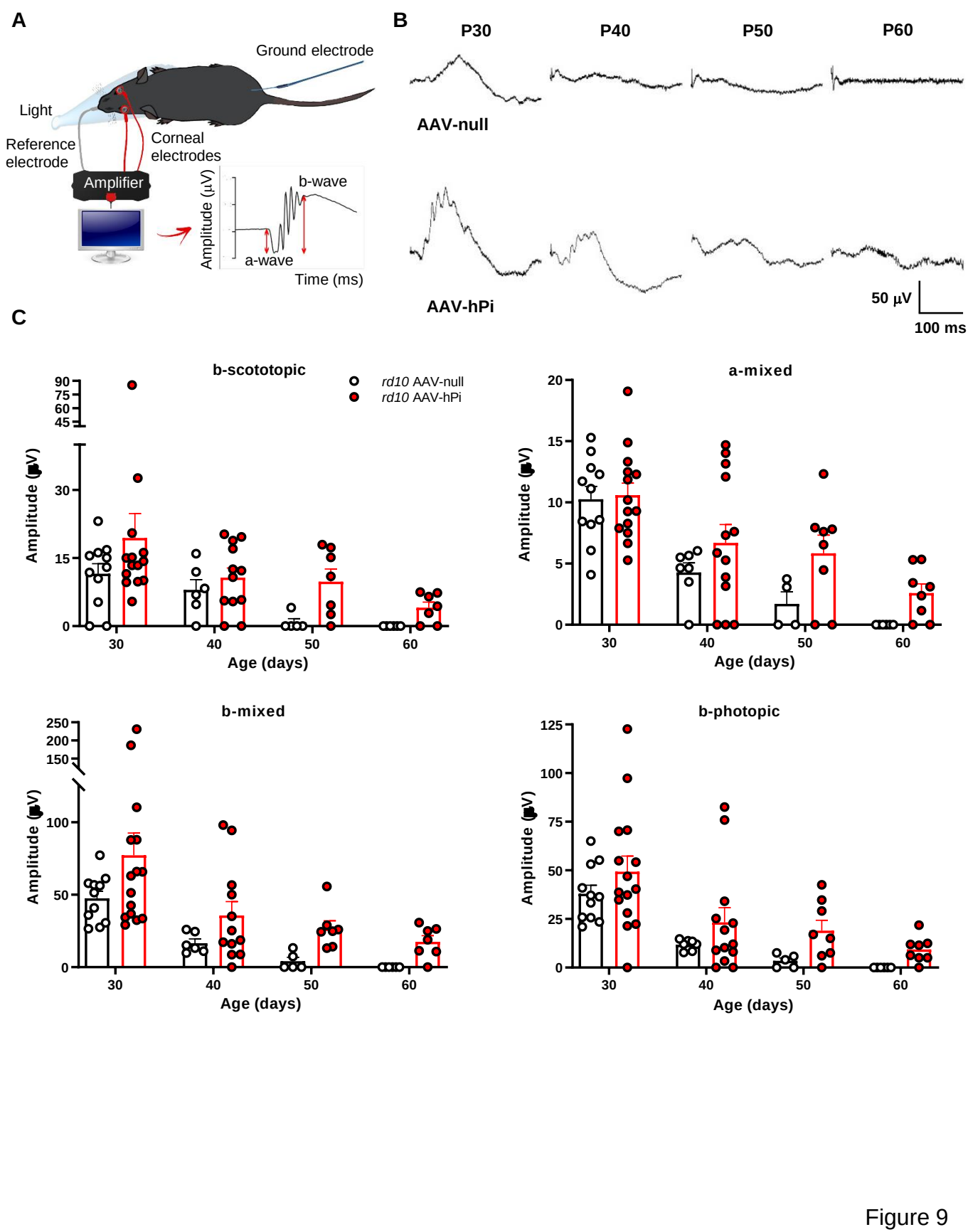
A
Ground electrode
Light
Reference electrode
Corneal electrodes
Amplifier
Amplitude (μV)
b-wave
a-wave
Time (ms)
B
P30
P40
P50
P60
AAV-null
AAV-hPi
50 μV
100 ms
C
b-scototopic
rd10 AAV-null
rd10 AAV-hPi
Amplitude (μV)
Age (days)
a-mixed
b-mixed
b-photopic

Figure 9

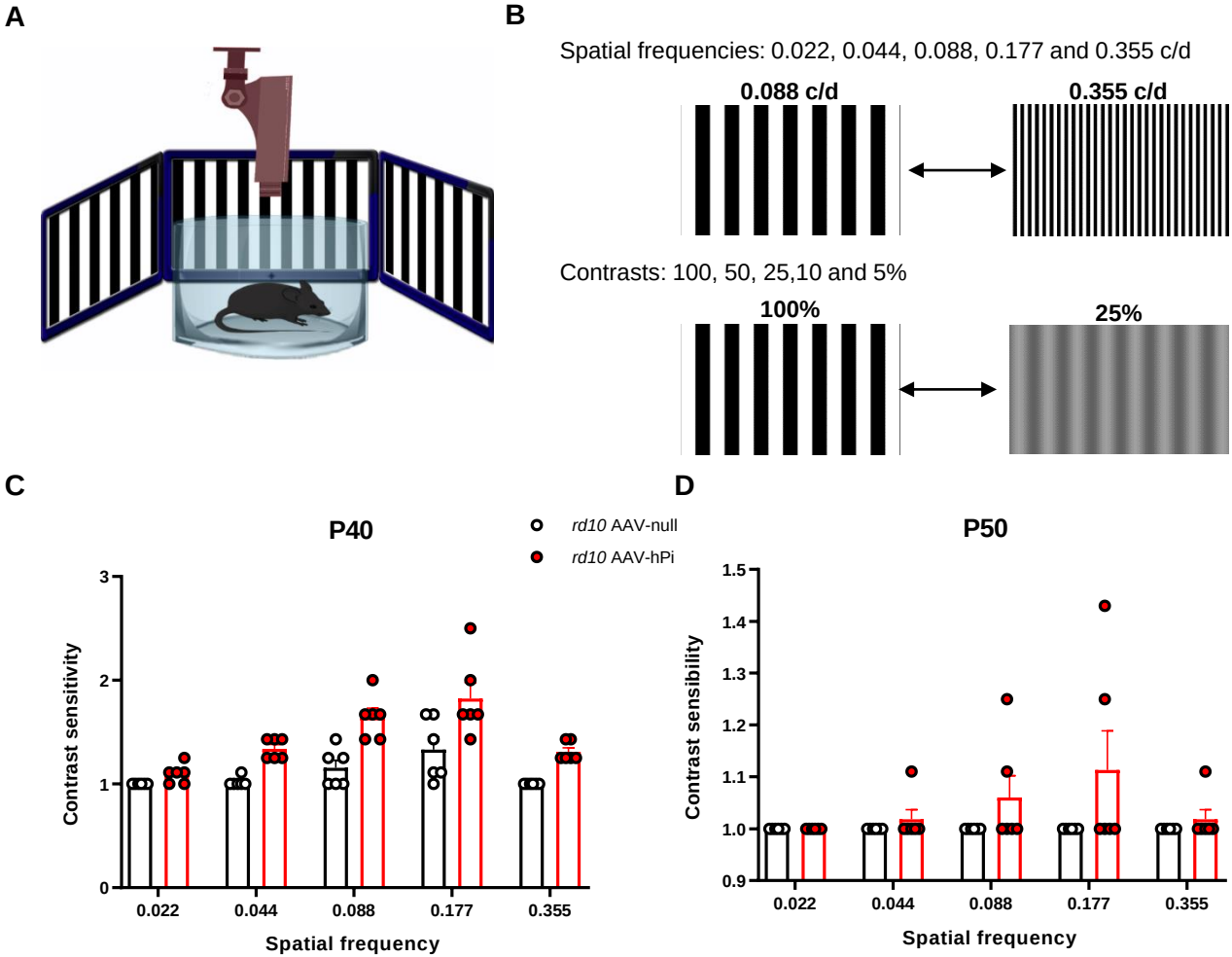
A
B
Spatial frequencies: 0.022, 0.044, 0.088, 0.177 and 0.355 c/d
0.088 c/d
0.355 c/d
Contrasts: 100, 50, 25,10 and 5%
100%
25%
C
P40
rd10 AAV-null
rd10 AAV-hPi
Contrast sensitivity
Spatial frequency
0.022
0.044
0.088
0.177
0.355
D
P50
Contrast sensibility
Spatial frequency

Figure 10

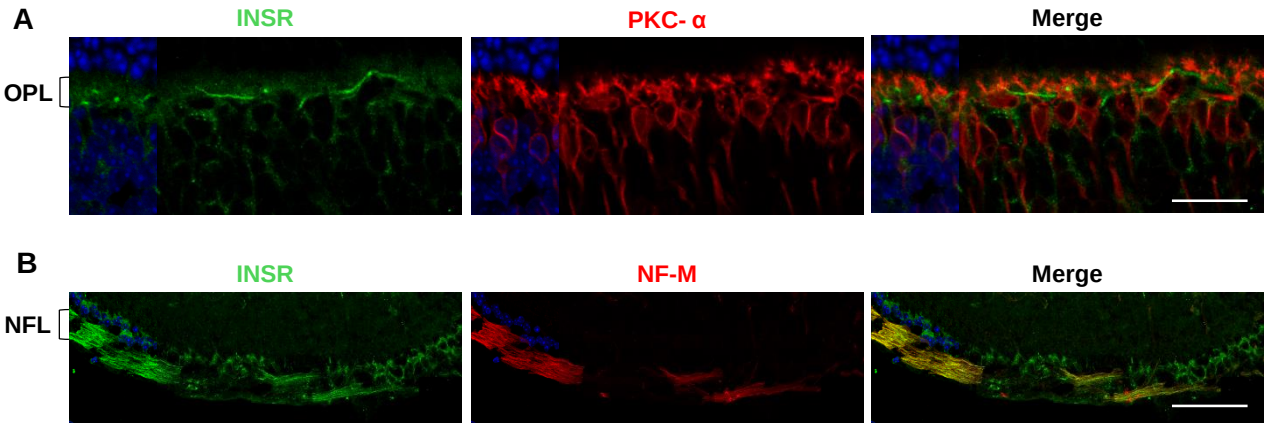

Suppl Fig. 1

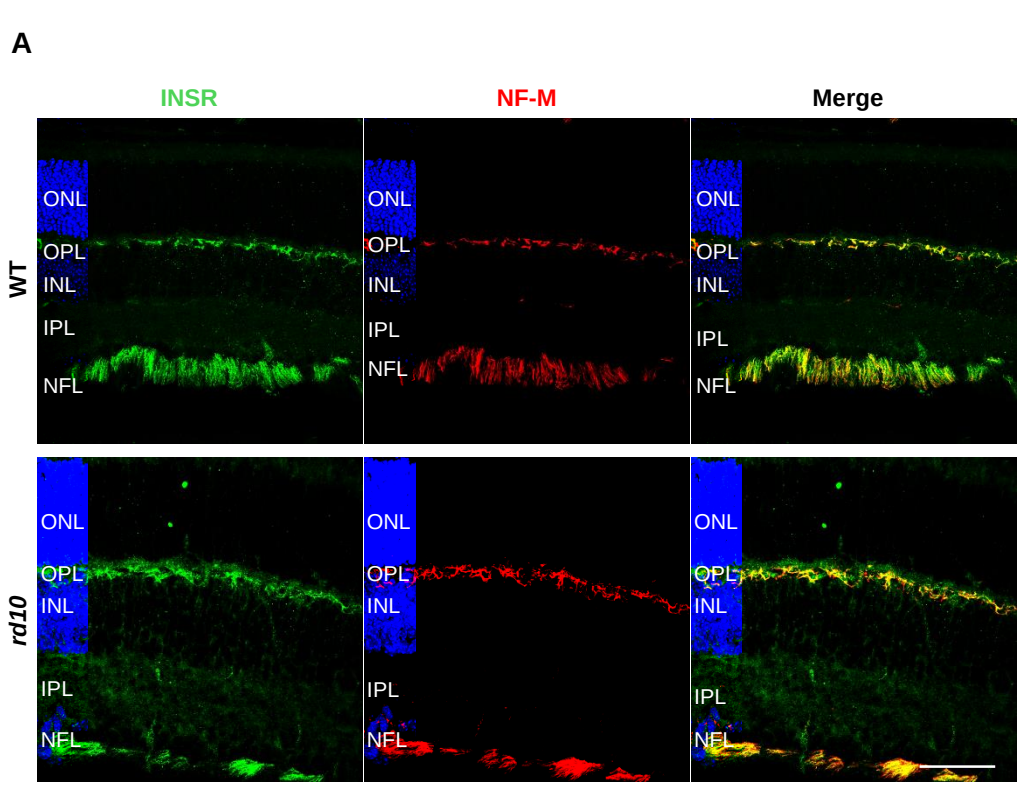
A
INSR
NF-M
Merge
WT
rd10
ONL
OPL
INL
IPL
NFL

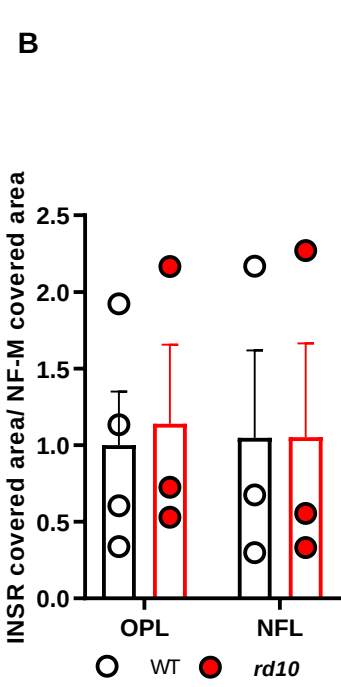
B
INSR covered area/ NF-M covered area
2.5
2.0
1.5
1.0
0.5
0.0
OPL
NFL
WT
rd10

Suppl Fig 2

A

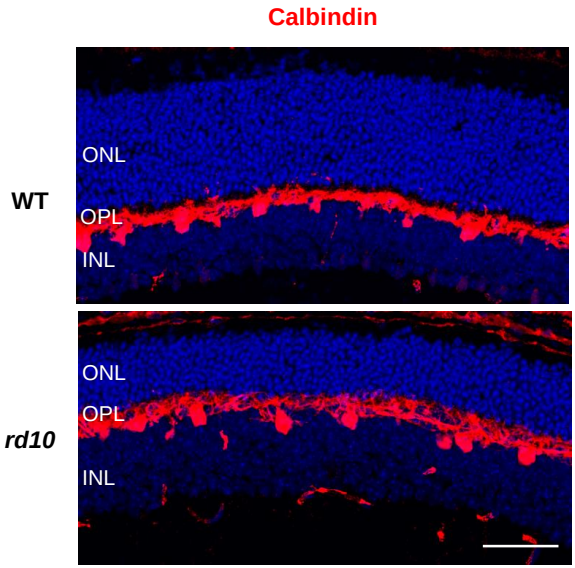

B

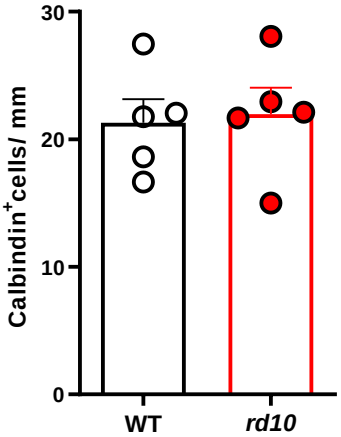

Suppl Fig. 3

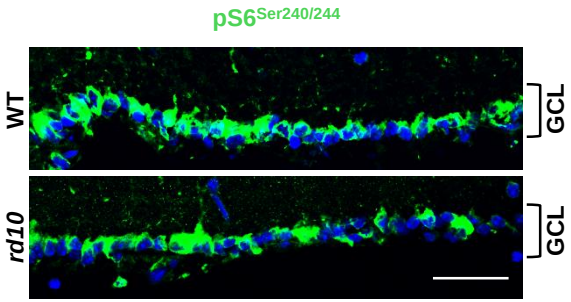

Suppl Fig. 4

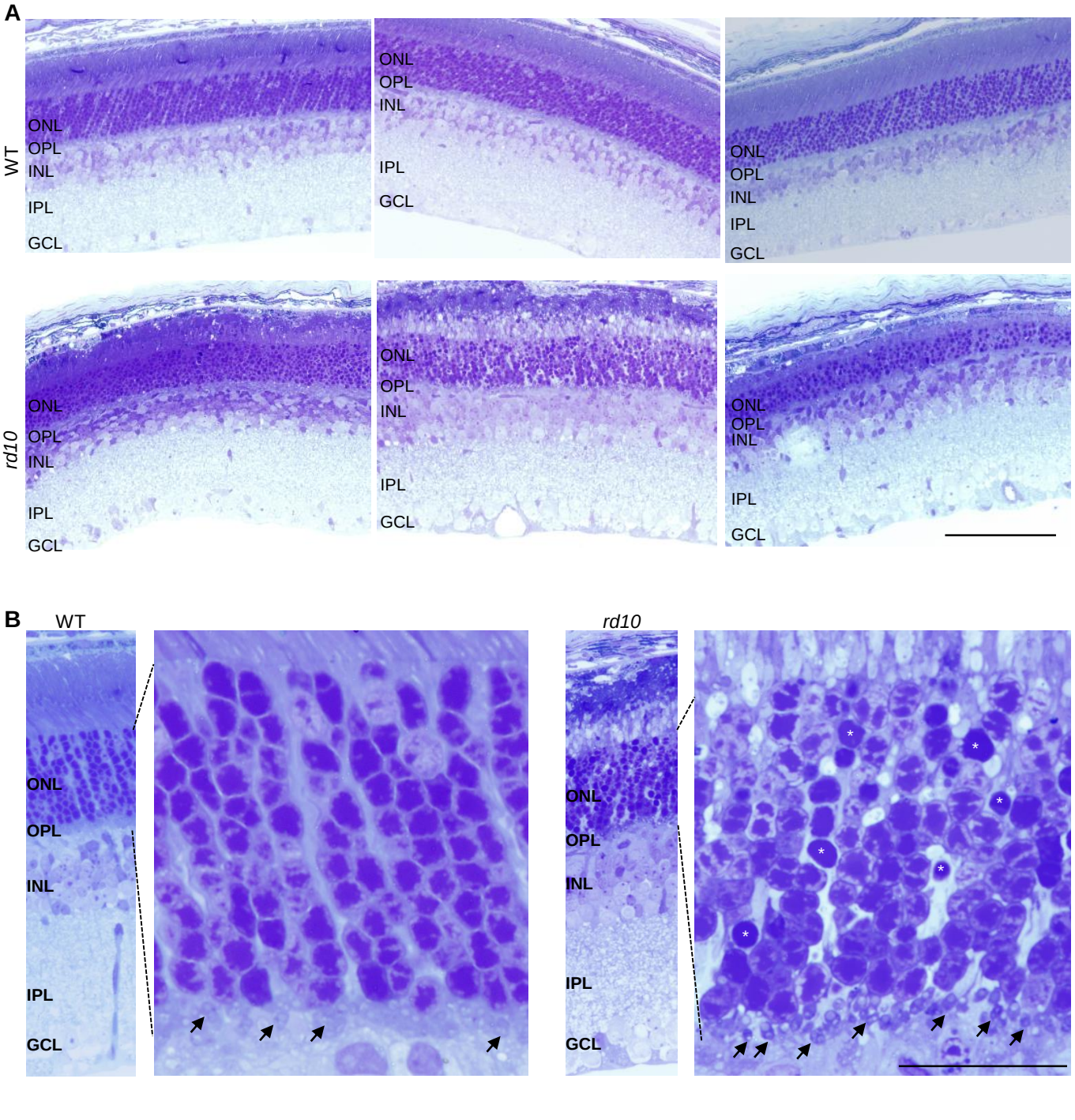

Suppl Figure 5

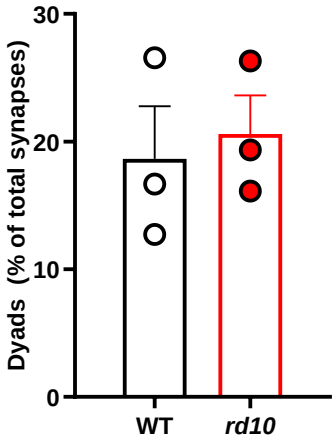

Suppl Fig. 6

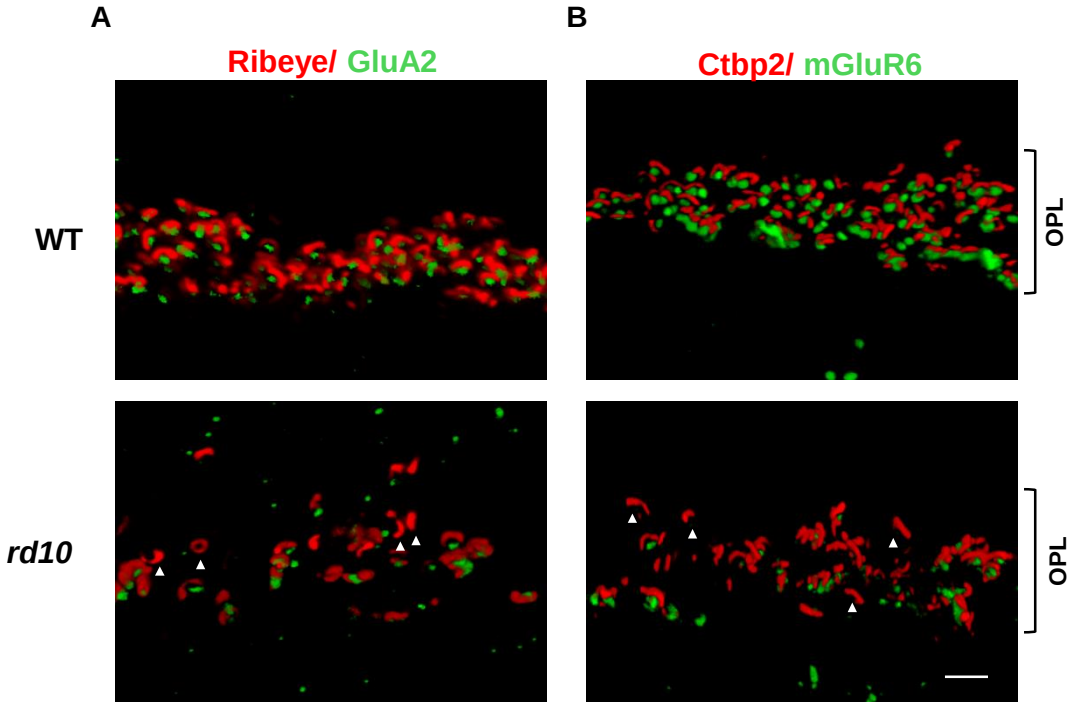

Suppl Fig. 7

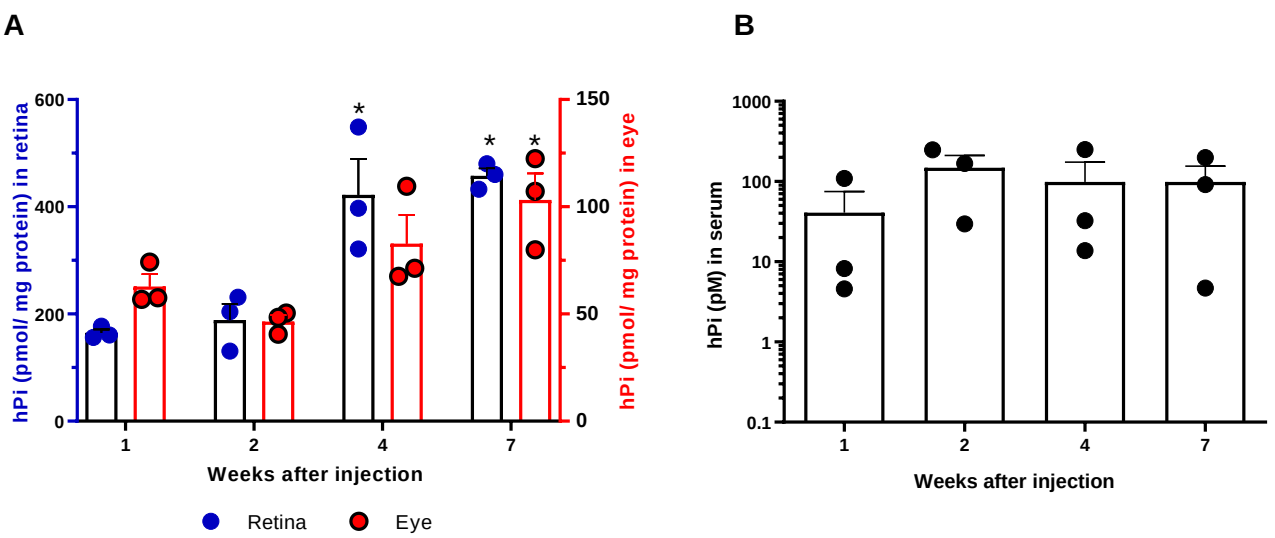
A
B
hPi (pmol/ mg protein) in retina
hPi (pmol/ mg protein) in eye
600
400
200
0
150
100
50
0
1
2
4
7
Weeks after injection
Retina
Eye
*
*
*
hPi (pM) in serum
1000
100
10
1
0.1
1
2
4
7
Weeks after injection

Suppl Fig. 8

Sánchez-Cruz et al. Molecular Neurodegeneration (2018) 13:19
https://doi.org/10.1186/s13024-018-0251-y

Molecular Neurodegeneration

RESEARCH ARTICLE Open Access

Modulation of GSK-3 provides cellular and functional neuroprotection in the *rd10* mouse model of retinitis pigmentosa

Alonso Sánchez-Cruz[1,2], Beatriz Villarejo-Zori[1], Miguel Marchena[1], Josefa Zaldivar-Díez[1], Valle Palomo[1], Carmen Gil[1], Ignacio Lizasoain[2], Pedro de la Villa[3], Ana Martínez[1], Enrique J. de la Rosa[1†] and Catalina Hernández-Sánchez[1*†]

Abstract

Background: Retinitis pigmentosa (RP) is a group of hereditary retinal neurodegenerative conditions characterized by primary dysfunction and death of photoreceptor cells, resulting in visual loss and, eventually, blindness. To date, no effective therapies have been transferred to clinic. Given the diverse genetic etiology of RP, targeting common cellular and molecular retinal alterations has emerged as a potential therapeutic strategy.

Methods: Using the *Pde6b*$^{rd10/rd10}$ mouse model of RP, we investigated the effects of daily intraperitoneal administration of VP3.15, a small-molecule heterocyclic GSK-3 inhibitor. Gene expression was analyzed by quantitative PCR and protein expression and phosphorylation by Western blot. Photoreceptor preservation was evaluated by histological analysis and visual function was assessed by electroretinography.

Results: In *rd10* retinas, increased expression of pro-inflammatory markers and reactive gliosis coincided with the early stages of retinal degeneration. Compared with wild-type controls, GSK-3β expression (mRNA and protein) remained unchanged during the retinal degeneration period. However, levels of GSK-3β^{Ser9} and its regulator Akt^{Ser473} were increased in *rd10* versus wild-type retinas. In vivo administration of VP3.15 reduced photoreceptor cell loss and preserved visual function. This neuroprotective effect was accompanied by a decrease in the expression of neuroinflammatory markers.

Conclusions: These results provide proof of concept of the therapeutic potential of VP3.15 for the treatment of retinal neurodegenerative conditions in general, and RP in particular.

Keywords: GSK-3, Retina, Retinitis pigmentosa, *rd10*, Neurodegeneration, Therapy

Background

Inherited retinal dystrophies, which include retinitis pigmentosa (RP), are a group of genetic diseases caused by mutations in over 300 genes and loci (http://www.sph.uth.tmc.edu/Retnet/disease.htm). RP is a retinal neurodegenerative condition characterized by primary dysfunction and death of photoreceptor cells, resulting in vision loss and, ultimately, blindness [1]. Although several experimental therapies have advanced to clinical trials (https://clinicaltrials.gov/ct2/results?term=retinitis+pigmentosa&Search=Search), neither approved treatments nor preventive therapies for RP are currently available. Its status as a rare disease and its diverse genetic etiology emphasize the importance of identifying shared pathological mechanisms independent of the causative mutation. Targeting common cellular and molecular retinal responses to mutations could benefit a significant number of RP patients, as well as those with other retinal dystrophies without an exclusively genetic etiology (e.g., glaucoma, age-related macular degeneration, diabetic retinopathy). Recent studies suggest that retinal neurodegeneration is associated with a broad inflammatory response in the retina. This response appears to be mutation-independent and involves

* Correspondence: chernandez@cib.csic.es
†Equal contributors
[1]Departments of Molecular Biomedicine (3D Lab) and Structural and Chemical Biology (IPSBB Unit), Centro de Investigaciones Biológicas-CSIC, C/ Ramiro de Maeztu 9, E-28040 Madrid, Spain
Full list of author information is available at the end of the article

microglial activation, reactive macrogliosis, and the production of pro-inflammatory cytokines [2–5].

GSK-3 is a serine/threonine kinase that exists as 2 highly homologous isoforms, GSK-3α and GSK-3β, each encoded by a distinct gene. GSK-3β is predominantly expressed in the central nervous system (CNS) [6]. Although initially identified as a glycogen synthesis enzyme (the role for which it was named), GSK-3 is currently considered a multitask enzyme involved in the regulation of diverse cellular functions owing to its broad substrate spectrum [7, 8]. In particular, GSK-3 plays a pivotal role in regulating the balance between pro-inflammatory and anti-inflammatory cellular responses. Consequently, GSK-3 is considered a potential therapeutic target for diseases with an inflammatory component. The therapeutic potential of GSK-3 modulators is currently being studied in a variety of neuroinflammatory diseases. These include psychiatric and neurodegenerative disorders, as well as retinal dystrophies; as part of the CNS, the retina shares many physiological and pathological traits with the brain [9].

Employing a chemical genetic approach, we recently investigated the neuroprotective effects of 3 chemically diverse GSK-3 modulators in photoreceptor cells [10]. In the present study we selected one of these compounds, VP3.15, based on its favorable pharmacokinetic and IC_{50} properties. This molecule is a 5-imino-thiadiazole that has been described not only as substrate-competitive GSK-3 inhibitor [11], but also as allosteric inhibitor of PDE7 [12].

We sought to validate in vivo the potential of GSK-3 as a therapeutic target for the treatment of RP, and to demonstrate the therapeutic potential of VP3.15 in this neurodegenerative condition. We characterized the expression of GSK-3β and its inactive serine-9-phosphorylated form in the dystrophic retina of the *rd10* mouse, a model of RP. Moreover, we demonstrated that chronic systemic in vivo VP3.15 treatment preserved visual function by delaying neurodegeneration. Our results indicate that VP3.15 is an innovative drug candidate for the treatment of RP.

Methods

Animals and drug delivery

The *rd10* mouse model of retinal neurodegeneration carries a homozygous phosphodiesterase 6b mutation (*Pde6b*$^{rd10/rd10}$) on a C57BL/6 J background. Mice were kindly provided by Bo Chang from The Jackson Laboratory (Bar Harbor, ME, USA). Wild type (WT) control mice of the same background were also obtained from The Jackson Laboratory. All animals were housed and handled in accordance with the ARVO statement for the Use of Animals in Ophthalmic and Vision Research, European Union guidelines, and those of the local ethics committees of the CSIC and the Comunidad de Madrid. Mice were bred at the CIB core facilities on a 12/12-h light/dark cycle.

VP3.15 was synthesized in our laboratory as previously described [11]. This small molecule is a member of the iminothiadiazole family, the first group of substrate-competitive GSK-3 inhibitors described ([11]; see Additional file 1: Figure S1 for the structure data). The dose administrated was selected based on pharmacokinetic and IC_{50} data ([11–13] and data not shown). Mice received daily intraperitoneal injections of vehicle (10% DMSO, 0.9% NaCl) or VP3.15 (10 mg/kg) for the indicated period of time.

IP administration was selected based on the ability of VP3.15 to cross the brain blood barrier [13] and the necessity of performing repetitive administration without damaging the eye.

Electroretinography

Mice underwent electroretinographic recordings (ERG) at different time points, using a previously described ERG protocol [14]. ERGs were performed by an observer blind to treatment. ERG signals were amplified and band filtered between 0.3 Hz and 1000 Hz (CP511 Preamplifier, Grass Instruments, Quincy, MA, USA) and digitized at 10 kHz using a PowerLab acquisition data card (AD Instruments Ltd., Oxfordshire, UK). Graphical representations of the signals recorded and the control light stimuli were generated using Scope v6.4 PowerLab software. ERG wave amplitudes were measured off-line and the results averaged.

Histology and immunostaining

Mice were euthanized at the indicated ages and their eyes enucleated. The right eye was processed for histological analyses and the left eye for retinal RNA extraction. For histological analyses, eyes were fixed for 1 h in 4% (*w*/*v*) paraformaldehyde in 0.1 M phosphate buffer (PB), pH 7.4, and then cryoprotected by incubation in increasing concentrations of sucrose (final concentration 50% (w/v) in PB). The eyes were then embedded in Tissue-Tek OCT (Sakura Finetec, Torrance, CA, USA) and frozen on isopropanol/dry ice. Cryostat equatorial sections (12 μm) were mounted on Superfrost® Plus slides (Thermo Scientific, Massachusetts, USA), dried at room temperature, and stored at − 20 °C. Before performing further analyses, sections were fixed in acetone for 10 min at − 20 °C and dried at 65 °C for 10 min. After rinsing in PBS and permeation with 1% (w/v) Triton X-100 in PBS, sections were blocked in BGT (2.5 g/L BSA, 100 mM glycine, 0.25% (w/v) Triton X-100 in PBS) for 1 h and then incubated overnight at 4 °C with primary antibodies (Table 1) diluted in BGT. Sections incubated in the absence of primary antibody were used as specificity controls. After rinsing in PBS and incubation

with the appropriate secondary antibodies (Table 1), sections were stained with DAPI (4′,6-diamidino-2-phenylindole; Sigma-Aldrich Corp., St. Louis, MO, USA) and coverslipped with Fluoromont-G.

To assess preservation of the photoreceptor layer, we compared the thickness of the ONL (which primarily contains photoreceptors) with that of the corresponding INL (which contains bipolar, horizontal, and amacrine neurons and Müller glial cell bodies), and quantified the length of rod and cone outer segments (OS). Three sections per eye were analyzed: for each section, one image was captured for each of the 6 retinal zones (T1, T2, T3, T4, T5, and T6; Additional file 2: Figure S2). In each image, 3 measurements were recorded at random positions to obtain an average value per retinal zone per section. Measurements were performed using the "freehand line" and "measure" tools in Fiji software. The ONL thickness was normalized to that of the INL (not affected by the degeneration at this stage) to correct for possible inclinations of the sectioning plane.

Immunoblots

Protein extraction was carried out by sonicating individual retinas in RIPA lysis buffer (containing 2 mM Na_3VO_4, 10 mM NaF, and 4 mM $Na_4P_2O_7$) and chilling the resulting solution on ice for 30 min. Protein (30 μg) from each sample was fractionated by electrophoresis on precast 10–12% (*w*/*v*) SDS-polyacrylamide gels (Criterion TGX, Bio-Rad, Munich, Germany), after which proteins were transferred to PVDF membranes using the Trans-Blot Turbo system (Bio-Rad). Blots were incubated overnight at 4 °C with primary antibodies (Table 1) diluted in TBS (Tris-buffered saline) containing 1% (w/v) Triton-X100, followed by incubation with the appropriate peroxidase-conjugated secondary antibody (Table 1). Proteins were visualized using the Pierce® ECL Western Blotting Substrate (ThermoFisher Scientific, Waltham, MA, USA), and quantified using Chemi-Doc™ Touch Imaging System (Bio-Rad).

RNA isolation and quantitative PCR

Total RNA from individual retinas was extracted using TRIzol Reagent, and 2.5 μg of RNA was typically reverse transcribed using the Superscript III Kit and random primers (all from ThermoFisher Scientific). Quantitative PCR (qPCR) was performed with the ABI Prism 7900HT Sequence Detection System using TaqMan Universal PCR Master Mix, no-AmpErase UNG, and Taqman assays (listed below) for detection (all from Thermo Fisher). The relative change in gene expression was calculated using the $2^{\Delta Ct}$ method, normalizing to expression levels of the *Tbp* (TATA-binding protein) gene. The primer-probe sets used are listed in Table 2.

Statistical analysis

Statistical analyses were performed with GraphPad Prism software 6.0 (GraphPad Software Inc., La Jolla, CA, USA). Protein levels were compared using an unpaired t-test. Gene expression levels were compared using either one-way or 2-way ANOVA tests as indicated in the Figure

Table 1 Antibodies

Antibody against	Host species	Dilution	Manufacturer	Catalog number
Rhodopsin	Mouse	IH,1:500	Abcam, Cambridge, UK	AB3267
L/M-opsin	Rabbit	IH,1:200	Abcam	AB5405
Mouse-Igs, Rabbit-Igs Alexa 488-546-647 labeled	Goat	IH, 1:200–500	ThermoFisher Scientific, Waltham, MA	A-11001
				A-11008
				A-11004
				A-11011
				A-21235
GSK-3Bβ	Mouse	IH,1:100	Cell Signaling Technology, Danvers, Massachusetts, USA	9832S
pGSK-3Bβ^{S9}	Mouse	IH,1:400	Cell Signaling Technology	93,235
Recoverin	Rabbit	WB,1:5000	Millipore, Billerica, Massachusetts, USA	AB5585
GSK-3Bβ	Mouse	WB,1:1000	Cell Signaling Technology	9832S
pGSK-3Bβ^{S9}	Rabbit	WB,1:1000	Cell Signaling Technology	93,235
Akt	Rabbit	WB,1:1000	Cell Signaling Technology	9272
pAkt^{S473}	Rabbit	WB,1:1000	Cell Signaling Technology	9271 L
pAkt^{S473}	Rabbit	IH,1:100	Cell Signaling Technology	4060
GFAP	Rabbit	IH, 1:500	Dako, Glostrup (Denmark)	Z0334

IH immunohistochemistry, *WB* Western blot

Table 2 Taqman assays

Gene	Taqman assay
a2m	Mm00558642_m1
Gfap	Mm01253033_m1
Il1β	Mm00434228_m1
Tbp	Mm00446971_m1
Tnfa	Mm00443260_g1
Rho	Mm01184405_m1
Iba1	Mm00479862_g1
Cd68	Mm03047343_m1
Cd11b	Mm00434455_m1

Legend. For ERG data, differences in wave amplitudes over time between vehicle- and VP3.15-treated mice were assessed using a 2-way ANOVA. Histological differences between vehicle- and VP3.15-treated mice were assessed by 2-way ANOVA. In all cases, *p*-values ≤0.05 were considered statistically significant.

Results

Inflammatory genes are upregulated in rd10 mice during the early stages of retinal neurodegeneration

Pathological neuroinflammation is a hallmark of neurodegeneration in many retinal dystrophies [2–5]. We analyzed temporal alterations in pro-inflammatory gene expression in the *rd10* retina between P14 (before the appearance of morphological signs of retinal degeneration) and P21 (at which stage the degenerative process has become clearly established) to identify the optimal period for therapeutic intervention. Quantitative PCR analysis of WT and *rd10* retinas revealed increased expression of the pro-inflammatory markers *α2m*, *Il1β* and *Tnfα* in the degenerating retinas, beginning in the early stages of degeneration (P18) and increasing dramatically (by 25 to 50 fold) by P21 (Fig. 1). Reactive gliosis in response to retinal damage, as measured by upregulated *Gfap* expression, correlated with the increased expression of inflammatory markers. Likewise, the expression of the microglia genes *Cd68* and *Cd11b* also showed a 4–5 fold increase (Fig. 1).

GSK-3β expression in wild type and rd10 retinas

We next determined expression levels of GSK-3β, the most abundant GSK-3 isoform in the CNS [6], during the same degenerative period as above. We measured the expression of total GSK-3β and of its inactive Ser9-phosphorylated form (GSK-3β^{Ser9}) in *rd10* mouse retinas. No significant differences in GSK-3β RNA levels were observed between *rd10* and WT retinas (Fig. 2a). Furthermore, despite the morphological differences caused by the degenerative process, we observed similarly broad distribution patterns for GSK-3β protein in both P21 *rd10* and WT retinas (Fig. 2b).

GSK-3β is an unusual kinase in that it is constitutively activated but is inhibited upon stimulation of its regulatory signaling pathways (reviewed in [7]). Activation of the PI3K/Akt pathway induces phosphorylation of GSK-3β at Ser9, and subsequent downregulation of GSK-3β activity [15]. During early retinal degeneration (P16 and P18), no differences in Ser^{473}-phosphorylated Akt (pAkt^{Ser473}) or Ser^{9}-phosphorylated GSK-3β (pGSK-3β^{Ser9}) levels were observed between WT and *rd10* retinas (data not shown). Conversely, at P19 and P21, at which point the degenerative process is well established, as evidenced by decreased expression of the photoreceptor protein recoverin, pAkt^{Ser473} and pGSK-3β^{Ser9} levels were significantly higher in *rd10* versus WT retinas (Fig. 3a and b). These observations in retinal extracts were in agreement with the immunostaining pattern observed at P21, which showed an increment in pAkt^{Ser473} and pGSK-3β^{Ser9} in the *rd10* retina (Fig. 3c).

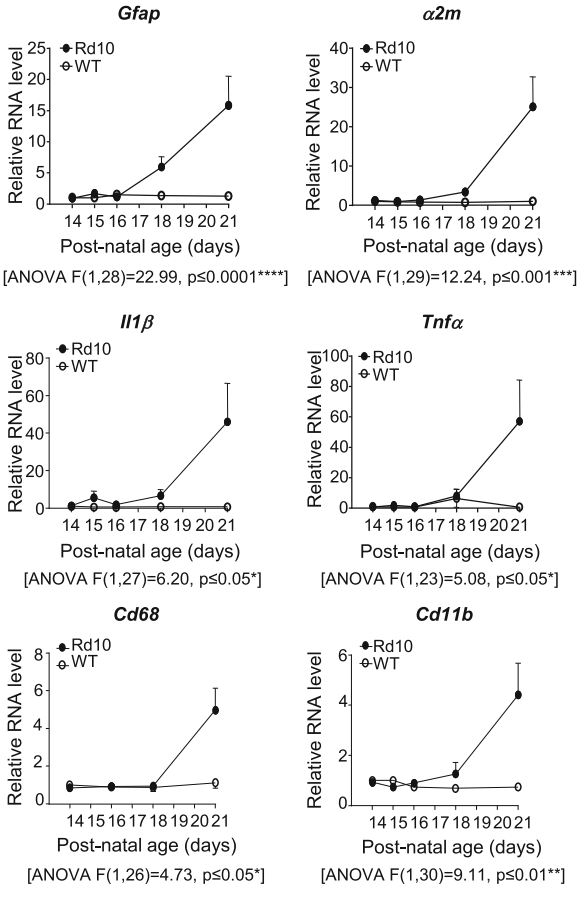

Fig. 1 Expression of inflammatory genes in the retina. RT-qPCR of WT and *rd10* retinas at the indicated ages. Levels of different transcripts were normalized to those of *Tbp* RNA and relativized to P14 WT level (= 1). Results represent the mean + SEM. $n = 3–4$, $^{*}p \leq 0.05$, $^{**}p \leq 0.01$, $^{***}p \leq 0.001$, $^{****}p \leq 0.0001$ (2-way ANOVA)

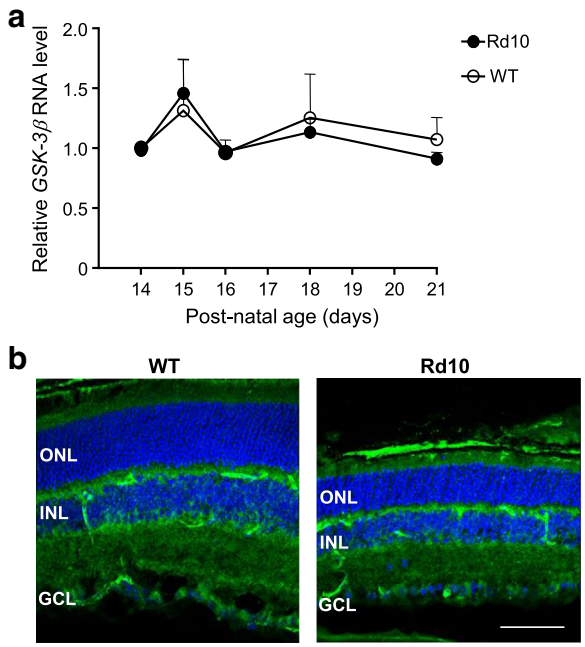

Fig. 2 GSK-3β expression in the retina. **a** RT-qPCR of WT and *rd10* retinas at the indicated ages. *Gsk-3β* transcript levels were normalized to *Tbp* RNA levels and relativized to P14 WT level (= 1). Results represent the mean + SEM. $n = 4$. **b** Representative images of P21 retinal sections from WT and *rd10* mice, immunostained for GSK-3β (green). Nuclei are stained with DAPI (blue). ONL, outer nuclear layer; INL, inner nuclear layer; GCL, ganglion cell layer. Scale bar: 60 μm

This inhibitory phosphorylation of GSK-3β, which coincided with activation of the pro-survival Akt signaling pathway, may represent an intrinsic neuroprotective response to the genetic damage caused in the retina. To test this hypothesis, we sought to potentiate this intrinsic response by pharmacologically inhibiting GSK-3 activity.

In vivo VP3.15 treatment decreases inflammatory and degenerative signs in the rd10 mouse retina

In light of our findings concerning proinflammatory gene expression and GSK-3β modulation, we selected the P15–P21 interval to assess the effects of short-term treatment with VP3.15, a GSK-3 inhibitor. VP3.15 inhibitory activity on GSK-3 was confirmed by determining its effect on the β-catenin levels in the microglia cell line N9 (Additional file 3: Figure S3). *rd10* littermates received daily intraperitoneal injections of either vehicle or VP3.15 (10 mg/kg). One eye from each animal was analyzed for gene expression and the other for retinal morphology. VP3.15 treatment significantly decreased the expression of the proinflammatory genes *Il1β* and *α2m*. A similar trend was observed for *Tnfα* expression (Fig. 4a), and secretion by *rd10* retinal explants (Additional file 7: Figure S7b), although these failed to reach statistical significance. The microglia genes

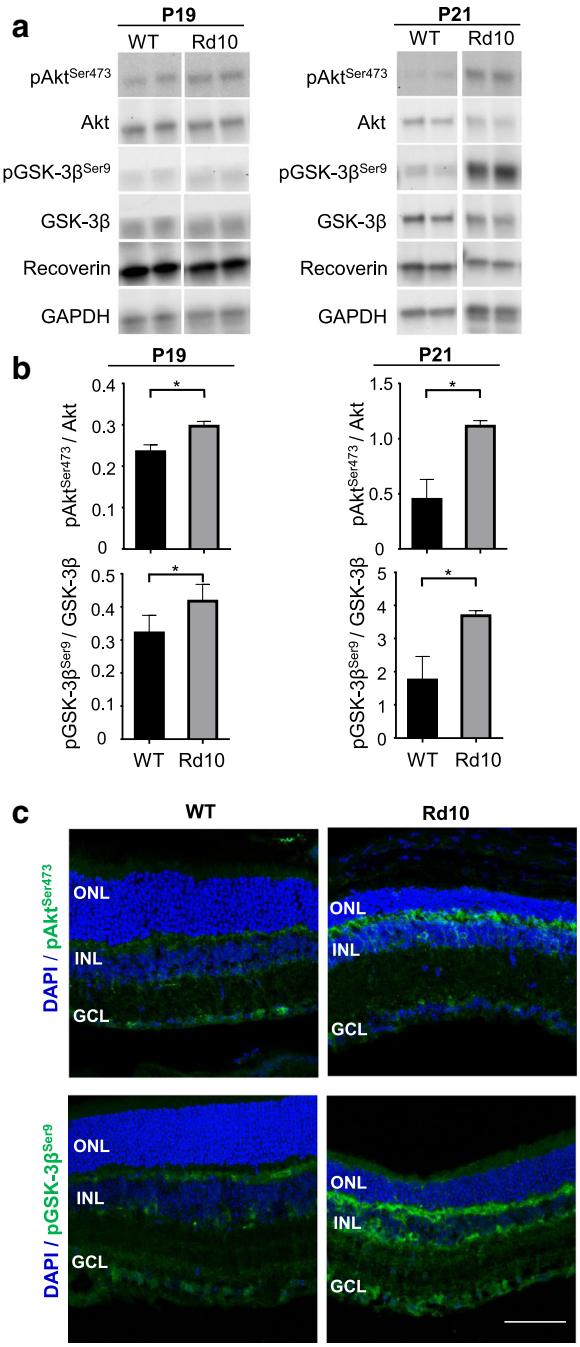

Fig. 3 GSK-3β activation in the retina. **a** Representative Western blots of protein extracts from WT and *rd10* retinas (at P19 and P21). **b** Densitometric analysis of several membranes as those shown in **a**. Levels of phosphorylated Akt and GSK-3β were normalized to those of total Akt and GSK-3β, respectively. Results represent the mean + SEM. $n = 4–5$, $^*p \leq 0.05$ (unpaired 2-tailed Student's t test). **c** Representative images of P21 retinal sections from WT and *rd10* mice, immunostained for $pAkt^{Ser473}$ and $pGSK\text{-}3\beta^{Ser9}$ (green). Nuclei are stained with DAPI (blue). ONL, outer nuclear layer; INL, inner nuclear layer; GCL, ganglion cell layer. Scale bar: 60 μm

Cd11b and *Iba1* were also decreased upon VP3.15 treatment, while the activated microglia marker *Cd68* showed a decline trend (Fig. 4b). In parallel, VP3.15 significantly reduced the expression of *Gfap*, an effect that correlates with a reduced GFAP staining depicted by the radial process of Müller glial cells and by the most inner retinal layer formed by Müller end feet and astrocytes (Fig. 4c and d). Conversely, a trend towards increased gene expression of rod photoreceptor-specific rhodopsin was observed in VP3.15-treated *rd10* mice (Fig. 4e). This observation correlated with the maintenance of ONL thickness and OS length, both of which were better preserved in VP3.15-treated than in the vehicle-treated *rd10* mice (Fig. 4f). Moreover, while rhodopsin expression was specifically localized in the photoreceptor outer segment (OS) in WT and VP3.15-treated *rd10* retinas, vehicle-treated *rd10* retinas displayed shortening of the OS and mislocalization of rhodopsin in the ONL (Fig. 4f).

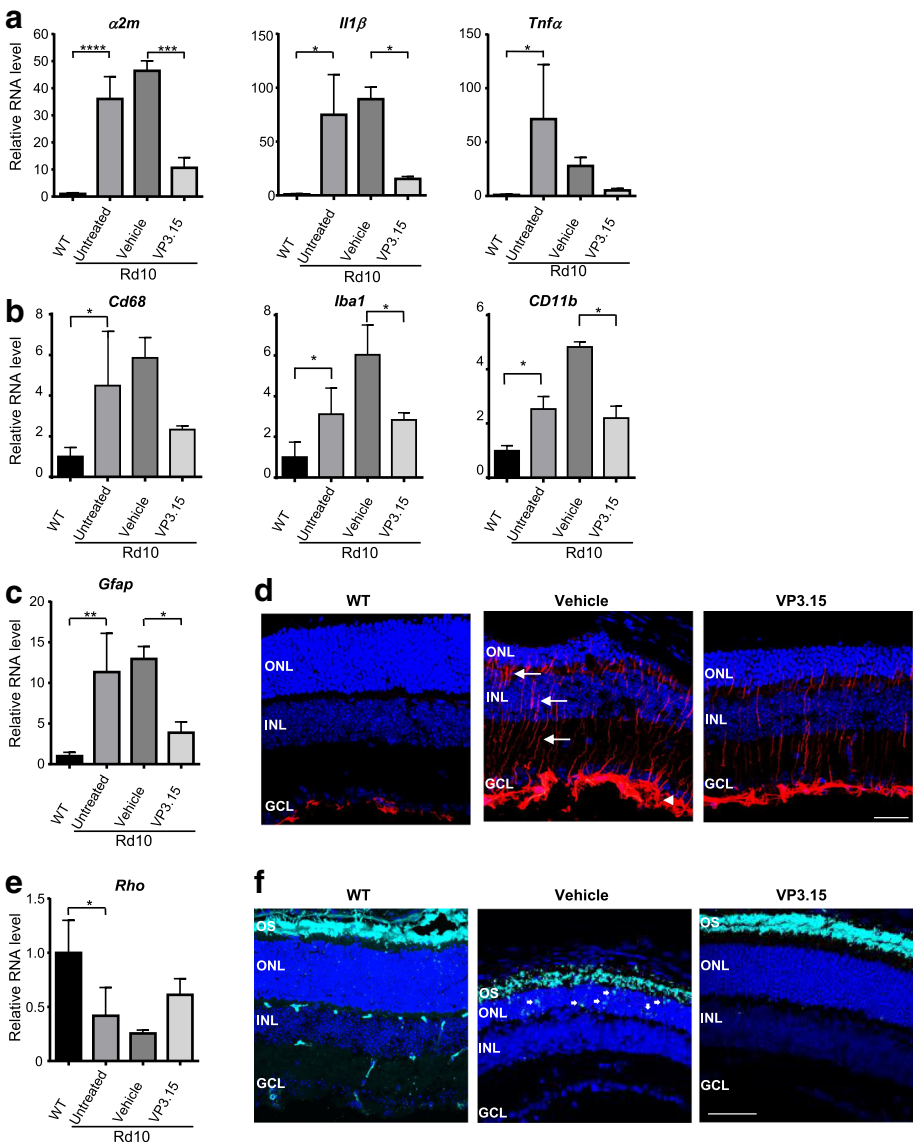

Fig. 4 In vivo effect of short-term VP3.15 administration. *rd10* mice received daily intraperitoneal injections of vehicle or VP3.15 from P15 to P21, and were analyzed one day after the last injection (P22). **a-c** and **e** RT-qPCR of WT as well as untreated *rd10* retinas, and vehicle- and VP3.15-treated *rd10* retinas (all harvested at P22). Levels of all transcripts were normalized to those of *Tbp* RNA and relativized to WT levels (= 1). Results represent the mean + SEM. $n = 2–4$, *$p \leq 0.05$, **$p \leq 0.01$, ***$p \leq 0.001$, **** $p \leq 0.0001$ (one-way ANOVA). **d** and **f** Representative images of P22 retinal sections from WT mice and from vehicle- and VP3.15-treated *rd10* mice, immunostained for GFAP (**d**, red) and rhodopsin (**f**, cyan). Nuclei are stained with DAPI. In **d** arrows point to the radial processes of Müller cells and the arrow head to the most inner retinal layer containing the Müller end feet and astrocytes. Arrows in **f** point to mislocalized rhodopsin in the ONL. OS, outer segments; ONL, outer nuclear layer; INL, inner nuclear layer; GCL, ganglion cell layer. Scale bar: 60 μm

In vivo treatment of rd10 mice with VP3.15 delays the loss of visual function

Based on the promising results obtained following short-term GSK-3 inhibition, we investigated whether a longer treatment period preserved visual function in the *rd10* mouse model. *rd10* littermates received daily injections of either vehicle or VP3.15 from P15 to P46 inclusive. Visual function was assessed weekly by ERG between P25 and P46. Compared with vehicle-treated counterparts, VP3.15-treated *rd10* mice displayed better-defined ERG waves of greater amplitude (Fig. 5 and Additional file 4: Figure S4). The amplitude of ERG waves (a-mixed, b-mixed, b-photopic, and oscillatory potential [OP]) was significantly higher in VP3.15-treated than in vehicle-treated mice, indicating a prolongation of both rod- and cone-mediated vision function by VP3.15 (Fig. 5).

Histological evaluation of retinas at the end point of the study (P47, after the last ERG) revealed a greater relative ONL thickness in VP3.15- versus vehicle-treated retinas despite the advanced degeneration stage (Fig. 6a and b). The photoreceptor preservation effect of VP3.15 was more evident at mid-degeneration stages (P33; Additional file 5: Figure S5). Moreover, specific immunostaining showed better preservation of photoreceptor structure in VP3.15-treated retinas (Fig. 6a). Rhodopsin immunostaining in rod outer segments confirmed the partial preservation of rod outer segments in VP3.15-treated retinas. By contrast, rod outer segments were barely present in vehicle-treated retinas. Similarly, M-L opsin immunostaining revealed longer cone outer segments in VP3.15- versus vehicle-treated *rd10* retinas (Fig. 6a and b).

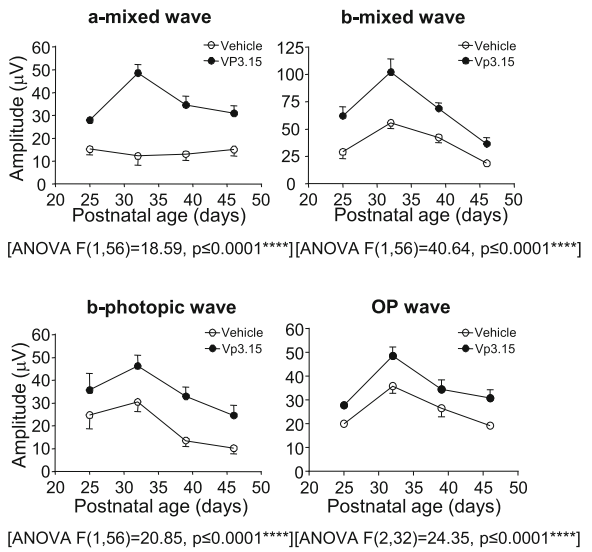

Fig. 5 In vivo effect of long-term VP3.15 administration on visual function. *rd10* mice received daily intraperitoneal injections of vehicle or VP3.15 from P15 to P45. ERG were performed at the indicated ages. Graphs show averaged ERG wave amplitudes, plotted as a function of animal age. Results represent the mean ± SEM. $n = 10$, **** $p \leq 0.0001$ (2-way ANOVA)

Moreover, no toxic effect of VP3.15 administration was observed in other neuronal populations of the retina, particularly rod-bipolar and ganglion cells (Additional file 6: Figure S6).

Taken together, these results demonstrate a neuroprotective effect of VP3.15 on neuroinflammation, retinal structure, and visual function. Our findings thus support the potential of VP3.15 as a novel therapy for retinal dystrophies.

Discussion

This study describes GSK-3β expression and activation of the Akt-GSK-3β pathway during the early stages of retinal neurodegeneration in the *rd10* mouse model of RP. Our findings support the involvement of GSK-3 in retinal decay and provide proof of concept of the neuroprotective effect of GSK-3 inhibition on photoreceptor cells [10]. In vivo administration of VP3.15, a small-molecule GSK-3 inhibitor, reduced photoreceptor cell loss and extended visual function. This neuroprotective effect was accompanied by a decrease in the expression of neuroinflammatory genes in the retina, indicating the potential of VP3.15 as a candidate RP therapy.

GSK-3 is a constitutively activated multitask enzyme, the activity of which is regulated by several inhibitory signaling pathways [7]. Inhibitory phosphorylation of GSK-3 at Ser9 is one of the main regulatory mechanisms. Our analysis of GSK-3β RNA and protein levels during the degenerative period in *rd10* retinas revealed no differences with respect to WT counterparts. However, at both P19 and P21, by when photoreceptor degeneration is well established, inhibitory phosphorylation of GSK-3β at Ser9, and phosphorylation of its Akt regulator, were increased in *rd10* retinas. This endogenous activation of the prosurvival Akt-GSK-3β pathway in the *rd10* retina is in agreement with previous observations in a photoreceptor cell line subjected to a variety of insults, and in the dystrophic retina [16, 17]. We speculate that the activation of endogenous prosurvival pathways in the dystrophic retina constitutes an attempt to control the degenerative process, a response that, however, results insufficient to counteract the permanent genetic damage underlying the degeneration. In our experiments, administration of the GSK-3 inhibitor VP3.15 may have exogenously potentiated the prosurvival pathway, thus delaying photoreceptor cell death and preserving visual function. Indeed, several agents with neuroprotective effects in the retina exert common stimulatory effects on the Akt-GSK-3β pathway [18–20]. GSK-3 is a downstream substrate of the insulin receptor [15, 21] and is thus inhibited upon insulin receptor

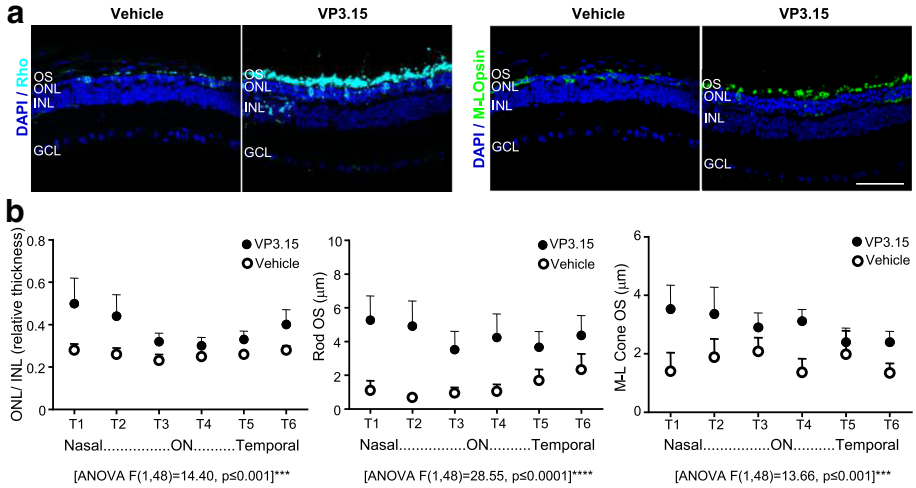

Fig. 6 In vivo effect of long-term VP3.15 administration on photoreceptor cell preservation. Retinal sections from the same animals described in Fig. 5 were immunostained to assess photoreceptor cell structure. **a** Representative images of P47 retinal sections from vehicle- and VP3.15-treated *rd10* mice immunostained for rhodopsin (cyan) and M/L opsin (green). Nuclei are stained with DAPI (blue). OS, outer segments; ONL, outer nuclear layer; INL, inner nuclear layer; GCL, ganglion cell layer. Scale bar: 60 μm. **b** ONL and INL thickness and the length of rod and cone outer segments were measured in equatorial sections corresponding to 6 regions of the retina, following a nasotemporal sequence (T1–T6; see Methods and Additional file 2: Figure S2). Plots show the mean + SEM. $n = 5$ mice, 3 sections per retina, 3 measurements per region and section. ON, optic nerve. ***$p \leq 0.001$, **** $p \leq 0.0001$ (2-way ANOVA)

stimulation. We have previously demonstrated that pro-insulin, which binds with high affinity to the A isoform of the insulin receptor in the retina and activates Akt [22, 23], similarly prolongs rod survival and preserves visual function [14, 22, 24].

Neuroinflammation is a key component of neurodegenerative processes affecting the brain and retina, and thus constitutes a promising non-cell-autonomous target for treatments of CNS diseases in general, and of the retina in particular [2–5, 25]. GSK-3 plays a pivotal role in the regulation of peripheral and central pro-inflammatory cytokine production [26, 27], and its inhibition reduces both systemic and brain inflammation [26, 27]. The specific molecular events that occur in the *rd10* retina upon GSK-3 inhibition remain to be established. This is a complicated task since GSK-3 is implicated in the regulation of multiple cellular processes including metabolism, cell structure, cell death, proliferation, and gene expression, with over 100 confirmed and 500 predicted substrates [7]. Exploratory studies employing *rd10* retinal explants showed that VP3.15 attenuated NF-kB activation (Additional file 7: Figure S7). NF-kB is a key regulator of the inflammatory response by enabling the transcription of the genes encoding many pro-inflammatory cytokines. Indeed, our results suggest that levels of pro-inflammatory cytokines (*Il1β* and *Tnfα*) are reduced in VP3.15-treated *rd10* retinas. This could explain, at least in part, the attenuation of photoreceptor degeneration and loss, and the preservation of vision. Moreover, the reduced inflammatory response observed in VP3.15-treated retinas was accompanied by decreases in the reactive gliosis marker GFAP as well as in *α2M* expression, for which a role in retinal neurodegeneration has been recently described [28–30].

In addition to its inhibitory effect on GSK-3, VP3.15 also acts as an allosteric inhibitor of PDE7, an effect that contributes to its neuroprotective activity in other CNS pathologies [13]. However, PDE7 inhibition, via increasing cAMP levels and PKA activation, also converges on GSK-3 inhibition [31]. PKA is able to phosphorylate GSK-3β at Ser9 and, subsequently, to inactivate it [20, 31]. Besides, previous findings by our group support that the prosurvival effect of VP3.15 in photoreceptors may be primarily due to GSK-3 inhibition, since the specific GSK-3 inhibitor tideglusib exerted an even more potent neuroprotective effect in photoreceptors [10].

Most forms of RP involve primary death of rod photoreceptors, in which the mutated gene exerts its function, followed by secondary loss of cone photoreceptors. VP3.15 treatment prolonged photoreceptor survival, as evidenced by the preservation of ONL thickness and rod outer segment length. Furthermore, VP3.15 preserved the integrity of the cone outer segment, the first site of morphological alterations during cone degeneration. Human vision primarily relies on cones, which mediate daylight, color, and high-acuity vision. Accordingly, a mutation-independent treatment for RP that specifically prolongs cone survival would be highly beneficial. VP3.15 had a marked effect on cone cytoarchitecture and visual function, as indicated by an increase in the

amplitude of the photopic b-wave compared with the untreated *rd10* animals. It remains unclear whether VP3.15 exerts a direct effect on cone integrity, or whether this effect is secondary to the prosurvival effect on rods (present study and [10]). Regardless, VP3.15 resulted in a marked attenuation of the loss of both daylight and dim-light vision.

Conclusion

Our in vivo findings, together with the results of a recently published in vitro study [10], support the therapeutic potential of GSK-3 modulation for the treatment of retinal neurodegeneration, as described for other neurodegenerative diseases [32], and underscore the potential of GSK-3 inhibitors, in particular VP3.15, as pharmacological therapies for RP.

Additional files

Additional file 1: Figure S1. Chemical structure of VP3.15. (PPTX 49 kb)

Additional file 2: Figure S2. Scheme of the retinal sections. The 6 retinal zones defined for quantification as T1, T2, T3, T4, T5 and T6 are indicated. ON, optic nerve. (PPTX 593 kb)

Additional file 3: Figure S3. Effect of VP3.15 on β-catenin levels. N9 microglia cell cultures were treated either with vehicle or with 10 μM VP3.15 for 1 or 7 h. **a** Representative Western blots of protein extracts from cultured N9 cells at the indicated times. **b** Densitometric analysis of membranes as those shown in **a**. Levels of β-catenin were normalized to those of GAPDH. Results represent the mean + SEM. $n = 3$, $^{*}p \leq 0.05$ (unpaired 2-tailed Student's t test). Methods are provided in Additional file 8. (PPTX 11435 kb)

Additional file 4: Figure S4. VP3.15 treated mice show better light-evoked responses than vehicle-treated ones. Standard ERG representative trace recordings from one VP3.15-treated and one vehicle-treated overnight dark-adapted animal. See for comparison the differences between the two experimental groups in the trace amplitudes. Rod and cone mixed response (a-mixed and b-mixed, 1.5 log cd·s/m^2), and oscillatory potential (OP, 1.5 log cd·s/m^2) were recorded sequentially under scotopic conditions. Cone (b-phot, 2 log cd·s/m^2) responses were recorded after 5 min light-adaptation (30 cd/m^2 background light) under photopic conditions. All light responses were separated in the vertical axis to better present the ERG waveform. Animal age is indicated to the left of each trace recording. (PPTX 1167 kb)

Additional file 5: Figure S5. Mid-term effect of VP3.15 on photoreceptor preservation. *rd10* mice received daily an intraperitoneal injection of vehicle or VP3.15 from P15 to P32 and the retinas were analyzed one day after the last injection (P33). Representative images of P33 retinal sections from WT and vehicle- and VP3.15-treated *rd10* mice stained with DAPI (blue). ONL, outer nuclear layer; INL, inner nuclear layer. Scale bar: 60 μm. **b** ONL and INL thickness were measured in equatorial sections corresponding to 6 regions of the retina, following a nasotemporal sequence (T1–T6; see Methods and Additional file 2: Figure S2). Plot shows the mean + SEM. $n = 3$ mice, 3 sections per retina, 3 measurements per region and section. ON, optic nerve. $^{****}p \leq 0.0001$ (2-way ANOVA). (PPTX 360 kb)

Additional file 6: Figure S6. In vivo effect of VP3.15 treatment on rod-bipolar and ganglion cells. *rd10* mice received daily an intraperitoneal injection of vehicle or VP3.15 from P15 to P32 and the retinas were analyzed one day after the last injection (P33). **a** Representative images of P33 retinal sections from vehicle- and VP3.15-treated *rd10* mice, immunostained for PKCα or RBPMS to label rod-bipolar or ganglion cells respectively (green). Nuclei are stained with DAPI (blue). **b** The number of PKCα- and RBPMS-positive cells were scored in equatorial sections corresponding to 6 regions of the retina, following a nasotemporal sequence (T1–T6; see Methods and Additional file 2: Figure S2). The plots show the mean + SEM. n = 3 mice, 3 sections per retina, 3 measurements per region and section. ONL, outer nuclear layer; INL, inner nuclear layer; GCL, ganglion cell layer. Scale bar: 38 μm. Methods are provided in Additional file 8. (PPTX 924 kb)

Additional file 7: Figure S7. Effect of VP3.15 on NF-kB activation and TNFα secretion. P22 rd10 retinas were cultured in the absence (vehicle) or presence of 3.2 μM VP3.15 for 16 h. **a** Representative images showing Western blots of protein extracts. **b** Densitometric analysis of membranes as those shown in **a**. Levels of pNF-kB^{Ser536} were normalized to those of GAPDH. Results represent the mean + SEM. $n = 5–6$, $^{*}p \leq 0.05$ (unpaired 2-tailed Student's t test). **c** TNFα concentration was quantified in the culture media by ELISA. Methods are provided in Additional file 8. (PPTX 6297 kb)

Additional file 8: Additional Methods. (DOCX 20 kb)

Abbreviations

CD11B: Cluster of differentiation molecule 11B; CD68: Cluster of differentiation 68; CNS: Central nervous system; ERG: Electroretinographic recording; GCL: Ganglion cell layer; GFAP: Glial fibrillary acidic protein; GSK: Glycogen synthase kinase; IBA1: Ionized calcium-binding adapter molecule 1; IC_{50}: Half maximal inhibitory concentration; IL1-β: Interleukin-1β; INL: Inner nuclear layer; NF-κB: Nuclear factor kappa-light-chain-enhancer of activated B cells; ON: Optic nerve; ONL: Outer nuclear layer; OP: Oscillatory potential; OS: Outer segment; PB: Phosphate buffer; PDE: Phosphodiesterase; PKA: Protein kinase A; PKCα: Protein kinase C alpha; qPCR: Quantitative polymerase chain reaction; RBPMS: RNA binding protein with multiple splicing; RP: Retinitis pigmentosa; RT: Reverse transcription; TBP: TATA-binding protein; TNFα: Tumor necrosis factorα; WT: Wild-type; α2M: α-2-macroglobulin

Acknowledgements

We thank Cayetana Murillo, Laura Ramírez and the staff of the CIB animal house and microscopy facilities for technical support. We thank Violeta Gómez-Vicente for advice on GSK-3 immunostaining. We thank Dr. García-Pardo and Dr. Labandeira-García for providing the pNF-kB^{ser536} antibody and the N9 cell line, respectively. ASC and JZD are recipients of UCM and MECD (FPU13-00362) predoctoral fellowships, respectively.

Funding

This work was supported by grants from the Spanish MINECO (SAF2012-37979-C03-01 and SAF2016-76639-R to AM, SAF2013-41059-R and SAF2016-75681-R to EJdlR, and PI13-02098 to PdlV) and Instituto de Salud Carlos III and cofinanced by FEDER (PI17/01601 and RETICS RD16/0019/0009 to IL).

Availability of data and materials

The datasets used and/or analyzed during the current study are available from the corresponding author on reasonable request.

Authors' contributions

ASC, BVZ and MM and JZD performed experimental procedures. VP synthesized VP3.15. CG and AM supervised the medicinal chemistry work. PdlV designed and analyzed the functional studies. EJdlR and CHS designed and supervised the biological experiments. AM, EJdlR and CHS, analyzed and discussed the results. ASC, VP, IL, PdlV, AM, EJdlR and CHS contributed to the writing and edition of the manuscript. All authors read and approved the final manuscript.

Ethics approval

Animal handling and experimental procedures followed the 3Rs principles, and were revised by the Animal Welfare Committee of the Centro de Investigaciones Biológicas (CIB) and the Bioethics Committee of the Consejo Superior de Investigaciones Científicas (CSIC) and authorized by the Comunidad de Madrid (Ref: PROEX 157/14), in accordance with the Spanish legislation and the European Union (EU) Directive 2010/63/EU for animal research.

Consent for publication

All authors consent for the publication of this study.

Competing interests
CSIC has filed a patent for the VP3.15 (AM, VP and CG inventors).

Publisher's Note

Author details
[1]Departments of Molecular Biomedicine (3D Lab) and Structural and Chemical Biology (IPSBB Unit), Centro de Investigaciones Biológicas-CSIC, C/ Ramiro de Maeztu 9, E-28040 Madrid, Spain. [2]Neurovascular Research Unit, Department of Pharmacology, Facultad de Medicina, Universidad Complutense de Madrid, Madrid, Spain. [3]Department of Systems Biology, Facultad de Medicina, Universidad de Alcalá, Alcalá de Henares, Spain.

Received: 15 June 2017 Accepted: 9 April 2018
Published online: 16 April 2018

References

1. Hartong DT, Berson EL, Dryja TP. Retinitis pigmentosa. Lancet. 2006;368:1795–809.
2. Chinskey ND, Besirli CG, Zacks DN. Retinal cell death and current strategies in retinal neuroprotection. Curr Opin Ophthalmol. 2014;25:228–33.
3. Cuenca N, Fernandez-Sanchez L, Campello L, Maneu V, De la Villa P, Lax P, Pinilla I. Cellular responses following retinal injuries and therapeutic approaches for neurodegenerative diseases. Prog Retin Eye Res. 2014;43:17–75.
4. Mustafi D, Maeda T, Kohno H, Nadeau JH, Palczewski K. Inflammatory priming predisposes mice to age-related retinal degeneration. J Clin Invest. 2012;122:2989–3001.
5. Yoshida N, Ikeda Y, Notomi S, Ishikawa K, Murakami Y, Hisatomi T, Enaida H, Ishibashi T. Clinical evidence of sustained chronic inflammatory reaction in retinitis pigmentosa. Ophthalmology. 2013;120:100–5.
6. Pardo M, Abrial E, Jope RS, Beurel E. GSK3beta isoform-selective regulation of depression, memory and hippocampal cell proliferation. Genes Brain Behav. 2016;15:348–55.
7. Beurel E, Grieco SF, Jope RS. Glycogen synthase kinase-3 (GSK3): regulation, actions, and diseases. Pharmacol Ther. 2015;148:114–31.
8. Jope RS, Johnson GV. The glamour and gloom of glycogen synthase kinase-3. Trends Biochem Sci. 2004;29:95–102.
9. Jindal V. Interconnection between brain and retinal neurodegenerations. Mol Neurobiol. 2015;51:885–92.
10. Marchena M, Villarejo-Zori B, Zaldivar-Diez J, Palomo V, Gil C, Hernandez-Sanchez C, Martinez A, de la Rosa EJ. Small molecules targeting glycogen synthase kinase 3 as potential drug candidates for the treatment of retinitis pigmentosa. J Enzyme Inhib Med Chem. 2017;32:522–6.
11. Palomo V, Perez DI, Perez C, Morales-Garcia JA, Soteras I, Alonso-Gil S, Encinas A, Castro A, Campillo NE, Perez-Castillo A, et al. 5-imino-1,2,4-thiadiazoles: first small molecules as substrate competitive inhibitors of glycogen synthase kinase 3. J Med Chem. 2012;55:1645–61.
12. Redondo M, Palomo V, Brea J, Perez DI, Martin-Alvarez R, Perez C, Paul-Fernandez N, Conde S, Cadavid MI, Loza MI, et al. Identification in silico and experimental validation of novel phosphodiesterase 7 inhibitors with efficacy in experimental autoimmune encephalomyelitis mice. ACS Chem Neurosci. 2012;3:793–803.
13. Medina-Rodriguez EM, Bribian A, Boyd A, Palomo V, Pastor J, Lagares A, Gil C, Martinez A, Williams A, de Castro F. Promoting in vivo remyelination with small molecules: a neuroreparative pharmacological treatment for multiple sclerosis. Sci Rep. 2017;7:43545.
14. Corrochano S, Barhoum R, Boya P, Arroba AI, Rodriguez-Muela N, Gomez-Vicente V, Bosch F, de Pablo F, de la Villa P, de la Rosa EJ. Attenuation of vision loss and delay in apoptosis of photoreceptors induced by proinsulin in a mouse model of retinitis pigmentosa. Invest Ophthalmol Vis Sci. 2008;49:4188–94.
15. Cross DA, Alessi DR, Cohen P, Andjelkovich M, Hemmings BA. Inhibition of glycogen synthase kinase-3 by insulin mediated by protein kinase B. Nature. 1995;378:785–9.
16. Finnegan S, Mackey AM, Cotter TG. A stress survival response in retinal cells mediated through inhibition of the serine/threonine phosphatase PP2A. Eur J Neurosci. 2010;32:322–34.
17. Nakazawa T, Shimura M, Tomita H, Akiyama H, Yoshioka Y, Kudou H, Tamai M. Intrinsic activation of PI3K/Akt signaling pathway and its neuroprotective effect against retinal injury. Curr Eye Res. 2003;26:55–63.
18. Baek SM, Yu SY, Son Y, Hong HS. Substance P promotes the recovery of oxidative stress-damaged retinal pigmented epithelial cells by modulating Akt/GSK-3beta signaling. Mol Vis. 2016;22:1015–23.
19. Rajala A, Gupta VK, Anderson RE, Rajala RV. Light activation of the insulin receptor regulates mitochondrial hexokinase. A possible mechanism of retinal neuroprotection. Mitochondrion. 2013;13:566–76.
20. Wyse Jackson AC, Cotter TG. The synthetic progesterone Norgestrel is neuroprotective in stressed photoreceptor-like cells and retinal explants, mediating its effects via basic fibroblast growth factor, protein kinase A and glycogen synthase kinase 3beta signalling. Eur J Neurosci. 2016;43:899–911.
21. van Weeren PC, de Bruyn KM, de Vries-Smits AM, van Lint J, Burgering BM. Essential role for protein kinase B (PKB) in insulin-induced glycogen synthase kinase 3 inactivation. Characterization of dominant-negative mutant of PKB. J Biol Chem. 1998;273:13150–6.
22. Isiegas C, Marinich-Madzarevich JA, Marchena M, Ruiz JM, Cano MJ, de la Villa P, Hernandez-Sanchez C, de la Rosa EJ, de Pablo F. Intravitreal injection of proinsulin-loaded microspheres delays photoreceptor cell death and vision loss in the rd10 mouse model of retinitis Pigmentosa. Invest Ophthalmol Vis Sci. 2016;57(8):3610.
23. Malaguarnera R, Sacco A, Voci C, Pandini G, Vigneri R, Belfiore A. Proinsulin binds with high affinity the insulin receptor isoform a and predominantly activates the mitogenic pathway. Endocrinology. 2012;153:2152–63.
24. Fernandez-Sanchez L, Lax P, Isiegas C, Ayuso E, Ruiz JM, de la Villa P, Bosch F, de la Rosa EJ, Cuenca N. Proinsulin slows retinal degeneration and vision loss in the P23H rat model of retinitis pigmentosa. Hum Gene Ther. 2012;23:1290–300.
25. Ransohoff RM. How neuroinflammation contributes to neurodegeneration. Science. 2016;353:777–83.
26. Beurel E, Michalek SM, Jope RS. Innate and adaptive immune responses regulated by glycogen synthase kinase-3 (GSK3). Trends Immunol. 2010;31:24–31.
27. Jope RS, Cheng Y, Lowell JA, Worthen RJ, Sitbon YH, Beurel E. Stressed and inflamed, can GSK3 be blamed? Trends Biochem Sci. 2017;42:180–92.
28. Barcelona PF, Saragovi HU. A pro-nerve growth factor (proNGF) and NGF binding protein, alpha2-macroglobulin, differentially regulates p75 and TrkA receptors and is relevant to neurodegeneration ex vivo and in vivo. Mol Cell Biol. 2015;35:3396–408.
29. Shi Z, Rudzinski M, Meerovitch K, Lebrun-Julien F, Birman E, Di Polo A, Saragovi HU. Alpha2-macroglobulin is a mediator of retinal ganglion cell death in glaucoma. J Biol Chem. 2008;283:29156–65.
30. Platon-Corchado M, Barcelona PF, Jmaeff S, Marchena M, Hernandez-Pinto AM, Hernandez-Sanchez C, Saragovi HU, de la Rosa EJ. p75 NTR antagonists attenuate photoreceptor cell loss in murine models of retinitis pigmentosa. Cell Death Dis. 2017;8:e2922.
31. Morales-Garcia JA, Palomo V, Redondo M, Alonso-Gil S, Gil C, Martinez A, Perez-Castillo A. Crosstalk between phosphodiesterase 7 and glycogen synthase kinase-3: two relevant therapeutic targets for neurological disorders. ACS Chem Neurosci. 2014;5:194–204.
32. Eldar-Finkelman H, Martinez A. GSK-3 inhibitors: preclinical and clinical focus on CNS. Front Mol Neurosci. 2011;4:32.